United Graduate School of Agricultural Sciences, Iwate University (UGAS)
Yamagata University, Faculty of Agriculture

PhD thesis

Influence of snow dynamics on mountainous forest soil hydrology cycle

積雪動態が森林土壌の水循環におよぼす影響

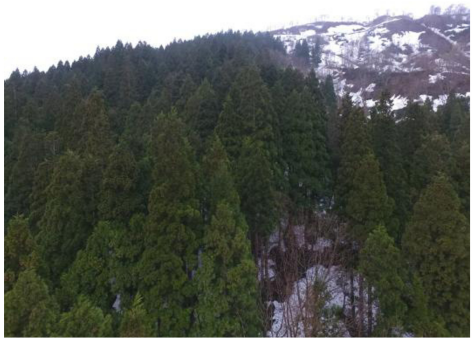
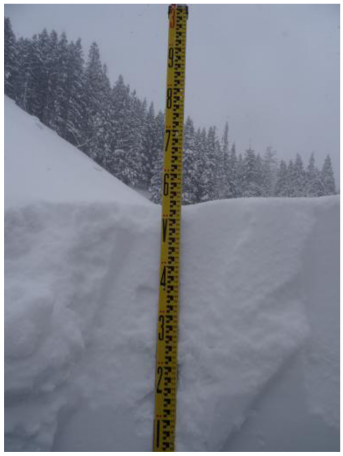
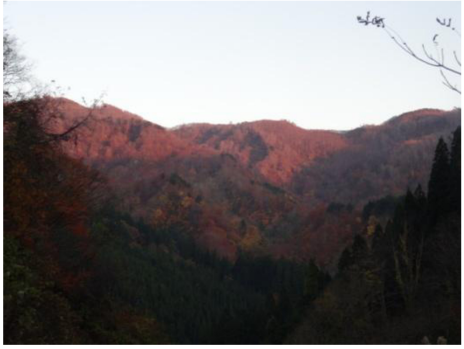

Alexander Christian Brandt

Yamagata University, Faculty of Agriculture
Yamagata-ken, Tsuruoka-shi, Wakabamachi 1-23, 997-8555 Japan
山形大学農学部、山形県鶴岡市若葉町 1－23

Supervisors: Prof. Hideki Murayma, Yamagata University, Tsuruoka, Japan

Prof. Larry Lopez, Yamagata University, Tsuruoka, Japan

Ass. Prof. Chihiro Kato, Hirosaki University, Hirosaki, Japan

I hereby certify that the thesis I am submitting is entirely my own original work except where otherwise indicated. I am aware of the University's regulations concerning plagiarism, including those regulations concerning disciplinary actions that may result from plagiarism. Any use of the works of any other author, in any form, is properly acknowledged at their point of use.

Signature: A.C. Brandt

This thesis was submitted at the Faculty of Agriculture, Yamagata University, part of the United Graduate School of Agricultural Sciences, Iwate University (UGAS) to acquire the degree of *Doctor philosphiae* in the Speciality of *Plant Production* belonging to the Major of *Bioproduction Science*.

Tsuruoka, 7th of September 2020

Table of contents

Table of Figures

Table of Tables

Abstract (English)

Snow covers provide one of the most important water reservoirs on earth. Snowmelt in spring distributes water to plants, animals and humans, ensuring the life of all living organisms. This process is particularly important in regions with low precipitation in spring, when plants start to transpire and soils start to dry due to increasing air temperatures. These regions rely on snowmelt water from mountains in sufficient quantity to bridge the time of low precipitation. In times of climate change and especially global warming, many regions around the world suffer droughts because snowfall in winter has decreased significantly, and therefore the total amount of accumulated snow before spring did, too.

One region that uses snowmelt water intensively is Tōhoku region (東北) in Japan. Two thirds of the surface is covered by forests, which are mainly growing in the Ōu Mountain range (奥羽山脈), which divides Tōhoku region into West and East. The plains closer to the Japan Sea and the Pacific are mainly used for rice farming. Hence, the demand of water for trees in the forest and for paddy fields is high in spring. Since the mountains, especially on the western side, are receiving heavy snowfall in every winter, the amount of water stored in the mountains results in long-running snowmelt processes, lasting until June or July in every year. However, winter precipitation and snow accumulation decreased in the last decades, and air temperature in winter, especially in the Asahi Mountain Range (朝日連峰) of Yamagata prefecture (山形県), is around 0°C. This temperature implies that small differences in air temperature make a difference between snow accumulation and snowmelt, and the timing of precipitation determines the proportion of rain and snow. Since winter precipitation is high, with usually more than 1500 mm, snow depths of more than three metres are common in the mountains. In recent years snow depth has shown high annual variability. Years with high snow depth were followed by a year with small snow cover two years later. Small temperature differences can then result in significant changes of water supply to the Shōnai plains (庄内), the coastal area of Yamagata.

The hydrological cycle in Shōnai and the Asahi mountains was subject of this study in order to understand the mechanisms in mountainous forests in winter and to detect changes in snow cover and snow dynamics over the last decade. Meteorological data, soil physical properties and soil moisture have been continuously monitored in the Yamagata University Research Forest (YURF) in order to run a model for soil moisture estimations, which can be

used for various applications. The modelling software used, HYDRUS 1D, calculates soil moisture, snow accumulation and other parameters using the data obtained from field and laboratory work.

The recent winter (2019/2020), with high air temperature and without heavy precipitation events, resulted in the shallowest snow cover in YURF which was measured. Snow depth was combined with snow density, which was higher in years with greater snow depth, because snow was compacted more in those years. Furthermore, snow at the surface melted on days with temperatures of more than 0°C and moved downwards in the snowpack. Water refroze in deeper layers of the snowpack, where it changed the snow crystal structure and increased the snow density. The same process was observed after rain-on-snow (ROS) events. Knowing the snow density after those events means knowing the amount of water which will be supplied to the Shōnai plains in spring. Modelling of snow density for the snow accumulation period and also for the snowmelt period was performed for every winter starting in the year 2011. Using precipitation data and degree-day factors (DDFs), accurate calculations for the snow water equivalent (SWE) of the snowpack were carried out.

ROS events caused increases in snow density, and were also found to affect soil moisture under the snowpack. In order to measure these effects, soil moisture was monitored at three spots of a slope, vegetated with Japanese cedar (*Cryptomeria japonica*). Two winters with significantly different snow depth were measured and analysed in this thesis in order to understand the relation between snow cover and rainwater infiltration. Soil moisture was also affected by numerous small rain events of less than 10 mm in the winter 2019/2020, where the maximum snow depth was 1.3 m. In contrast to the highly variable soil moisture in this winter, water infiltrated the soil only a few times in the winter 2018/2019, when the snow cover was 3 meters at its maximum. Further it was found that different parts of the slope receive different amounts of water. While most water reached the soil surface at the top and at the bottom of the slope, soil at the slope was less affected by ROS events. Consequently lateral flow of water in the snowpack downwards the slope was of higher rate than vertical flow into soil.

Infiltration of the snowpack by water resulted in a constant soil moisture level at the matric potential of the soil. High precipitation in autumn filled most pores of the soil, and the last pores to reach field capacity were filled in early winter. ROS events and partial snowmelt supplied water to fill quickly draining pores. However, due to high sand contents and high

hydraulic conductivity, soil never became saturated. Soil moisture increased insignificantly in spring during snowmelt, which caused higher surface runoff of snowmelt water and less subsurface runoff. Soil moisture decreased significantly, due to transpiration and evaporation, shortly before snowmelt ended. Soil moisture reacted immediately to rain events in summer and autumn. However, soils in YURF had high water repellency, resulting in higher surface runoff when the soil was dry. Runoff measurements confirmed that surface runoff was higher after dry periods and after heavy rain events.

Significant differences in soil physical properties were found between the soils in YURF and the soils of the second study site in Kaminoyama city (上山市). Soils at the Kaminoyama sites contained more clay and silt and were therefore able to store water and nutrients better than the soils in YURF, which results in better fertility. The experiments were done in order to characterise the efficiency and yield of wine production. Since soils in Kaminoyama were better evolved than soils in YURF, the potential for agriculture and fruit cultivation was, based on the soil physical properties, significantly higher.

The application of the HYDRUS 1D model for YURF was found to be a good approach but introduced also some difficulties. Differences in between model and reality were small in seasons without snow cover. In contrast, thick snow cover caused problems for the model, resulting in an overestimation of soil moisture contents in winter. Snow depth was not predicted correctly either. The best results for soil moisture modelling were obtained for the top of the slope, where water moves vertically in the snowpack. However, in general the model worked well and can be improved in the future, also by the use of the more sophisticated versions HYDRUS 2D and 3D.

In conclusion, this study demonstrated water storage and water movement in the soil in winter, and the potential for using models for the calculation of hydrological processes. Winter precipitation became more important, since a shift in the amount of snowfall is followed by smaller SWE in the Asahi Mountains. The results confirm changing climate conditions and introduce new methods for the estimation of water availability.

Abstract (Japanese)

地球上で積雪は水を貯水するのに大切なものの一つだ。春の融雪は植物や動物に水を配給し、すべての生物の生命を保証する。この過程は植物が蒸散を始め、気温の上昇で土壌が乾燥し始める春に降水量の少ない地域で特に大切だ。これらの地域は山からの雪解け水に依存しており、降水量が少ない期間も水量が十分である必要がある。気候変動、とりわけ地球温暖化によって世界中多くの地域で干ばつが起こり、冬の降雪量が大幅に減少したため春前の積雪量も減少した。

東北は雪解け水を多く使っている地方である。東北地方の中心を走る奥羽山脈の周辺に森林は存在し、東北地方の三分の二を占める。日本海側と太平洋側の平野は水田に使われる。したがって、森林の樹木と水田に水は使われるため春の水の需要は高くなる。毎年東北地方特に西部は大雪に見舞われるので山に蓄えられた水の量は、毎年 6, 7 月まで続く長期にわたる融雪プロセスをもたらす。しかしながら冬の降水量と積雪量はここ数十年で減少し、冬の気温は朝日連峰（山形県）で 0 ℃付近である。この温度は、気温のわずかな違いが積雪と融雪の間に違いをもたらし、降水のタイミングが雨と雪の割合を決定することを意味する。たいてい冬の降水量は 1500mm を超えるため、山では 3mを超える積雪深が一般的である。ここ数年、積雪深が変化ししていることが分かった。積雪量の多い年の二年後に積雪量の少ない年になるのである。山形の海岸地域において小さな気温の差は庄内平野への水の供給に大きな変化をもたらす可能性があります。

過去十年間の雪の力動や天気の力動を調べるために、庄内朝日の水の循環を研究した。山形大学演習林(YURF)で気象データと土壌物理特性と土壌水分を量って、水分モデルに入力しました。このモデルを HYDRUS1D と呼ぶ。演習林のデータをこのモデルを用いて土壌水分や雪の深さなど色々なパラメーターを算定する。

2019-2020 は気温が高く、降水量も多くなかったためここ十年で積雪深は一番低かった。雪は圧縮できるため、積雪の深い年は積雪の浅い年より雪の密度は大きかった。温度が０℃以上の日は雪の上部が解け、積雪の中に浸透し下部で凍ることで結晶組織が変化し雪の密度が増加した。同じプロセスは雨の日に起こった。雪の重さが分かれば、春の雪解け水の量を推測できる。2011 年冬から毎年、積雪の期間と融雪の期間に雪密度の測定を行い、降水量データと度・日係数（DDF）を使用して、積雪の雪水当量（SWE）の正確な計算をした。

冬の降水は雪密度を増加させるだけでなく、雪の下の土壌水分にも影響をもたらす。山腹の杉林に三つのサンプリングポイントを作り土壌水分を量った。積雪と雨水の浸透との関係を理解するために、雪の深さが大きく異なる 2 つの冬を測定して分析しました。2019－2020 年の最深雪は 1.3mであり、1 日の降雨が 10 ㎜以下の場合も土壌水分にしばしば影響した。2018－2019 年の最深雪は 3mであり、水は土壌に数回しか浸透しなかった。さらに、斜面の異なる部分が異なる量の水を受け取ることがわかった。雨水は斜面の上部と下部の土壌表面には到達したが、斜面途中の土壌には雨水による影響は少なかった。斜面の一番高い所と一番下所で雨水は大概を届けてが、斜面中の所に水が土にあまり浸潤しなかった。そのため水は雪の中を通り下部へ移動した。

冬の雪解け水の浸透が土壌のマトリックポテンシャルで土壌水分を一定に保つことができた。秋の高い降水量は土壌の孔隙の大方を埋めて、冬の初めに最後の孔隙が埋まった。冬の雪解け水と雨水が大きい土の孔隙を埋めたのである。しかし、砂の量が多く、水伝導性が高いことから、土壌は決して飽和状態にならなかった。

雪解けの終わりに土壌水分はすぐに大幅に減少した。木の蒸散が始まって、蒸発が高い土壌温度で始まった。夏と秋では、雨がすぐに土壌水分に影響を与えた。それでも山形大学演習林の土壌の撥水性が高いため、土壌が乾燥していると地表面の流出量は多くなった。流出の測定により、乾季の後および雨が激しく降っているときに、地表面での流出量がより高いことが確認された。

山形大学演習林において HYDRUS１D モデルは良い結果を見せたが、様々な困難もあった。雪が無い場合、モデルの土壌水分と本当の土壌水分がほとんど同じレベルであったため。対照的に、冬に高い深雪がある場合、土壌水分含有量を過大評価するという結果となった。積雪深はモデルでも正しく計算されなかった。土壌水分モデルにおいて最も良い結果は斜面のトップで見られた。それは水が雪の中を垂直に流れたためである。このモデルは将来 HYDRUS 2D と 3D がさらに向上していくことでより良いものになっていくだろう。

結果としてこの卒業論文では水の貯蓄や土壌中での流れ、そして、水文学的プロセスの計算のモデルの使用の可能性が分かった。降雪量の変化に続いて、朝日連峰での SWE が小さくなってきたため積雪量は最も重要な指標となった。この研究では東北地方の気候が変化していることを指摘し、水や雪の利用可能性を算定するための新しい方法を提示した。

Abstract (German)

Schnee ist eine der wichtigsten Wasserquellen der Erde. Schneeschmelze im Frühling verteilt Wasser and Pflanzen, Tiere und Menschen, wodurch es das Leben aller Organismen sichert. Dieser Prozess ist vor allem in Regionen mit wenig Niederschlag im Frühling, wenn die Transpiration der Pflanzen beginnt und die Böden aufgrund höherer Temperaturen trocknen, von Bedeutung. Diese Regionen benötigen ausreichend Schmelzwasser aus den Bergen, um die regenarme Zeit zu überbrücken. In Zeiten des Klimawandels, und hauptsächlich der Klimaerwärmung, leiden viele Regionen an Wassermangel, da der Schneefall im Winter und daher auch die akkumulierte Menge an Schnee zu Beginn des Frühlings signifikant abnehmen.

Eine Region, die intensiv Schmelzwasser nutzt, ist die Region Tōhoku in Japan. Zwei Drittel der Landmasse sind mit Wald bedeckt, der Großteil liegt im Ōu Gebirge, welches Tōhoku in West und Ost teilt. Die Ebenen nahe des Japanischen Meers und des Pazifiks werden hauptsächlich zum Anbau von Reis genutzt. Daher ist der Wasserbedarf sowohl im Wald als auch in den Ebenen im Frühling hoch. Da die Berge, vor allem auf der Westseite, intensiven Schneefall im Winter erhalten, resultiert die große Menge an akkumuliertem Schnee in einer langen Schmelzsaison, die bis spät in den Juni oder sogar Juli andauern kann. Allerdings verloren Niederschläge und Schneeakkumulation im Winter in den letzten Dekaden an Intensität, begleitet von einer durchschnittlichen Lufttemperatur von etwa 0°C in den Asahi Bergen in der Präfektur Yamagata. Diese Temperatur hat zur Folge, dass bereits kleine Schwankungen und das Timing des Niederschlags den Unterschied zwischen Schneeakkumulation und Schneeschmelze machen. Da Niederschlag, mit normalerweise 1500 mm im Winter, hoch ist, sind Schneetiefen von mehr als drei Metern in den Bergen nicht ungewöhnlich. Jahre mit überaus großen Schneetiefen wurden zwei Jahre später gefolgt von einem Winter mit signifikant weniger Schneeakkumulation. Geringe Unterschiede in Lufttemperatur können folglich in großen Unterschieden in der Wasserversorgung der Shōnai Ebene, der Küstenregion der Präfektur Yamagata, resultieren.

Der Wasserkreislauf in Shōnai und dem Asahi Gebirge war, mit dem Hintergrund, die Dynamik des Winters und der Veränderung von Schneedecke in den letzten zehn Jahren zu verstehen, der Hauptbestandteil dieser Forschung. Meteorologische Daten, bodenphysikalische Eigenschaften und Bodenfeuchte wurden kontinuierlich im

Forschungswald der Yamagata Universität (YURF) aufgezeichnet, um ein Modell für Bodenfeuchte zu entwickeln, welches für verschiedene Forschungszwecke angewandt werden kann. Die Modellierungs-Software (HYDRUS 1D) berechnet Bodenfeuchte, Schneetiefe und andere Parameter auf Grundlage der im Feld und Labor gemessenen Bodeneigenschaften.

Der vergangene Winter (2019/2020), mit hoher Lufttemperatur und ohne Starkniederschläge, resultierte in der geringmächtigsten Schneedecke seit Beginn der Aufzeichnungen in YURF. Schneetiefe wurde mit Schneedichte verknüpft, welche aufgrund von Kompaktion in Jahren mit tiefem Schnee höher war. Darüberhinaus schmolz Schnee an der Oberfläche an Tagen, die wärmer als 0°C waren, und das entstandene Schmelzwasser infiltrierte die Schneedecke. Das Wasser fror erneut in tieferen Lagen der Schneedecke, wodurch sich Kristallstruktur und Dichte des Schnees änderten. Der gleiche Prozess wurde nach Regenfällen auf der Schneedecke festgestellt. Ist die Dichte des Schnees nach diesen Ereignissen bekannt, lässt sich auch die Menge an Wasser abschätzen, die während der Schneeschmelze in die Ebenen von Shonai geliefert wird. Modellierungen, sowohl für die Schneeakkumulation, als auch die Schneeschmelze wurden für jedes Jahr, ausgehend vom Winter 2011/2012, entwickelt. Mithilfe der Niederschlagsdaten und des Degree-Day factors (DDF) wurden akkurate Berechnungen für das Schnee-Wasser-Äquivalent (SWE) des Schnees durchgeführt.

ROS Ereignisse waren nicht nur verantwortlich für eine Zunahme der Schneedichte sondern wirkte auch unter der Schneedecke auf die Bodenfeuchte ein. Um den Effekt der Infiltration von Wasser in den Boden zu messen wurden drei Messpunkte an einem mit Japanischer Zedar (*Cryptomeria japonica*) bepflanztem Hang gewählt. Zwei Winter mit deutlich unterschiedlichen Schneemächtigkeiten wurden für diese Arbeit beprobt und analysiert, um den Zusammenhang zwischen Schneemächtigkeit und Regenwasser-Infiltration zu qualifizieren. Im Winter 2019/2020, wo die maximale Schneetiefe 1,3 Meter betrug, wirkten sich zahlreiche Regenevents von weniger als 10 mm Intensität auf das Bodenwasser aus. Im Gegensatz zu der stark variierenden Bodenfeuchte in diesem Winter infiltrierte Wasser den Boden nur selten im Winter 2018/2019, als die Schneetiefe drei Meter betrug. Zudem wurde festgestellt, dass die verschiedenen Punkte am Hang unterschiedlich auf die Regenereignisse reagierten. Während Oben und Unten am Hang das meiste Wasser den Boden erreichte war der Boden im Hang kaum von Regenereignissen beeinflusst. Dies ist eine Konsequenz aus

dem lateralen Wasserfluss hangabwärts innerhalb der Schneedecke, der höher war als der vertikale Fluss von Wasser hinunter zur Bodenoberfläche.

Die Infiltration von Wasser in die Schneedecke resultierte darüberhinaus in einer konstanten Bodenfeuchte bei einem Wassergehalt des Matrixpotentials. Starke Niederschläge im Herbst füllten die meisten Poren des Bodens, während die restlichen Mittelporen, die noch zum erreichen des Matrixpotentials fehlten, im frühen Winter gefüllt wurden. ROS Ereignisse und Schneeschmelze im Winter führten den schnell trocknenden Grobporen immer wieder Wasser zu. Dennoch war der Boden aufgrund des hohen Sandgehalts und der hohen Wasserleitfähigkeit nie vollständig gesättigt. Die Bodenfeuchte stieg signifikant während der Schneeschmelze an, was darüberhinaus zu einem höheren Oberflächenabfluss führte. Der Bodenwassergehalt nahm kurz vor Ende der Schneeschmelze aufgrund der startenden Transpiration und Evaporation wieder signifikant ab. Der Wassergehalt des Bodens stieg unmittelbar nach Regenereignissen im Sommer und Herbst an. Die hohe hydrophobe Eigenschaft des Oberbodens resultierte jedoch in stärkerem Oberflächenabfluss, wenn der Boden trocken war. Messungen bestätigten, dass hauptsächlich lange Trockenperioden und Starkregenereignisse den Oberflächenabfluss im Vergleich zum Untergrundabfluss signifikant erhöhten.

Signifikante Unterschiede wurden auch zwischen den Böden in YURF und Kaminoyama gefunden. Böden in Kaminoyama hatten höhere Anteile an Schluff und Ton, was bessere Wasser- und Nährstoffspeichereigenschaften und somit eine höhere Fruchtbarkeit im Vergleich zu YURF ermöglichte. Die Experimente wurden durchgeführt, um die Effektivität und den Ertrag von Weinstöcken in der Gegend zu charakterisieren. Da die Böden in Kaminoyama deutlich besser entwickelt sind als die Böden in YURF ließ sich ein signifikant höheres Potential für Landwirtschaft und Obstanbau erkennen.

Die Anwendung des HYDRUS 1D Modells für YURF war eine sehr gute Annäherung and die Messwerte, zeigte aber zeitgleich auch Schwächen auf. In Zeiten ohne Schneedecke waren die Unterschiede zwischen modellierter und gemessener Bodenfeuchte klein. Im Gegensatz dazu sorgte Schnee für eine Überschätzung des Wassergehalts im Modell. Auch Schneetiefe wurde nicht korrekt modelliert. Die besten Ergebnisse wurden für den Messpunkt oberhalb des Hangs erzielt, wo sich das Wasser größtenteils vertikal im Schnee bewegte. Trotz der guten Übereinstimmung für diesen Messpunkt kann das Modell noch deutlich verbessert

werden, hauptsächlich durch die Benutzung der weiterentwickelten Programme HYDRUS 2D und 3D.

Zusammengefasst verdeutlicht diese Studie Wasserspeicherung und Wasserbewegung in Böden im Winter sowie das Potential der Verwendung von Modellen für die Berechnung wichtiger hydrologischer Prozesse in den Bergen in Japan. Niederschläge im Winter wurden wichtiger, da in den Asahi Bergen kleine Veränderungen in der Menge des Schneefalls zu starken SWE Änderungen führen können. Die Ergebnisse bestätigten die Veränderung der meteorologischen Situation in Zeiten des Klimawandels und stellten neue Modelle zur Berechnung von Schmelzwasser vor.

1. Introduction

1.1 General introduction

The hydrological cycle and the use of water in forests and agricultural fields have become more important in times of climate change and have been studied in many regions around the world. Especially regions with intensive snowfall and snowmelt as their main water source in spring are expected to suffer water shortages in the future due to higher air temperatures and less snow accumulation in winter (Luo et al., 2011). Since Japan receives most of the precipitation in winter by winter monsoons (Dorman et al., 2004) and by the Yamase winds in summer (Kanno, 1997), small changes in air temperature may have major impact on these weather phenomena. It has been found in many regions around the world, that small changes of air temperature either increase or decrease the number of events of extreme precipitation significantly (Anagnostopoulou and Tolika, 2012). Tōhoku (東北) in Japan is one of the regions with the characteristic of high winter precipitation. It is divided into West and East by the 500 km long Ōu Mountain range (奥羽山脈), which also causes different meteorological conditions on both sides of the mountain range (Kominami et al., 2005, Lopez et al., 2014a, Kudo et al., 2017). Forests cover more than 60 % of the land surface of Japan (Kumagai et al., 2008, Seidel et al., 2017) and agricultural fields more than 20 % (Osumi et al., 2003). Especially Tōhoku is mainly composed of these two types of land use. One prefecture, receiving precipitation of several thousand millimetres per year (Nagata, 1987, Dorman et al., 2004), is Yamagata, which faces the Japan Sea. The study area in the Asahi Mountains (朝日連峰), south of the Shōnai plains (庄内), has an annual precipitation of around 3000 mm (Yasunaga and Tomochika, 2017, Seidel et al., 2019). Half of this precipitation falls as snow in winter and creates snow covers of more than 3 m depth (Kazama et al., 2008, Kudo et al., 2017, Kawase et al., 2018). Wind streams from Siberia bring clouds and storms to the Japan Sea coast, and cause high precipitation in winter and significant cooling of the air (Ebuchi et al., 1992, Kanno, 1997, Dorman et al., 2004). Compared to other regions around the world, the annual precipitation is high (Kominami et al., 2005, Lopez et al., 2014a). However, precipitation is at its lowest in the spring and therefore agricultural and forest ecosystems rely on water from snowmelt. Agriculture in Shōnai, mainly paddy fields for rice production, consumes immense amounts of water from snowmelt (Richard and Gratton, 2001, Hayashi et al., 2005, Tanaka and Sato, 2005). In

addition, forests start transpiration in spring and have high water demand (Tague and Peng, 2013).

Climate change affects regions with unstable meteorological conditions and weather more than regions, which are not influenced by winds from other regions (Davis et al., 1999). The effect of air temperature increase might cause more intensive changes than in other regions of the world, because winter air temperature is on average around 0 °C (Sinha and Cherkauer, 2010, Fujita et al., 2014), which causes snowmelt and frequent rainfall in winter (Shimada and Kawamura, 2004). Due to increasing temperatures in winter a trend of increasing amounts of rain and a decrease of snowfall over the years were already expected (Ishizaka, 2004, Takeuchi et al., 2008, Yasunaga and Tomochika, 2017). Temperature does also influence the snow water equivalent (SWE) of snowpacks, therefore air temperature increases could result in significant decreases of SWE (Davis et al., 1999). Thus, the rain/snow ratio in the snowfall region of Tōhoku has been increasing as winters are becoming warmer (Godsey et al., 2018). As a consequence of climate warming, Tōhoku region and also Shōnai may suffer water stress in spring if the snow cover decreases in winter.

Whereas snow cover reaches depths of three metres and more in winter, air humidity is almost 100 % in summer, creating a tropical environment in forests (Lopez et al., 2014a, Sasaki et al., 2014). Hence, Tōhoku region is also in summer of major interest and importance for forests and agriculture, since meteorological conditions create an environment of extreme precipitation and temperature differences. Moreover, Japanese mountains, especially the Ōu Mountain range and the Asahi Mountains, are characterised by steep slopes and sandy soils (Matsuoka, 1996, Kazama et al., 2008, Kudo et al., 2017). Hence, water movement and the hydrological cycle in Tōhoku and especially in the mountains are more pronounced than in many other regions of the world (Ninomiya, 1964, Spreitzhofer, 1999, Kominami et al., 2005, Kazama et al., 2008).

Precipitation, snowmelt and soil moisture need to be analysed in detail, in order to understand the movement and distribution of water in forest ecosystems and agricultural fields. Therefore, this study focussed on a small part of the Asahi Mountains, the Yamagata University Research Forest (YURF). YURF represents the typical meteorological conditions of the Asahi Mountains which allows its extrapolation of water availability and dynamics with this study. Thus, this study was divided into the following objectives:

1. Analyse soil physical properties in order to understand the mechanism of water movement in soils in YURF and Kaminoyama
2. Characterise water inputs, outputs and seasonal soil water dynamics by monitoring soil moisture for all four seasons
3. Determine snow dynamics in mountainous forests vs. clear cut sites by measuring snow density and snow depth continuously
4. Characterise reactions of snow cover to air temperature increases and rain-on-snow events
5. Model snow water equivalent for snow accumulation and snowmelt period based on measured meteorological conditions
6. Analyse snow melt dynamics and comparability between different years by using the degree-day factor approach
7. Model soil water conditions in order to estimate soil moisture dynamics in future by using the software HYDRUS 1D

The research for this thesis was done with the aim to introduce simple models for the management of snowmelt water and soil moisture progression over the years. The idea was to combine short term measurements with long term monitoring of meteorological data. All objectives were chosen based on the special meteorological characteristics of the study area and the effect of climate change and future changes were discussed. Hence, continuous snow and soil measurements were conducted and meteorological data was used to establish models for the prediction of SWE and the local snowmelt degree-day factor (DDF) based on changing meteorological conditions. Soil physical properties were used to run the HYDRUS 1D model, which models soil moisture.

1.2 Snow dynamics

Winter temperatures have increased significantly since the early 1990's in Tōhoku, developing a higher number of rain events during winter (Japan Meteorological Agency). As a result of increases in winter air temperature not only in Japan but also in other regions, snow cover is showing higher intra- and inter-annual fluctuations (Cayan, 1996, Bowen, 2008, Luo et al., 2011), shortening the period of snow cover as has been reported in several regions (Callaghan et al., 2011, Krasting et al., 2013). Tōhoku is sensitive to climate change

because of varying spatial air temperatures and a high hydrological variability (Ishizaka, 2004, Kominami et al., 2005). Over the last decades, multiple studies have focussed on the dynamics of snowfall and rainfall (Godsey et al., 2018), soil hydrological processes (Asanuma and Kamimera, 2004, Callaghan et al., 2011) or soil frost (Hardy et al., 2001). Soil frost has been studied to characterise its importance on the winter hydrological cycle (Stadler et al., 1996, Edwards et al., 2007), since forest ecosystems rely on the availability of water in spring (Ohta et al., 2001, Osumi et al., 2003). Frozen soil prevents water from infiltrating and increases surface runoff, affecting water cycling, microbial processes and root water uptake (Kohl et al., 2001, Callaghan et al., 2011, Iwata et al., 2011). Soil frost can further negatively affect forest soils more intensively than it can damage barren soils. In contrast, unfrozen soils not only store but also transport water. Soil temperature is the critical parameter that is influenced in winter by snow depth, snow density and duration of snow coverage (Zhang, 2005). Snow can lower soil surface temperature because of its high albedo (Cline, 1997, Edwards et al., 2007, Nishimura et al., 2019) but it can also increase the temperature by its high thermal insulation potential due to low thermal conductivity (Zhang, 2005). In particular, soil temperature can be up to 20°C higher than the air temperature in winter due to the effect of insulation in extremely cold regions (Zhang et al., 2005).

Approximately one third of the northern hemisphere landmasses are covered with snow for three months of the year or longer (Edwards et al., 2007). Nevertheless, most of these regions have either only a shallow snow cover (less than 50 cm) or are exposed to low mean annual temperatures (-10 °C or colder) (Zhang, 2005, Callaghan et al., 2011, Bulygina et al., 2015, Lopez et al., 2015). In regions with winter air temperatures ±0 °C, the presence or absence of snow cover determines whether soil freezing occurs or not (Cohen and Rind, 1991, Hardy et al., 2001). Even unfrozen soils are may be in a near frozen state during winter. Air temperatures in winter are around 0°C in the western part of Tōhoku (Kominami et al., 2005) and the Japanese Sea coastline receives heavy snowfall (Asaoka and Kominami, 2013) from the cold Siberian winds, which hit the Asahi Mountains and produce around 1500 mm snowfall in winter (Dorman et al., 2004, Yamaguchi et al., 2011). Such high precipitation results in snow depths of more than three meters and snow coverage lasting until May. Hence, soil temperature behaviour and absence of soil frost may be similar to other regions around the world (Cayan, 1996, Bales et al., 2011). However, snow depth in the Asahi Mountains of Tōhoku is significantly higher than in most other regions in the world.

Forests and areas with less vegetation differ in soil hydrological processes as well as in snow accumulation (Lopez et al., 2007, Jost et al., 2012, Lopez et al., 2015, Potopová et al., 2016). Evergreen trees accumulate snow in the canopy, resulting in significantly lower SWE in forested sites compared to clear cut sites (Berris and Harr, 1987). In heavy snowfall regions of Tōhoku, the difference between forest and clear cut sites resulted in some hundreds of millimetres SWE (Brod, 2018). However, snow depths in the forest were still more than two meters. Moreover, snow melted at a lower rate in forested sites than in open areas (Jost, et al., 2012). As a result, snowmelt in forested areas lasts longer and provides longer availability of water for trees in spring when precipitation is the lowest.

Long and thick snow cover periods control how plants grow and how snowmelt water relates to soil moisture (Lopez et al, 2015). Snow cover protects plants from frost damage, and the duration of coverage and snowmelt determine the rate of plant growth (Beniston et al., 2003, Wang et al., 2008). The dominant tree species in Japanese forests are beech (*Fagus Crenata*) and Japanese cedar (*Cryptomeria japonica*), which is the main planted species in Japan (Seidel et al., 2017, Seidel et al., 2019). These tree species start transpiration when snow cover is still several meters high (Osonoi, 2018). Since a snow depth of 40 cm already results in a decoupling of soil and air temperature (Cline, 1995, Venäläinen et al., 2001, Zhang, 2005), we introduced the hypothesis, that thick snow cover prevents soil from freezing and plays a significant role in the winter hydrological cycle.

Interactions between precipitation, snow cover, soils and rivers are pronounced in Tōhoku (Osumi et al., 2003, Asanuma and Kamimera, 2004). Snowmelt processes are known to increase soil moisture in spring (Lundmark and Jansson, 2008, Potopová et al., 2016), but also rain-on-snow events (ROS) are common due to variable air temperature and winter monsoons (Shimada and Kawamura, 2004, Bokhorst et al., 2016). Minimum air temperatures in most forests of Tōhoku are -10°C, but nevertheless, under this temperature regime ROS events could in theory occur (Magono and Kikuchi, 1980, Kondo and Yamazaki, 1990). However, air temperature in north-eastern Japan is in general higher than -5 °C, which increases the possibility of ROS events. ROS events as well as snow melting and refreezing processes increase snow density irreversibly (Coléou and Lesaffre, 1998), which causes avalanches in many regions of the world (Hestnes, 1985, Kattelmann, 1987). During winter snowmelt water is produced in the upper layers of the snowpack before it refreezes in deeper layers, increasing the snow density (Giddings and LaChapelle, 1962, Akitaya, 1974,

Reiweger and Schweizer, 2013). The more snow density increases, the sooner water storage capacity of the snowpack is reached. Water retention of snow is not unlimited (Yamaguchi et al., 2010), thus, water is expected to move from the snowpack into the soil. However, soil moisture under a thick snowpack is rarely measured and not well understood (Yamaguchi et al., 2011).

1.3 Research plan

Soil plays an important role in the hydrological cycle, since it is the medium which supplies plants with water. Soil type and structure influence water storage capacity, water retention and hydraulic conductivity, three parameters which are essential in the characterisation of plant water availability (Boyer et al., 1997, Grayson et al., 1997, Marthews et al., 2014). Sandy soils can store and transport water much faster than fine grained soils but need less energy and pressure to be drained. However, soils with high clay contents have many fine pores, which makes it difficult for plants to uptake and use the stored water (Hillel, 1998). Hence, it is essential to know the texture and hydrophysical properties of the present soils in the research sites. Texture and soil density can be expressed in pF-diagrams showing the relation between water potential and soil water content (Madi et al., 2018). Mountainous forest soils are known for fast increases and decreases of soil moisture and increased lateral runoff in comparison to flat sites (Gerke et al., 2015, Dusek et al., 2017). High soil moisture in slopes leads furthermore to a better connection between soil patches, resulting in higher hydraulic conductivity (McNamara et al., 2005). The connection of different hydrological parts at the slope increases lateral water flow and results in water runoff.

Soil water runoff is divided into surface runoff and subsurface runoff (Gerke et al., 2015). Subsurface runoff is further divided into intra soil runoff, bedrock runoff and groundwater recharge (Grayson et al., 1997, Hillel, 1998, Salve et al., 2008). The intensity of surface runoff depends especially on the soil water repellency, which increases with higher content of organic matter in the soil (Lamparter et al., 2009, Wissolek et al., 2009). Furthermore, the potential of soils to uptake water is furthermore lower when the soil is dry and higher when it is wet.

In highly permeable sandy soils of steep slopes, bedrock runoff is the dominant subsurface water movement (Clow and Mast, 1995). Quantification of bedrock runoff is essential for the

understanding of the hydrology of watersheds, because nutrients are washed out and transported with bedrock water (Clow and Mast, 1995). Furthermore, bedrock runoff is not plant available and supplies streams and rivers, rather than the groundwater (Notaro et al., 2014). Hence, the relationship between precipitation, surface runoff and bedrock runoff needed to be studied for YURF. Water repellency measurements as well as collection and quantification of surface and bedrock water flow were done in order to determine differences and hydrological patterns. Surface runoff and snowmelt are the major influences of river water discharge variations (Hirayama et al., 2002). Since rivers are the main transport medium for water over larger distances, the connection between precipitation, slope water runoff and snowmelt in spring needed to be studied. River discharge reflects the water runoff of slopes in the study site and indicates the main snowmelt period of areas in higher altitudes upstream (Hirabayashi et al., 2002, He et al., 2014). Hence, river water level measurements and discharge calculations were conducted for the snowmelt season and linked to water input sources.

Changing meteorological conditions and the duration of the annual winter period introduced snow as a fundamental part of this study. Since snow covers in YURF accumulate three metres of snow and more due to heavy snowfall, snow depth and snow density can change significantly over a short period of time. Manual measurements combined with automatic monitoring were needed in order to understand the mechanisms inside and also under the snow cover (Perry, 1998, Kohl et al., 2001, Uchida et al., 2005, Tague and Peng, 2013, Iijima et al., 2016). Midwinter snowmelt events and ROS could infiltrate the soil; therefore soil moisture was not only measured in the summer season but also in winter.

Better understanding of the hydrological cycle is important, because of the relation of forests to water and the reliance of agricultural fields in the Shōnai plains especially on snowmelt water. Obtained data were used as input for the HYDRUS 1D model, which can be a useful tool to estimate soil moisture and later on water mobility in the whole study area. Being able to model soil water processes provides opportunities to transfer the mechanism to other sites within the Asahi Mountains.

1.4 HYDRUS 1D

The software HYDRUS 1D is a sophisticated modelling software for soils and especially soil moisture (Šimůnek et al., 2013 a). It was programmed for the use in flat agricultural areas (Soylu et al., 2014, Jin et al., 2015, Kato and Nishimura, 2017) but was also applied in mountain areas to model soil moisture (Kato et al., 2011, Caiqiong and Jun, 2016). HYDRUS uses various soil physical and meteorological parameters to estimate hydrological processes and nutrient transport in and above soil. The modelling software uses many smaller models, which are implemented in the main user interface. Hence, for many years HYDRUS has already been the most powerful and accurate modelling software for soil moisture. However, it was not often used for snow modelling (Sandór and Fodor, 2012), therefore discrepancies and inaccuracies were expected in the model for this study, when heavy snowfall was applied and snow cover increased. The model is complex and offers many options for input and output data (Šimůnek et al., 2013 a). Its successful application can be a valuable tool for future work and research in Japanese mountain forests.

2. Material and Methods

2.1 Sites

2.1.1 YURF

Most of the conducted measurements took place in the Yamagata University Research Forest (YURF) in the Asahi mountain range (38°33’18.86’’N, 139°542.63’’E). It is located approximately 25 km south-east of Tsuruoka (鶴岡). The forest covers 753 ha and elevations between 243 m and 844 m (Brod, 2018). The Wasada stream (早田川) divides YURF into West and East exactly in half. Slope angles of the two mountain ridges east and west of the stream reach 55°; the mean slope angles are between 30° and 40°. More than ten different tree species can be found in YURF (YU, 2014), but most of the mountains are covered with beech (*Fagus crenata*) and Japanese cedar (*Cryptomeria japonica*). Japanese cedar is with 22 % one of the most abundant plantation tree species in Japanese forests (Kumagai et al., 2008).

The measurements, especially during winter, focused on soils and snow in a Japanese cedar forest slope which is located near the main building in the centre of YURF. The slope aspect is NE with an average inclination of 12°, the lower half of the slope reaches inclinations of more than 30°. Three sampling spots at the slope have been chosen, one at the bottom (*SB*), one in the middle (*SM*) and one at the top (*ST*) (Figure 2.3). ST was located on top of a ridge which runs SSW. The hydrology of the analysed slope was considered as not being influenced by water runoff down the ridge, hence the small angle of the ridge in comparison to the slopes.

Two other sites were selected for research (Figure 2.2); especially snow measurements have been conducted there. One was close to the meteorological measuring tower, surrounded by the Wasada stream in a deciduous forest (*Isle*). Another one was approximately 300 m to the north in front of a barren slope, which was previously used for the Japanese Yakihata, a procedure of shifting cultivation (*Yaki*). The forest slope was used for all soil moisture measurements and multiple snow density measurements were conducted at the sites *Yaki* and *Isle*.

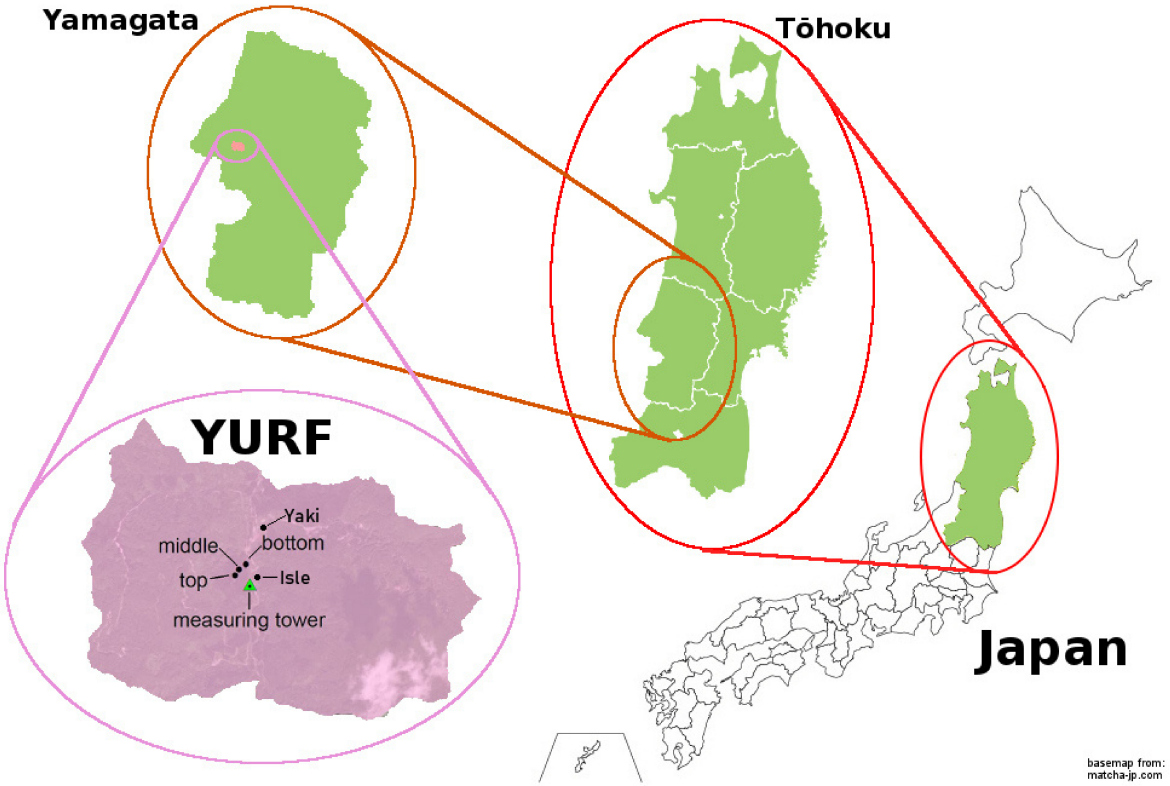

Figure 2.1: Location of YURF in Japan

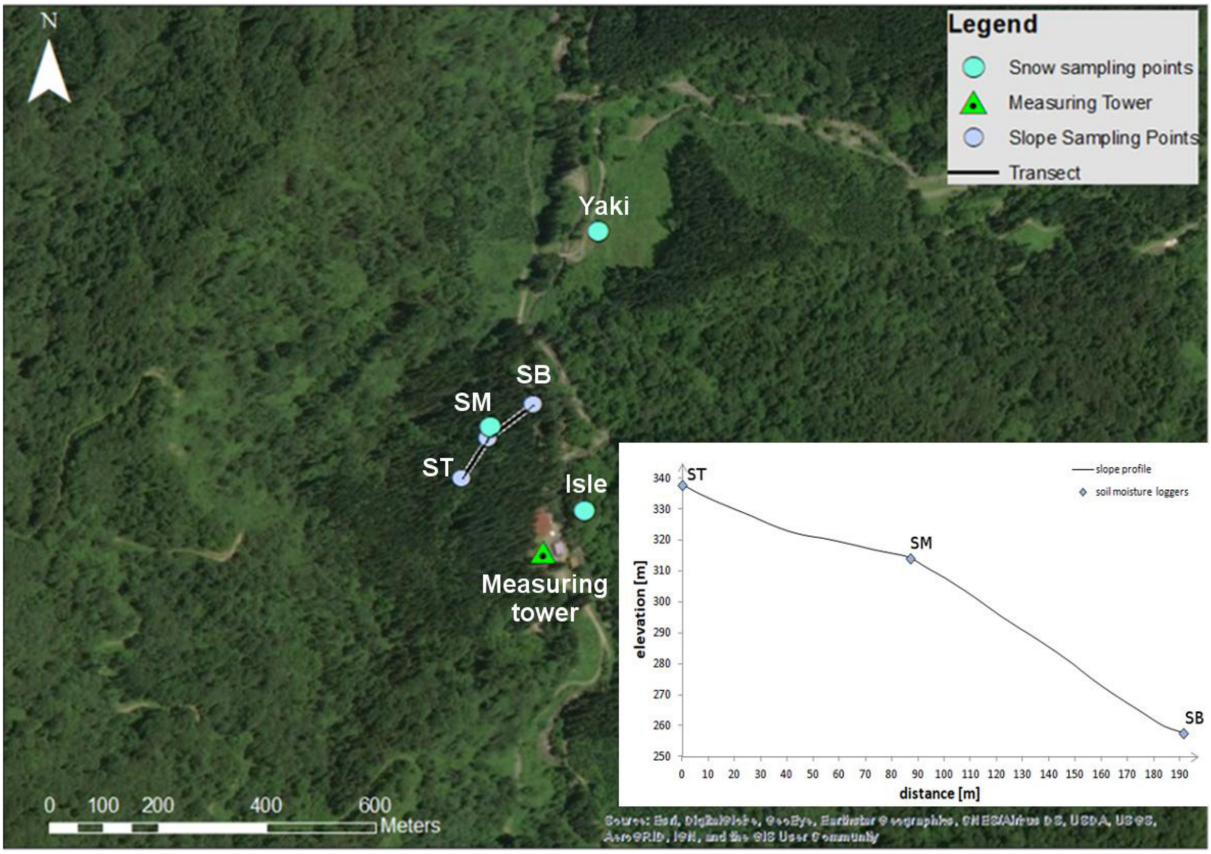

Figure 2.2: Sampling points in YURF

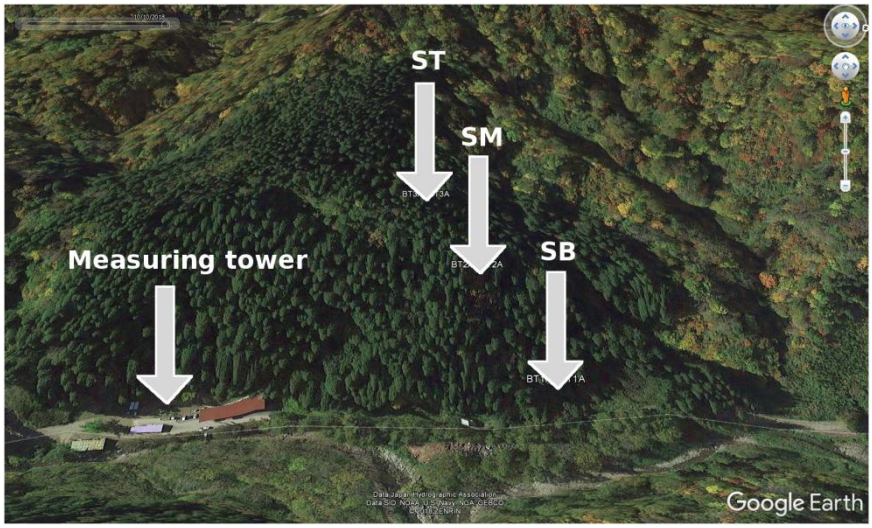

Figure 2.3: Sampled slope and location of measuring tower

2.1.2 Kaminoyama

Soil analyses have further been conducted in vineyards in Kaminoyama, south of Yamagata city (Figure 2.4). Samples were taken from three sites with different types of grape. The first site (*A*) was a Merlot plantation at a slope of less than 5° inclination (38°6'43.15"N, 140°19'1.97"E). Cabernet Sauvingon was planted at the second site (*B*), which was flat (38°6'43.06"N, 140°18'25.69"E). The third site (*C*) was at a steeper slope (around 15°) beneath paddy fields and a dam (38°7'14.83"N, 140°19'24.07"E). The elevation of sites *A* and *C* was approximately 300 m a.s.l., site *B* was 250 m a.s.l. and further away from the mountains. Sites *A* and *B* have been sampled at two spots each, site *C* was sampled at three spots along the slope.

Because grape production is the main land use in the study sites, the focus of the sampling was on the water use potential and on the nutrient supply. Therefore, not only soil physical analysis but also a measurement of CN ratio was conducted.

Figure 2.4 a-b: Location of the sampling sites in Kaminoyama

2.1.3 Meteorological conditions

Annual precipitation is around 3000 mm in YURF, with half of it falling as snow in winter, resulting in snow covers of usually more than three metres in slopes and valleys and more than five metres on the mountain tops. Snow starts falling in December, and snowmelt ends in May. Precipitation over a one-year period is highest in winter and lowest in spring. Winter air temperatures are around 0 °C, in summer the temperature reaches 30 °C on daily average, combined with air humidity of almost 100 %.

Kaminoyama receives significantly less precipitation than YURF. Annual precipitation varies between 1000 and 1500 mm, and maximum snow cover is 150 cm. At -5 °C, the daily average air temperature in winter is significantly lower than in YURF, summer air temperature is similar in Kaminoyama and YURF.

2.2 Soil Samples

Soils at the three slope spots *SB*, *SM* and *ST* and at the Kaminoyama sites A, B and C have been analysed regarding soil type, texture and hydrological properties (water retention, hydraulic conductivity). For soil texture, YURF samples were taken every 10 cm starting at a depth of 5 cm and down to 55 cm (6 samples per spot). Two samples per spot have been taken in Kaminoyama, one at 15 cm and one at 45 cm soil depth.

For the HYPROP measurements nine samples at three different depths were taken at *SM*. The depths were 5 cm, 40 cm and 80 cm, with the middle of the sampling ring determining the depth. Only one depth (30 cm) was probed at each of the five other spots. Three samples per depth were taken, because especially in the soils in YURF many small stones and roots were prominent in the soils and were able to influence the measurements significantly. The samples needed to be undisturbed and originally orientated. Therefore metal rings (height = 5 cm; surface area: 50 cm²) were driven vertically in the soil as carefully as possible to minimize disturbance of the sample. The top of a sample was scraped with a knife in order to achieve a flat surface. The core was covered and carefully moved upside down, to flatten the bottom surface, too. Afterwards the bottom was also covered.

Water repellency experiments were done for the soil of the slope. At each of the spots (*SB*, *SM* and *ST*) six samples were taken. One from the organic layer and five from the soil (2 cm, 4 cm, 6 cm, 8 cm and 10 cm).

2.2.1 Soil texture

Soil samples were oven dried at 105°C and sieved < 2 mm. After sieving, both grain size fractions were weighed to calculate the proportion between < 2 mm and > 2 mm.

Organic matter might distort the soil texture values of each sample. To avoid this effect, organic matter was destroyed with hydrogen peroxide prior to the measurements. 0.5 g of soil was filled in 200 ml - beakers. The soils were expected to have rather low clay contents. Hence, an equal mass for all samples could be used. Before weighing, all samples were homogenized to avoid a discrimination of grain fractions due to gravimetric sorting.

In order to destroy organic material, 25 ml of 35 % - hydrogen peroxide solution were added to all samples in beakers. Additionally, 10 % - hydrochloric acid were added to the samples to destroy calcite. After one night, all samples were heated at ~60 °C for four hours, until all hydrogen peroxide had vaporized, which was indicated by the solution clearing up. From time to time deionised water was added to retain a liquid level of around 2-5 mm above the sample. Afterwards the samples were cooled down and transferred to smaller beakers (50 ml). In order to destroy small aggregates, 5 ml of tetra sodium pyrophosphate were added. Samples without significant organic matter contents were not treated and were directly measured. Most of those samples were from depths of 20 cm and more.

The measurements were done with a laser ablation spectrometer (Type Coulter LS 200). This spectrometer divides grain sizes into 92 classes between 0.4 and 2000 µm. Depending on the grain size the laser beam is diffracted in a specific angle, the resulting counts and intensity in the detectors give the percentiles of each grain size.

Samples were inserted into an integrated water cycle in the spectrometer. The water cycle ensured the separation of all particles and an equal distribution. Ultrasonic waves have been used to destroy remaining aggregates (Kachaoski et al., 1988). Depending on the sample amount and the number of particles, different volumes of water were used for the measurements. A low obscuration of sample in the water results in weaker repeatability of the measurements. A high obscuration will result in multiple diffractions due to many particles in the measuring chamber. An optimal obscuration ranges between 7 % and 13 %. An obscuration of 11 % was intended for most measurements.

Every measurement was repeated two times; afterwards the average of all three measurements was determined.

2.2.2 HYPROP

Figure 2.5: Core sampling method

The HYPROP system measures hydraulic conductivity and the water retention curve of soils. The water retention curve is calculated by soil sample weight loss due to drying and the hydraulic pressure difference between two tensiometers (1.25 and 3.75 cm deep).

In the laboratory, the samples needed to be water saturated for analysis. Therefore, the sample bottom cover of every soil ring sample was removed. A linen cloth was used as water-permeable cover and fixed (HYPROP delivered). Thereafter the top cover was removed and the sample core was put in 4 cm deep tap water for at least 24 hours (UMS, 2015).

The HYPROP sensor unit was filled with deionised water and set under vacuum in order to eliminate all air in the tensiometer shafts. The two small tensiometers were treated in the same way. The vacuum conditions were set for 24 hours.

In preparation for the measurements two small holes were drilled in the sample using the HYPROP special drilling tool. A few milligrams of silt were put into the holes to increase the connection between soil and tensiometer head. The tensiometers and the sensor unit were carefully adjusted to air pressure again. Both tensiometers were screwed into the sensor unit and sealed air-tight with silicon rings and a silicon mat, which was placed on the sensor unit in the end. The sensor unit was placed on the sample, fitting the tensiometers into the prepared holes in the soil, and fixed.

After the installation of the tensiometers and the sensor unit on the sample, the measurements started. During the measurements, all samples were weighed on the HYPROP balance, which is connected to a computer. The weight of the samples and the tensiometer pressure were checked every hour (every 10 minutes for the first 2 hours) and prompted to the HYPROP software. The measurements were run until both tensiometers fell dry (tension dropped down to 0 hPa). A 12 V fan was used to expedite the drying process of the sample. The measuring time was shortened from 16 down to 5 days with this modified instrumentation.

The HYPROP system can only provide measurements up to a pF of 3.0. To measure the dry weight of the soil, the samples were oven dried at 105 °C for 48 hours. Furthermore, the wilting point of plants is at pF 4.2 and the corresponding water content needs to be measured. An autoclave was used to create a pressure of 15 kPa, which is equal to pF 4.2.

Around 10 g of wet soil per sample were fit into a PVC-ring, which was attached to the porous pressure plate of the autoclave. Depending on the soil texture, the duration of the experiment varied. With the start of the experiment and the pressure boosting water starts to flow and leave the autoclave. The experiment was regarded as finished when no water left the autoclave any more. A typical duration for the analysed soils of YURF was one week. After pF 4.2 was reached, the soil was removed from the autoclave and weighed with a precise balance (accuracy: 0.1 mg). The weighed soil was oven dried at 105°C and weighed again after 48 hours. The mass difference between soil at pF 4.2 and dry soil was considered as evaporated water. The mass percentage of soil was calculated and extrapolated for the whole 250 ml HYPROP core sample (Equations 2.1 – 2.3).

$$\textbf{Equation 2.1}: \frac{H_2O_{\text{sample}}}{m.\%} = \frac{m_{\text{wet}} - m_{\text{dry}}}{m_{\text{dry}}} * 100$$

$$\textbf{Equation 2.2}: \frac{H_2O_{\text{total}}}{g} = \frac{H_2O_{\text{sample}}}{\text{m.\%}} * \frac{m_{\text{core}}}{g} * 0.01$$

$$\textbf{Equation 2.3}: \frac{H_2O_{\text{total}}}{\text{vol.\%}} = \frac{H_2O_{\text{total}}}{ml} * \frac{100}{250\ ml}$$

Because the density of water is almost 1 g/cm³, H_2O_{total} in gram from Equation 2.2 could be written as volume in millilitres in Equation 2.3. Dry soil weight of the core sample and the volumetric water content at pF 4.2 were entered into the HYPROP software. Soil volumetric water content was plotted versus pF value in the software. Thereafter the water retention curve was interpolated, using the bimodal Kosugi-Mualem model (Romano et al., 2011). Parameters were modified until the best fitting was achieved. The resulting water retention curve was exported as a graph into an excel sheet.

The most important parameters calculated were the residual water content θ_r (in vol.%), the maximum water content θ_s (in vol.%), the hydraulic conductivity K_s (in cm/d) and two shape parameters α (in 1/cm) and n. These parameters were later used to run the HYDRUS model. Usually the hydraulic conductivity of soil is described by the parameter k_f, but since HYPROP

and HYDRUS use K_s instead, the latter expression was used in this thesis for hydraulic conductivity.

2.2.3 CN ratio

Soil samples were oven dried at 40 °C and sieved < 2 mm. Between 20 and 150 mg of every sample were weighed and filled into tin cups for the analysis. The amount of sample material used for the analysis was determined on the basis of the estimated content of organic matter. The darker the colour of the soil sample, the more organic matter was assumed. 20 mg of samples with high organic matter content was used; the less organic matter the more sample material was used for analysis.

Measurements were conducted in the soil science institute of the Leibniz University Hannover (Germany). Samples were burned in a CN-analyser *Elementar Vario EL* using one blank and one standard at the beginning of the analysis and after every 15 samples. Burning of the samples releases carbon dioxide and nitrogen which can be measured using a thermal conductivity detector (TCD). Every sample has been measured with one replicate and the average data has been used for the calculation of the CN ratio.

2.2.4 Contact angle

The contact angle of water drops on dry soil was determined in order to characterise hydrophobia of soil. Soil samples were oven dried at 40 °C for 72 hours to avoid destruction of organic matter. Dry soil was spread on a sticky microscope slide. The sticky surface needed to be covered completely, because it is hydrophobic and would distort the measurement. However, the layer of soil should optimally consist of single grains sticking to the slide. After spreading the soil on the slide, grains were fixed with a metal spatula. The slide was turned upside down afterwards to remove unfixed parts of the soil. The organic layer samples were fixed by the same method.

The prepared samples were installed under a pipette and in the focus of a microscope camera. A water drop of 1 µl was automatically created at the end of the pipette and the pipette was lowered manually to the sample. Once the water drop gets in contact with the sample it disconnects from the pipette and moistens the soil grains. Hydrophobic soils have bad moistening characteristics and the contact angle between surface and water drop is

more than 95° (Bachmann et al., 2000). If the contact angle is smaller than 45° the soil has good wetting properties. Hydrophilic soils are considered to have no contact angle between water and surface, resulting in immediate wetting of the surface. The initial contact between soil and water was recorded with the camera and the contact angle was analysed with the software SCA20. Every measurement was repeated four times per sample and the average contact angle was calculated. Based on the contact angles the water repellency characteristics of the samples were classified.

2.3 Soil moisture

Soil moisture is an essential parameter that indicates infiltration of rain and snowmelt water. Changes in soil moisture represent lateral movement within the soil column or vertical infiltration/runoff of water. Therefore, three data loggers were installed in each of the spots at the slope (*SB*, *SM* and *ST*) to minimize errors and to prevent data loss due to possible defects of sensors or loggers during winter. All sensors were installed at more than five meters distance to trees to reduce the effect of tree canopies and major root systems on soil moisture.

Soil moisture sensors (*S-SMC-M005 ECHO EC-5 Soil Moisture HOBO Smart Sensors*) measured continuously every two hours at three different soil depths: 15 cm, 30 cm and 50 cm. Data were recorded by *H21-002 HOBO Micro Station Data Logger*s. The data loggers were equipped with Lithium batteries, wrapped in plastic and covered with soil to secure them beneath the snowpack. All data loggers were set up in October 2018 and ran until May 2020. Soil moisture was displayed in volume percent. Sensors were calibrated with dry soil, wet soil, water and air before installation (Sakaki et al., 2008).

2.4 Slope water runoff

Water moves in a slope on top of the soil surface, on top of the bedrock or within the bedrock as ground water. Ground water could not be measured in this study due to high porosity of the parental rocks in YURF.

Two metal plates with a width of 1.85 m were installed at the bottom of the slope (*SB*); one directly under the organic layer of the soil and one on top of the bedrock. The plates collected runoff water from the slope and directed it to two dipping bucket rain gauge

measurement systems. The data was saved every hour from July 2019 until November 2019. Because rain on the plates gave an additional input to the system, the direct precipitation on the plates was subtracted.

Runoff data of surface and bedrock were correlated with soil moisture and precipitation in order to determine the infiltration into the bedrock.

2.5 Stream water level

The water level of the Wasada stream was measured in the melting season 2019 from March 26 until May 12 in front of the meteorological tower in YURF, where the stream runs straight with a streambed width (*b*) of 4 m. The channel of the stream has a manmade concrete wall with an angle of 75° on the western side and a rocky natural stream bank with an inclination of 50° on the eastern side. No hydrological sensors were used for the measurements; instead a pole and a wildlife camera were installed. The camera took one picture per hour of the pole; the water level was read off the pictures manually after image collection. The water level was used to estimate the stream discharge. The slope of the streambed was calculated based on the height difference in terrain, measured with a theodolite, and the distance between the two measurement points.

$$\textbf{Equation 2.4}: (slope_{\text{stream}} * \frac{m}{m}) = arctan\left(\frac{\Delta_{\text{height}}}{\text{distance}}\right)$$

The discharge of the river has been calculated using Manning's equation for open channel flows (Akgiray, 2004). For the calculation, the Manning coefficient of roughness needed to be estimated. This coefficient is between 0.4 and 0.7 for mountain streams with cobbles and rocks. The geometry of the channel and the water level (*h*) were used to calculate the flow area A, the wetted perimeter O and the hydraulic radius R_h (Equation 22).

$$\textbf{Equation 2.5}: \frac{A}{m^2} = \left(\frac{b}{m} + \frac{\frac{h}{m}}{\tan(50°) * 2} + \frac{\frac{h}{m}}{\tan(75°) * 2}\right) * \frac{h}{m}$$

$$\textbf{Equation 2.6}: \frac{O}{m} = \frac{b}{m} + \frac{\frac{h}{m}}{\sin(50°)} + \frac{\frac{h}{m}}{\sin(75°)}$$

$$\textbf{Equation 2.7}: \frac{Rh}{m} = \frac{A}{m^2} / \frac{O}{m}$$

The hydraulic radius was used together with the flow area and the slope (in m per m distance) to calculate the potential discharges for the given Manning coefficients of 0.4 and 0.7.

$$\textbf{Equation 2.8}: (Q * \frac{s}{m^3}) = \frac{\frac{A}{m^2}}{n} * \frac{Rh^{\frac{2}{3}}}{m} * (slope^{\frac{1}{2}} * \frac{m}{m})$$

The calculated stream discharge was compared with daily precipitation data in order to determine the runoff of water to the stream. Based on the daily precipitation and snowmelt the relation between water input and stream water discharge was analysed.

2.6 Oxygen and Hydrogen isotope ratio

Soil and snow samples were collected in the snowmelt season in order to confirm the uptake of snowmelt water by the soil. One sample of mixed snow was taken every sampling day at four different sites (*Yaki*, *SB*, *SM* and *ST*). These 4 samples were collected in glass bottles once a week and always put directly into a freezer. The freezing of the samples prevents the change of the isotopic composition of soil water.

The snow samples were slowly melted in a fridge and afterwards filtered with 0.45 µm membrane filters. The filtered water was put into 2 ml vials for auto samplers. All samples were analysed at the University of Tsukuba. The $\delta^{18}O$ and δD data of the snow samples was plotted against each other in order to analyse differences between the open and the forested sites.

2.7 Meteorological data

A meteorological measuring tower (installed by the Yokogawa Denshikiki Co., Ltd.) next to the main building in YURF measured various meteorological parameters in an hourly interval. These parameters are wind speed (in m/s), wind direction, precipitation (in

Figure 2.6: Measuring tower in winter and summer

mm), air temperature (in °C) as well as soil temperature (in °C) at 10 cm, 30 cm and 50 cm depth, sunshine (in h/d), accumulated solar radiation (in MJ/d), snow depth (in cm) and SWE (in kg/m²).The tower measured continuously since December 2011, and the data is available on the Yamagata University server. The tower recorded meteorological conditions hourly and calculated daily and monthly average. Hourly data has been used especially for snow depth and SWE analyses and for the determination of snow and rain. Daily averages were used for most of the diagrams including precipitation. Average monthly data were used to show differences in meteorological conditions between different years. Further relationships have been analysed in the following sections.

2.7.1 Temperature analysis

Soil and air temperature data were used to determine whether soil in YURF froze in winter or not. Differences between air and soil temperature throughout the year are an indicator for the thermal conductivity of the soil. Eight years of temperature data were included in the analysis. Plotting daily average data and using a linear regression between air and soil temperature, the dependency between both parameters was determined (Zhang, 2005). The daily average has been chosen in order to reduce the effect of fluctuating air temperatures. By plotting all years together the dependency of both temperatures as well as the effect of insulation by snow on soil frost can be determined.

2.7.2 Rain/snow ratio

Precipitation data of the meteorological station in YURF are not automatically separated into rain and snow. Therefore, changes in snow depth were used to characterise precipitation as rain or snow. Precipitation linked to decreasing snow depth was considered as rain (Avanzi et al., 2018). Increasing snow depth was considered as snowfall. The proportion of rain was calculated for every winter since 2011 for the four winter months (December – March) in order to analyse differences in seasons and changes between years. Increases in the proportion of rainfall and its variability in different months were interpreted as indicators of climate change in the study area.

2.7.3 Snow density

Snow density and SWE were not only obtained from the measuring tower but also measured manually with 100 cm³ metal sampling boxes. A snow profile was dug first. Snow density was then measured every ten centimetres (starting from the soil surface) with three replicates. Every snow sample was weighed and the density was calculated based on the known volume (Equation 2.9). The average of all density values was calculated and multiplied with the snow depth of the profile to achieve the SWE. Measurements were conducted at least once a week always in the same spot to assure the same topographic condition every time. Every new snow profile was dug one meter apart from the previous one.

$$\textbf{Equation 2.9}: \quad (\rho_{sample} * \frac{cm^3}{g}) = \frac{\frac{m_{snow}}{g}}{100\ cm^3}$$

$$\textbf{Equation 2.10}: \quad (SWE * \frac{m^2}{kg}) = mean\ (\rho_{sample} * \frac{cm^3}{g}) * \frac{h_{snow}}{m}$$

The mean snow density and the standard deviation were calculated for every depth and for the whole profile in order to achieve the standard deviation of the SWE.

2.7.3.1 SWE snow accumulation period

In some years, the SWE measured by the measuring tower was significantly smaller than the manually measured SWE. In order to solve this problem, the data was calibrated and a modelling of SWE for the snow accumulation period was done. In order to model the SWE in YURF, the characteristics of the climate and meteorology of this region were rather important. Therefore no standard models were used but the SWE was calculated manually using precipitation data and the water storage potential of snow cover. The SWE was calculated for every day based on the total precipitation from the start of snow accumulation. Snow cover was assumed to be able to store 8 mm of rain. This value was used based on the results of the soil moisture peak analysis in winter (see chapter 3.4 or Brandt et al., 2020). For days with a daily average air temperature above 0°C, the potential snowmelt was calculated using a DDF of 5 mm/°C. This factor was obtained based on the DDF calculations of the melting seasons (see chapter 2.7.4) and modified empirically. The SWE of every day was calculated as follows depending on the meteorological conditions of day *n*:

- If rainfall (R) > 8 mm and air temperature (T_{air}) > 0°C:

Equation 2.11: $$\frac{\mathrm{SWE}\ (n)}{\mathrm{mm}} = \frac{\mathrm{SWE}\ (n-1)}{\mathrm{mm}} + \frac{\mathrm{P}\ (n)}{\mathrm{mm}} - \left(\frac{\mathrm{R}\ (n) - 8mm}{\mathrm{mm}}\right) - \frac{T_{air}\ (n)}{°C} * 5$$

- If R > 8 mm and T_{air} < 0°C:

Equation 2.12: $$\frac{\mathrm{SWE}\ (n)}{\mathrm{mm}} = \frac{\mathrm{SWE}\ (n-1)}{\mathrm{mm}} + \frac{\mathrm{P}\ (n)}{\mathrm{mm}} - \left(\frac{\mathrm{R}\ (n) - 8mm}{\mathrm{mm}}\right)$$

- If R < 8 mm and T_{air} > 0°C:

Equation 2.13: $$\frac{\mathrm{SWE}\ (n)}{\mathrm{mm}} = \frac{\mathrm{SWE}\ (n)}{\mathrm{mm}} - \frac{T_{air}\ (n)}{°C} * 5$$

- If R < 8 mm and T_{air} < 0°C:

Equation 2.14: $$\frac{\mathrm{SWE}\ (n)}{\mathrm{mm}} = \frac{\mathrm{SWE}\ (n-1)}{\mathrm{mm}} + \frac{\mathrm{P}\ (n)}{\mathrm{mm}}$$

Hence, the SWE depended on the daily precipitation and on the daily average air temperature. Because conditions varied, it was not possible to use one single equation for the entire accumulation period.

2.7.3.2 SWE snowmelt period

The automatic weighting scale of the measuring tower malfunctioned every year from the beginning of the snowmelt season. The difference between the automatically obtained and the real SWE increased within the snowmelt season. Hence, snow density and SWE for the snowmelt season were calculated based on continued manual measurements in the year 2018/2019. Since snow density increased continuously, a coefficient of increase (c_d) was calculated, which expresses how much snow density increases if 1 cm of snow cover melts. This increase was based on the difference in snow height (Δh_{snowT}) and snow density ($\Delta \rho_{first}$) between the day with the maximum SWE and the last day of the snow melt season (based on the manual measurements):

Equation 2.15: $$(c_d * \frac{cm^4}{g}) = \frac{(\Delta\rho_{\mathrm{first}} * \frac{cm^3}{g})}{(\Delta h_{snowT} * \frac{1}{cm})}$$

The resulting coefficient c_d of the year 2018/2019 was further used for all previous years, because only few manual measurements were conducted in the other years. The coefficient

c_d was used to calculate the basic snow density (ρ_{base}) of the snowpack (Equation 2.16). If fresh snow fell, it was added on top of the snowpack with a lower density (ρ_{fresh}), obtained from the amount of precipitation (P) causing the increase of snow cover. The density of the already existing snowpack ρ_{base} was assumed constant if the density of the fresh snow cover was smaller than the density of the existing snowpack. Δh_m is the snow depth decrease in centimetres in one day (Equation 2.17).

$$\textbf{Equation 2.16}: (\rho_{base}(n) * \frac{cm^3}{g}) = \frac{\Delta h_m(n)}{cm} * \left(c_d * \frac{cm^4}{g}\right) + (\rho_{base}(n-1) * \frac{cm^3}{g})$$

$$\textbf{Equation 2.17}: \frac{\Delta h_m(n)}{cm} = \frac{h(n-1)}{cm} - \frac{h(n)}{cm}$$

δ_{fresh} was calculated based on the snow cover increase and precipitation, when snowfall occurred during the melting period. Δh_a is the height of the additional snow cover and was calculated for every day after a snowfall event, based on the initial height difference ($\Delta h_{snowfall}$). Δh_a is the difference in snow depth between the day before snow accumulation and day n and it is calculated day by day. Precipitation was accumulated for all days with fresh snow events. Increasing sum of precipitation (ΣP) and decreasing additional snow height (Δh_a) were used to calculate the density of fresh snow cover (δ_{fresh}) on day n (Equation 2.18).

$$\textbf{Equation 2.18}: (\rho_{fresh}(n) * \frac{cm^3}{g}) = \frac{\sum_{d=1}^{n}(P(d) * \frac{cm^2}{g})}{(\Delta h_a(n) * \frac{1}{cm})}$$

$$\textbf{Equation 2.19}: \frac{\Delta h_a(n)}{cm} = \frac{\Delta h_{snowfall}}{cm} - \frac{\Delta h_m(n)}{cm}$$

Equation 2.17 was only applied when $\Delta h_m > 0$, in other cases ρ_{base} was set equal to the density of the previous day. ρ_{base} did not change when $\Delta h_m > 0$ but $\rho_{fresh} < \rho_{base}$. Hence, Equation 2.19 was always applied when the density of fresh snow was smaller than the density of the base snowpack.

SWE for every day n was calculated with both density values; ρ_{base} and ρ_{fresh}. Density and snow depth (h_{snow}) were expressed in kg/m³ and m respectively. The snow depth was partitioned into ripened and fresh snow and multiplied with the associated density:

$$\textbf{Equation 2.20}: \left(SWE * \frac{m^2}{kg}\right) = \left(\rho_{base} * \frac{m^3}{kg}\right) * \left(\frac{h_{snow} - \Delta h_a}{m}\right) + (\rho_{fresh} * \frac{m^3}{kg}) * \frac{\Delta h_a}{m}$$

In most of the cases (since fresh snow is prominent only for a few days) the equation only used ρ_{base} and h_{snow}, because Δh_a was 0 in those cases. The SWE was calculated for every snowmelt season and every day for the years 2011/2012 to 2019/2020.

2.7.4 Degree-day factor

The Degree-day factor (DDF) is a parameter which describes the amount of snowmelt produced by a daily average air temperature of 1 °C. It is calculated with the daily decrease in SWE and the daily average air temperature. SWE was calculated as described in chapter 2.7.3 (Snow density), air temperature was measured by the meteorological tower (chapter 2.7). The difference in SWE between two consecutive days was calculated in order to obtain the snowmelt (Equation 2.21).

$$\textbf{Equation 2.21}: \frac{melt(n)}{mm} = \frac{SWE(n-1)}{mm} - \frac{SWE(n)}{mm}$$

Every snowmelt season was divided into several snowmelt events. Whenever the melt of one day was negative, meaning snow accumulation, the snowmelt event ended, and a new event started when positive melt was calculated. Snowmelt and temperature were accumulated for every snowmelt event, starting with the first day of the snowmelt period.

Four different approaches were used to obtain the DDF.

(1) Graphical analysis by plotting the accumulated melt against the accumulated temperature and use a linear regression. The inclination of the regression gives the DDF.

(2) A graphical analysis, where only days without precipitation were considered for the DDF calculation. With this procedure it can be ensured that only snowmelt originated by air temperature was regarded, and no effect of snowmelt caused by rain occurs.

(3) 10-day interval time analysis (Martinec, 1960): Degree Days and daily snow melt are summed up and precipitation is added to the amount of snow melt because rain and snow are additional inputs to the system. Three time intervals were assigned for every month: 1st to 10th, 11th to 20th and the remaining days of the month. Only days with positive amount of snow melt were used in the calculations

$$\textbf{Equation 2.22}: \left(DDF * \frac{°C}{mm}\right) = \frac{\sum_{n=1}^{10(8:11)} \frac{melt(n)}{mm} + \sum_{n=1}^{10(8:11)} \frac{precipitation\ (n)}{mm}}{\sum_{n=1}^{10(8:11)} \frac{T(n)}{°C}}$$

(4) 10-day interval time analysis (modified): Degree Days and daily snowmelt are summed up but precipitation is not considered. Rain- and Snowfall in the equation would have a doubled impact on the result, because the SWE of the snowpack in YURF was already calculated with inputs of precipitation.

$$\textbf{Equation 2.23}: \left(DDF * \frac{°C}{mm}\right) = \frac{\sum_{n=1}^{10(8:11)} \frac{melt(n)}{mm}}{\sum_{n=1}^{10(8:11)} \frac{T(n)}{°C}}$$

The four different approaches have been compared and the resulting DDFs of every year have also been compared in order to find a similarity and a relationship of snow density and DDF.

For the graphical approaches, the snowmelt season was portioned into sub-seasons. The main melting season started after the last increase of SWE and ended with the end of snowmelt. Shorter snowmelt periods intermitted by snowfall events were regarded separately as early snowmelt events. Separate DDFs were calculated for those events and compared with the DDF of the main snowmelt.

2.8 Rain/Snowmelt linked to soil moisture

Soil moisture responses to snow melt and ROS events were analysed for the winters 2018/2019 and 2019/2020. Because soil does not freeze in winter water can infiltrate the soil. It was therefore expected, that ROS and snowmelt would affect soil moisture in winter.

The recorded peaks in the soil moisture data were analysed in order to identify the sources of water causing them. The average soil moisture content 72 hours before a measured peak was calculated. The difference between the peak maximum and the 3-day-average value was analysed for significance. Only peaks after the end of soil moisture fluctuations during the initial snow accumulation and before snowmelt season soil moisture variations were analysed because they were easy to identify and a homogeneous soil moisture level before their occurrence was found. If the time gap between two analysed peaks was less than 72 hours, only 48 hours or 24 hours, respectively, were used for the calculation of the soil moisture average level.

The soil moisture difference between the calculated average prior to the peak and the peak soil moisture was divided by the time that the peak needed to reach its maximum ($\Delta t_{increase}$). This time difference was measured between the first increase of soil moisture and the peak maximum. The calculated increase rate was compared with rainfall and with SWE changes 24 hours prior to the event. Based on the increase rate and the meteorological data, it was determined whether the peak was most likely caused by rain, by snowmelt (decrease in SWE) or by both factors.

After this, the intensity of rain events causing peaks as well as the SWE decrease at melting processes was used to determine infiltration events in the past. Based on the results of soil moisture measurements in the winter of 2018/2019 boundary values of rainfall and snowmelt were chosen to predict the number of events affecting soil moisture. Hence, the change of SWE within one day and the daily precipitation of January and February of every year were ordered and analysed. Only January and February were used, because December and March were in some years influenced by a late start of snow accumulation or an early beginning of snowmelt.

2.9 HYDRUS 1D

The software *HYDRUS 1D* is free to use and models soil moisture dynamics. Input values are soil physical properties, hydrothermal parameters and meteorological information. Furthermore a graphical editor was used to distribute the soil into horizons, to apply roots and to modify the initial temperature of the soil profile.

The model was applied for the three slope spots in YURF, where soil moisture was also measured (*SB*, *SM*, and *ST*). The measured soil moisture was used to confirm the modelled data. The software was further used to model snow depth and surface runoff.

2.9.1 Model windows

In the *Main Processes* window the different processes to be modelled can be chosen. For this study, water flow, including vapour flow and snow hydrology, heat transport and root water uptake were selected.

In *Geometry Information* the length unit was set to cm and three soil materials were chosen based on the horizons of the soil profiles. Three layers for mass balances were chosen and the soil depth was 60 cm at all spots.

The time unit was set to days in the *Time Information* window. In order to model every spot month by month, the initial day was set to 0 and the final time to 28, 29, 30 or 31, depending on the month. Initial time step, minimum time step and maximum time step remained unchanged at 0.001, 0.00001 and 1 days. The time variable boundary conditions and the meteorological data were activated and set to 31, each. The Penman-Montheith Equation was used for evapotranspiration-calculations in *HYDRUS* (Monteith, 1981).

The output should be given for every day; hence the time interval and print step in the *Print Information* window were set to 1 day. The number of print times was set equal to the number of days of the month. The options "Screen Output" and "Hit Enter at End?" were activated.

The maximum number of iterations was adjusted to 15 in the *Iteration Criteria* window. The other parameters in this window remained unchanged.

The *Soil Hydraulic Model* window is the important model to choose the model which will be used for calculations based on the porosity. Different modelling runs were done; the *van Genuchten-Mualem Single Porosity Model* (van Genuchten, 1980) and the *Durner Dual-porosity model* (Durner, 1994) were used.

Soil physical parameters (θ_r, θ_s, K_s, α and n), obtained by the *HYPROP* measurements, were input in the next window, called *Water Flow Parameters*. A second approach used the *Neural Network Prediction* function, calculating the soil hydrological parameters based on soil texture, density and water content with the implemented software *Rosetta Lite v. 1.1* (Šimůnek et al., 2008). After input and test runs of the model, the modelled soil moisture was compared with the actual measurements, the parameters were manually adjusted and the model was executed again. This procedure was repeated until the modelled soil moisture curves fit the measured soil moisture data.

After assigning the parameters to the soil materials, the model proceeded to the *Water Flow Boundary Conditions* window. "Atmospheric BC with Surface Run Off" was selected for the Upper Boundary Condition and "Free Drainage" for the Lower Boundary Condition. The initial condition was selected to be given as water content.

The *Heat Transport Parameters* window showed a table for the input of detailed soil thermal parameters. Because measurements were not conducted to analyse heat transport, the default values for Sand were used.

The next window, called *Heat Transport Boundary Conditions*, introduced the snow cover. The snow melting constant was manually calculated for every month and assigned to the model. The snow sublimation constant was 0.4 and the initial snow layer was the snow depth of the first day of the modelled month. Upper and Lower Boundary Conditions were set to "Temperature BC".

The *Root Water and Solute Uptake Model* window was only used to apply the Feddes model (Feddes et al., 1977) for water uptake reduction and to assign "No Solute Stress".

The Database "Deciduous Fruit" was used to estimate the Feddes parameters in the *Root Water Uptake Parameters* window.

The following window, named *Time Variable Boundary Conditions*, showed columns for entering precipitation, soil temperature at surface and bottom as well as the soil temperature amplitude within one day.

To keep the modelling process reproducible, the geographical location was entered in the *Meteorological Parameters* window. "Solar Radiation" was selected as input data for radiation, and latitude (38.5°) and altitude (270 m) were assigned to the corresponding sections. The measurement height for wind speed and temperature was set to 300 cm. The remaining values in the parameter section of the window were left at default. The option "No Crop" was selected and the albedo was set to 0.13, which represents the mean value of evergreen coniferous forests (Betts and Ball, 1997, Kuusinen et al., 2012). Cloudiness was calculated by measured sunshine hours.

The sunshine hours were entered together with radiation, air humidity, wind speed and air temperature data for every day in the *Meteorological Conditions* window.

After entering all data and proceeding to the next window, the graphical editor opens. The three soil materials needed to be assigned to the soil column. Material 1 was assigned to the first 17.5 cm depth, followed by material 2 until 37.5 cm and material 3 for the lower part of the soil column. Initial soil moisture and soil temperature were assigned and three observation nodes were created. After saving the edits the window was closed and the model was run.

The model results were accessible in graphical and numerical form. The window of the observation nodes offered data for pressure head, soil temperature and, most importantly for the comparison with measured data, soil water content. The following windows showed graphs for water content, water flux and other data on a daily basis over the soil profile. Surface runoff, infiltration and snow depth were plotted in the section *Water Flow – Boundary Fluxes and Heads* and could be compared with the measured data.

The results of every HYDRUS 1D modelling process are shown as graphs inside the software but can also be accessed in form of data tables in the *.out* output files. These files can be opened either with a text editor or with excel. The *.out* files were used to plot the modelled soil moisture for the whole year 2019 and the winter season 2020.

2.10 Data comparison

The data for soil moisture, snow depth and surface runoff modelled with HYDRUS were compared with the manually obtained values for every month from October 2018 to April 2020. Differences were plotted in graphs in order to illustrate the precision and the weak points of the HYDRUS model. Snow depth and surface runoff were compared on a daily basis and soil moisture was analysed graphically using the graphs over time.

2.11 Statistical analysis

Soil moisture peaks were analysed with a one-way ANOVA and a *post-hoc Tukey HSD test*. Averages and standard deviations (SD) of soil moisture and snow density were used to define whether differences were significant or not.

Linear regressions were made for soil and air temperature comparisons for all data with soil temperature higher than 2°C. Linear regressions were also made for the DDF plots of approaches 1 and 2, water runoff measurements and stream discharge. Box and whiskers plots including a *Grubbs outlier test* were used for all meteorological data. The outlier tests and box and whisker plots for meteorological data were programmed in R-Studio.

Averages and SD have been further used for snow density and SWE as well as for the soil moisture curves and water retention measurements.

3. Results

3.1 Soil analysis

3.1.1 Soil texture

Samples collected from all sites contained only small stones, gravel and finer texture, and were only analysed for the fractions < 6mm. Soil texture was classified with the standard soil texture diagram (Figure 3.1). Since all soils were mainly composed of sand, no soils were classified as clay soil type or silt soil type.

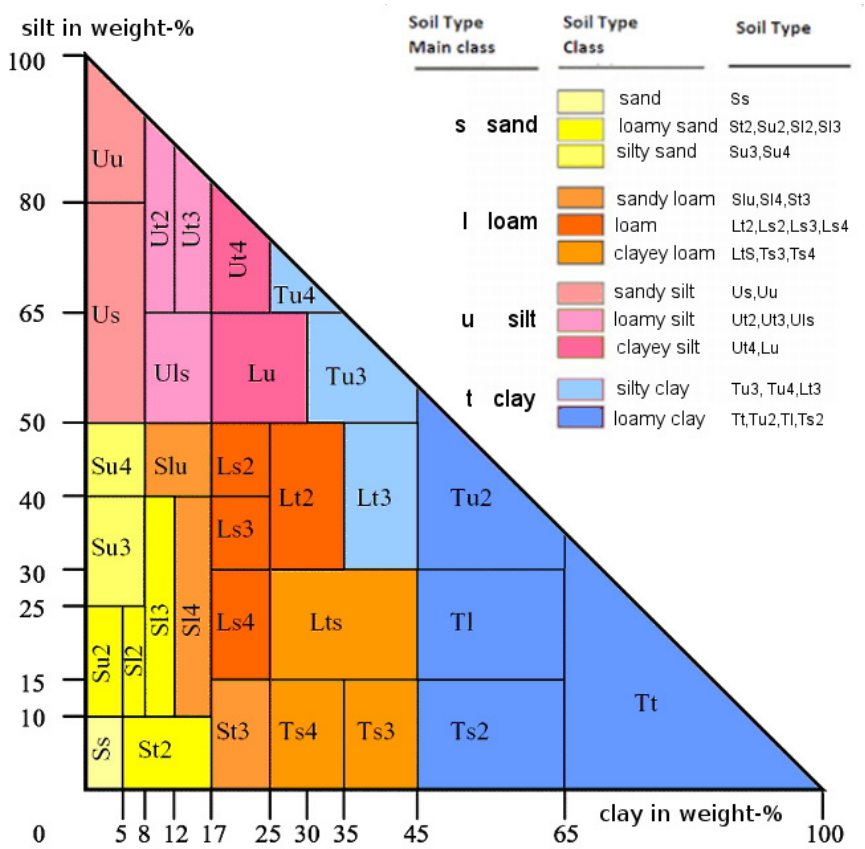

Figure 3.1: soil type diagram (after Eickelmann et al., 2005)

3.1.1.1 Soil texture in YURF

Soils at the three spots in YURF contained high amounts of gravel and larger grain fractions. Large rocks prominent at the bottom of the slope. Soil profiles in the slope were not deeper than 90 cm; the steeper the slope, the shallower the soil profile. On average, soil depth between the sampling points *SB* and *SM* was 50 cm, and between *SM* and *ST* 70 cm. The organic-rich A-horizon was thin at *ST* and *SM* (less than 5 cm). At *SB*, the A-horizon was thicker and the soil profile more than 1 m deep.

3.1.1.1.1 Spot *SB*

Figure 3.2: Soil profile (*SB*)

Soil texture at SB was sandy; the sand content was, except at 15 cm depth, always higher than 75 % in comparison to the other fractions < 2 mm. Clay content was always lower than 5%. Silt and fine sand decreased with depth, medium sand stayed stable around 20%, and the coarse sand content increased significantly with increasing depth. The soil type varied between *loamy sand* (Su2) at 5 cm and *silty sand* (Su4) at 15 cm. In deeper layers, the soil type was *sand* (Ss). Fractions > 2 mm made up more than 50 % of the soil texture, except for 5 cm depth. However, many rocks with diameters of more than 60 cm were found at *SB*, which were not included in the fraction > 6.3 mm, because they were too big to analyse in the laboratory, especially in depths greater than 50 cm, big boulders constituted the major part of the soil (Figure 3.3). Therefore, the proportion of the fraction > 2 mm was in reality even higher than the results show. Soil particles < 2 mm were smaller proportions in the matrix, filling the pores between stones and boulders.

Soil density of the fraction < 2 mm was 1.1 g/cm³ at 15 cm depth, 1.12 g/cm³ at 30 cm depth and 1.18 g/cm³ at 45 cm depth.

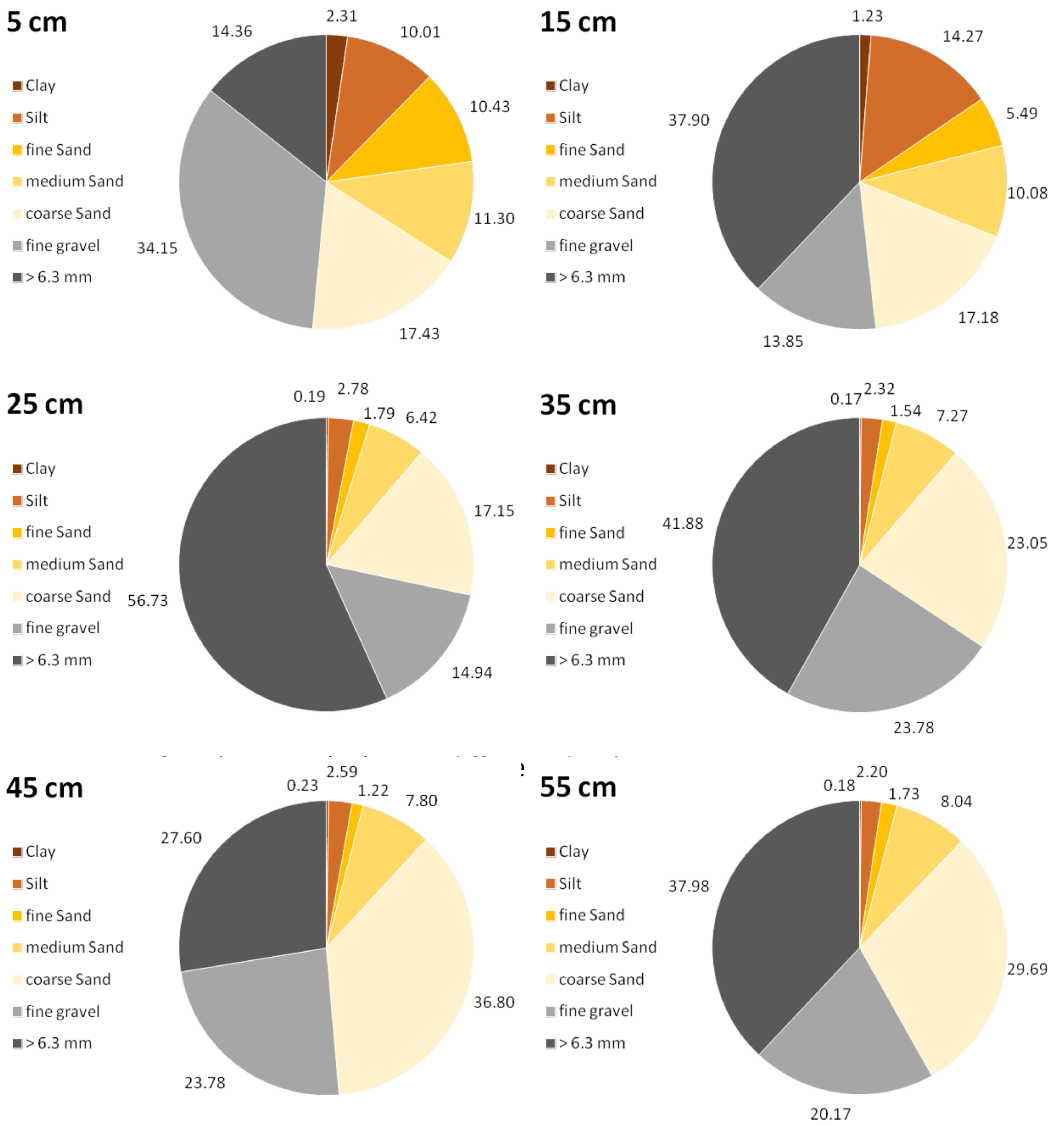

Figure 3.3 a-f: Soil texture (*SB*) at six different depths

3.1.1.1.2 Spot *SM*

Total sand content was higher than 45 %, and always higher than 75 % in comparison to the other fractions < 2 mm. Clay was negligible at 1 % or less. Silt and fine sand were decreasing with depth, medium sand decreased down to a depth of 35 cm from 24.5 % to 11 % and increased again in deeper horizons again. The coarse sand content increased from 19 % at 5 cm to 39 % at 45 cm. Fractions > 2 mm increased from 25.5 % at 5 cm to 49 % at 25 cm. With greater depth, the small gravel content increased slightly, but the fraction > 2 mm decreased significantly. The soil type changed from *loamy sand* (Su2) at 5 cm and 15 cm to *sand* (Ss) at all greater depths.

Figure 3.4: Soil profile (*SM*)

Soil density increased from 0.9 g/cm³ at 15 cm depth to 1.04 g/cm³ at 45 cm depth.

Figure 3.5 a-f: Soil texture (*SM*) at six different depths

3.1.1.1.3 Spot *ST*

The fraction > 2 mm, at around 25 % of the total mass, was smaller than at the spots *SB* and *SM*. The coarse sand fraction was also, with a maximum of 40 % at 15 cm depth, smaller than at the other spots. In total, the sand content varied between 50 % and 75 %. Clay content was smaller than 4 %. Silt content was 22.9 % at 5 cm, 7.8 % at 15 and at 25 cm, and was between 11.4 % and 14.1 % at deeper horizons. Coarse sand content was always higher than 23 %, with its maximum of almost 40 % at 25 cm. That resulted in the soil types Su3 for 5 cm, Ss at 15 cm and Su2 at all deeper soil samples.

Soil density of the undisturbed samples increased from 0.9 g/cm³ at 15 cm depth to 1 g/cm³ at 45 cm.

Figure 3.6: Soil profile (*ST*)

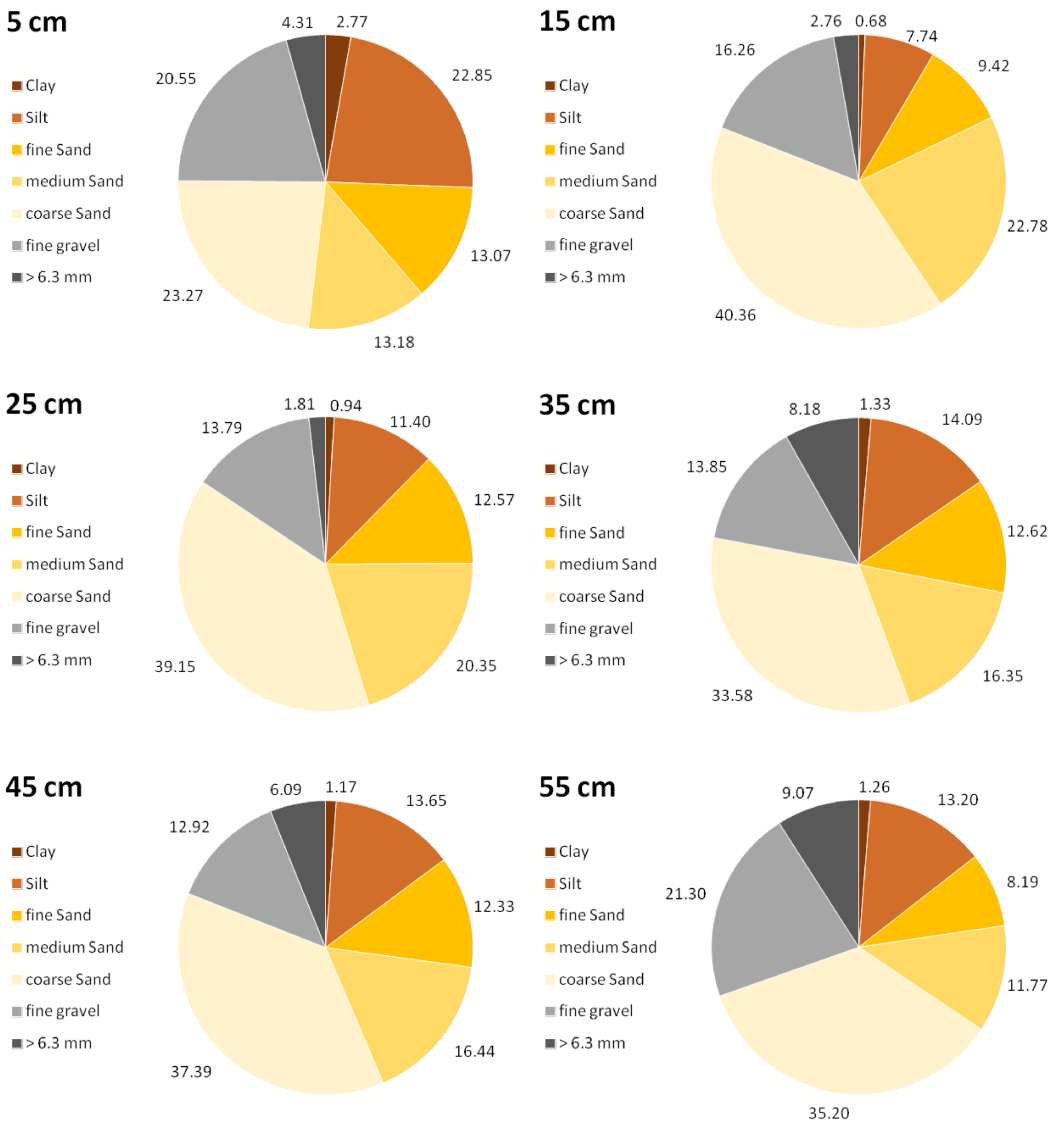

Figure 3.7 a-f: Soil texture (*ST*) at six different depths

3.1.1.2 Soil texture in Kaminoyama

In general, gravel and stones were not as prominent in Kaminoyama as in YURF. At all sampling sites the fraction > 2 mm was smaller than at the YURF sites. Soils were better developed and had significantly higher silt and clay contents. Sites A and B (Figure 3.8 a and b) were mull soils (developing to Cambisols) and dominated by a carbon-rich A-horizon. The soil type of site C was Pseudogley, developed under the influence of a paddy field which was located uphill and caused permanently high groundwater. In the upper soil horizon were areas of oxidized Iron and Manganese (Figure 3.8 c). The lower horizon was colourless, because of reducing conditions. Site B had a clear boundary between A and B horizon (Figure 3.8 b), the B-horizon in site A had high contents of organic matter and was therefore almost as dark as the A horizon.

Figure 3.8 a-c: Soil profiles of sites A, B and C

3.1.1.2.1 Site A

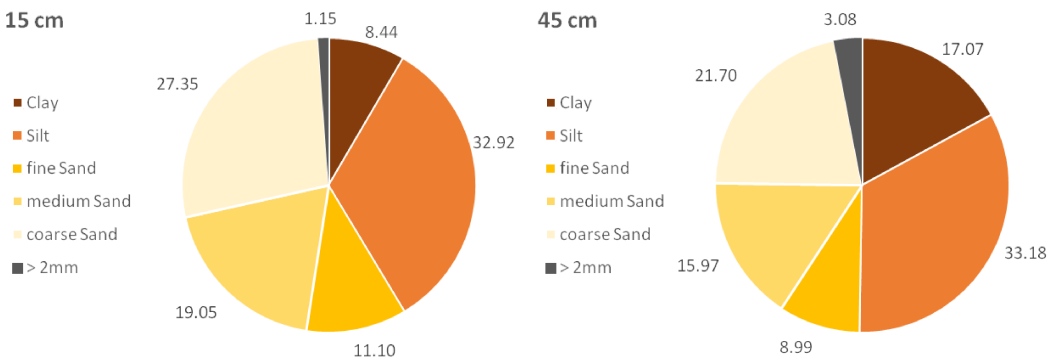

Figure 3.9 a-b: Soil texture (site A) at two depths

Soil at site A was composed to 97 % of fractions < 2 mm. The fraction > 2 mm increased from 1.1 % at 15 cm depth to 3.1 % at 45 cm depth. Clay content increased significantly from 8.4 % to 17.1 %. At more than 30 %, silt was the largest fraction of all soil texture classes. While silt content increased slightly with depth, all three sand class contents decreased with depth. The soil type was *loamy sand* (Sl3) at 15 cm and *loam* (Ls3) at 45 cm depth.

3.1.1.2.2 Site B

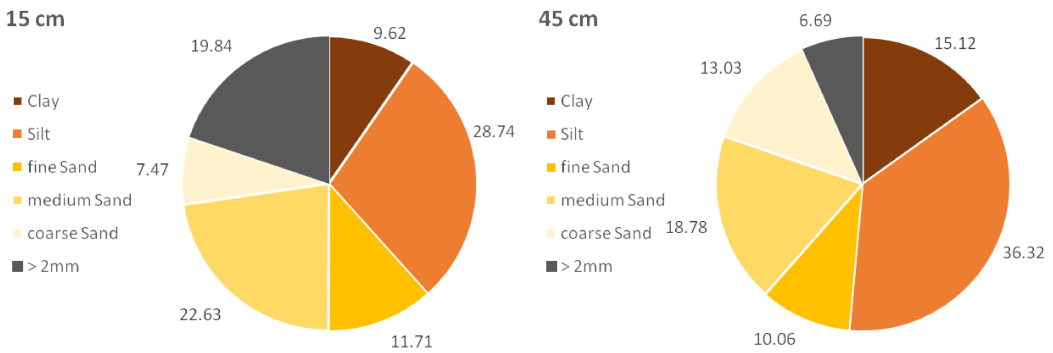

Figure 3.10 a-b: Soil texture (site B) at two depths

Clay content increased from 9.6 % at 15 cm to 15.1 % at 45 cm. Silt content increased from 28.7 % to 36.3 % with increasing depth. The individual contents of fine and medium sand fractions decreased slightly. The fractions > 2 mm decreased from almost 20 % to 6.7 %, whereas the coarse sand fraction increased from 7.5 % to 13 %. The soil was classified as *loamy sand* with soil types Sl3 at 15 cm and Sl4 at 45 cm depth.

3.1.1.2.3 Site C

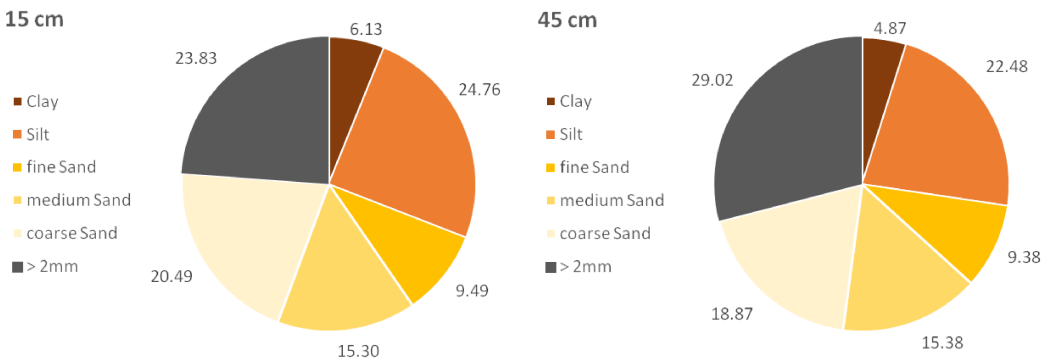

Figure 3.11 a-b: Soil texture (site C) at two depths

Site C had the highest contents of gravel and larger grains of the three Kaminoyama sites, with 23.8 % at 15 cm and 29 % at 45 cm depth. In contrast, sand, silt and clay contents decreased with greater depth. Clay content decreased from 6.1 % to 4.9 %, silt from 24.8 % to 22.5 % and coarse sand from 20.5 % to 18.9 %. Fine and medium sand remained at the same proportion in both depths. The soil types were *loamy sand* (Sl3) at 15 cm and *silty sand* (Su3) at 45 cm depth.

3.1.2 Soil water retention curves and physical parameters

The following figures show the average water retention curves for the three soil cores collected at every site. All soil moisture contents are given in vol.% for the HYPROP system and also for the soil moisture measurements in the field. The water retention curves were interpolated on the basis of measured soil moisture contents at specific matrix potentials (pF values) between pF0 and pF3 and the measured water content at pF4.2. The shape of the curve at pressures higher than pF4.2 was not realistic in the figures and only a theoretical assumption. The shape of the water retention curve was further determined by fitting parameters, which were iterated by HYPROP automatically during the calculation process.
HYPROP calculated also hydraulic conductivity, which was evaluated for the sites below. However, HYPROP usually underestimated the hydraulic conductivity, therefore the following values were significantly different from those used in the HYDRUS 1D model.

3.1.2.1 YURF

3.1.2.1.1 Spot *SB*

The HYPROP cores for spot *SB* were taken in a distance of approximately 10 m from the end of the slope, because too many big rocks made it impossible to take undisturbed samples directly at the end of the slope. The maximum soil moisture content at *SB* was 51.2 %, decreasing gradually with increasing pF value. The soil water content at the wilting point (pF = 4.2) was 13.8 %. The field capacity (pF = 1.8) was 40 %.

The shape parameters of the curve, obtained by iteration processes in HYPROP, were as follows:

Q_r = 13.9%, Q_s = 51.3%, α_1 = 0.00567 1/cm, n = 1.327, w_2 = 0.236, α_2 = 0.0518 1/cm, n_2 = 2.629

The calculated hydraulic conductivity K_s was 10.9 cm/d.

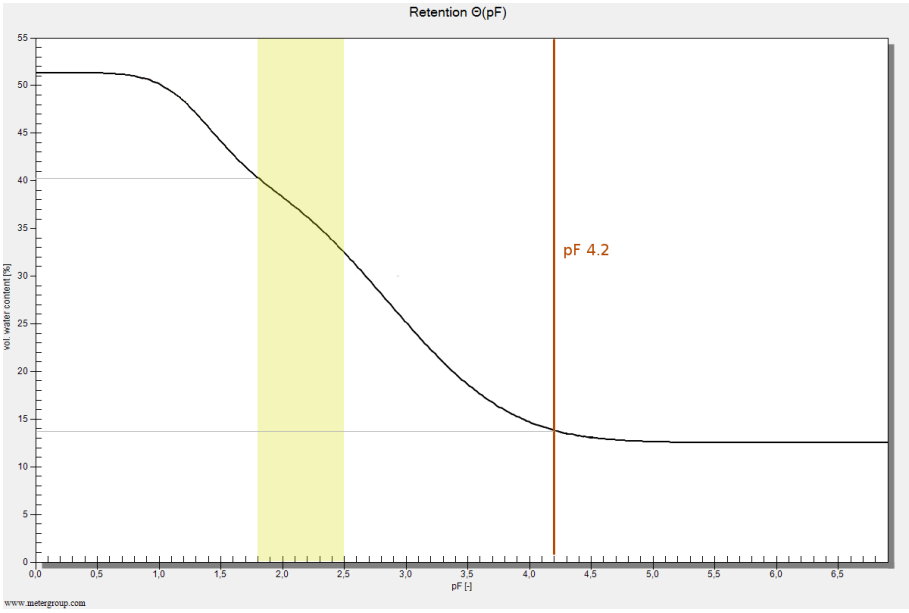

Figure 3.12: Water retention curve of spot *SB* (30 cm depth)

3.1.2.1.2 Spot *SM*

All three depths of *SM* had a water capacity between 42.5 % and 47 %, whereas the wilting point at pF = 4.2 was related to a soil moisture content of around 10 %. The field capacity increased slightly with depth from 20.3 % at 5 cm to 23.6 % at 85 cm depth. The total plant available water increased from 8 % in 5 cm to 11.5 % at 40 cm to 14.5 % at 85 cm depth. Hydraulic conductivity increased from 6.7 cm/d at 5 cm depth and 13.8 cm/d at 45 cm depth to 20.2 cm/d at 85 cm depth.

The calculated shape parameters of the water retention curves were:

<u>5 cm</u>:

Q_r = 12.6%, Q_s = 44.9%, α_1 = 0.115 1/cm, n = 2.179, w_2 = 0.404, α_2 = 0.0457 1/cm, n_2 = 1.07

<u>45 cm</u>:

Q_r = 10.8%, Q_s = 42.5%, α_1 = 0.0163 1/cm, n = 1.223, w_2 = 0.61, α_2 = 0.0631 1/cm, n_2 = 2.579

<u>85 cm</u>:

Q_r = 10%, Q_s = 47%, α_1 = 0.2303 1/cm, n = 1.607, w_2 = 0.236, α_2 = 0.0507 1/cm, n_2 = 1.02

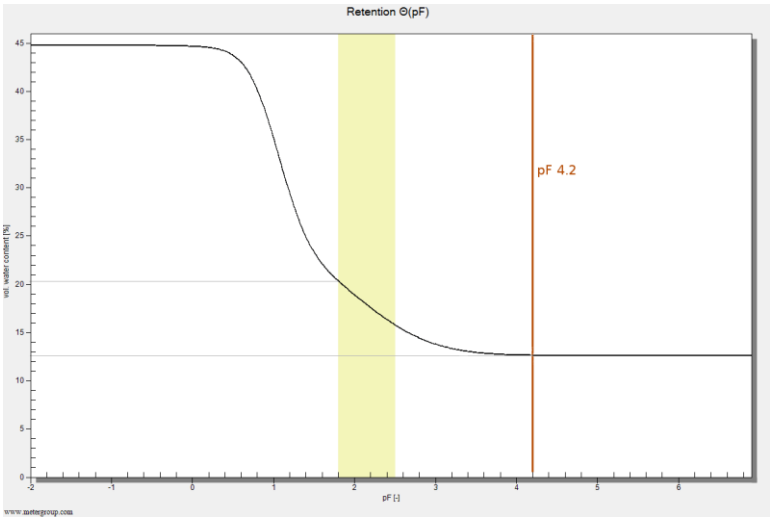

Figure 3.13: Water retention curve of spot *SM* (5 cm depth)

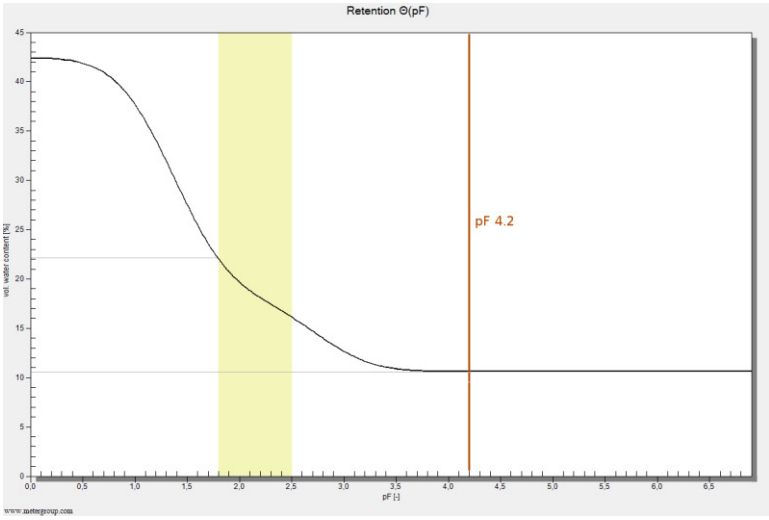

Figure 3.14: Water retention curve of spot *SM* (45 cm depth)

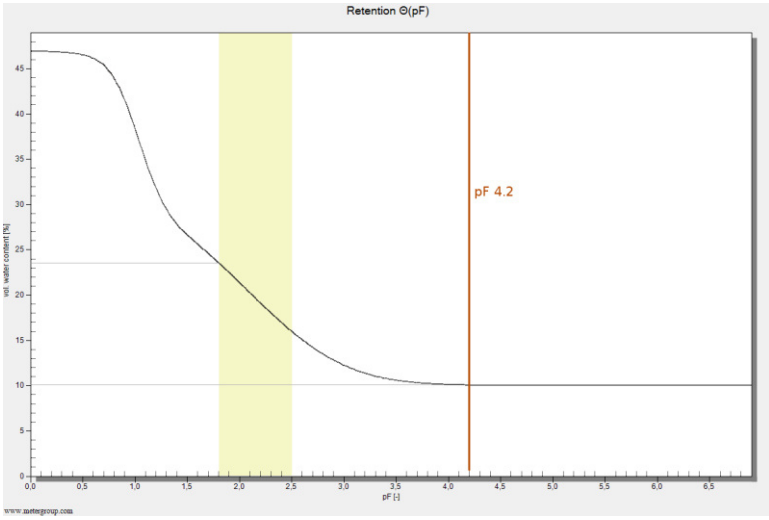

Figure 3.15: Water retention curve of spot *SM* (85 cm depth)

3.1.2.1.3 Spot *ST*

The pF curve of spot *ST* at 30 cm depth showed a steep decrease of soil moisture at pF3.7, near the wilting point. The field capacity was 32 %, and the water content at the wilting point was 9.5 %. The maximum water content was 49 %. The water retention curve in the low-pressure region (below pF2.5) was not as steep as the curves at *SB* and *SM*. The hydraulic conductivity for *ST* was 11.8 cm/d. Other soil hydraulic parameters were:

Q_r = 9.5%, Q_s = 49%, α_1 = 0.155 1/cm, n = 1.422, w_2 = 0.28, α_2 = 0.00008 1/cm, n_2 = 15

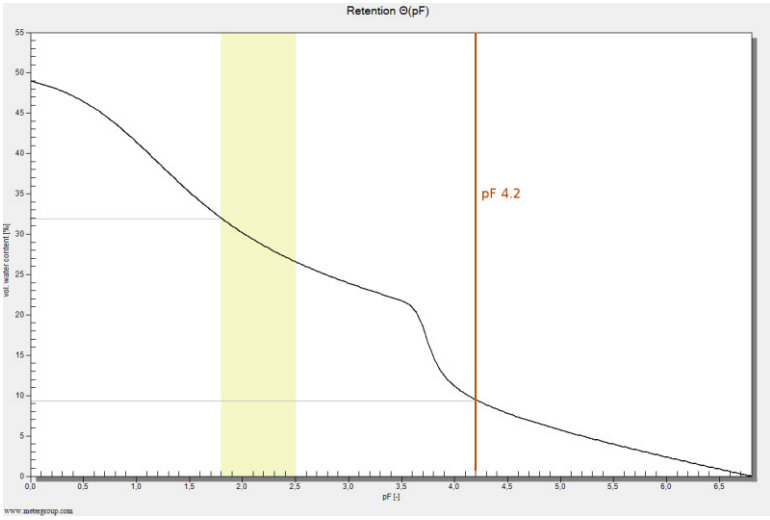

Figure 3.16: Water retention curve of spot *ST* (30 cm depth)

3.1.2.2 Kaminoyama

The soils of Kaminoyama had lower maximum soil moisture contents but higher soil moisture contents at pF 4.2 due to the higher clay and silt contents in comparison to the soils of YURF. The water retention curves showed smaller differences in soil moisture between pF0 and pF4.2 than the soils in YURF. HYPROP cores were in better shape and easier to take because of the small amount of stones and other large soil components.

3.1.2.2.1 Site A

The maximum water content at site A was 44 %, the field capacity 29.2 % and the wilting point at 21.5 %. The high clay content in the soil caused the high water content at the wilting point. Less sand but a lot of silt shape the retention curve. The high water content at the wilting point results in 7.7 % of plant available water under normal conditions. The K_s value for site A was 453.1 cm/d and therefore significantly higher than the K_s value of the soils in YURF. The curve shaping parameters were:

Q_r = 21.4%, Q_s = 44%, α_1 = 0.1008 1/cm, n = 1.383, w_2 = 0.166, α_2 = 0.2107 1/cm,

n_2 = 2.365

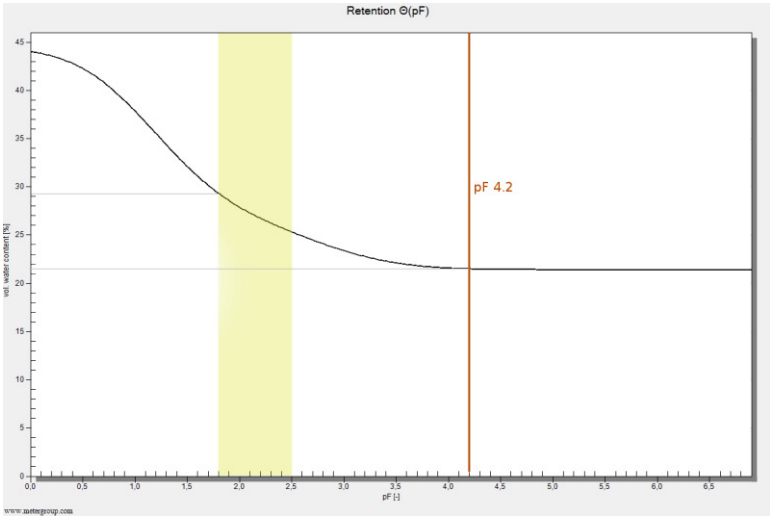

Figure 3.17: Water retention curve of site A (30 cm depth)

3.1.2.2.2 Site B

The maximum soil moisture content in site B was 46.3 %, the residual water content at wilting point 27.2 %. The high silt content in the soil increases the amount of water which is plant available. The air capacity is less than 10 % because of the small amount of sand. The plant available water was 12 % (water contents from 27.2 % to 39.2 %) and therefore higher than at site A, the hydraulic conductivity was smaller with 9.22 cm/d. The curve shaping parameters were:

Q_r = 27.2%, Q_s = 46.3%, α_1 = 0.0436 1/cm, n = 2.115, w_2 = 0.764, α_2 = 0.0113 1/cm,

n_2 = 1.09

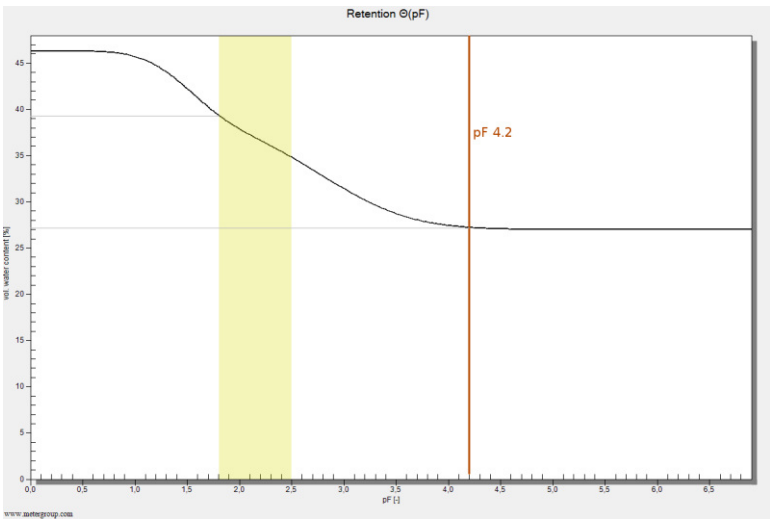

Figure 3.18: Water retention curve of site B (30 cm depth)

3.1.2.2.3 Site C

The shape of the water retention curve of site C looked similar to the shape of the curve of site B. The maximum water content was 46.1 %, and the water content at pF4.2 was 25.5 %. At pF1.8 the soil can store 38.3 % water, resulting in 12.8 % plant available water. Soil hydraulic conductivity K_s was 15.8 cm/d, whereas the curve shaping parameters were:

Q_r = 25.5%, Q_s = 46.1%, α_1 = 0.00776 1/cm, n = 1.58, w_2 = 0.476, α_2 = 0.0711 1/cm, n_2 = 1.659

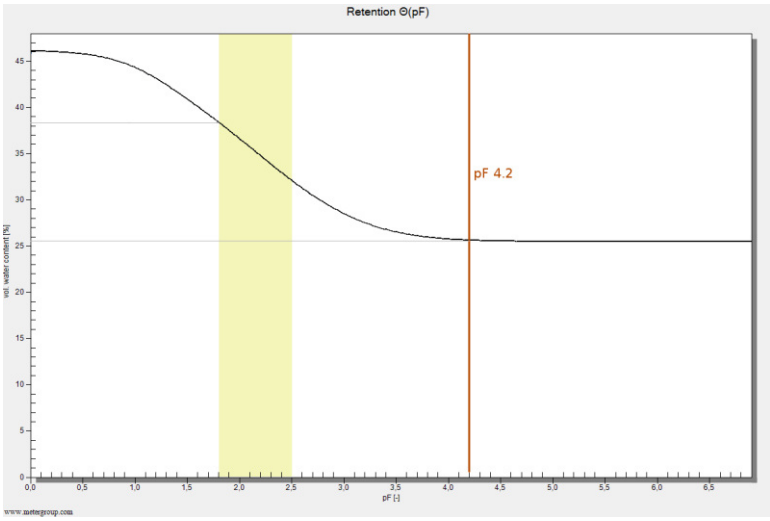

Figure 3.19: Water retention curve of site C (30 cm depth)

3.1.3 Contact angle

Table 3.1: Contact angle of soil samples of the slope site in YURF

Soil depth	*SB*	*SM*	*ST*
Organic layer	135°	146°	138°
2 cm	103°	77°	109°
4 cm		43°	
6 cm		51°	
8 cm		50°	
10 cm	87°	48°	91°

The contact angle of the organic layer of the soil profiles in YURF was 135° or higher in all samples. The organic-rich first 2 cm of the soil profile at the spots *SB* and *ST* produced also contact angles of more than 95°. These five samples had therefore high water repellency values. All soil samples of *SM* had contact angles lower than 95°. Hence, the soil at *SM* was better wettable than the soils at *SB* and *ST*, but the organic layer of *SM* was more hydrophobic than at the other two spots.

3.1.4 CN ratio

The CN ratio for the soils in Kaminoyama was calculated based on the results of the CN-analyser. Soil Carbon content varied between 2.1 and 47.3 g/kg, with site C having the lowest Carbon contents and site A the highest. The highest Nitrogen content was measured as 3.65 g/kg in the A-horizon of site C, which had also the lowest Nitrogen content of 0.33 g/kg in 45 cm depth. All sites had high Nitrogen and Carbon contents in 15 cm depth and low contents in 45 cm depth. The average contents for the two profiles in site A and B, the three profiles in site C and the calculated CN ratio are shown in Table 3.2.

Table 3.2: Carbon and Nitrogen contents of soils in Kaminoyama

Site	C in g/kg	N in g/kg	CN ratio
A – 15cm	21.50	1.65	13.064
A – 45 cm	47.12	2.56	17.641
B – 15 cm	28.28	2.17	13.014
B – 45 cm	6.85	0.72	9.418
C – 15 cm	18.26	1.74	8.921
C – 45 cm	3.79	0.43	8.409

The highest CN ratio was calculated for site A. Carbon, Nitrogen and CN ratio did even increase with greater depth in this site. The CN ratio of the A-horizon in site B was similar to site A, but it decreased with greater depth. Site C had the lowest CN ratios, with values < 9. However, Carbon and Nitrogen contents were significantly lower than at the other two sites.

3.2 Soil water interactions

3.2.1 Soil moisture

Soil moisture has been divided into two periods in the following graphs. The first, one-year period of measurements started on October 10, 2018. The second period was shorter; the data acquisition occurred from October 10, 2019 until May 10, 2020. Both periods included summer and winter soil moisture measurements, and data loggers were maintained after snowmelt seasons. The highest soil moisture was recorded at 15 cm depth at all three spots; the lowest was always recorded at 50 cm depth.

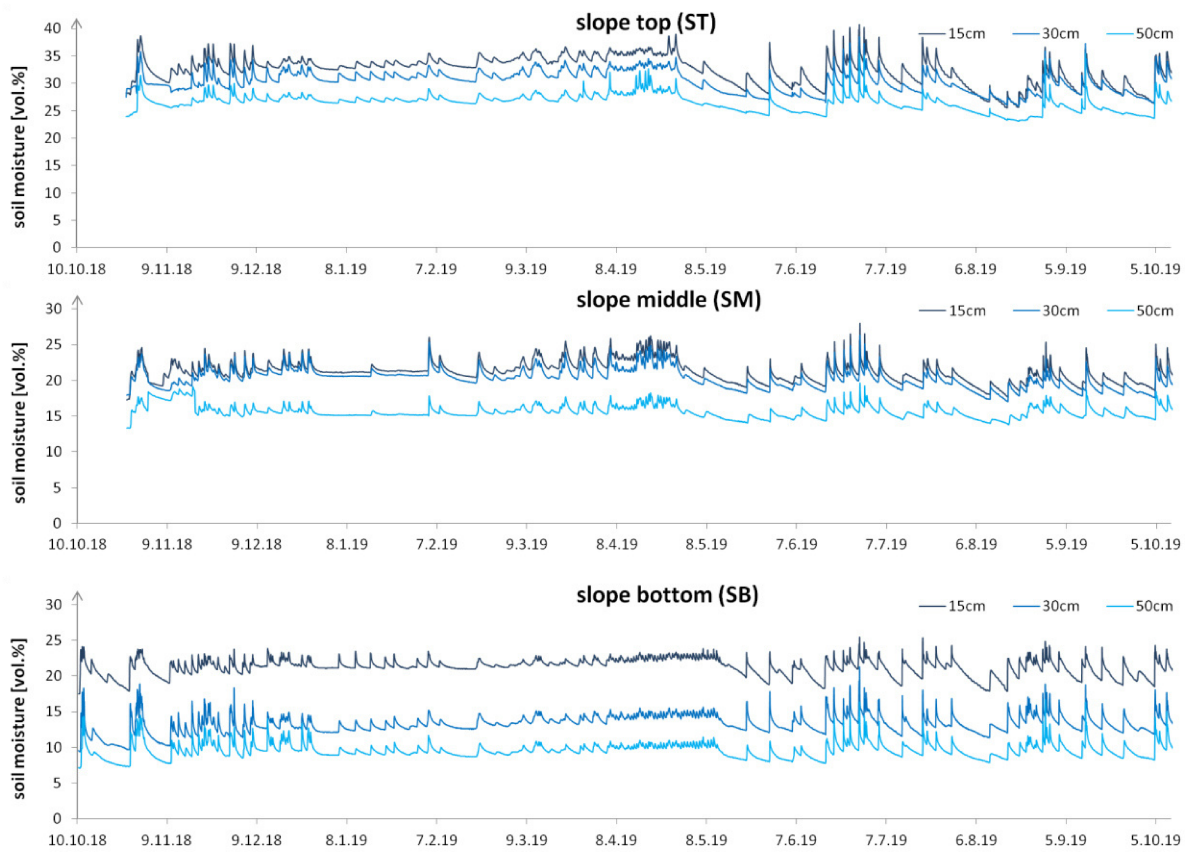

Figure 3.20 a-c: Soil moisture 2018/10 - 2019/10 at the spots *ST*, *SM* and *SB*

The highest soil water contents were measured at *ST*, with always more than 25 % at 15 cm depth (Figure 3.20 a). Water content at 15 cm depth was more than 30 % in autumn and winter 2018 and decreased after the snowmelt period ended in May 2019. Soil moisture at 30 cm and 50 cm depth decreased with smaller intensity, so that the difference of around 7 % in winter between 15 cm and 50 cm became smaller. Soil moisture decreased after peaks faster at 15 cm than at 30 and 50 cm. On some days in May and especially August and September the sensors at 15 and at 30 cm depth recorded the same soil water content.

Peaks after rain events represented increases of up to 10 %, with peaks in the 15 cm curve higher than in the 30 cm or 50 cm curves.

Soil moisture at *SM* was more uniform than at the other two spots, especially in the winter months (Figure 3.20 b). Significant decreases in soil moisture were recorded after the end of the snowmelt season, occurring at 15 cm and 30 cm almost simultaneously and with the same intensity. The difference of soil water content between 15 cm and 30 cm therefore stayed almost the same throughout the whole year, at around 1 %. Soil moisture at 50 cm reacted less intensely to precipitation and to drying processes than the topsoil. Peaks in soil moisture during winter were almost of the same height as peaks after heavy rain events in seasons without snow cover.

At spot *SB*, soil moisture at three depths (15, 30 and 50 cm) oscillated synchronously during the period October 2018 to May 2019 (Figure 3.20 c). The highest values were observed at 15 cm depth, and values decreased with depth. Soil moisture at 15 cm depth was, on average, 7 to 10 % higher than at 30 cm depth. Soil moisture fluctuation decreased in the period mid-November to end of December, followed by smaller peaks during the period of snow cover.

However, increases in precipitation in July and August refilled soil moisture that was readily used for tree transpiration. The amplitude of soil moisture changes was greater at 15 cm than at 50 cm. Soil moisture in winter was 21 % on average at 15 cm, while it was 13 % and 10 % at 30 cm and 50 cm, respectively. During the forest growing season, soil moisture ranged from 17 % to 25 % at 15 cm depth. Peaks in summer were higher at 30 cm and 50 cm depth in comparison to 15 cm depth.

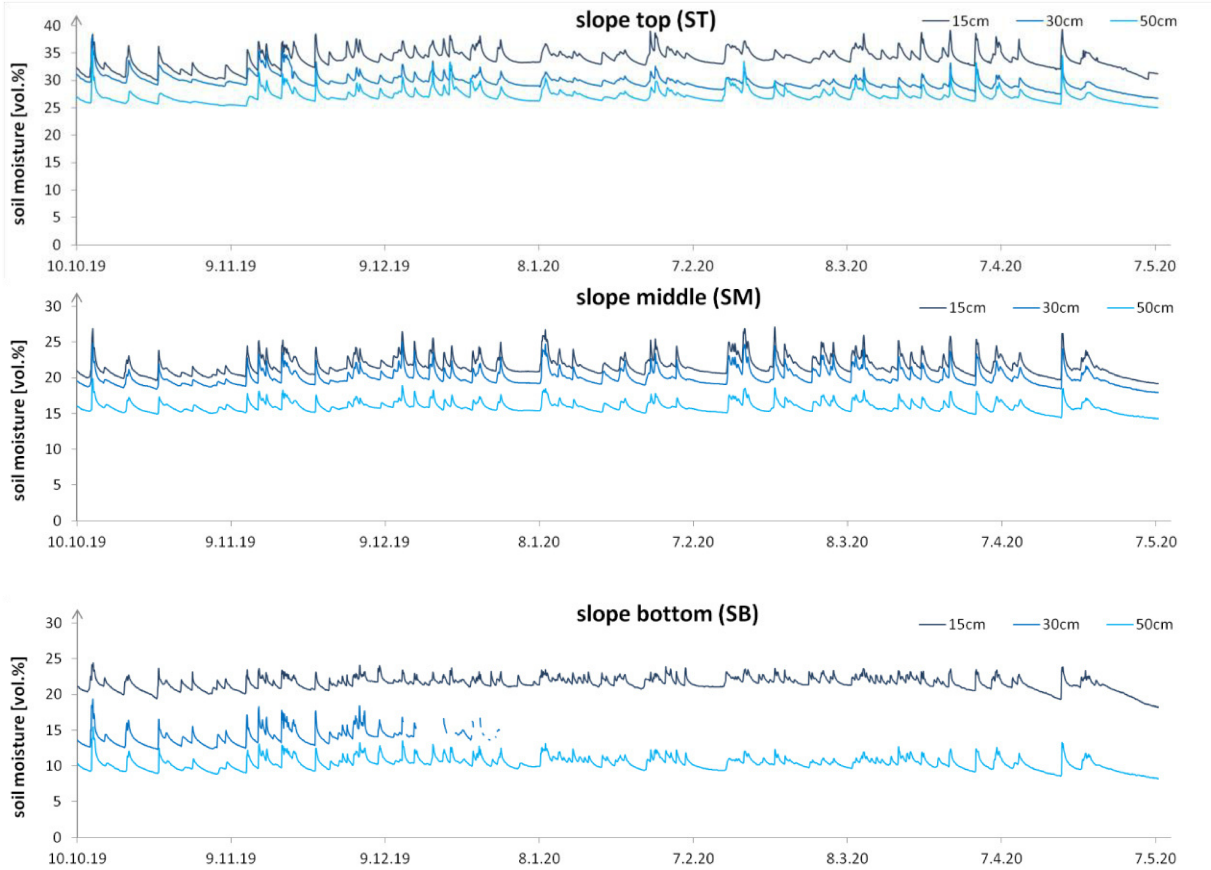

Figure 3.21 a-c: Soil moisture 2019/10 - 2020/05 at the spots *ST*, *SM* and *SB*

Soil moisture curves of the winter season 2019/2020 contained more peaks than the curves of the winter season 2018/2019. The soil water content at 15 cm depth at *ST* was around 32 % before snow accumulation started and increased to 34 % under snow cover. After the end of snowmelt soil moisture decreased, at 15 cm more than in deeper horizons. However, the decrease was not as pronounced as in the previous year.

Soil moisture at *SM* was relatively constant over the whole measuring period 2019/2020. As in the previous year, the soil moisture at 15 cm and at 30 cm changed almost at the same rate. Soil moisture at 15 cm and 30 cm was generally around 20 %.

The sensor in 30 cm depth at SB stopped working in January 2020. Therefore, the trend of soil moisture was not recorded at this depth. However, the 15 cm and 50 cm curves showed a constant soil moisture minimum level but many peaks during winter. After the end of the snowmelt, soil water content at 15 cm decreased significantly.

3.2.2 Slope water runoff

Soil surface and bedrock runoff was measured for one summer season, from end of June 2019 until end of November 2019. Soil moisture of the spot *SB* was plotted together with the runoff data in order to link rain events to soil moisture decreases (Figure 3.22). The highest total runoff was measured as 1875 mm on November 18. The second highest peak was recorded as 1859 mm on July 18. Both peaks, and also most of the other peaks, had major contribution of bedrock runoff. The surface runoff was larger than the bedrock runoff only at the end of June, the end of September, and in October.

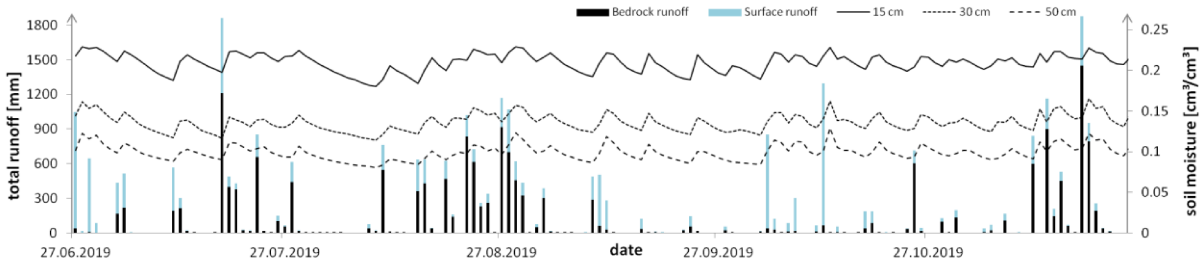

Figure 3.22: Surface and bedrock runoff versus soil moisture at *SB*

Soil moisture varied throughout the whole summer and autumn period. Increases in soil moisture were observed simultaneously to runoff events. However, the soil moisture data alone was no indicator for the relation between surface runoff and bedrock runoff. In order to understand the mechanism and the occurrence of surface runoff, the difference between surface and bedrock runoff was calculated for every day and plotted against the daily precipitation. Negative differences mean a high fraction of bedrock runoff; positive differences mean a higher surface runoff.

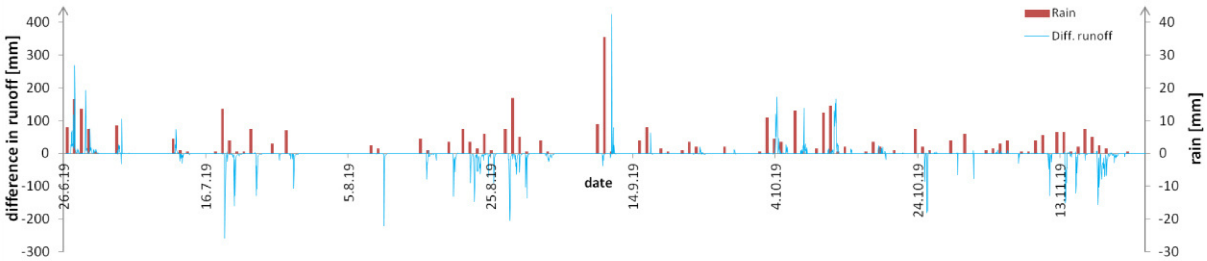

Figure 3.23: Difference between surface and bedrock runoff versus rainfall

Surface runoff was higher than bedrock runoff when precipitation was high. The largest rain event of 35.5 mm on September 10 was one day before the highest peak in the runoff

difference. Other events of more than 10 mm rain on one day were also followed by high soil surface runoff. Negative differences were calculated especially during longer rain periods.

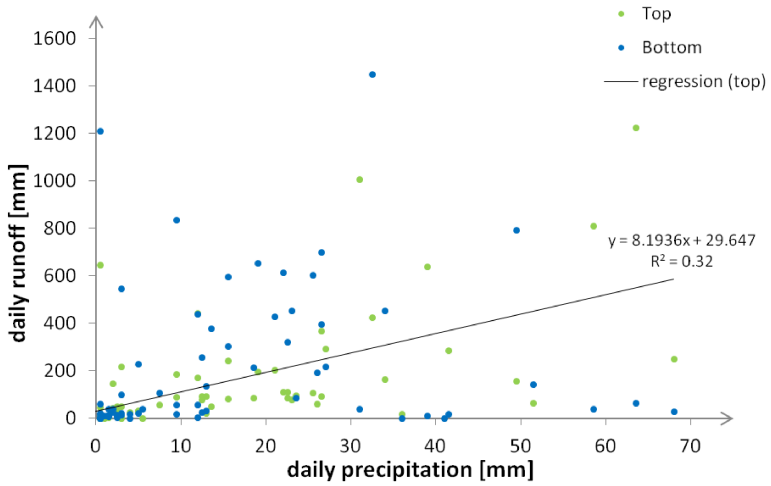

Figure 3.24: Slope water runoff plotted versus rainfall

The runoff data was plotted against the precipitation data of one day before in order to compensate the delay of precipitation water being measured as runoff water. However, the relation between surface runoff and precipitation was weak (R^2 of 0.32) (Figure 3.24). Further, the best R^2 was achieved, when one day time offset was assumed. Higher precipitation related to higher runoff, but the points were widely scattered in the graph. Surface runoff (top) and bedrock runoff (bottom) occurred both after heavy rain events and after smaller rain events without separation of both processes.

3.2.3 Stream water discharge

The water level of the Wasada stream ranged between 40 cm and 90 cm. Only pictures taken during the day could be analysed, because, even using the night picture capturing mode, the scale bar of the river was not readable at night. The monitoring period of less than three months was rather short, but the peak discharge of the snowmelt season could be measured.

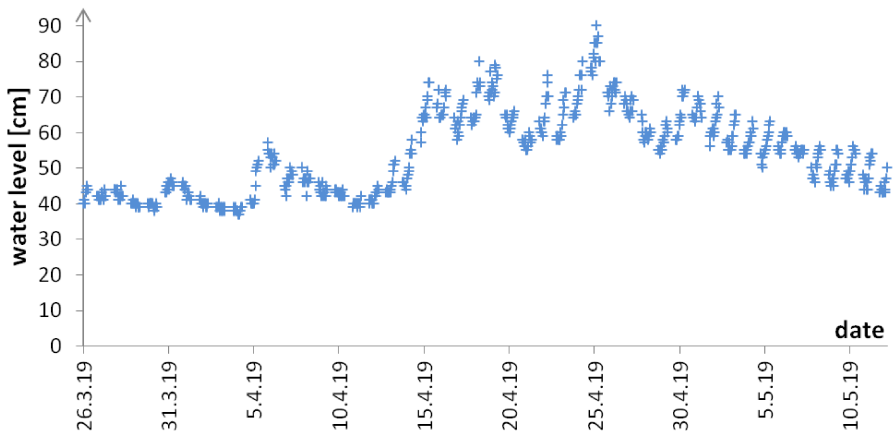

Figure 3.25: Stream water level

The Wasada stream was at a normal water level of 40 cm during the first weeks of the snowmelt season. The water level and therefore the water discharge increased significantly on April 15, 2019, which was two weeks before the end of the snowmelt season in YURF. The peak river water level of 90 cm was measured on April 25 and decreased afterwards. The level at the end of a day was usually about 10 cm higher than in the morning.

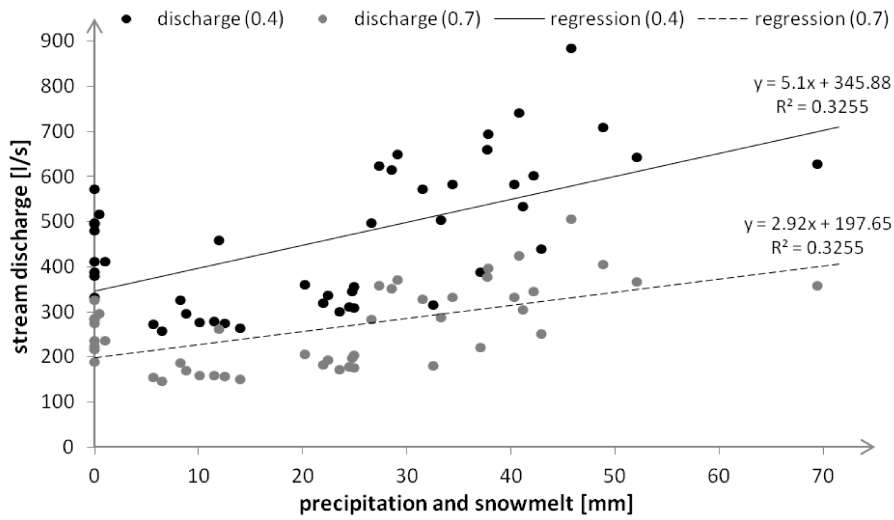

Figure 3.26: Stream discharge calculations versus precipitation and snowmelt

Daily precipitation and snowmelt were added and plotted against the calculated stream discharge in order to find a relationship of higher discharge linked to high water runoff. Based on the peaks in the water level graph (Figure 3.26) a delay of one hour reaction time for the water level was chosen. Rain and snowmelt water needed a certain time to be reflected in the stream water level; therefore the precipitation and snowmelt water volume of a day *n* was plotted against the water level of the day *n*+1. Stream discharge was also

variable when no additional water affected the stream. Higher runoff resulted in general in greater discharge of water in the Wasada stream. Based on the expected Manning coefficients between 0.4 and 0.7 for the stream, two regressions were calculated, as the real water discharge values were expected to be found between the two regression lines.

3.2.4 Oxygen and Hydrogen isotope ratio

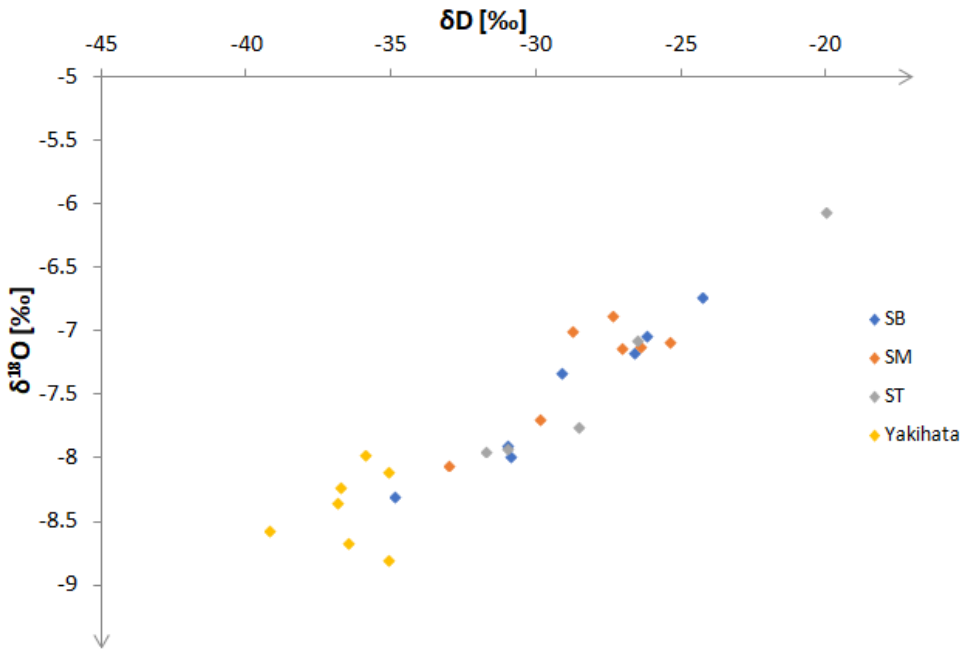

Figure 3.27: Oxygen and Hydrogen isotope ratios of snow

The snow isotopic composition was different in the forested slope and in the *Yaki* site. The lighter Hydrogen and Oxygen isotopes were present in a higher proportion in the *Yaki* site, resulting in lower $\delta^{18}O$ and δD values. All *Yaki* samples were between -8 and -9 ‰ and between -35 and -40 ‰, respectively. The snow of the forested sites was heavier and ranged between -6 and -8.3 for $\delta^{18}O$ and between -35 and -20 for δD. The heaviest water molecules were measured at *ST*, the lightest at *SB*. No connection in time series was found for any of the four spots. The isotope ratio at different spots varied without any pattern, neither increased nor decreased with ongoing snowmelt.

3.3 Meteorological data

Precipitation, air temperature and snow depth showed the highest annual variability. All meteorological conditions and their variability were averaged for every year from 2011-2020. The summer in YURF is usually humid and hot, the winters are moderate with high precipitation.

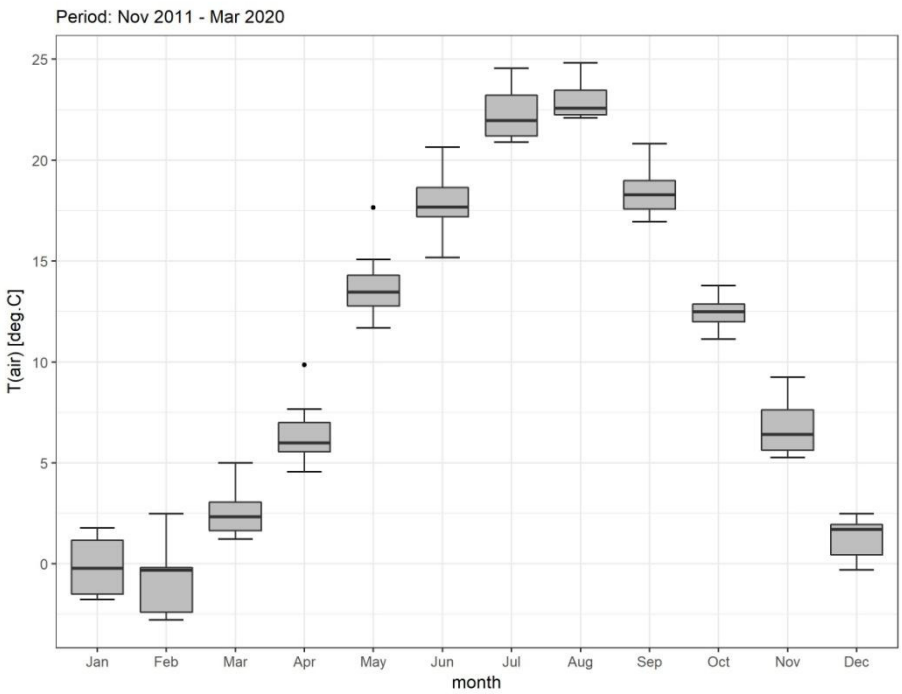

Figure 3.28: Temporal variability of air temperature in YURF

Average air temperature was lowest in January and February slightly below 0 °C and highest in August above 22.5 °C. The temperature differences between years were less than 5 °C, which means that snow depth characteristics were not significantly influenced by air temperature.

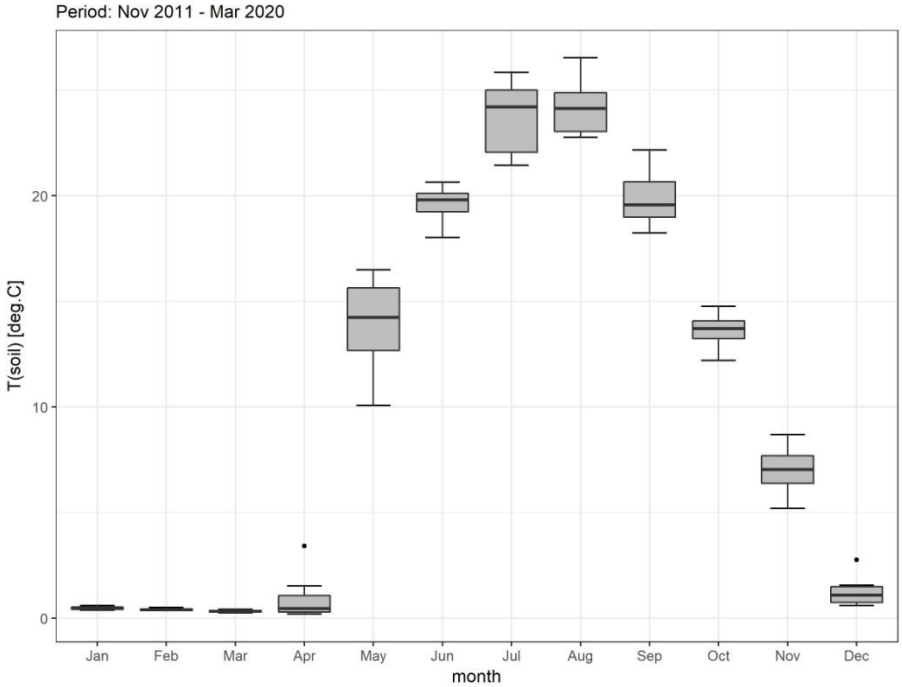

Figure 3.29: Temporal variability of soil temperature in YURF

During the eight years, soil temperature measured at 10 cm, 30 cm and 50 cm never registered values below 0.2 °C. Even the soil surface under snow cover did not show temperatures < 0 °C. Hence, soil did not freeze in winter. Every year, soil temperature was around 0.5 °C in December and January and decreased to 0.2 °C in April until the snow cover disappeared (Figure 3.29). The highest monthly averages of soil surface temperatures were measured at almost 25 °C in July and August, which was higher than the monthly averages of the air temperature of these months. The increase of soil temperature in spring was faster than the decrease in autumn. The temperature decreased from September to December at a constant rate of approximately 6 °C per month.

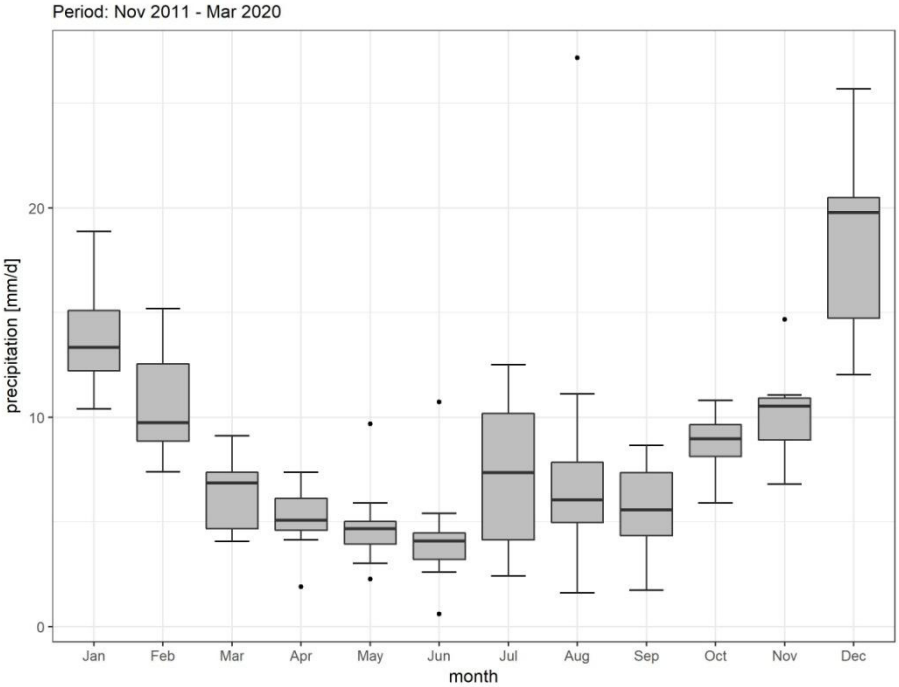

Figure 3.30: Temporal variability of precipitation in YURF

Precipitation varied substantially among years, especially in summer and winter the differences can be 10 mm/d or more, resulting in more than 300 mm for the whole month. December had the highest precipitation of all months with approximately 20 mm/d, but at the same time the highest variability (Figure 3.30). January had the second highest precipitation, followed by all summer and autumn months, which had similar precipitation of 5 to 10 mm/d. The lowest precipitation, linked to the smallest variation, occurred in spring, with the lowest value of 4 mm/d in June.

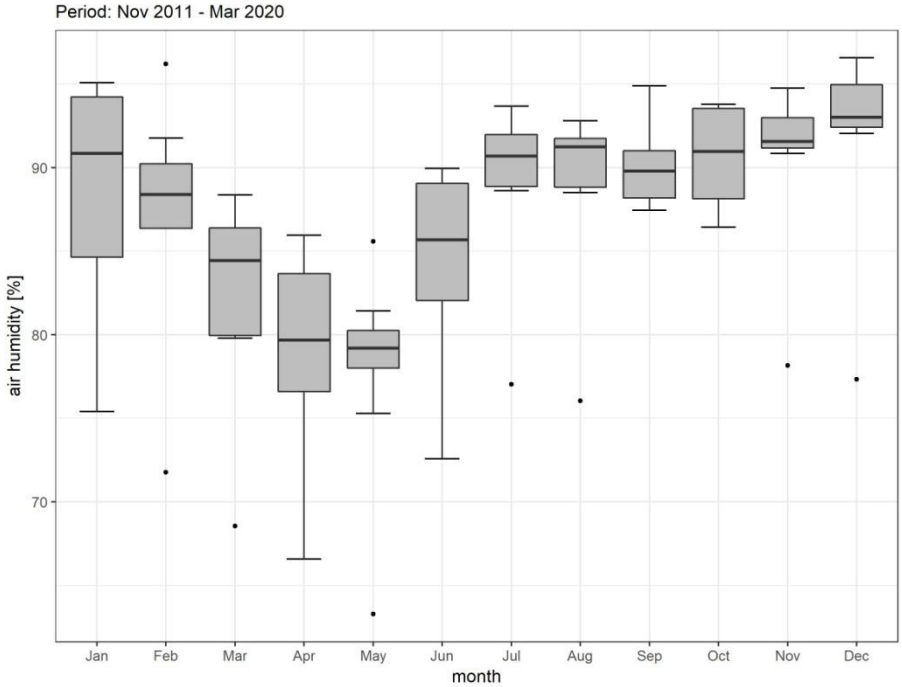

Figure 3.31: Temporal variability of air relative humidity in YURF

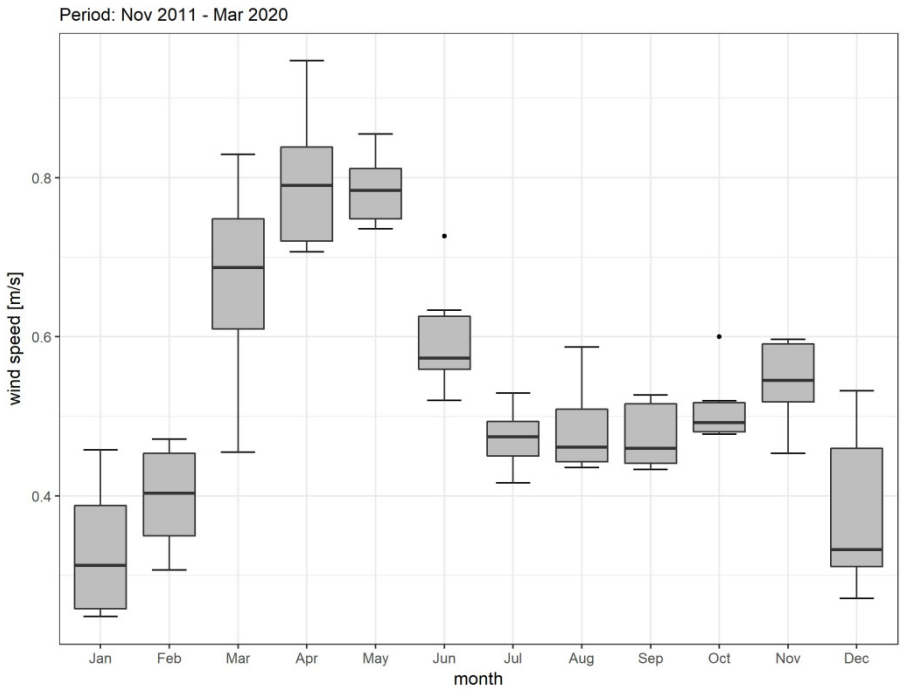

Figure 3.32: Temporal variability of wind speed in YURF

Wind speed reached its highest monthly average value (0.8 m/s) in April and May, while it was lowest (0.3 m/s) in December and January (Figure 3.32). The average wind speed was between July and November relatively constant at 0.5 m/s. Variations between years were small in summer and autumn but high in March and April. While wind speed had the highest values in April and May, the relative humidity was lowest in these months (Figure 3.31). The

lowest air humidity was in May with 80 % and the highest in December was 93 %. Several days in winter had relative humidity of almost 100 %, but the monthly average was mostly 90 %. Relative humidity decreased almost linearly between January and April from 90 % to 80 %.

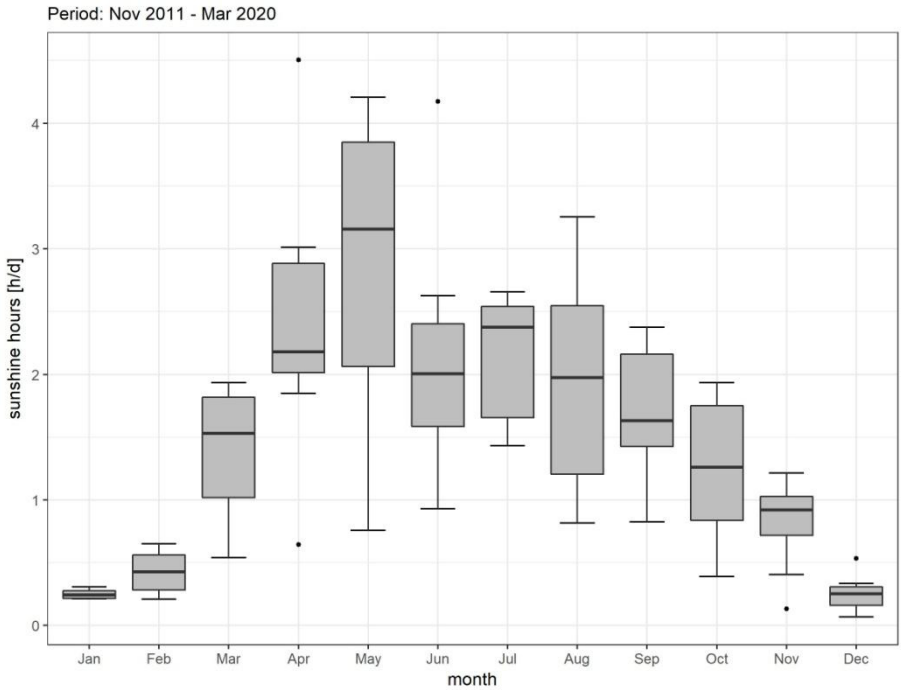

Figure 3.33: Temporal variability of sunshine hours in YURF

Due to snowfall and clouds, sunshine hours averaged less than 1 hour per day in winter. The sunshine average peaked in May, and the highest variability, with more than 3 h/d, occurred in the same month. Similar to the relative humidity, sunshine hours maintained an almost constant average in the summer and autumn months.

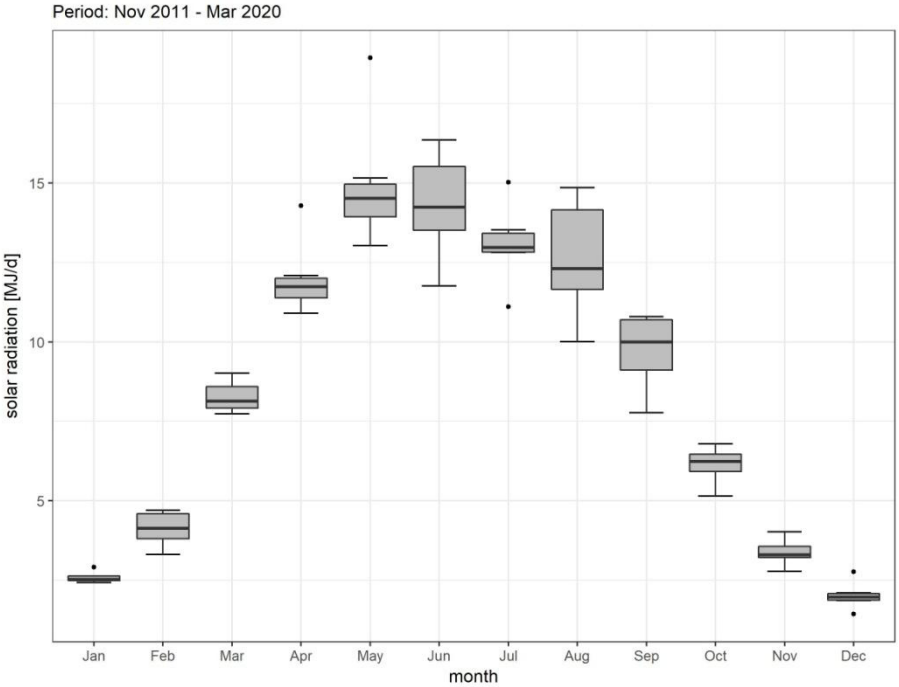

Figure 3.34: Temporal variability of solar radiation in YURF

The solar radiation was the lowest in December (2 MJ/d) and the highest in May and June (almost 15 MJ/d). The trend of the solar radiation followed the typical pattern for the northern hemisphere, having the highest values in summer and the lowest in winter. However, solar radiation was not as constant from June to September, as the sunshine hours were.

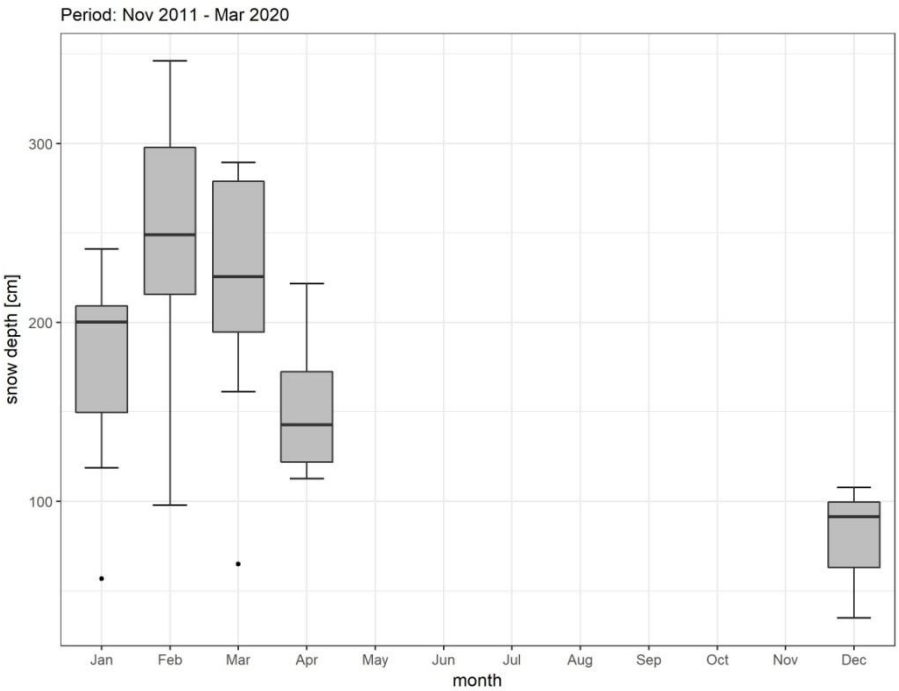

Figure 3.35: Temporal variability of snow depth in YURF

Snow depth was highest in February, but the variation between years was also highest in this month, especially the winter 2019/2020 with significantly smaller snow depth influenced the average considerably (Figure 3.35). The winter 2019/2020 was regarded as outlier for the months January and March. In general, snow depth variations from year to year were less than 1 m on monthly average. May was disregarded in Figure 3.35, because the snow cover disappeared already before May in most years, and in the remaining years within the first or second week of May. Therefore the monthly average would be unrepresentative for the graph.

3.3.1 Temperature analysis

The lowest recorded daily average air temperature since November 2011 was -7 °C and was associated with a soil temperature of 0.4 °C. The highest recorded air temperature was associated with significantly lower soil temperature and was measured during the snowmelt season in April 2012 (daily averages: T_{air} = 15 °C, T_{soil} = 0.2 °C). The linear regression (Equation 3.1) between air and soil temperature was calculated only with the daily data without snow coverage. It shows an almost 1:1 relationship between air and soil temperature (R^2 = 0.89). Since hourly soil temperature showed lower fluctuations than air temperature, differences in daily average datasets were usually caused by day-night variations. This also explains the scatter of data points (Figure 3.36).

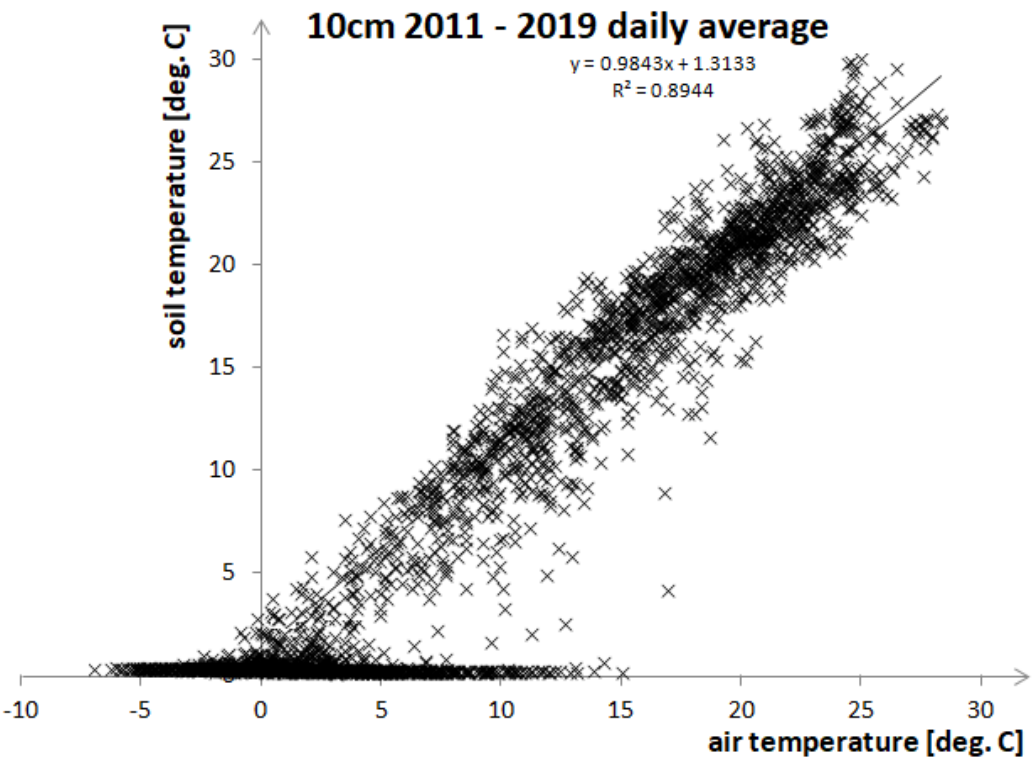

Figure 3.36: Daily average air temperature versus soil temperature

$$\textbf{Equation 3.1}: T_{soil} = 0.98 * T_{air} + 1.31\ °C$$

The linear regression of Figure 3.36 shows that soil temperature was similar to air temperature, being on average 1.3 °C higher than air temperature. Furthermore, variations in daily average air temperature and soil surface temperature (10 cm) were not significantly different (Figure 3.36).

Monthly average air and soil temperatures for the period 2011 – 2019 were calculated and plotted in order to analyse changes over the year (Figure 3.37). Soil and air temperature have been compared because the soil temperature was constant in winter. With increasing air temperature in spring, the difference between soil and air temperature increased until the snow has melted. To eliminate the effect of day-and-night cycles on the temperature, monthly averages were calculated and represented in box and whiskers plots.

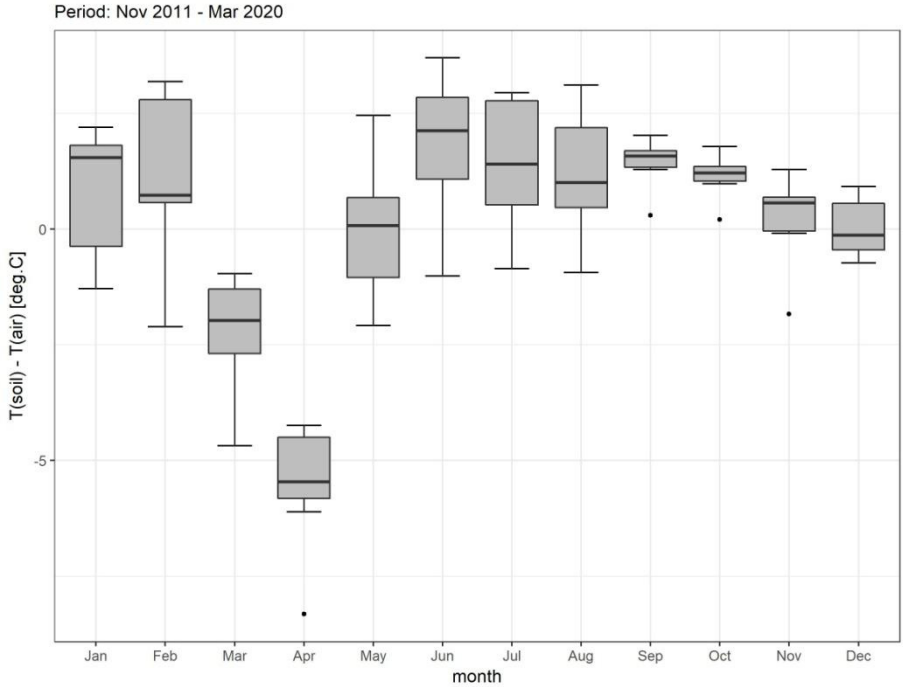

Figure 3.37: Temporal variability of differences between soil and air temperature

Except for March and April, soil temperature was always higher than air temperature (Figure 3.37), with the temperature difference never exceeding 2.5 °C. In March soil temperature was 2 °C lower, in April 5 °C lower than air temperature. The highest variation between temperature differences was found in February (-2.1 °C to 3.2 °C) and the lowest in October (0.2 °C to 1.8 °C) (Table 3.3).

Table 3.3: Monthly soil and air temperature differences from 2011-2019

Month	2011	2012	2013	2014	2015	2016	2017	2018	2019
January	-	3.0	2.9	1.8	-1.3	1.3	1.0	2.2	1.6
February	-	3.2	2.8	2.0	-2.1	0.6	0.6	2.8	0.7
March	-	-0.7	-0.9	-1.1	-4.7	-1.5	-1.1	-2.3	-1.9
April	-	-5.1	-4.4	-5.4	-8.4	-4.3	-5.5	-6.2	-4.7
May	-	-1.6	-0.8	0.2	-2.1	0.1	2.1	0.1	2.5
June	-	3.7	1.5	-0.2	-1.0	2.2	2.8	3.6	2
July	-	2.9	0.2	0.5	-0.8	0.5	3.0	2.2	2
August	-	3.1	0.8	0.6	-0.9	0.3	2.7	2	1.3
September	-	1.4	1.6	1.3	0.3	1.9	2.0	1.6	1.6
October	-	1.3	1	0.2	1.1	1.8	1.5	1.1	1.3
November	-0.5	0.7	-0.1	-1.9	0.6	0.6	0.6	0.6	1.3
December	1.1	0.9	-0.2	-0.8	0.3	-0.1	0.8	0.6	-0.6

All values are calculated from monthly average air Temperature (T_{air}) and soil Temperature (T_{soil}) with the formula: $T_{diff} = T_{soil} - T_{air}$. All values are given in °C.

The year 2015 was significantly warmer than the other years (monthly averages > 0 °C), which resulted in negative values for $T_{soil} - T_{air}$. Hence, most of the values of 2015 were

considered as outliers, except in February, which explains the long whiskers (Figure 3.37), while in November and December the difference between soil and air temperature was small (Table 3.3). When the first snow fell, it cooled the surface, which resulted in negative temperature differences, because air temperature decreased faster than soil temperature. As air temperature continued to decrease, the difference became positive, until snowmelt started. Ongoing snowmelt resulted again in negative differences that increased until the end of the snowmelt due to increasing air temperatures. Soil temperature in April was at least 4.3 °C lower than air temperature, a temperature difference which increased by 3 °C to 5 °C in March. The winter 2014/2015 was warmer than all other winters, resulting in negative differences throughout all months.

3.3.2 Rain/snow ratio

Monthly precipitation was evaluated for the four winter months December, January, February and March (Table 3.4). During the winters 2015/2016 and 2016/2017 the rain gauge malfunctioned during that period. Therefore, the detected precipitation and especially snowfall were significantly smaller than in reality. Snow depth in both years was similar to other years, therefore the precipitation data did not reflect snow depth, and thus the rain/snow ratio was not representative. Because of the malfunction and the incorrect data, these two years were not plotted in Figure 3.38.

The four-month average of rain/snow ratio (Table 3.4) showed an increase in rain and simultaneously a decrease in snowfall from 2011/2012 to 2019/2020. The rain/snow ratio was 0.47 in the first years and increased to a ratio of 1.01 in 2019/2020 (Figure 3.38). This means that in the winter 2019/2020 the same amount of rain and snow fell. An increase was found for every month; only in February the ratio increased less than in the other months (Table 3.4). Within every winter season, December and March had higher ratios while they were lower in January and February. However, the total amount of precipitation did not change among years. Total precipitation was around 1500 mm for the four month period for every year, except for the winters 2015/2016 and 2016/2017 when the precipitation meter malfunctioned and the total precipitation was recorded as less than 1100 mm.

Table 3.4: Rain, snow and rain/snow ratio for nine winter seasons

Month	2011/ 2012		2012/ 2013		2013/ 2014		2014/ 2015		2015/ 2016*		2016/ 2017*		2017/ 2018		2018/ 2019		2019/ 2020	
December	179 330	0.54	185 430	0.43	262 336	0.78	338 456	0.74	342 31	11	226 235	0.96	217 438	0.50	335 262	1.28	230 223	1.03
January	82 299	0.27	143 333	0.43	175 254	0.69	87 311	0.28	102 12	8.46	161 28	5.85	210 371	0.57	311 362	0.86	158 165	0.96
February	135 298	0.45	132 257	0.49	52 200	0.26	108 152	0.71	154 69	2.25	192 13	15.4	130 146	0.89	121 195	0.62	145 230	0.63
March	139 211	0.66	106 107	0.99	176 151	1.17	97 130	0.75	72 55	1.32	99 124	0.8	91 44	2.07	83 70	1.19	189 94	2.01
all months	535 1138	0.47	566 1127	0.50	665 941	0.71	630 1049	0.60	670 117	4.03	678 400	1.7	648 999	0.65	850 889	0.96	722 712	1.01
	rain in mm snow in mm		rain/snow ratio															

*The years 2015/2016 and 2016/2017 have low values, because the precipitation meter in YURF did malfunction during these winter periods.
Rain/snow ratio was calculated in the following way: rain ratio= rain [mm] / snow [mm]

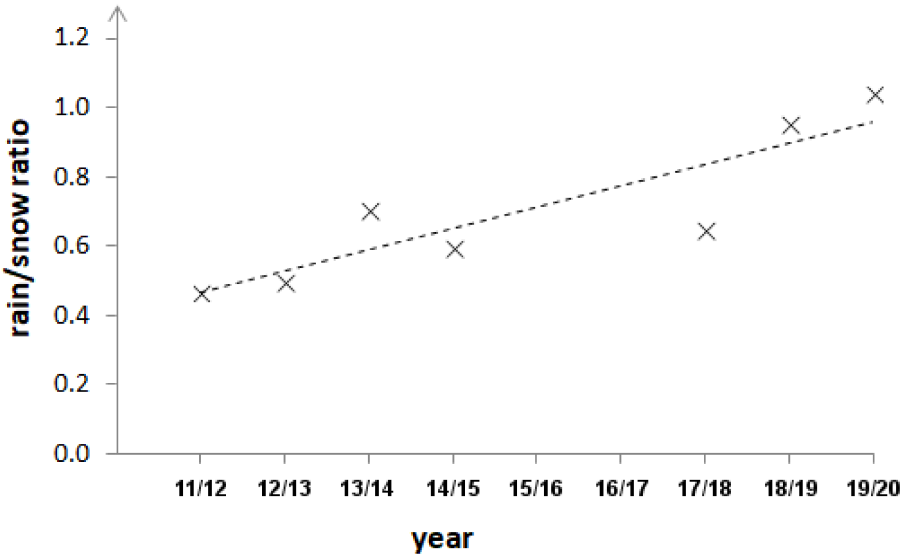

Figure 3.38: Trend of rain/snow ratio in YURF

3.3.3 Winter precipitation and air temperature

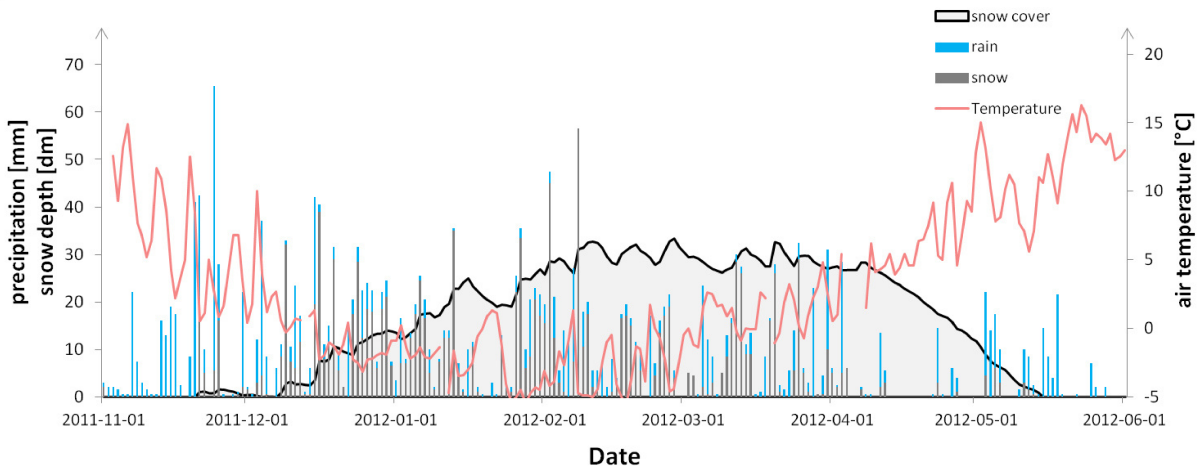

Figure 3.39: Precipitation and temperature variability in the winter 2011/2012

Except in April, precipitation occurred on almost every day during the winter season 2011/2012. The largest snowfall event was on February 8, 2012 with 56.5 mm. In almost every precipitation event, a small proportion was rain, even in December and January, when air temperature was below 0°C. Minimum daily average air temperatures were -5 °C between the middle of January and end of February, and in January the temperature was below 0 °C on most days. Three peaks in snow depth were recorded in February, each of them with more than 3 m of snow depth. The first snow accumulated already in the last week of November 2011, the snowmelt started in the second week of April and ended in the middle of May.

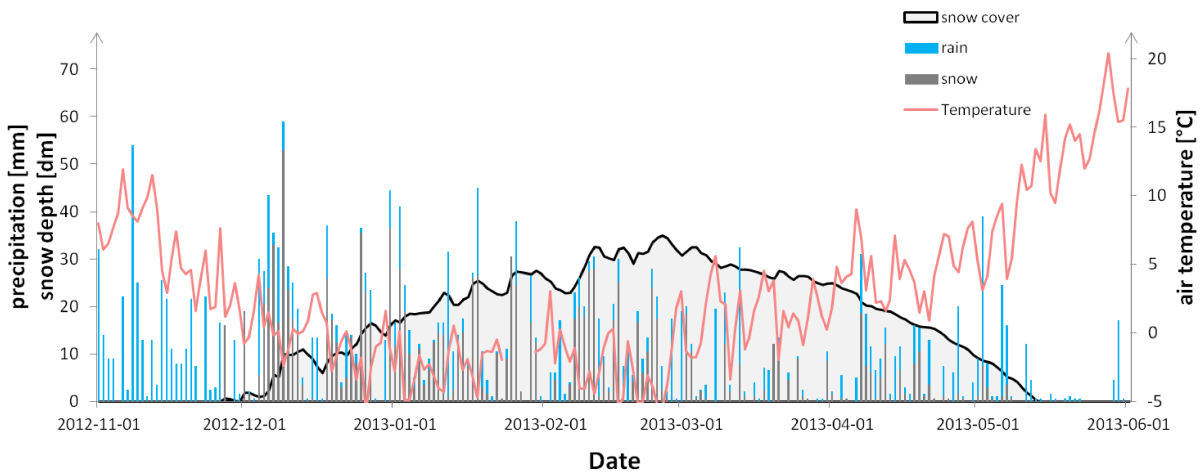

Figure 3.40: Precipitation and temperature variability in the winter 2012/2013

The number of days with precipitation in the winter 2012/2013 was higher than in the previous year. However, precipitation events were not as intense. The most intensive event occurred at the beginning of the snow accumulation period on December 9, 2012 with 53 mm. Rain and snow fell throughout the whole winter period, snow was also still falling in April, when the air temperature was already higher than 0 °C and snow depth decreased. The minimum daily average air temperature was -5.5 °C and was reached in the end of February, similar to the year before. However, air temperature was six times lower than -5 °C during the winter, representing more cold days than in most of the other winter seasons. First snow accumulated in the beginning of December and the snowmelt ended after the second week of May. The maximum snow depth was reached on February 25 with 3.5 m. The snowmelt period was longer, but not shorter than in the previous winter season.

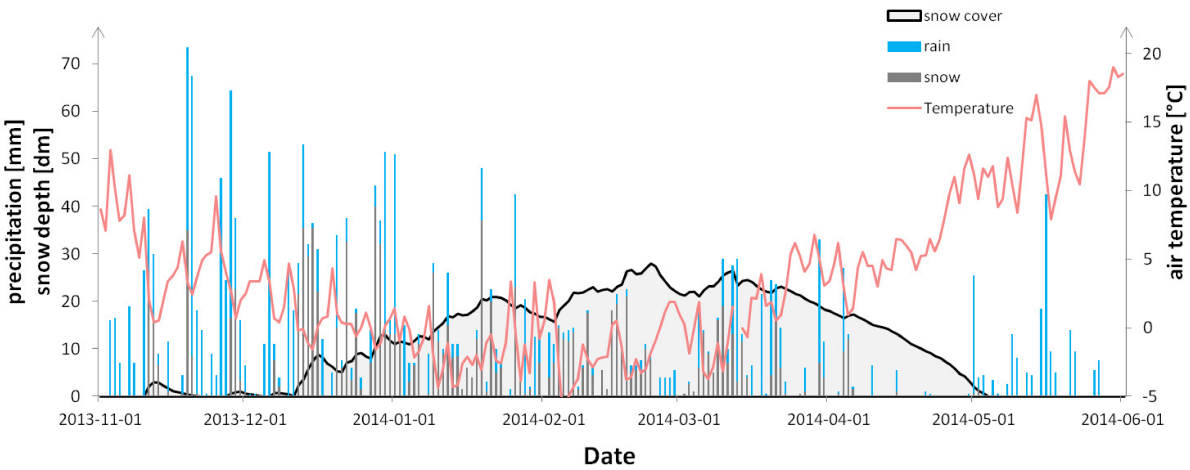

Figure 3.41: Precipitation and temperature variability in the winter 2013/2014

The winter 2013/2014 was dominated by rain events and less snowfall in mid winter. First snow fell already in the second week of November 2013, but melted again. Snowfall was high in the early winter but total precipitation was low in February 2014 and from April on. In March rain and snowfall were almost evenly distributed. The minimum air temperature of -5 °C was reached in the beginning of February and increased afterwards faster than in the winter 2012/2013. The daily average air temperature was already above 0 °C from the second week of March 2014 on. Snow depth was less than in the two previous years with its maximum of 2.8 m on February 23. Snowmelt ended by the end of April.

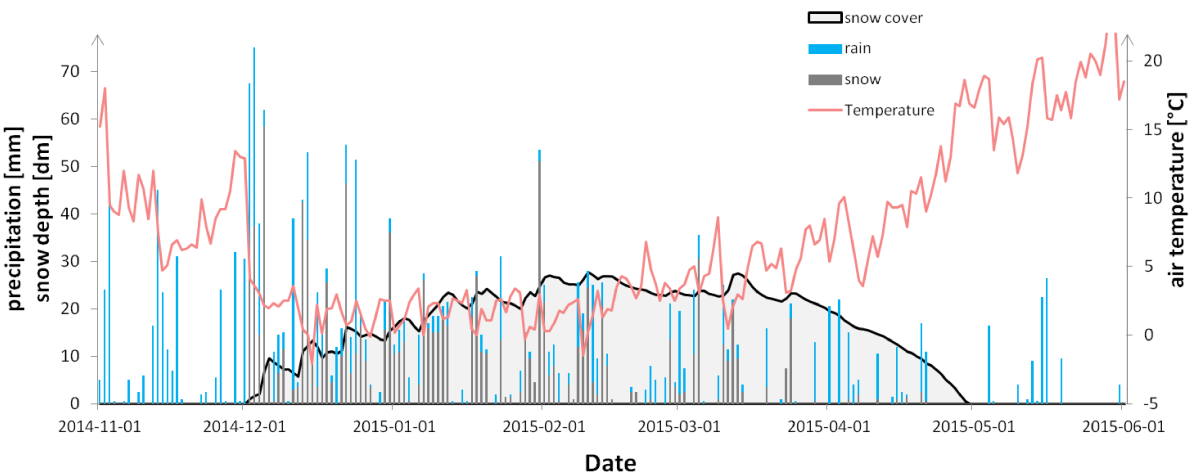

Figure 3.42: Precipitation and temperature variability in the winter 2014/2015

The total precipitation of the winter 2014/2015 was insignificantly lower in comparison to the previous years. The first days of January 2015 had high precipitation of more than 60 mm on three days and still more than 30 mm on the fourth day. There was less rain during the snow cover period, but also no snowfall during the snowmelt season. The air

temperature was always consistently above 0 °C, which indicates that a lot of snowmelt occurred during winter. However, the snow depth was similar to the winter 2013/2014. The maximum snow depth was 2.8 m on February 10, and the snow depth remained relatively stable in the following weeks. The snowmelt period was faster than in the previous years, especially when the snow depth was < 1 m.

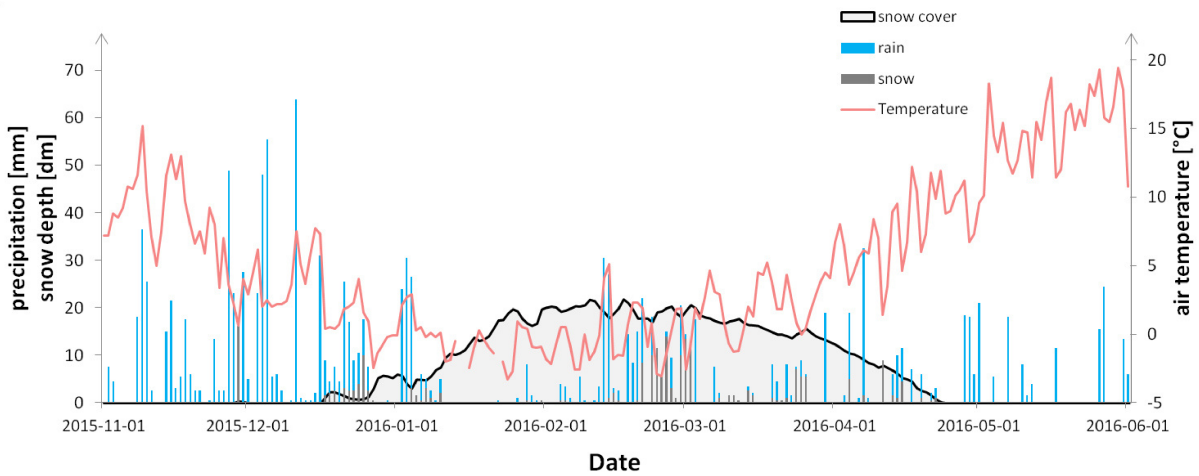

Figure 3.43: Precipitation and temperature variability in the winter 2015/2016

The winter 2015/2016 had the second smallest and second shortest snow cover. Snow accumulation started in the middle of December 2015 and snowmelt ended in the last week of April. Air temperature fluctuated around 0 °C between January and middle of March and increased to 10°C during the snowmelt season. Snow depth was almost constant for about one month from the beginning until the end of February. The maximum of 2.2 m was reached on February 10, 2016. The precipitation data was erroneous, as stated earlier (Table 3.4), due to malfunction of the precipitation meter. The error was apparent especially between January 11 and January 27, when the snow depth increased significantly but almost no precipitation was measured.

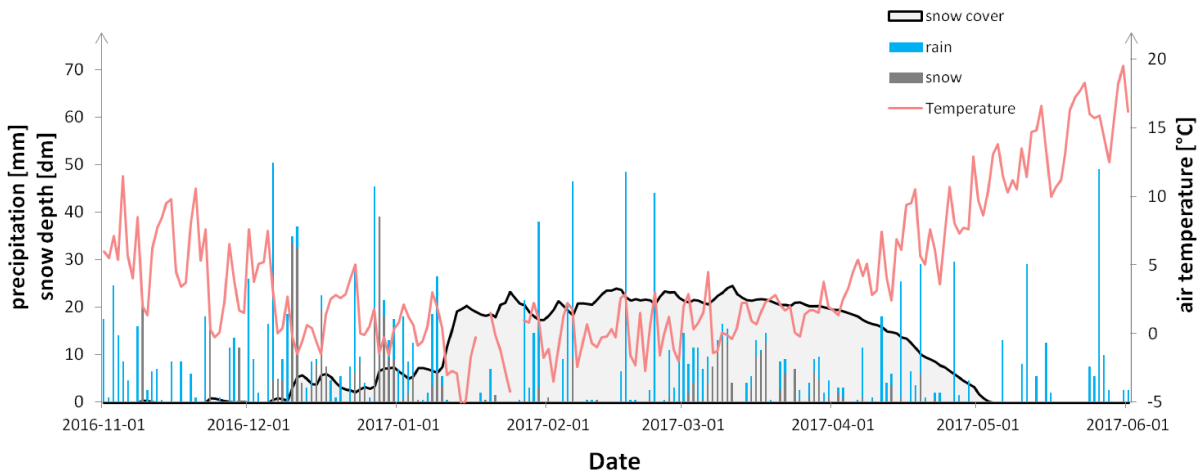

Figure 3.44: Precipitation and temperature variability in the winter 2016/2017

Precipitation data of the winter 2016/2017 was, due to the precipitation meter malfunction, smaller than in the other years. A high volume of rain was detected but especially during the intensive snow accumulation period in the second week of January 2017 the data was corrupted. In general, rain was high also in mid winter. A second snowfall period was detected in March. The maximum snow depth of 2.35 m was reached on February 13 and snow depth was almost constant at 2.1 m between the middle of January and the end of March. Minimum air temperature was -5 °C in the middle of January, but on average around 0 °C during the rest of the winter.

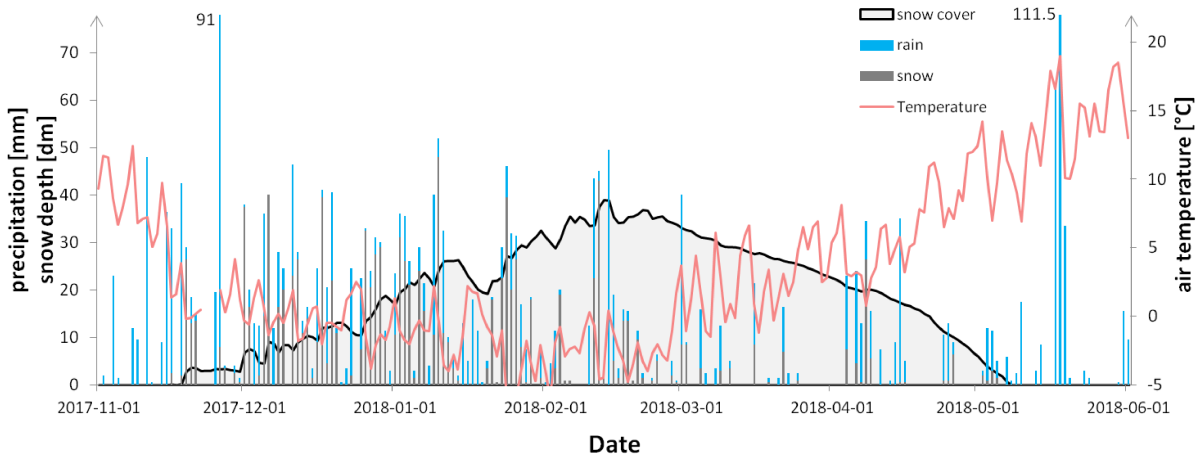

Figure 3.45: Precipitation and temperature variability in the winter 2017/2018

The winter 2017/2018 had the highest snow accumulation of all the years. The total precipitation was 1600 mm between December and March on average (Table 3.4), but the rain/snow ratio was below the trend, and lower than in the following years (Figure 3.38). Two events of extreme precipitation were detected, the first on November 26 with 91 mm,

the second on May 18 with 111.5 mm. The snow cover reached the maximum snow depth of 3.9 m on February 13, which was significantly higher than the maximum snow depth of the other years. The snowmelt period started one week after the peak in snow depth. Air temperature was significantly lower than in the previous years, with an average of -3 °C, and fell below -5 °C three times; the minimum of -6.3 °C was recorded on January 25.

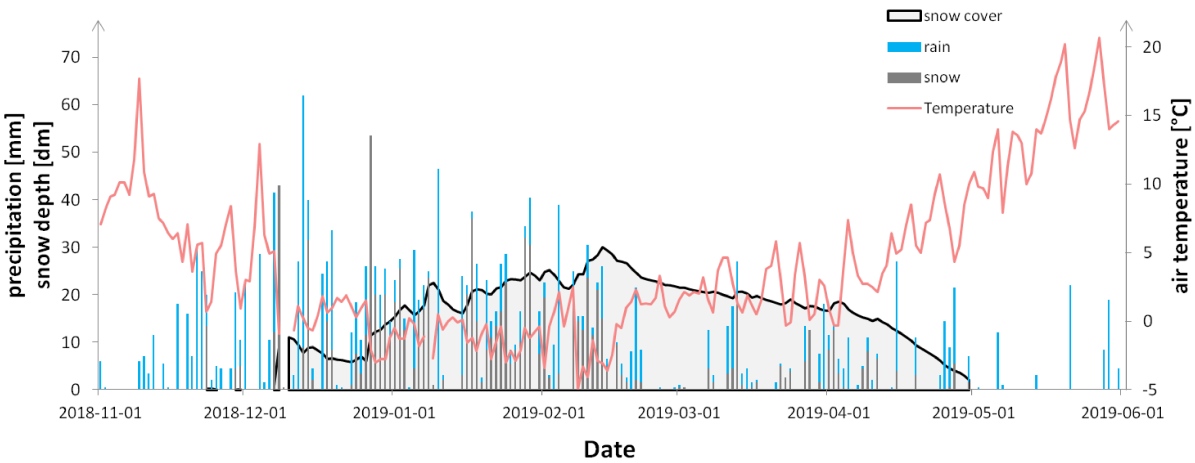

Figure 3.46: Precipitation and temperature variability in the winter 2018/2019

The winter season 2018/2019 showed an increasing intensity of precipitation from the beginning of November until the mid of December, where the precipitation peaked with 62 mm. The intensity of events decreased gradually until the last week of February, shortly after the maximum snow depth. The last week of February and the first week of March had almost no precipitation, as well as the third week of March. The ratio between rain and snowfall was higher than in all previous years. Nevertheless, snow cover peaked at 3 m on February 13. Since snow accumulation started in the first week of December with a heavy snowfall event of 55 mm within two days, snow depth increased faster than in other years, with snowmelt ending exactly on April 30. Air temperature was around -1 °C from the beginning of December until the beginning of February, when also the minimum air temperature of -5 °C was measured. After that day air temperature increased significantly and was around 2 °C until the beginning of April.

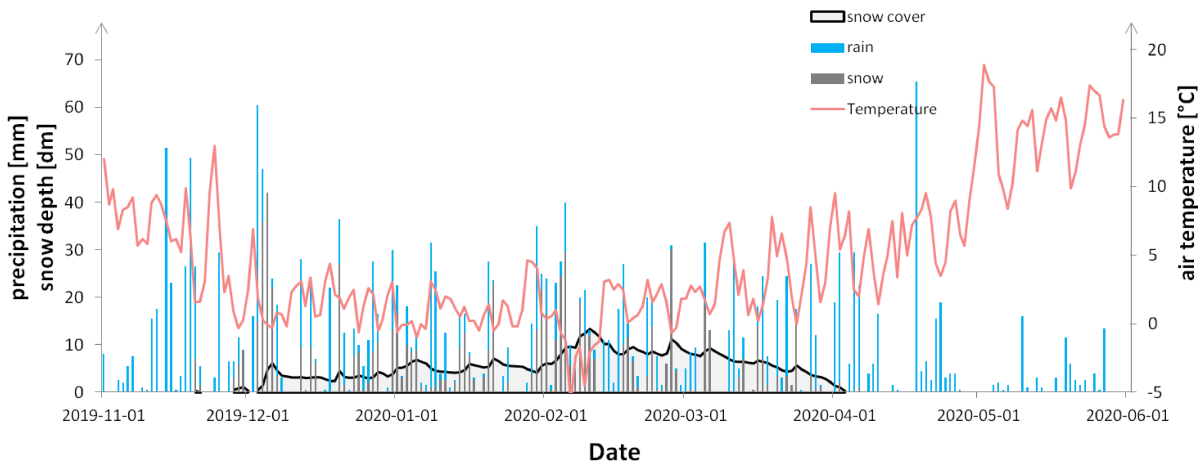

Figure 3.47: Precipitation and temperature variability in the winter 2019/2020

Meteorological conditions were unusual in the winter season 2019/2020. Total precipitation from December until end of April was 1400 mm, lower than in most of the other years. However the major difference was that precipitation occurred on almost every day throughout the winter season. Snow and rain fell almost equally. High air temperatures of approximately 2 °C were measured for almost the whole winter, causing constant snowmelt and therefore immediate decreases in snow depth after snowfall events. During the second week of February 2020 the air temperature became significantly colder and reached the minimum of -5 °C. The maximum of snow depth was recorded in the same time period, with 1.3 m on February 10 significantly lower than in all of the other recorded winters. After February 12, air temperature increased again and snow depth decreased. The snowmelt season could not be identified clearly, because snow fell on many days in March, increasing the snow depth during the snowmelt season. Since the snow cover was less than 1 m before the snowmelt season started, the decrease in snow depth was slower because snow melted already before April, when air temperatures were still < 5 °C.

3.3.4 Manual snow density measurements

3.3.4.1 Snowmelt season 2019 – *Yaki*

The snow depth and density were measured every week in the *Yaki* site and the *Isle* site. Snow density measurements were started shortly after the maximum snow depth of the winter was reached. The increment sampling depth was 10 cm, the total snow depth between the *Yaki* and the *Isle* site differed only insignificantly on most of the sampling days.

Three samples per depth were averaged and the average snow density of both sites is shown in the following figures.

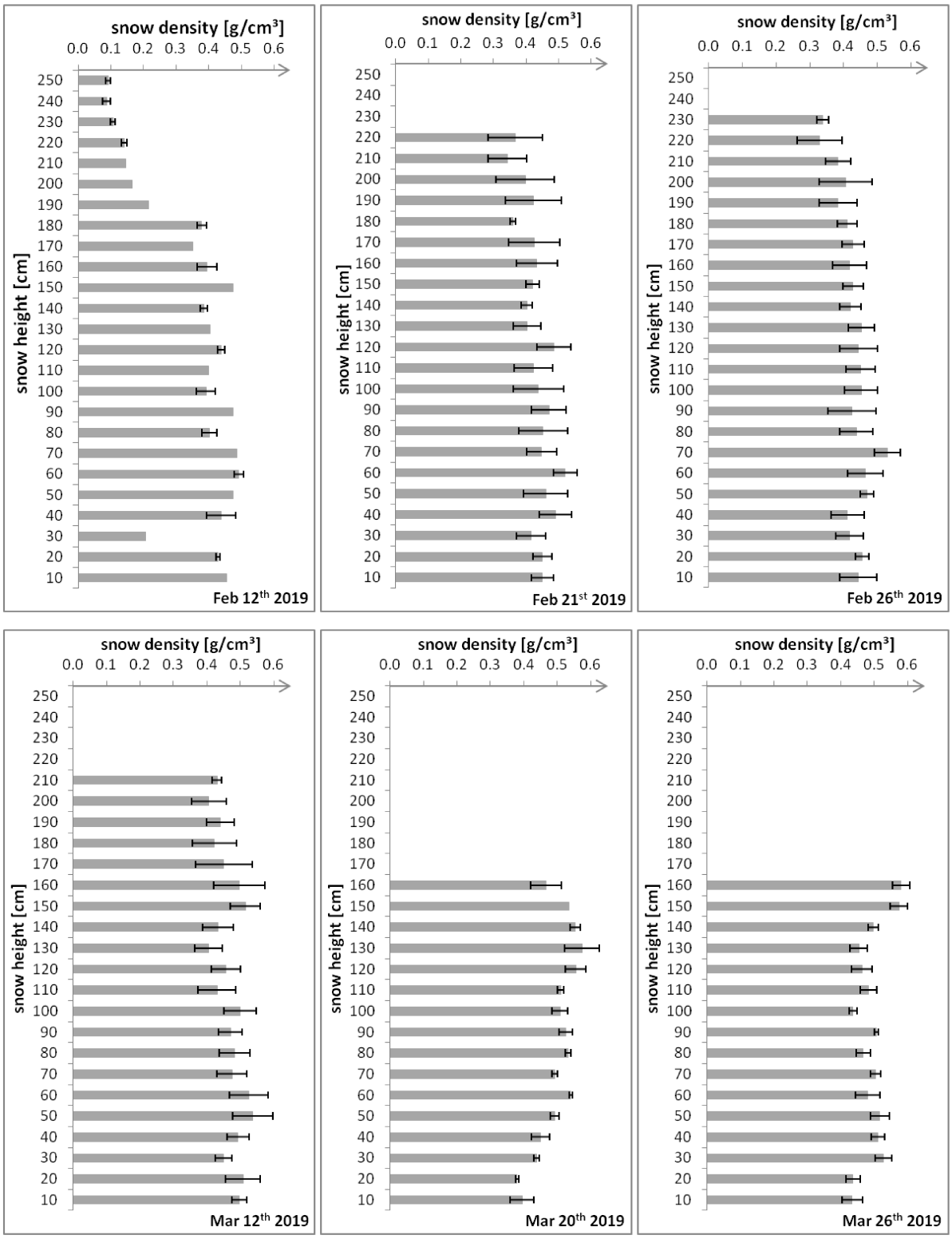

Figure 3.48 a-f: Snow density profiles of the sites *Yaki* and *Isle* (2019)

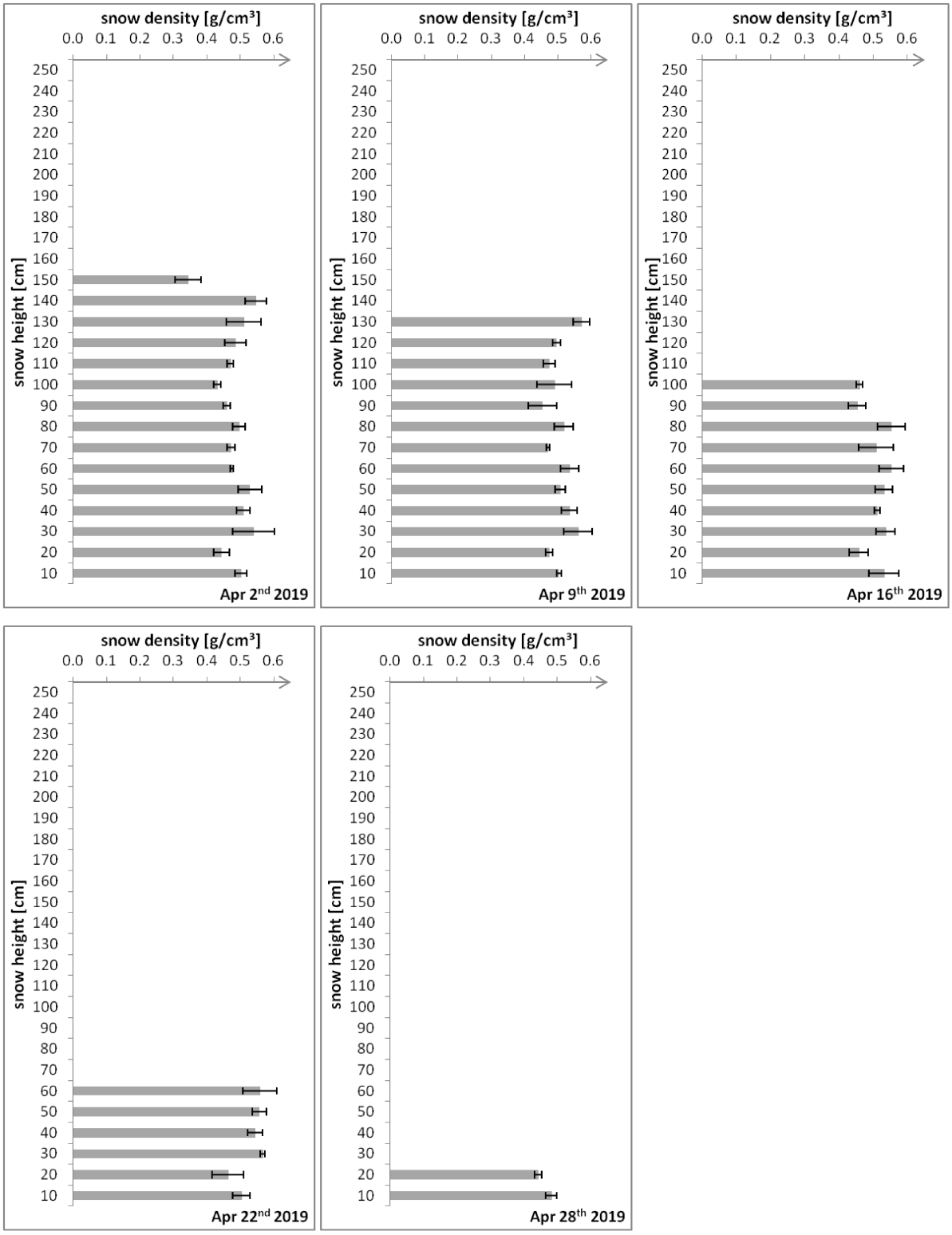

Figure 3.48 g-k: Snow density profiles of the sites *Yaki* and *Isle* (2019)

The maximum snow depth was measured on the first sampling day, February 12, 2019 (Figure 3.48 a). The top 60 cm were fresh snow with snow densities < 0.2 g/cm³. All samples below 190 cm had snow densities of more than 0.35 g/cm³, except at 30 cm depth. The samples at 30 cm depth had also a lower density than the surrounding layers in the following

weeks (Figures 3.48 b-e). The sampling on February 12 was less representative, because replicate samples were only taken every 20 cm. The remaining samplings were done at 10 cm increments and resulted in more homogeneous snow density values. On February 21 the top of the snowpack already reached densities of more than 0.3 g/cm³. Snow density increased for the snowpack slightly with every day.

The snow cover showed a trend of snow density decreasing with depth for March 20, 2019, but snow density increased further on the following sampling days. However, at 20 cm and 70 cm depth, local minima of snow density were measured.

3.3.4.2 Snowmelt season 2019 – *SM*

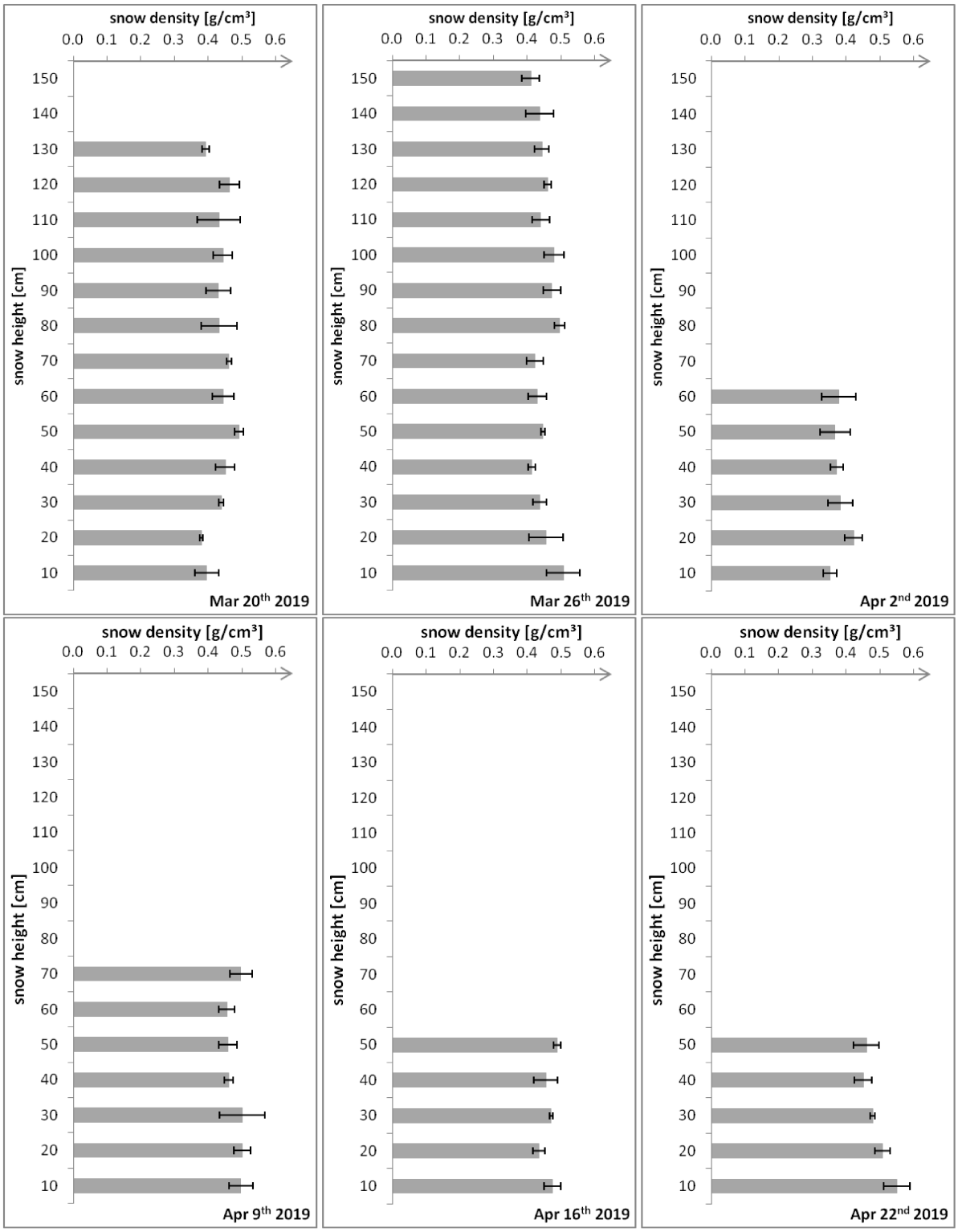

Figure 3.49 a-f: Snow density profiles of the spot *SM* (2019)

On almost every day, snow depth at *SM* was smaller than at *Yaki* and at *Isle*. The snow profile on March 26 had almost the same depth as the snow profiles at the other sites and was also deeper than in the previous week (Figure 3.49 b), even though no snow fell. The

sampling spot differed, because the slope was in the forest and therefore no continuous transect for snow sampling could be assigned. Hence, snow depth depended on the location. Snow depth decreased from April 8 and snow density increased simultaneously. Snow density within the profile was less variable than in the two open sites.

3.3.4.3 Snow cover 2020

The year 2020 had only small snow cover and therefore the snow profiles were shallow with 90 cm and 80 cm (Figure 3.50). Snow density measurements were only conducted on February 19, 2020 and March 3 at the *Yaki* and the *Isle* sites. The snow profile of February 19 showed snow with smaller density in 80 cm and 90 cm height, while the snow density on March 3 was homogeneous from top to bottom. The snow density at each depth was smaller than with the same snow depth in the previous year.

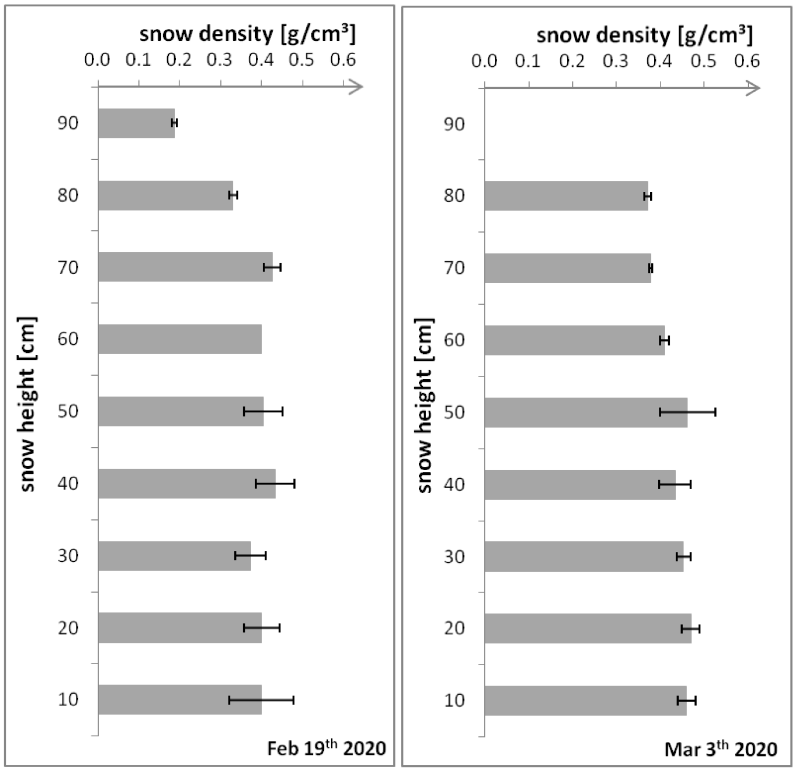

Figure 3.50 a-b: Snow density profiles of the sites *Yaki* and *Isle* (2020)

3.3.5 Modelled snow density and SWE

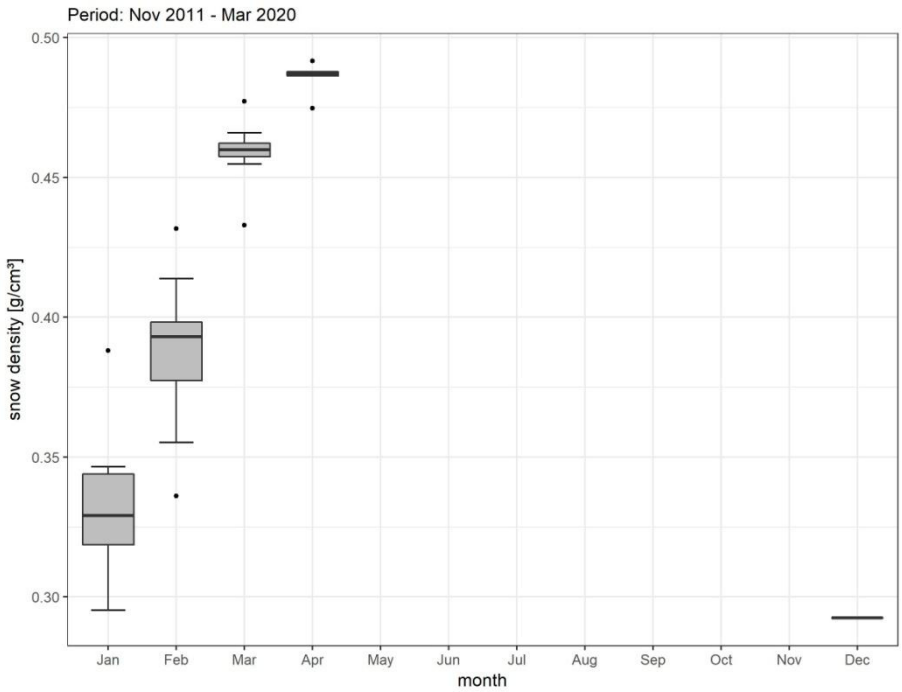

Figure 3.51: Temporal variability of snow density in YURF

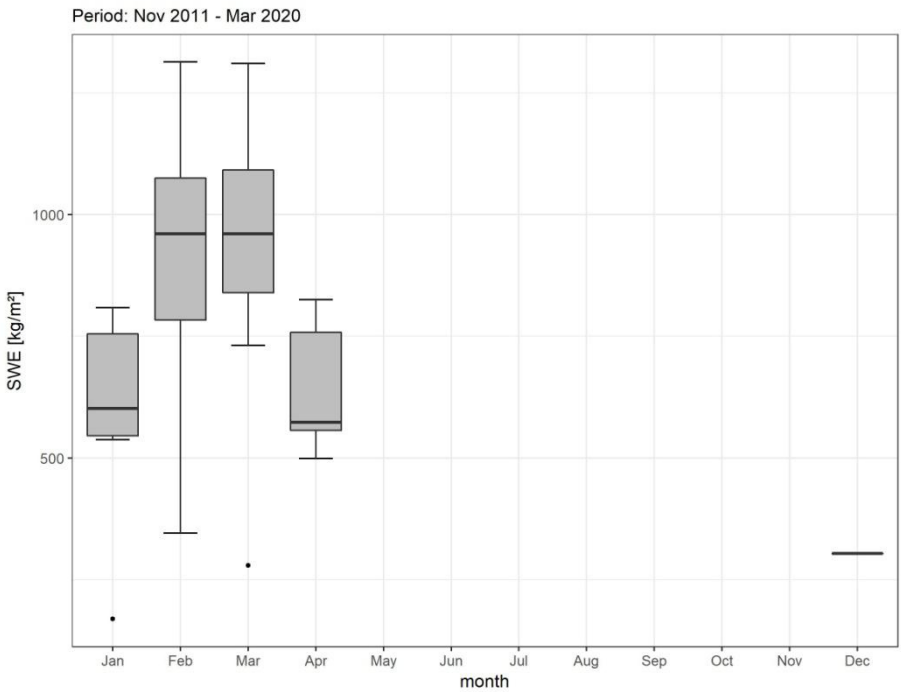

Figure 3.52: Temporal variability of snow water equivalent in YURF

Snow density increased gradually every year. Fresh snow, falling mainly in December and January, had snow densities smaller than 0.3 g/cm³. Snow density of the snowpack increased more in February and March, until it reached the maximum of almost 0.5 g/cm³ in April (Figure 3.51). With increasing snow depth less influence of fresh snow on the snowpack was

observed. Therefore, the differences in snow density between the years became smaller by the end of the winter. The snowmelt season in April caused maximum snow densities in every year; therefore the whiskers in Figure 3.51 were the shortest in April.

SWE was more variable from one year to another. Years with high precipitation and more snowfall had higher SWEs than years with more rain and shallow snow cover. February and March had on average the highest SWE with almost 1000 mm, January and April had SWEs of around 500 mm (Figure 3.52). That means that the increase and decrease in SWE due to snowmelt had almost the same rate. The small SWE values in the plot were from the winter 2019/2020, which had an unusually shallow snow cover and therefore small SWE.

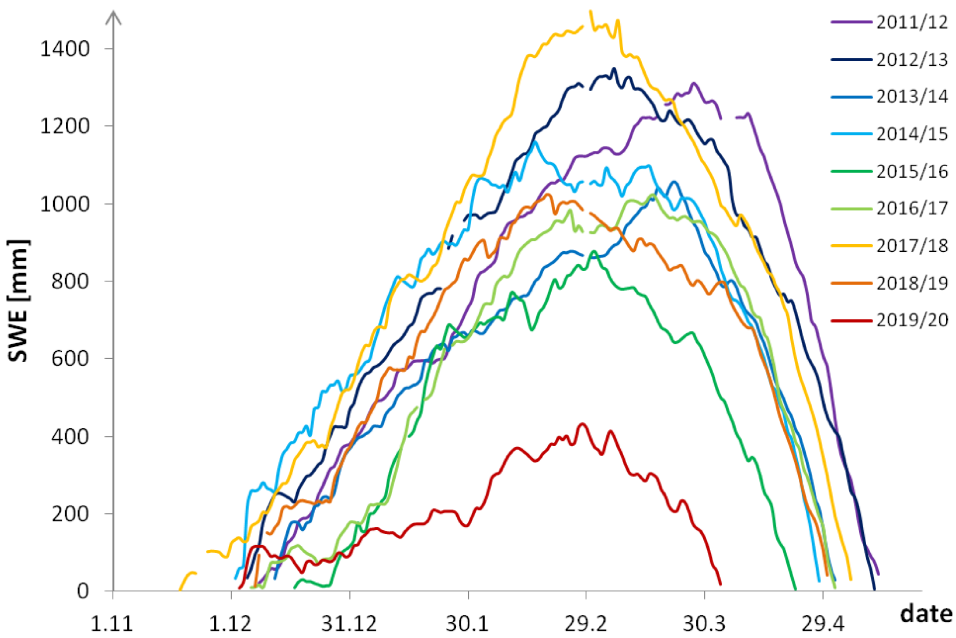

Figure 3.53: Snow water equivalent variability of every year

The highest SWE was calculated, and also measured, in the year 2017/2018 (Figure 3.53), which was also the year with the greatest snow depth (Figure 3.45). Similarly, the smallest SWE was measured in the year 2019/2020, when the smallest snow depth was measured (Figure 3.47). With 400 mm SWE in 2019/2020, the volume of water stored in the snowpack was significantly smaller than in all of the other years, as also detected by the outlier test for the average calculations (Figure 3.52). For most years the maximum SWE was calculated to be at the end of February. In the years 2011/2012 and 2013/2014 the maximum SWE was almost one month later, by the end of March. The maximum SWE was already in the middle of February in the winters 2014/2015 and 2018/2019. It can be said that SWE increased at similar rates in almost every year, and also the snowmelt also occurred at almost the same

rate in every year, because the SWE graphs of the years run almost parallel (Figure 3.53). However, the winter 2019/2020 had significantly lower SWE values and the SWE line was not parallel to the other years.

3.3.6 Degree-day factor

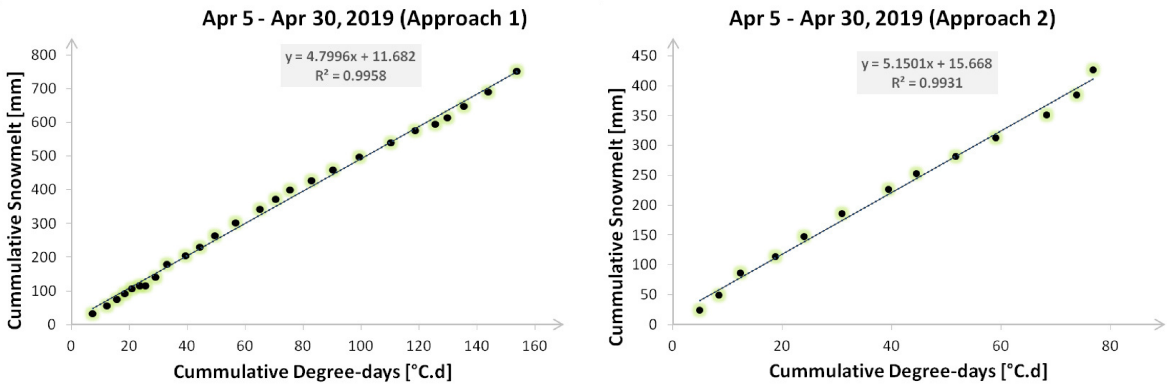

Figure 3.54 a-b: DDF graphs for the snowmelt season 2019

The graphical analysis of DDF values resulted in some short periods for early snowmelt events (7-12 days) and one main snowmelt event (> 20 days) for every year. The main snowmelt event for the year 2019 is plotted as an example in Figure 3.54 a and in Figure 3.54 b using only days without rain. The DDF evaluation graphs of the other years and of the early snowmelt events can be found in the supplementary material section (chapter 9). The formulas for the linear regressions of cumulative snowmelt vs. cumulative Degree-Days and ranged between y = 3x and y = 6x for the gradient of the graph. All graphs showed excellent correlations with $R^2 > 0.99$. The gradient of the slope was equivalent to the DDF and therefore the DDFs in different years had values between 3 mm/d°C and 6 mm/d°C. The mean DDF was found to be 4.5 mm/d°C. The high precision of the linear regression along all data points means further that the DDF did not increase or decrease significantly within one snowmelt season.

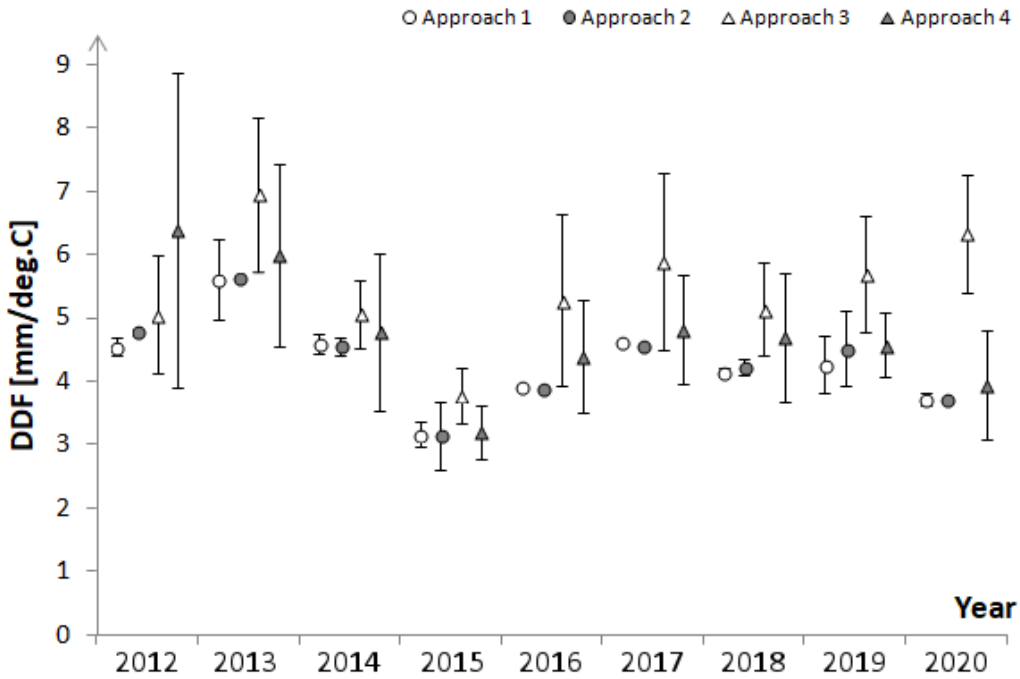

Figure 3.55: Comparison of four different approaches to calculate DDF

The four different approaches to calculate the DDF in YURF produced values between 3 and 7 mm/°C on average. The average values of approaches 1, 2 and 4 were similar for most years, approach 3 had higher values. The error bars of the graphical approaches were small; the method of Martinec (1960) produced larger error bars. Furthermore, the difference between the graphical approach excluding rainy days and the approach including all days is insignificant.

3.4 Link of soil moisture and rain or snowmelt

3.4.1 Winter 2018/2019

Since all three loggers per spot gave similar soil moisture contents (within a 95% significance interval), the average soil moisture per spot and depth was used. The highest soil moisture was measured at 15 cm, 30 cm and 50 cm depth (Figure 3.56) at all measuring points. The soil at the top of the slope (*ST*) had higher soil moisture contents than the soil at the middle (*SM*) and at the bottom (*SB*). At the beginning of winter (November, December) and during the snowmelt season (from April on), soil moisture was highly variable at all spots.

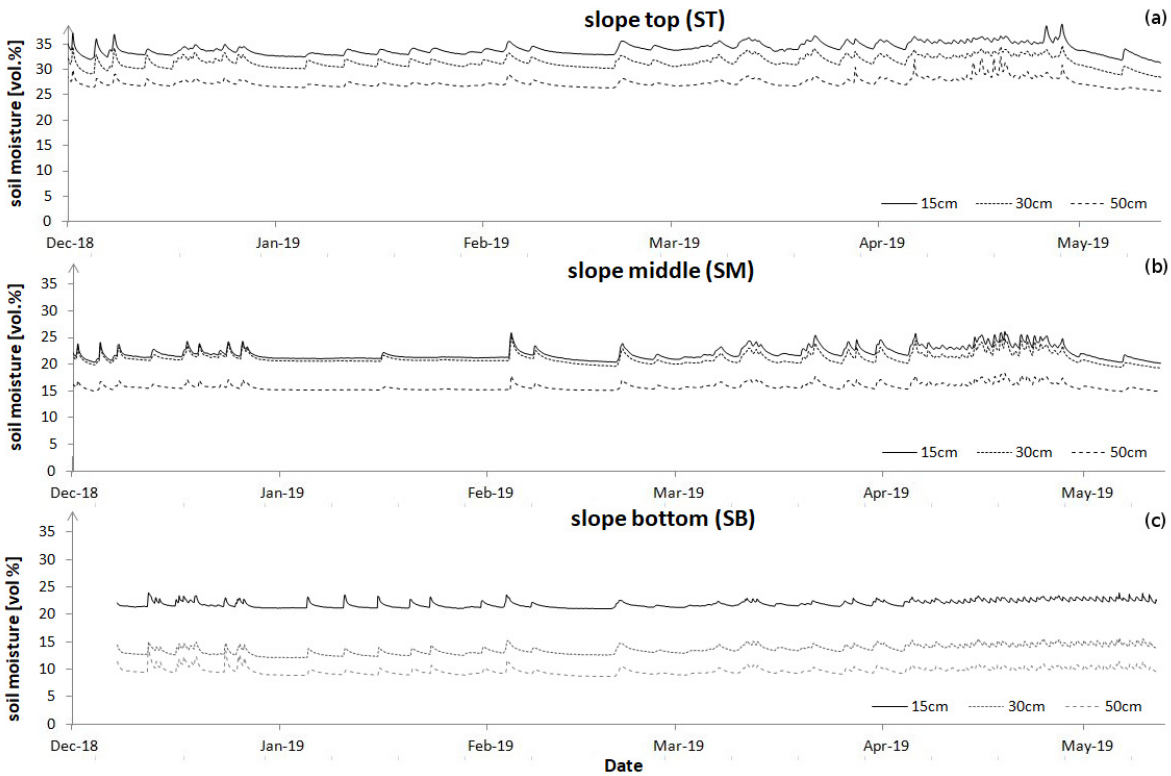

Figure 3.56 a-c: Soil moisture curves for the winter 2018/2019

Soil moisture was stable from the end of December until the beginning of March, meaning that the soil reached the field capacity. The volumetric water contents at 15 cm depth were 21.2 % (SD: 0.17 %) on average at *SB* and 21.3 % at *SM*. Only *ST* (Figure 3.56 a) had higher values with a water content of 33.5 % at 15 cm depth. The higher content of silt and clay at *ST* in comparison to *SB* and *ST* imply more micro pores and better water storage ability. The soil moisture of approximately 22 % at *SB* and *SM* corresponds to a pF value of 1.2 for the soils at the slope, the 33.5 % at ST correspond to a pF value of 1.5.

During the winter, several peaks in soil moisture were observed at all three spots. The number and shape of peaks was different at each spot, based on soil texture and position at the slope. During the period December 24, 2018 to March 7, 2019, 15 sharp peaks were detected at *SB* (Figure 3.56 c), which were in synchrony with the peaks at *ST*. They occurred on the same dates but the increase of soil moisture was slower at *ST*, while fewer peaks were recorded at the middle of the slope (*SM*). In January only one peak was measured at *SM* (Figure 3.56 b), in contrast to the six recorded peaks in the same month at *ST* and *SB*. The amplitude of the peaks at *SM* was greater than that of the peaks at *ST* and *SB*. All peaks recorded at all three spots were recorded at every depth simultaneously. The mean soil moisture content in all spots started to increase slightly with the beginning of the snowmelt.

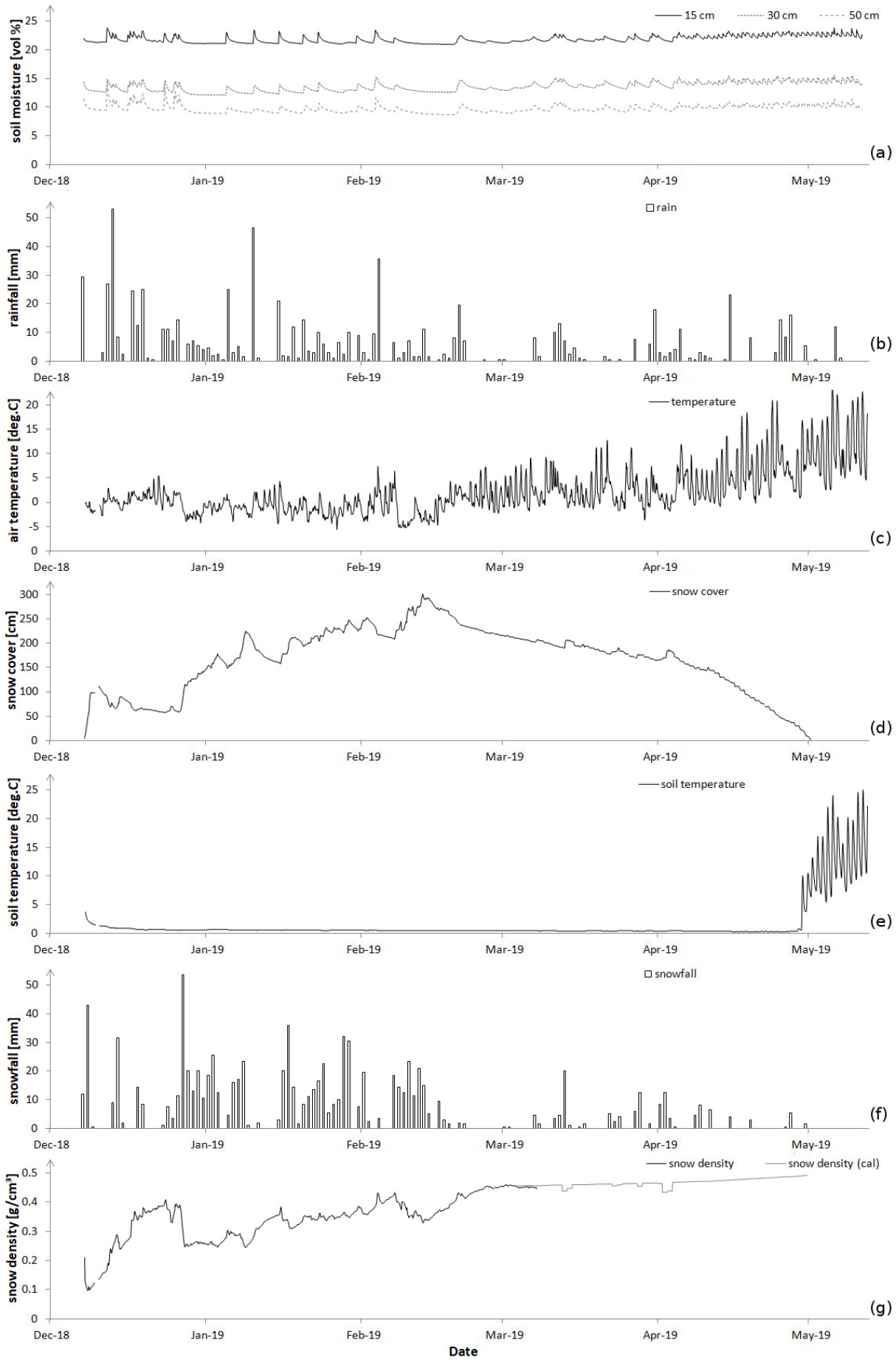

Figure 3.57 a-g: Meteorological conditions of the winter 2018/2019

All 15 peaks at *SB* between December 24, 2018 and March 7, 2019 were analysed. These peaks showed a significant increase of soil moisture at 15 cm soil depth (derived by a *post-hoc Tukey HSD test*). The standard deviations of the average soil moisture content of the three days prior to the peak event had values of 0.11 % or less, except for the peaks on February 4 and 8 (SD: 0.12 %), when the average of 48 hours was calculated (Table 3.5). Since the focus of this study was on winter soil moisture, only peaks after the initial fluctuations of soil moisture and before the snowmelt period were considered. Fluctuations of soil moisture at the beginning of winter and in March were caused by high temperatures, while soil moisture decrease at *ST* and *SM* by the end of April coincided with the earlier end of snowmelt in comparison to *SB*.

Table 3.5: Soil moisture peak analysis of rain and snowmelt events

date of peak	SM increase in vol.%	3 days SD in vol.%	$\Delta t_{increase}$ in h	increase rate in vol.%/h	Precipitation (rain) in mm	SWE change in mm	causing event		
24.12.2018	1.59**	0.11	6	0.2650	19.5 (18.5)	9	rain		
26.12.2018	1.6**	0.11†	16	0.1000	17 (14)	7		both	
05.01.2019	1.98**	0.02	4	0.4950	24.5 (24.5)	15	rain		
11.01.2019	2.35**	0.05	6	0.3917	46.5 (46.5)	14	rain		
15.01.2019	2.12**	0.06	2	1.0600	19.5 (19.5)	38	rain		
20.01.2019	1.52**	0.09	4	0.3800	18 (14)	22	rain		
23.01.2019	1.91**	0.06†	6	0.3183	20 (10)	25	rain		
31.01.2019	1.22**	0.09	4	0.3050	10.5 (8)	18	rain		
04.02.2019	2.2**	0.12‡	10	0.2200	30 (30)	43	rain		
08.02.2019	0.83**	0.12‡	4	0.2075	22.5 (6.5)	29	rain		
21.02.2019	1.45**	0.03	26	0.0558	21.5 (19.5)	14		both	
26.02.2019	0.3**	0.11	8	0.0375	0.5 (0.5)	-9			melt
03.03.2019	0.38**	0.06	16	0.0238	0 (0)	-8			melt
06.03.2019	0.23**	0.04‡	10	0.0230	0 (0)	-11			melt
07.03.2019	0.46**	0.08†	10	0.0460	9 (7.5)	-12		both	

†: The peak was too close to a previous event, only one day (‡: two days) before the event was/were regarded
**: significance level $p < 0.01$

Soil moisture peaks appeared simultaneously at all spots. However, more peaks were recorded at *SB* than at *SM*, and peaks at *SB* were more pronounced than at *ST*. Therefore, the peaks of *SB* were analysed first, and results were compared with the other two spots afterwards. The highest peak at *SB* was caused by a soil moisture increase of 2.35 % on January 11; the smallest peak (0.23 %) was recorded on March 6. Thereafter calculated soil moisture increase rates ranged between 0.02 %/h and 1.06 %/h, with the peaks in February and March taking longer to reach their maximum than the peaks in January.

The SWE of the snowpack, or simply the mass of water, was found to increase during the first eleven peak events and to decrease during the last four (Figure 3.58). All events were classified based on the SWE changes, where the decreasing SWE represented the loss of water as a result of snowmelt processes. Rainfall only occurred on one of the four days with decreasing SWE; therefore three events were labelled as 100% snowmelt induced. The fourth event was labelled as a mixed event, caused by rain and snowmelt combined. SWE increased during the remaining ten events. Out of these events eight increased with more than 0.2 %/h and were labelled as rain induced. Snowmelt processes took longer than rain water needed to infiltrate the snowpack; therefore, the two events with small soil moisture increase rates and moderate SWE increase were also labelled as mixed events. The difference between snowmelt induced and ROS events was significant for both parameters: SWE change and soil moisture increase rate (Figure 3.58). A ROS event of 15 mm precipitation was sufficient to increase soil moisture. On the other hand snowmelt influenced soil moisture when the SWE decreased by 8 mm or more.

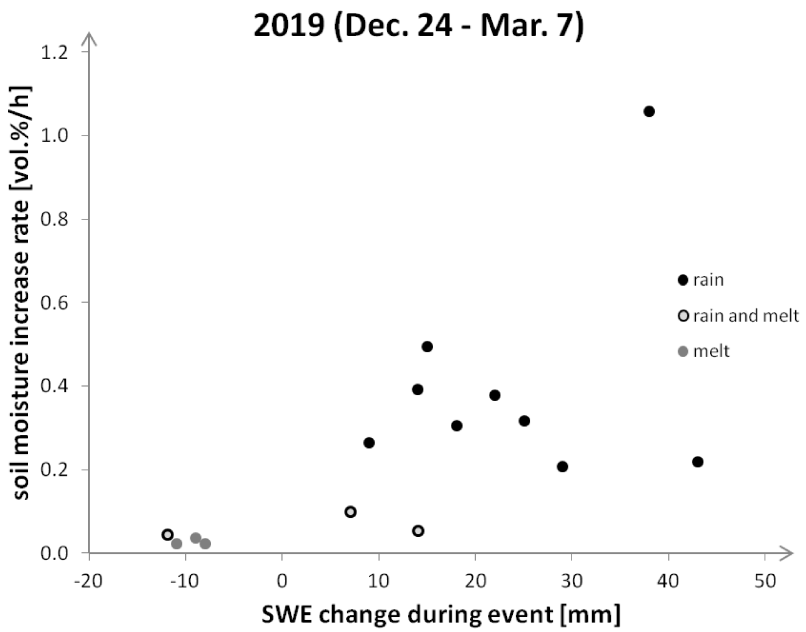

Figure 3.58: Soil moisture increase events under snow cover (2019)

Influences of rain events on soil moisture were predicted with the use of a critical value. Since all rain events of 15 mm or more influenced soil moisture in forest, this was used as the critical value for the prediction of rainfall influence on soil moisture. Snowmelt events were considered to affect soil moisture if the SWE decreased by 8 mm or more within 24 hours. Rain events for the year 2019 were found for January 5, 10 and 15 and for

February 4 and 20. Three days of snowmelt events increasing soil moisture were predicted in the year 2019: February 4, 21 and 26. All of these days were confirmed by the soil moisture measurements (Figure 3.56). The prediction of ROS and snowmelt for February 4, 2019 indicates a mixed event, as classified based on the soil moisture increase rate (Table 3.5).

Based on the 15 mm and 8 mm critical values for rain and snowmelt events during winter, ROS events appeared to affect soil moisture during all winters 2011-2018. In contrast, winter snowmelt events might have contributed to increase of soil moisture in six of the eight winters (Table 3.6). The estimated number of ROS events neither increased nor decreased significantly within the eight years. The maximum was counted in 2017 with a total of nine ROS events in January and February. While ROS events were found in both months, snowmelt increased soil moisture only a few times in January. Soil moisture increases caused by snowmelt were assumed for February of almost every winter (Table 3.6).

Table 3.6: Predicted soil moisture increase events

Year	> 15mm rain (January)	> 15mm rain (February)	> 8mm SWE loss (January)	> 8mm SWE loss (February)
2012	-	2	-	-
2013	2	3	-	9
2014	4	-	3	4
2015	1	1	-	4
2016	3	2	1	4
2017	5	4	-	2
2018	3	2	-	-
2019	3	2	-	3

3.4.2 Winter 2019/2020

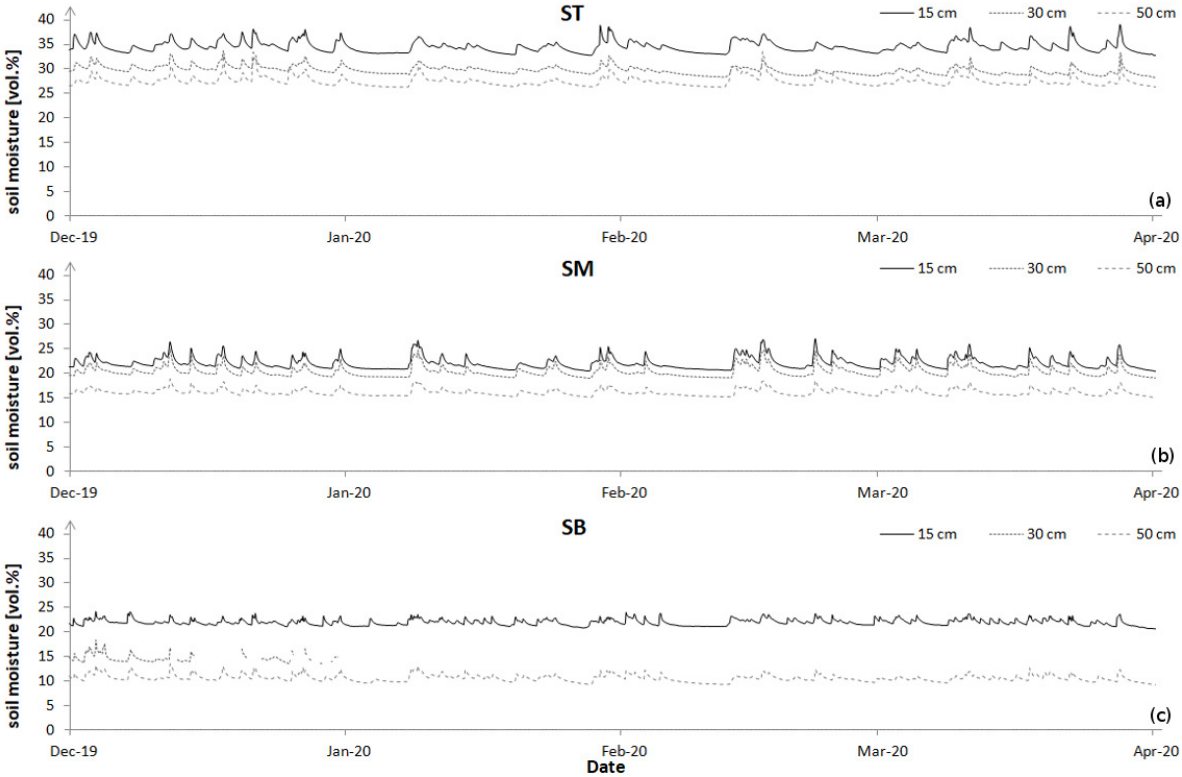

Figure 3.59 a-c: Soil moisture curves for the winter 2019/2020

The winter 2019/2020 was warmer than the previous ones, had smaller precipitation and resulted in soil moisture curves which were significantly different to the curves of the winter 2018/2019. At *SB*, many of the peaks observed were irrelevant in intensity and separation. In contrast to 2018/2019, more peaks were recorded at *SB* than at *ST*. Soil moisture at *SM* had, as in the previous winter, the smallest number of peaks but with greater peak heights than the peaks at *SB* and *ST*. The soil moisture level at all three spots was the same as in the winter 2018/2019. The sensor at 30 cm depth at *SB* started to malfunction in December 2019 and the other two data loggers at *SB* were removed before the start of the winter due to technical problems, therefore no soil moisture signal could be recorded in winter for the 30 cm depth.

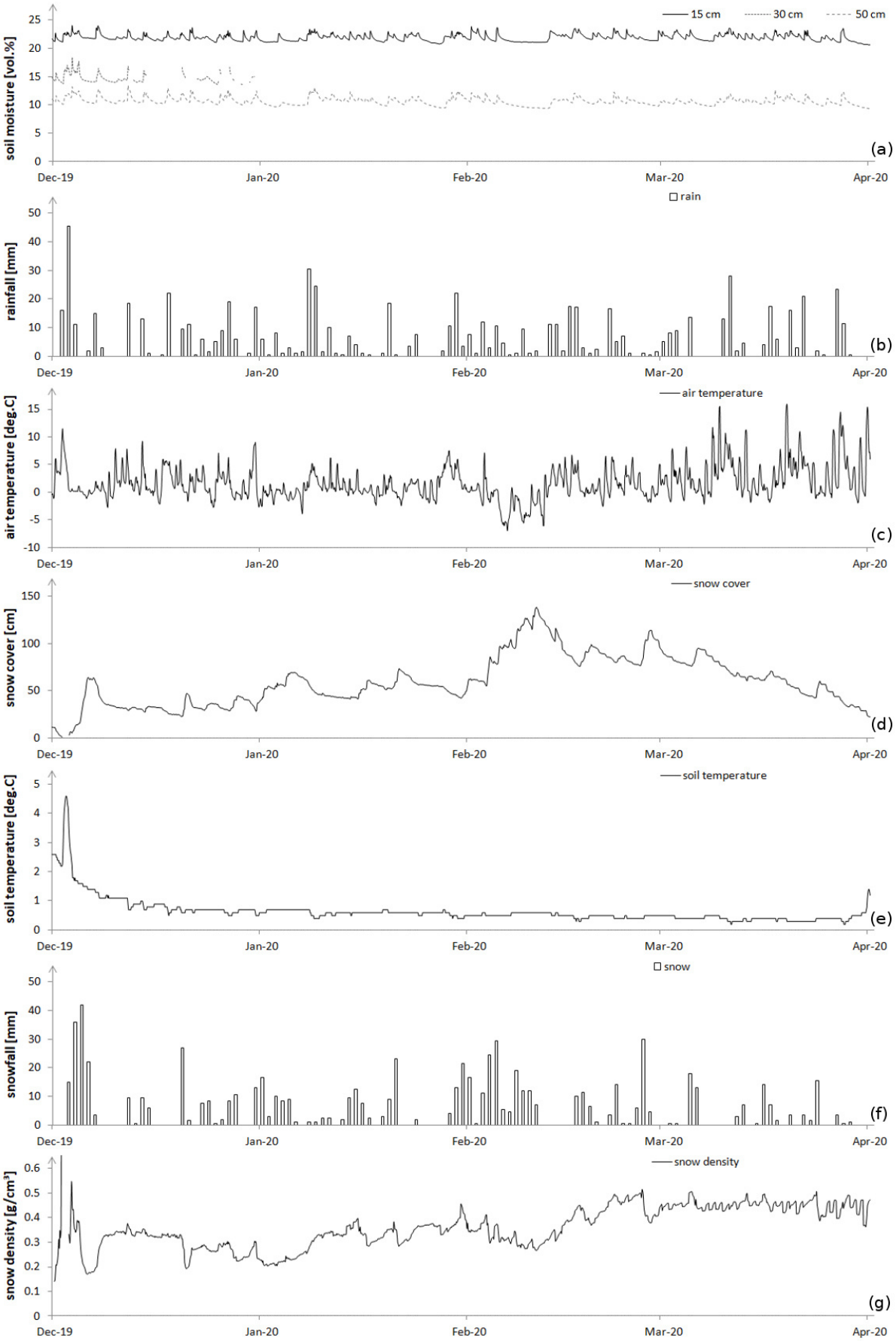

Figure 3.60 a-g: Meteorological conditions of the winter 2019/2020

Peaks in soil moisture at *SB* occurred after almost every rain event in winter. Only during the local maximum of snow depth in the first week of January 2020 and during the maximum snow accumulation in the second week of February, no peaks were recorded, even though rain fell. During the rest of the winter, peaks were observed even after small rain events, which implies that also snowmelt and runoff from higher parts of the slope also contributed to increases in soil moisture. Peaks at *SM* were less frequent and occurred only after ROS events of more than 10 mm of rainfall. Higher peaks at ST did also occur after intensive ROS events, while small precipitation was followed by smaller or no peaks.

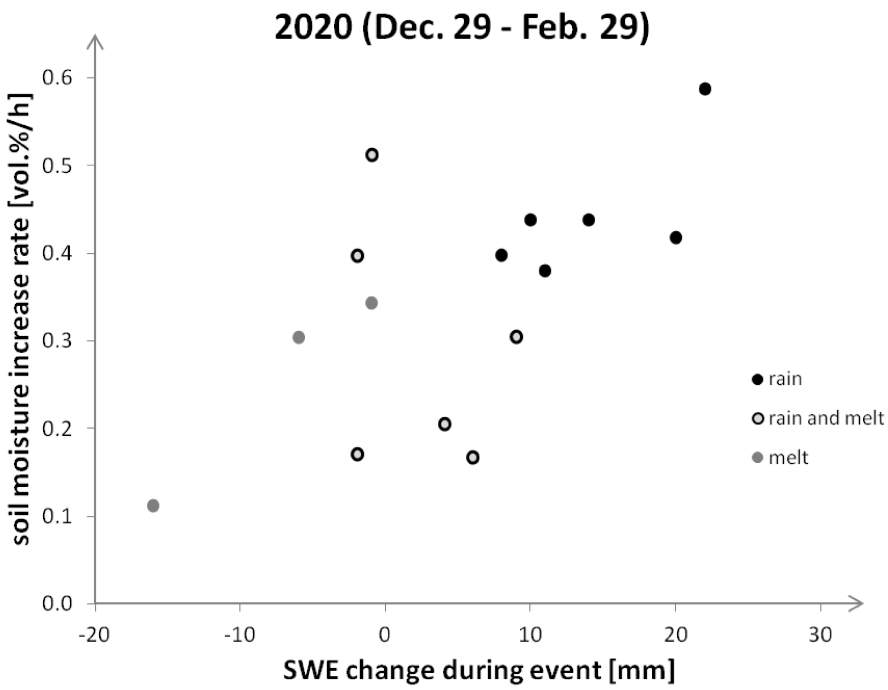

Figure 3.61: Soil moisture increase events under snow cover (2020)

3.5 HYDRUS 1D results

3.5.1 Soil moisture

The model setup worked well, and soil physical properties were adjusted based on trial runs. Overall, the model produced an error only in a few cases, which could be solved by adjusting the soil physical properties, especially the K_s value. In contrast to the measured soil moisture, modelled soil water content tended to increase during the modelled months, especially under snow cover. Peaks were modelled for the same day as they were measured, but after the event they were not decreasing as fast as the measured data showed. The HYDRUS model was applied for one year, for the period November 2018 until November 2019.

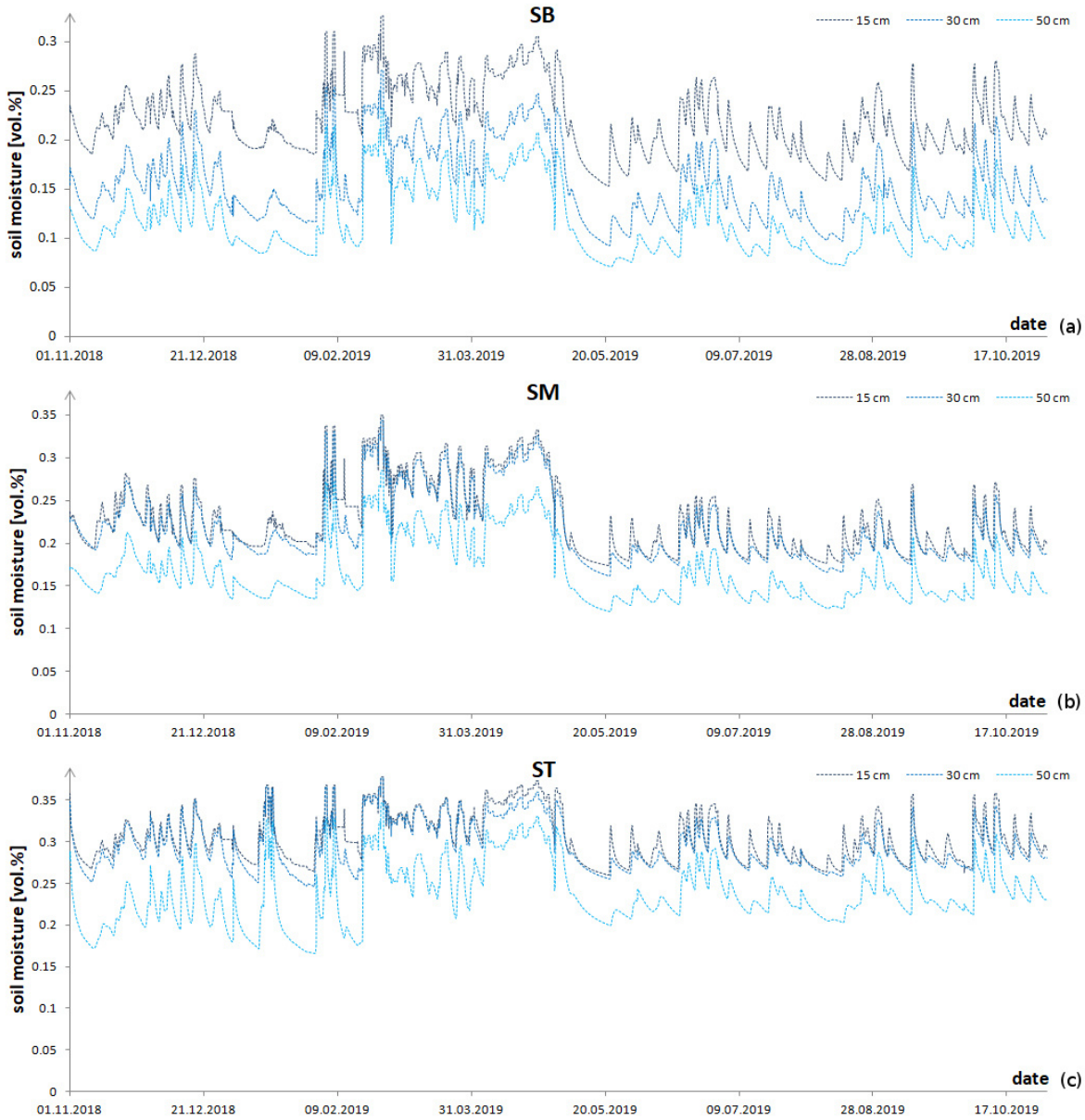

Figure 3.62 a-c: HYDRUS 1D modelled soil moisture for *SB*, *SM* and *ST*

The highest soil moisture was modelled for all three spots for the winter season. The highest soil moisture of almost 40 % was further modelled for *ST* in winter, followed by *SM* and *SB*, where the soil moisture exceeded 30 % only three times. Peaks of soil moisture increase were higher at *SB* than at the other two spots, especially in the periods without snow cover. The differences in soil moisture between 15 cm and 30 cm were less than 1 % at *SM* and *ST*, in *SB* it was greater but the difference between 30 cm and 50 cm was less than at *SM* and *ST*.

3.5.2 Accuracy of the model

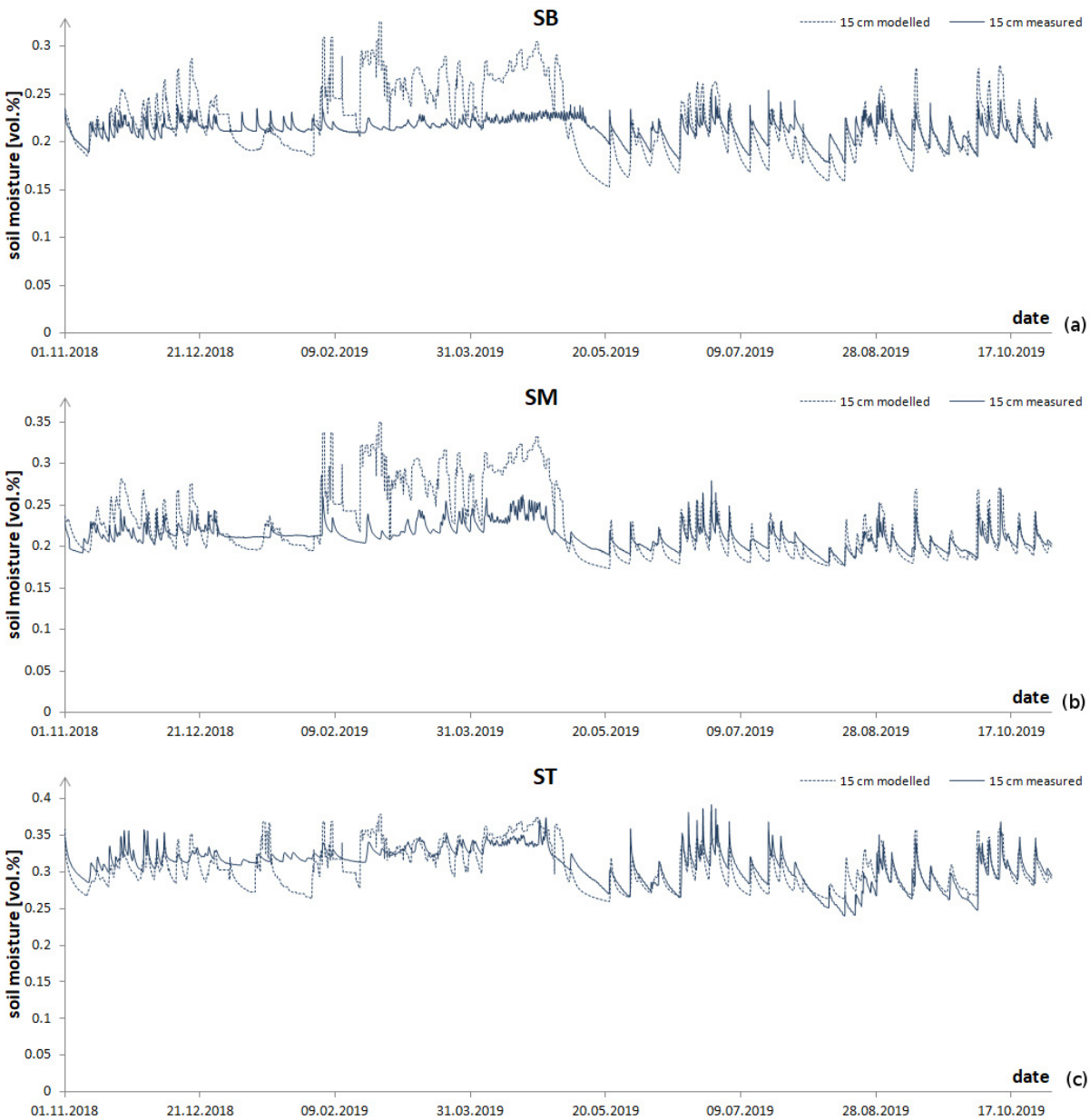

Figure 3.63 a-c: Modelled versus measured soil moisture (15 cm) at *SB*, *SM* and *ST*

The progression and trend of soil moisture was similar at all depths, therefore only the graphs for 15 cm depth were plotted for comparison (Figure 3.63). The figures for 30 cm and 50 cm can be found in the supplementary material section (chapter 9).

Peak heights of the modelled soil moisture were often greater than in reality, especially in winter the soil moisture at *SB* and *SM* was around 5 % higher than in snow free seasons. Increases and decreases in soil moisture have been more intensive in the model, while the measured data showed periods of almost constant soil moisture both in summer and in winter. Those patterns were not found in the modelled soil moisture. The modelled soil water content at ST was similar to the measured soil moisture; however the amplitudes of soil moisture variations were, as at the other spots, higher in the model than in reality. Soil moisture was modelled to decrease to lower water contents in dry periods with higher intensity than it was observed.

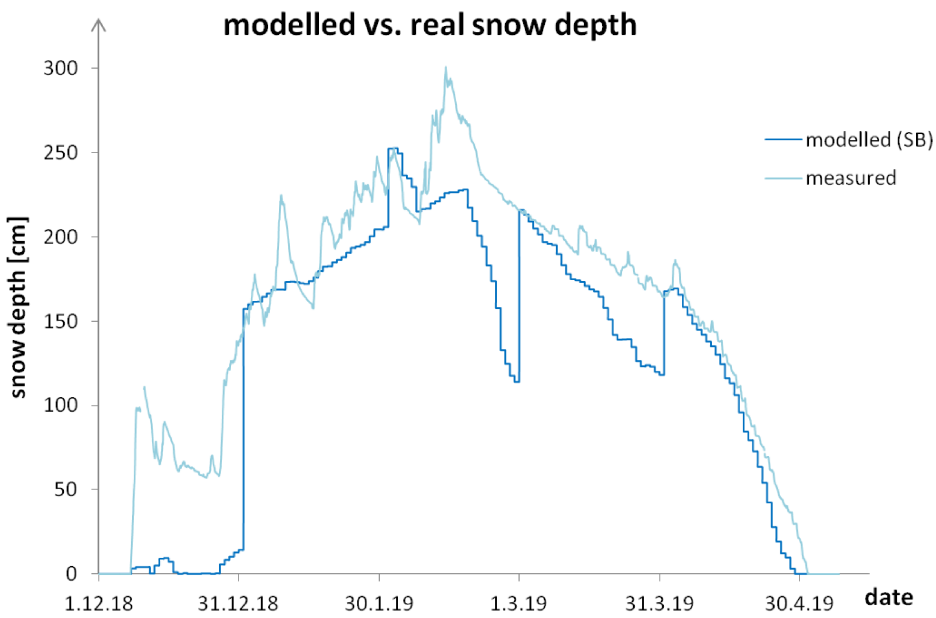

Figure 3.64: HYDRUS 1D modelled snow depth

Modelled snow depth did not differ from one spot to another. Because HYDRUS 1D forest cover was not included in the HYDRUS model, the modelling process did not make any difference in the calculation, because the same meteorological input data was used for all spots. Therefore, the calculated snow depth was the same at every spot and only the model data of *SB* was plotted as representative (Figure 3.64). At the beginning of every month jumps in the curve for the modelled snow depth were observed. Those jumps were generated because each HYDRUS model ran for one month, and the measured snow depth

was entered as the initial value for every new modelled month. The snow depth of the model and the measured snow depth were therefore always the same on the first day of every month. For January and April, the differences between model and reality were smaller than in the other months. The modelled snow depth was in general less than the real depth and had only few peaks.

Soil water runoff was modelled, but most of the days during the year had small surface runoff. Surface runoff is a lateral water flow, which could not be modelled in a one-dimensional model. Since every spot was regarded as a single point with no relationship to the other two spots, no exchange of water and therefore no surface runoff along the three spots were calculated. Hence, the measured and the modelled surface runoff at every spot could not be compared.

4. Discussion

4.1 Soil physical properties and water dynamics

The coarse texture of the soils in YURF supports the overall impression of young and not well developed soils. Bedrock was reached after 60 cm at most of the soil profiles. Granodiorite as host rock has high contents of quartz, which is the main fraction in the soil and characterises the sand fraction (Blume et al., 2010). The common soil type was Cambisol, which is typical for soils developing from plutonic, especially granitic, host rocks (Blume et al., 2010, Lopez et al., 2014a). Cambisols, or also brown forest soils, have been found in various places in YURF (Seidel et al., 2017) and in other Japanese mountains (Matsuoka, 1996, Uchida et al., 2005). The steep slopes of the mountains, combined with the high precipitation, result in increased soil erosion and the loss of fine soil particles like silt or clay, because those particles are easier to erode than sand. Furthermore erosion explains the shallow A-horizon in the soils of the sampling slope. Higher content of organic matter in *SB* in comparison to *ST* and *SM* can be explained by the continuous increase in soil depth due to accumulation of eroded soil from the slope. Soil surface needs to redevelop after erosion events. In addition, the accumulation of big stones and boulders disturbs the soil community and needs time to weather. In contrast to the bedrock surface, accumulated stones are well rounded, which makes it more difficult for water and plants to enter and weather those rocks (Røyne et al, 2008, Salve et al., 2008). Because of the high content of particles > 2 mm and even > 60 cm it was difficult to extrapolate the hydrological properties of the soil fraction to the whole pedon. In particular, in a soil with stones the hydraulic conductivity K_s is significantly higher than the laboratory measurements with soil < 2 mm prompt.

The described characteristics of the sampling spots in YURF resulted in higher standard deviations of the calculated pF-curve. The soil texture and matrix of the samples were not identical in the three replicates, which resulted in differences of up to 5 % for the saturated water content at pF0. The variance in water content decreased with increasing steepness of the pF-curve and increased again before pF4.2. However, the difference between the three replicates was smaller at pF4.2 than at pF0. The variations in the pF-curve show the uniqueness of every soil sample and elucidate the difficulty to unify soils and soil physical properties on a larger spatial scale, as it has been described in many other studies (Grayson et al., 1997, Assouline et al., 1998, Wessolek et al, 2009, Kojima et al., 2018). Especially the

pF-curve of *SB* did not reflect the measured soil texture ideally. Soils along the whole slope were sandy, but the shape of the pF-curve at *SB* was more similar to a silty soil than to a sandy soil. Thus, the soil in the HYPROP samples contained more silt than the texture samples.

The soil texture data and the pF curves of *SM* match more closely. The sharp decrease of soil moisture with small increases in pressure is typical for sandy soils (Assouline et al., 1998, Clark et al., 2006, Peters and Durner, 2006). The field capacity at 5 cm depth was smaller than at 45 cm (Figures 3.13 and 3.15), which was not supported by soil texture data, but the difference in water content is minor and therefore within the range of measurement errors.

The final pF-curve of *ST* at 30 cm depth did also reflect the soil texture (Figure 3.2). The shape of the graph was at *SM* less steep than curves for sandy soils are, which corresponds to higher silt and clay contents. The drastic decrease in water content between pF4.0 and pF4.2 could have two different reasons: One is a simple measurement error, because the HYPROP system measured all pressures < pF3.5 and pF4.2 was measured separately. If the difference between both plotted points is high, a slope in the graph is created. The second possibility is a realistic behaviour of soil, in detail a discrimination of a specific grain size in texture. This phenomenon is unusual but has been observed in different soils around the world (Abdu et al., 2008, Marthews et al., 2014). For *ST* it means, that the fraction of fine silt was small in the soil profile, because it is not as strongly bound in aggregates as clay is (Wessolek et al., 2009), but small enough to be washed out easily (Zhou et al., 2008, Detert and Parker, 2010).

The higher proportion of clay at *ST* in comparison to *SM* and *SB* was a result of the relief of the mountain. The ridge, where *ST* was located, was relatively flat and therefore soil could evolve better than at the steep slope, where soils erode frequently. *SM* was located at one of the steepest parts of the slope, therefore erosion, especially water erosion due to high precipitation, is high and smaller grains are washed out. The erosion resulted not only in a coarse texture of the soil but also in shallow soil profiles. The HYPROP core samples were taken at a spot where the slope was not as steep as at the sampling spot for soil texture and soil moisture, therefore also 80 cm soil depth was reached. The soil was only 40 cm deep at the steeper parts of the slope. All eroded soil material and also big stones accumulate at *SB* which explains the high content of gravel at *SB*.

Soil texture and the water retention curves suggest high hydraulic conductivity values for the soils in YURF. However, HYPROP calculated relatively small values for K_s (Dusek et al., 2017). The reason for these small values was the measurement itself, because HYPROP does not measure but only assumes hydraulic conductivity and because the fitting process favours the water retention. Therefore, K_s values obtained from HYPROP were assumed to be incorrect. Especially during observation of soil moisture peaks, increase and decrease of soil moisture are much faster than K_s values of around 10 cm/d would allow. Hence, significantly higher values between 500 and 1500 cm/d were used as input data for the HYDRUS 1D modelling process.

The large fraction of sand in the soils is equivalent to a high air capacity and consequently a low field capacity. The water retention curves predicted water contents of 22-24 % at *SM* and 32 % for *ST*. These values fit the measured soil moisture well, especially in winter. In winter, soil moisture at 30 cm depth at *ST* was in winter approximately 30 %, which expressed the equilibrium state and therefore the field capacity, because the soil was kept wet permanently by the snow cover. Other studies reported that soils reach their field capacity latest during snowmelt (Lundmark and Jansson, 2008, Conner et al., 2016). But in YURF the field capacity of soil was already reached at the beginning of the snow accumulation period. For *SM* the theoretical and the observed field capacity were also close together. Only at *SB* the water retention curve and the observed soil moisture did not match, because of the shape of the water retention curve.

An indicator for the fast movement of water along the slope was already given by the water retention curves, but soil moisture and water repellency measurements, together with the runoff measurements, confirmed the movement of water in different soil layers. The water repellency data was of high interest for the summer and autumn season, because the wetting of soil is especially poor when the soil is dry. Wet soil has already a high potential to transport water (Hillel, 1998, Kojima et al., 2018), but the hydrophobic behaviour of organic matter prevents water from infiltration when no water film has been established. Therefore, dry and warm seasons were of high interest for the determination of surface and subsurface runoff (Grayson et al., 1997, Gottfried et al., 2006). It has been documented that soils in Japan have different flow patterns, on the soil surface, on the bedrock and water movement in the soil (Salve et al., 2008, Gerke et al., 2015). The hydrophobic organic layer of the forest soil needed time after water penetration to let water pass into the soil (Goebel et al., 2011).

High water repellency explains why surface runoff was especially high after dry periods and why bedrock runoff was high when soil moisture was already high before a rain event. In the first case, rain did not infiltrate the soil and ran off on the surface, while the soil moisture was almost unaffected and consequently bedrock runoff not initiated. In the second case described, water filled organic layers, which passed most of the water to the topsoil. High hydraulic conductivity of the soil caused higher proportions of vertical movement of water, from the topsoil to the bedrock, than lateral flow down on the soil surface. Wet soil has increased hydraulic connectivity in comparison to dry states (McNamara et al., 2005). However, lateral flow takes place when the water saturation is between 60% and 80% (Grayson et al., 1997). Based on the average maximum water content of 45 % for *SM*, a 60 % saturation represents a water content of 27 %. Since the soil moisture content was usually smaller than 25 %, lateral flow was expected to be negligible. Peaks in the soil moisture data confirmed the minor role of matrix flow along the slope, because most peaks after rain events were recorded simultaneously at all spots and depths (Figures 3.20 and 3.21). Besides these peaks, there were no additional increases in soil moisture recorded at *SB* and *SM*. If water movement within the soil profile occurs on a large scale, the amount of water of the whole slope moving down would have an impact on the soil moisture at the bottom of the slope (Grayson et al., 1997, Dusek et al., 2017). Since significant peaks, which were not linked to rain events, were rarely observed at *SB*, subsurface matrix flow was only minor and surface and bedrock flow were the main forms of water runoff (Sidle et al., 2007, Gerke et al., 2015). High hydraulic conductivity of the soil resulted therefore in a preference of bedrock runoff.

The peaks in soil moisture and their simultaneous occurrence at all spots do not only show the direction of water movement and the influence on bedrock and surface runoff, but they were also good indicators for rain events. Every peak marked sudden increases of soil moisture, which usually relate to precipitation (Dusek et al., 2017).

4.2 Soil properties of Kaminoyama

The objective for the soils in Kaminoyama was to characterise the potential to produce wine. All results were therefore discussed regarding the fertility and water efficiency of the soils. The observed high clay and silt contents of the soils are unusual for the mountain soils in

Japan (Matsuoka, 1996). The clay content explained the high water content at the wilting point (pf4.2), as measured for all three sites, and further improved the nutrient availability for plants (Assouline et al., 1998). Clay particles have a large surface and the structure of clay minerals results in a high cation exchange capacity (Helling et al., 1964, Parfitt et al., 1995, Hepper et al., 2006). Hence, the amount of nutrients which can be bound in the soil is higher than in sandy soils (Blume et al., 2010). Especially in comparison to soils in YURF, with a high content of sand, the soils in Kaminoyama have much greater ability to store nutrients and water.

However, the high clay content does have a disadvantage for the soils. The plant available water, at less than 10 %, was lower than in soils of YURF. The maximum water content, at around 45 %, was a good value (Assouline et al., 1998, Blume et al., 2010), but the percentage of dead water, at 22 to 27 %, was significantly higher than in other soils with similar texture (Madi et al., 2018). The water bound by clay minerals was not available for plants, and was therefore not taken into account for the fertility of plants. Especially in seasons with small precipitation and high water demand of plants, grapevines suffer drought stress. Timing and duration of root-zone drying and drought can harm the growth of grapes significantly (De la Hera et al., 2007).

Despite water transport, Carbon and Nitrogen contents of soils are important for the nutrient supply and the growth of plants (Blume et al., 2010, Bramley et al., 2011). Not only the concentration, but also the ratio of the two elements is responsible for the growing of plants. If the ratio between Carbon and Nitrogen is too high or too low, plants might suffer nutrient stress. An optimal CN ratio is 10 (Mesic et al., 2012). The soils in Kaminoyama sites A and B have slightly higher values (around 14), which is still a normal value for vineyard soils (Wang and Schuchardt, 2010). The reason may be the high content of organic matter in the A-horizon (Table 3.2). The CN ratio for site C was lower. It lied between 8 and 9, which represented average values of soils for fruit trees (Blume et al., 2010). The normal Nitrogen content of moderate-humid climate soils ranges between 0.7 and 5 g/kg, which fits the concentration in the vineyards (Blume et al., 2010, Bramley et al., 2011). Overall, the results show favourable conditions for plants and also wine to grow better than in many other places in Japan (Osumi et al., 2003, Le Bissonnais et al., 2007). Sites A and B may be more suitable than site C because the iron in the soil is not oxidized and therefore better available. Furthermore higher Carbon and Nitrogen contents increase the fertility of plants. Further,

small concentrations and applications of fertilizers will be enough to supply the plants with nutrients, because the soils have high nutrient storage capacities. The Nitrogen concentration showed that there was no overfertilisation.

Further research might be done concerning heavy metals and the quality of the grapes themselves. Many countries used copper sulphate to fight mildew in vineyards. Japan, too, used this sulphate intensively, which resulted in poisoning of workers (Franchitto et al., 2008) and in the accumulation of Copper in soils (Besnard et al., 2001). Copper binds to organic matter and is an essential element for plants to grow leaves to reach the maximum yield (Blume et al., 2010). Usual concentrations of Copper in soil are between 2 and 40 mg/kg. However, if the concentration gets higher than 500 mg/kg, it can become toxic for plants (Besnard et al., 2001). Therefore, the management and monitoring of copper in orchards and fields, especially if they are treated with pesticides, is essential to maintaining ideal growing conditions.

4.3 Meteorology

The data of relative humidity and precipitation followed a pattern which has been documented for Tōhoku (Motoya et al., 2001). The high humidity in autumn and winter was linked to high precipitation, and the warm air with less precipitation in spring resulted, on average, in a relative humidity below 80 % in May (Figure 3.31). The snowmelt in spring did not seem to have a significant effect on the relative humidity, therefore sublimation processes in spring might be rather small (Neumann et al., 2008, Reba et al., 2012) and resulted in the majority of snowmelt water infiltrating or running off the soil. The daily variations in soil moisture at *SB* during the snowmelt seasons reflected the constant input of snowmelt water into the soil during daytime and the runoff at night. Low air relative humidity in early summer was also reflected in the soil moisture. Since lowest soil water contents, especially in the topsoil, have been found between May and September, soil dried during these months and could not increase the relative humidity due to small input of water. High relative humidity was linked to low average wind speed. The box plots (Figures 3.31 and 3.32) show the effect of wind on air relative humidity (Motoya et al., 2001). Strong wind causes circulations and mixing of air, increases the energy and therefore also the potential to take more water up (Fujita et al., 2014). However, lull does not move any air

masses, resulting in fast saturation of air with water (Hayashi et al., 2005). Since air had high relative humidity and precipitation occurred on almost every day, errors in the precipitation data due to wetting errors and therefore mistakes in the further analysis were assumed to be minimal (Wagner, 2009).

Significant differences were found in winter wind speed. At the Japan Sea coast, wind blows strong from the sea side (Dorman et al., 2004, Shimada and Kawamura, 2004). Those strong winds are caused by the air masses moving from Siberia to Japan and creating the winter monsoons (Ebuchi et al., 1992, Kudo et al., 2017). However, the wind speed measured in YURF was at its lowest in winter. Strong winds at the coast seemed not to reach YURF. Moreover, in the inland mountains, winds were not as strong in winter as in summer (Nagata, 1987). Hence, the massive snow covers in YURF were caused not only by the high precipitation, but also by the absence of wind, which resulted in less erosion and transport of snow and in less sublimation due to high air humidity (Neumann et al., 2008). The origination of snow in the winter monsoon from Siberia could also be confirmed by the snow isotopic data. The snow Oxygen isotopic composition at the *Yaki* site (Figure 3.27) was similar to precipitation values observed in Siberia (Meyer et al., 2002) and different from the isotopic composition in YURF in summer seasons (Zhang et al., 2019). The measured isotopic ratio supports the findings of other studies monitoring snow along the Japan Sea coast (Nakamura and Abe, 1993, Nakatsuka et al., 2004, Zhang et al., 2019).

Soil freezes before snow starts to accumulate in other regions of the world (Baker and Ruschy, 1995, Edwards et al., 2007, Shanley and Chalmers, 1999, Fu et al., 2018), but that was not observed in YURF because of relatively high air temperatures before snowfall. Observed soil temperatures (Figure 3.36) showed that soil remained unfrozen during winter, even before snow accumulation. Soil surface temperatures suggested that soil moisture and especially snowmelt water were in a phase close to freezing but did not crystallise. Still, water close to 0 °C can freeze partially and develop micro crystals (Matsumoto et al., 2002, Alabarse et al., 2012). Those crystals might decrease the infiltration speed of water and possibly the flow dynamics in the soil. The negative temperature differences in the winter 2014/2015 (Table 3.3) implied that snow insulation was low; in contrast the snow cover cooled the soil surface during the whole period.

Relatively warm air in winter and intensive precipitation were found in YURF, and they were common for the mountains along the Japan Sea coast (Takeuchi et al., 2008, Asaoka &

Kominami, 2013). It is likely that in most of these areas soil does not freeze in winter because daily air temperature needs to be -3 °C or lower to cause soil freezing (Baker and Ruschy, 1995). If snow cover is present, air temperatures need to be even lower (Cline 1997), especially in the heavy snowfall areas of Tōhoku (Hart and Lull, 1963, Takeuchi et al., 2008), in contrast to other studies in temperate regions, where a strong influence of snow cover on soil freezing was found (Stadler et al., 1996, Hardy et al., 2001, Niu and Yang, 2006, Kellomäki et al., 2010, Callaghan et al., 2011, Bulygina et al., 2015, Fu et al., 2018). Another controlling factor is forest cover, where soil temperature was higher than in uncovered soils (Hardy et al., 2001, Osumi et al., 2003); therefore forest ecosystems could be a buffer of soil frost in case of thinner snowpacks in mountainous areas, as the long-term data show in our study site. Regarding the data of YURF and different studies from previous decades, a change in the meteorological conditions was assumed.

Zhang et al. (2005) reported temperature differences of up to 20 °C between air and soil. Temperature differences of this magnitude have also been found in YURF. The highest difference was measured in spring, when the air was significantly warmer than the soil. Moreover, cooling of the soil was also found in spring, probably caused by snowmelt water infiltration, which had temperatures close to 0 °C because of high latent heat of fusion (Cline, 1997, Edwards et al., 2007). Further, increasing snow density increased thermal conductivity, which also affected soil temperatures and might also be responsible for the decrease in soil temperature during the snowmelt season (Saito et al., 2012).

The past eight years show a recurrent pattern of snow coverage. Years with heavy snowfall and great snow depths were usually followed by a year with less snow and a third year with even smaller snow cover. After this minimum was reached, snow depth started to increase again. This trend could be observed recently in the years 2017-2020 with heavy snow in 2017/2018 and only little snow in 2019/2020. The winter 2015/2016, too, was characterised by a shorter period of snow coverage (starting in late December) and smaller snow depth compared to previous years. The changes in snow depth require more observation in future years, but for now it can be assumed that the snow coverage in YURF follows a five-year-recurring trend. SWE, snowfall and rainfall affect this cycle, thus it can be expected that due to climate change the five-year-cycle will also have either an increasing or, as the data suggested until now, a decreasing trend. It is also worth noting that the maximum snow depth was reached in the second week of February in almost all years, and the snowmelt

ended with the last days of April in most years. Hence, disregarding the amount of snowfall and the air temperature, snow accumulation and snowmelt followed the same pattern and timing in most of the years. Even though the rain/snow ratio increased in the last decade, that seemed not to affect the timing of snow maximum and end of snowmelt.

Since relative humidity was almost 100% in winter, snow sublimation was negligible (Neumann et al., 2008, Reba et al., 2012). In contrast, low relative humidity during the snowmelt period enhanced melting and evaporation of snow cover. The percentage of sublimation and the difference to winter snow sublimation could be a subject of further research. Overall, the snowmelt season was observed to have a constant decrease in snow depth. Disregarding the amount of precipitation or the type of precipitation, the snow cover decrease was almost linear in every year (Figures 3.39 – 3.47). That means, that the snow density increased within the whole snowpack and homogenised it, which further resulted in the same amount of melt energy needed for every layer of the snowpack (Cline, 1997).

4.3.1 Rain/snow ratio

The observed increase of rain in winter over the last years is a phenomenon which can have a negative effect since less snow, especially in the early winter, decreases the maximum SWE in spring before snowmelt (Yamaguchi et al., 2011). As described above, small amounts of ROS increased snow density and were stored in the snowpack, but storage was limited by snow water retention capacity (Yamaguchi et al., 2012, Achleitner and Schöber, 2017). The increase of the rain/snow ratio has been drastic in YURF, from 0.47 in 2011/2012 to 1.04 in 2019/2020 (Figure 3.38), representing a significant decrease in snow depth, which has shown extremely low values (130 cm) in February 2020. Air temperature did not change significantly over the past eight years; therefore it seems that there were other major reasons for the transformation from snow to rain during the last decade. The number of days with snow and rain did not change, but the intensity of rain events increased while the intensity of snow events decreased. This finding was described by Krasting et al. (2016), who calculated rain-to-snow transitions and assumed wet snowpacks due to increasing rainfall. Therefore, higher precipitation on warm winter days (falling as rain) and less precipitation on cold winter days (falling as snow) were expected.

A shift of the rain/snow ratio, accompanied by less heavy snowfall events (Spreitzhofer, 1999), has decreased snow cover and correspondingly decreased SWE, as has already been observed in many other regions of the world (Ismail et al., 2015, Bokhorst et al., 2016, Potopová et al., 2016, Godsey et al., 2018), and was also predicted for Tōhoku and its heavy snowfall regions (Ogawa and Nogami, 1994, Mizuta et al., 2005). More frequent intra-differences during the winter monsoon season could be a reason for the observed shift. Temperature as well as total amount of rain in winter increased over the last decades (Fujita et al., 2014). Hence, shifts in precipitation have been observed recently (Fujita et al., 2014, Yasunaga and Tomochika, 2017).

4.4 Soil moisture

Soil moisture measurements fit the water retention curves accurately. The field capacity of the soils were reached at *SM* and *ST*, especially in winter, when soils were constantly supplied with water and no transpiration took place, the water content was exactly the field capacity. Under snow, matric potential becomes 0 cm, because no air pressure influences the soil (Peters and Durner, 2006, Kumagai et al., 2008). Since the water retention curves estimated water contents of 22 % for *SM* and 31 % for *ST*, which were almost reached in winter, the HYPROP measurements for these two spots seemed to be accurate and representative. In contrast to the good conformity at the slope, the soil moisture for *SB* did not confirm the water retention curve (Figure 3.12). However, the differences between water retention curve, soil texture and recorded soil moisture most probably originated from the spatial difference between the sampling points. The data loggers were set up directly at the bottom of the slope, while the HYPROP cores were taken in a spot closer to the small stream located about 10 metres apart from the bottom of the slope. Soils near rivers have higher silt and clay contents, as also seen in the soil texture (Wessolek et al., 2009, Blume et al., 2010, Marthews et al., 2014). Hence, the water retention curve did not have the typical S-shape that pF-curves of sandy soils usually have. Second, the high content of gravel and stones at *SB* decreased the volumetric water content which can be held by soil under atmospheric pressure (Hillel, 1998, Blume et al., 2010). Disregarding the differences in the HYPROP measurements, *SB* had soil moisture contents which were in the expected range for forest soils. Differences in water content between summer and winter were smaller at *SB*

than at *SM* and *ST*, which might originate from the constant supply of water to *SB* through surface runoff and lateral movement within the soil matrix (Grayson et al., 1997, Tague and Peng, 2013, Caiqiong and Jun, 2016). Peaks in the soil moisture curves after rain events were high, because the high hydraulic conductivity of the soils resulted in fast transport of water, which further resulted in drastic increases of soil moisture. Wetting and drying of the soil was fast, because the hydraulic conductivity enhanced the transport of water to the soil surface (Madi et al., 2018). However, at all spots increases in soil moisture were significantly faster than the decreases, because the capillary pressure requires more energy to extract water from pores than to add water to partially filled pores (Blume et al., 2010). Further, the organic layer on top of the soil, which creates biomat flow downwards a slope (Gerke et al., 2015), was thin in YURF and therefore the portion of water infiltrating the soil was high.

While soil moisture became significantly active in the snowmelt season 2019 at all spots, the melting season 2020 was not clearly visible in spring 2020. Only at spot *SB* a soil moisture variation pattern, similar to the previous year, was noticed between March 10 and March 30, 2020. Since the snow cover was small in the recent winter season, water did always filtrate into the soil during winter. The SWE of the snowpack was significantly smaller in 2020 and resulted in a much shorter and less intensive snowmelt period (Bokhorst et al., 2016). In comparison to 2019, more peaks in soil moisture were recorded at *SB*. The shallow snow cover in 2020 seemed to increase lateral movement of water and also the higher air temperature increased snow melt (Tague and Peng, 2013, Kudo et al., 2017). In addition to the lateral movement of water, snowmelt itself played an important role. *ST* and *SM* were within the Japanese cedar forest, SB was located at the end of the forest, where solar radiation played a significant role (Walsh et al., 1985, Yamazaki and Kondo, 1992). Hence, more snowmelt was produced at *SB* and less at *SM* and *ST*, which was further reflected by the soil moisture data, because the number of recorded peaks at *SM* and *ST* were significantly smaller.

Forest cover influenced not only snowmelt and snow cover, but also the response of soil moisture to rain events in summer. Peaks at *SM* and *ST* were usually smaller in intensity than at *SB*. Forest canopy reduces the amount of rainwater reaching the soil surface and therefore also the infiltration (Floyd and Weiler, 2008).

Daily changes of soil moisture before winter were apparently still controlled by tree transpiration until mid November 2018, since the decrease was sharper after soil moisture

refilling caused by precipitation. There was a change in pattern of oscillation from April to May, which was the most intense period of snowmelt. During this period, two opposite processes took place: soil moisture increase due to the supply of water from snowmelt, and the loss of water from the soil as trees started to use soil water (Osonoi, 2018). Therefore, during the snowmelt period there was a strong balance between these two processes that appeared to keep the soil water availability relatively constant. Soil moisture decreased rapidly after snow disappeared, in particular, if snowmelt has already ended before the end of March, since precipitation in April and May is relatively low due to wind direction changes (Dorman et al., 2004, Shimada & Kawamura 2004). From mid-May forward snowmelt water was not available anymore and for that reason the daily variation in soil moisture became larger since the supply of snowmelt or rainfall was not enough to keep up with transpiration rates for this period.

4.4.1 Soil moisture peak analysis

The analysis of soil moisture peaks confirmed the hypothesis of active soils in winter, as they have been found in other regions around the world (Hardy et al., 2001, Bales et al., 2011, Potopová et al., 2016). Field capacity was reached at the beginning of winter 2018/2019 (under snow cover) as indicated by the constant soil moisture value as it was also observed by Uchida et al. (2005). In contrast, soil moisture tends to be below field capacity in many other regions with seasonal snow cover (Harpold et al. 2015, Lopez et al., 2015, Conner et al., 2016, Potopová et al., 2016). High precipitation in autumn and warm winter temperatures in YURF might be the reasons for the comparatively high soil moisture values in early winter.
Based on texture differences of soils at *ST* and *SB*, soil moisture also differed. The higher soil moisture content at *ST*, indicated by the higher silt and clay content in comparison to *SB* and *SM*, where in contrast gravel and small stones are more present. Consequently, soil moisture changes were slower at *ST*, which was represented by the peaks with low increase rates (Figure 3.56a). In contrast, water moved faster in the sandy soil of *SB* and *SM*. Air filled macropores were more prominent than at *ST* and hydraulic conductivity was higher (Hillel, 1998, Blume et al., 2010, Kato and Nishimura, 2017); therefore the peaks were higher and steeper. High hydraulic conductivity explains furthermore the simultaneous development of peaks in all three depths of the soil profiles. Infiltrating water moved fast into deeper

horizons because the soil moisture level exceeds the suction pressure head (Hillel, 1998). This movement process is called redistribution.

All peaks in soil moisture were either caused by rain or by positive air temperatures melting a sufficient amount of snow (Stadler et al., 1996, Hayashi et al., 2005). A steep increase in soil moisture was more likely a rain event than a snowmelt one (Table 3.5). The background for this assumption was the physical properties of snow since rain penetrated wet snow fast, following Darcy's law (Wakahama, 1968, Stadler et al., 1996). In contrast, snowmelt is a slow process, because it demands huge amounts of energy (334 J/g ice) for the transformation from ice to water (de Quervain, 1973, Matsumoto et al., 2002, Zhang, 2005) and therefore snowmelt caused moderate soil moisture increase.

After ROS events, peaks in snow density (Figure 3.57f and 3.60f) can be explained by the input of water filling the pores of the snowpack. Water retention and permeability of snow were the controlling factors and explained movement, storage and distribution of water in the snowpack (Colbeck & Anderson, 1982, Yamaguchi, Watanabe, Katsushima, Sato & Kumakura, 2012). Water moves as film flow or creates preferential flow channels in snow (de Quervain, 1978, Coléou & Lesaffre, 1998). Since soil moisture was high in winter, the soils at the top and bottom of the slope were hydraulically connected (McNamara, Chandler, Seyfried & Achet, 2005). As a result vertical flow in soil profiles decreased. Snow and soil have similar hydro-physical properties like water retention, water films and hydraulic conductivity (de Quervain, 1973, Hardy et al., 2001, Yamaguchi et al., 2010, Yamaguchi et al., 2012). Hence, on the steep slopes of the mountain forests of Tōhoku, preferential flow appears to be rather lateral downwards the slope than vertical into the soil, which explained the smaller number of peaks at *SM* in comparison to *ST* and *SB* (Kohl et al., 2001). *ST* and *SB* were flat, therefore water moves vertically at these spots and infiltrated the soil.

The effect of snowmelt on soil moisture has been previously studied in many other regions of the world (Harpold et al., 2015, Conner et al., 2016, Potopová et al., 2016, Fu et al., 2018) and the results of this study confirm, that Tōhoku has similar dynamics. Furthermore, a significant impact of ROS events on soil moisture during winter was discovered, a new finding for studies on winter hydrology. Conner et al. (2016) mentioned the influence of rain, but rather during the snow melting period than in mid-winter, while Harpold et al., (2015), Potopová et al. (2016) and Fu et al. (2018) measured in regions with lower air temperatures

and less precipitation. Hence, this study is the first presenting the influence which ROS events have on soil moisture in heavy snowfall regions.

As stated earlier, water from rain or snowmelt increased snow density significantly. Fresh snow by the end of December and beginning of January buffered rain until the low snow density of approximately 0.2 g/cm^3 had increased to around 0.3 g/cm^3. This density increase was irreversible due to internal melting and refreezing processes (Kojima, 1967, Coléou and Lesaffre, 1998). Even small amounts of rain caused increases in soil moisture when snow density was high. When snow density was low, heavier ROS events were required to affect soil moisture. For that reason, snow depth and snow density were no reliable indicators for the analysis of ROS events affecting soil moisture. Even decreases of several centimetres in snow depth were accompanied by SWE increases as rain was falling. Rain events caused higher decrease of snow depth when snow density was low but caused smaller decreases in snow depth when the density was high. Snow density increased but also decreased in some cases during the rain events due to snow crystal structure changes. Therefore, the most reliable parameter for the relation with ROS was the SWE. SWE related directly to water masses and reacted to precipitation and snowmelt immediately. In contrast, snow depth and snow density reacted at different rates depending on the initial values.

Generally, all ROS events in mid-winter 2019 with rainfall of 15 mm/24 hours caused a peak in soil moisture at *SB*. However, the peaks in mid-winter 2020 were more numerous and appeared after smaller rain events (Table 3.5). Snow covers of less than 1 m buffers less rainwater than snow covers of more than 2 m. Consequently the water storage capacity, and therefore the buffer potential, of the snow cover was smaller with smaller snow depth (Kattelmann, 1987, Kawase et al., 2018). In addition to the small snow cover in 2020, the higher air temperatures caused snow densities of more than 0.3 g/cm³ from early winter on (Figure 3.60f). Moreover, melting of snow occurred on most days, which resulted in constantly wet snow (Saito et al., 2012). The snow density was still lower than in 2019, however, for a snowpack of less than 1 m it means that the snow water retention was almost reached (Kokkonen et al., 2006). Great snow depths increase compaction and structure changes of the lower snow layers to fern or ice (Kojima, 1967, Akitaya, 1974). Hence, high densities of 0.4 g/cm³ are common and still offer potential to take up and store water. However, shallow snowpacks do not create the necessary pressure on lower layers to change their structure. Deeper layers became icy because of water reacting with the snow.

This reaction closed pores and decreased the water storage capacity of the snowpack significantly (Kokkonen et al, 2006, Yamaguchi et al., 2012). A second water storing ability, which appeared frequently in thick snow covers, is given by the icy layers as capillary barrier. Those layers are less permeable and in some parts of the snowpack almost impermeable (Bartsch et al., 2010, Avanzi et al., 2015). Some water infiltrating the snow from the top gets trapped in ponds on boundaries between snowy and icy layers (Hirashima et al., 2016). The shallow snowpack in 2020 did not produce many icy impermeable layers, which resulted in fewer possibilities for the water to pond within the snowpack. Based on the high air temperatures, the snow density and the shallow cover 2020, the critical value of rain affecting soil moisture was significantly smaller than in 2019. For the time with less than 1 m of snow cover, all rain events with more than 7 mm/d affected soil moisture. However, the majority of peak events were identified as mixed events, since snowmelt added to rainfall on most days (Figure 3.61).

The different critical values corresponding to different snow depths allowed the prediction of events with increase of soil moisture due to rainfall, which is necessary for the further understanding of soil moisture activity and the influence of ROS events on soil hydrological processes (Iwata et al., 2010, Iwata et al., 2011). Since snow density and SWE are high in YURF and ROS events of different intensities, based on the snow depth, induced infiltration of the soil, it can be expected that the critical value will be higher or lower depending on the climate and snow density of a given region.

4.4.2 Simulation of events

With the meteorological data of the past eight years the number of events causing soil moisture increase since the year 2012 was estimated. The predicted events for January and February 2019 (Table 3.6) were all confirmed by soil moisture measurements. Some of the measured peaks were not predicted because rainfall was rather small on some days, but our aim was to calculate how many events happened at least in the past nine years. Since all events were simulated correctly, also all events in previous years were assumed to have affected soil moisture. No significant change in the number of ROS or snowmelt events was found along the years in January and February, where snowmelt seemed to affect soil

moisture in February, while ROS was more evenly distributed within January and early February.

However, the results for 2020 indicated that the critical value should be used in connection with the snow depth. A rain event of 8.5 mm on Dec. 14, 2018 did also cause a peak in the soil moisture curve of *SB* (Figure 3.57). Since the amount of rain which was required to exceed the water storage capacity of the snow cover depended on the snow density and air temperature prior to ROS events, the critical value needs to be regarded as indicator for the minimum number of events increasing soil moisture. Moreover, with more than 1 m of snow depth, 8 mm of rain were sometimes enough to induce outflow (Table 3.5), especially when the snow was already wetted after minor snowmelt.

Using rainfall data and snow depth, three critical values for ROS events were defined: rainfall of 7 mm for snow covers less than 1 m, 10 mm for less than 2 m, and 15 mm for less than 3 m. These values implied the dependence on snow depth but were not sufficient for the prediction of the exact amount of events affecting soil moisture. In fact, they were the indicator for the minimum number of soil moisture increases. If fresh dry snow with low density fell, rain of the described intensity should still affect soil moisture. Consequently, wet snow required less rain to reach its water capacity. Since changes in precipitation resulted in changes in soil moisture even under snow cover conditions, the possibility to predict soil moisture changes based on meteorological data can be a powerful tool for future characterisations of the hydrological cycle.

4.5 Snow dynamics

Snow depth, density and SWE varied considerably in the last decade. In particular, few snow fell in the winter 2019/2020, which resulted in a shallow snow cover (Figure 3.47) and a SWE significantly smaller than in the previous winters (Figure 3.53). Overall, the snow cover decreased in the last decade, highly influenced by the winter 2019/2020 (Figure 4.1). However, the observed tendency of recurring snow depths and alternating snow conditions implies that winters of small or large snowfall (Figure 3.45) were not exclusively the result of climate change, but follow a certain pattern

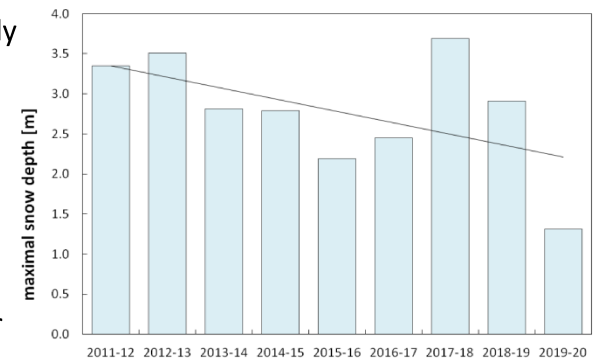

Figure 4.1: Trend of maximum snow depth

of natural variation (Beniston et al., 2003, Ishizaka, 2004, Yamaguchi et al., 2011). However, since the amount of snow falling in the winter has decreased over the last years and rainfall increased instead, the possibility of occurrence of winters with deep snow covers decreased (Kawase et al., 2018, Nishimura et al., 2019). If rain and snow fall equally and alternating, fresh snow of the snowpack can uptake rain water by increasing snow density, which results in a minimum of rainwater runoff. This process happens multiple times in every winter, resulting in snow densities between 0.45 and 0.55 g/cm³ in spring, which is the maximum theoretical snow density for ripened snow (Wakahama, 1968, Abe and Shimizu, 2004). However, the SWE differed based on the snow depth. Hence, as the snowfall determines the snow depth, the decrease in snowfall limits the depth of a potential snow cover.

Snow density increased not only when rain fell but also due to snowmelt. The relatively high air temperature in winter caused minor snowmelt events on several days of the winter season. Those events did not result in water discharge and a decrease in SWE, as it is usual for snowmelt, but in an increase in SWE linked to a decrease in snow depth. Top snow melted and moved down the snowpack, where it refroze in deeper layers. This process did not only increase snow density but also changed the structure of the snow to bigger and harder fragments (de Quervain, 1973, Colbeck, 1982). During winter the amount of ice grains increases and forms icy layers (Forbes and Stammler, 2016). Because the snow depth is usually more than three metres and thus higher than in many other regions of the world (Beniston et al., 2003, Inoue and Yokoyama, 2003, Kudo et al., 2017), the icy layers formed in the snowpack were not directly exposed to temperatures > 0 °C. When one layer reached its maximum density and all snow crystals were transformed into ice grains, snow layers above started to change their structure and to increase density. The more minor melt events occurred in winter and the less fresh snow fell, the earlier the whole snowpack transformed to a homogeneous icy structure with a density of 0.55 g/cm³.

Associated with the change of crystal structure is a change in snow water retention and preferential water flows of water within the snowpack (de Quervain, 1973, Avanzi et al., 2015). Therefore, changes in snow structure and snow density, including the formation of icy layers (Matsumoto et al., 2002), affected the mobility of water within the snowpack. Icy layers were found every year at all sites. They were hard, almost impossible to sample with the snow density sampling box, and formed barriers for water. The occurrence of icy layers in years with higher air temperature and more minor snowmelt events was more common

than in years with smaller air temperature. Icy layers seemed therefore to be formed during a snowmelt event. The snow surface becomes very wet and some water stays on top of the snow (Hirashima et al., 2018). When the air temperature decreased, water froze and created icy layers, which were covered by fresh snow of the next snowfall event. Those icy layers prevented lower snow layers from compaction, because they were more resistant to pressure of overlaying snow (Skogland, 1978, Forbes and Stammler, 2016) and blocked water moving down the snowpack (Avanzi et al., 2015, Hirashima et al., 2016). The formation of a dense icy layer and a snow layer with smaller density were found at the *Yaki* site at 20 and 30 cm snow depth (Mar. 20, 2019 – Apr. 22, 2019) and between 70 and 90 cm (Mar. 26, 2019 – Apr. 16, 2019). A second effect was the formation of depth hoar, which is the formation of an icy layer by snow, which sublimated on the soil surface and migrated upwards until it refroze in the snowpack (Giddings and LaChapelle, 1962, Akitaya, 1974, Reiweger and Schweizer, 2013). Since soil was not frozen in YURF, this process is likely to happen every year and was also confirmed in other regions of Japan (Iwata et al., 2010).

4.5.1 Snow in evergreen forest

The snowpack at *SM* was more homogeneous than the snowpacks at *Yaki* and *Isle*, and snow density did not increase significantly during the snowmelt season. Furthermore, now depth was in the forested area about 50 cm lower than in the open field. Evergreen forests influenced snow accumulation because the canopy accumulated snow which evaporated or sublimated and did not reach the snow surface (Giddings and LaChapelle, 1962, Fujihara et al., 2017). The Oxygen and Hydrogen isotopic data suggested further, that the forest canopy does not have only a physical but also a chemical effect on the snow (Figure 3.27). Higher isotope ratios of snow in the forested site were caused by interactions of trees and falling snow. Japanese cedar has usually $\delta^{18}O$ values between -7 and -10 ‰ (Zhang et al., 2019), which fits the observed values for *SB*, *SM* and *ST*. Snow, staying in the tree canopy, melted faster than on the ground, because it was surrounded by air and faced the sunlight directly (Sicart et al., 2004, Musselman et al., 2012). Hence, during the melting process it reacted with the air, which resulted in a shift in the isotopic composition. Snow under forest cover was thus heavier than snow in open sites. Since the isotopic composition of precipitation

changes seasonally (Bowen, 2008, Leonelli et al., 2017), snow in forested and in open sites influenced the isotopic composition of the soil moisture.

However, forest cover influenced the snowpack also during the snowmelt season, because the canopy blocked sunlight and therefore less energy reached the snowpack to melt snow (Yamazaki and Kondo, 1992, Harpold et al., 2015). The measured differences in snow depth of about 50 cm between evergreen forest sites and open sites resulted in differences of SWE. Applying an average density of 0.5 g/cm³ resulted in a SWE difference of 200 to 300 mm, which was significantly higher than in forests in other regions of the world (Winkler et al., 2005, Schelker et al., 2013). However, that represents around 20% of the total SWE in midwinter, which is the same percentage, Schelker et al. (2013) observed, and it was in the range of snow accumulation differences, calculated by Fujihara et al. (2017). Snow density was more homogeneous in the forested site, because snow, falling from the branches increases snow density of the top part of the snow cover (Floyd and Weiler, 2008). Manual measurements at *SM* in the snowmelt season 2019 confirmed further the variability in snow depth and SWE caused by the relief of the slope. Less snow accumulated in steep parts and snow depth was higher in less steep parts of the slope, which controlled the timing of snow disappearing (Jost et al., 2012). Because of the slope, including erosion processes and lateral water movement, and due to the forest cover, snow density in the slope reached values of up to 0.5 g/cm³ (Jost et al., 2009).

4.5.2 Snow modelling

Manual snow density measurements in the *Yaki* site proved that the snow covers in YURF with typical small densities on top and increasing density with snow depth (Akitaya, 1974, Saito et al., 2012) compacted to snowpacks with uniform density within less than two weeks. The homogenisation of the snowpack was noticed especially from February 12, 2019 to February 21, 2019 (Figure 3.48). Ongoing snowmelt and changes in the structure of the snow and ice crystals resulted in a further gradual increase of snow density (Kojima, 1967, de Quervain, 1973). The average density increasing from 0.43 g/cm³ on February 21 to 0.53 g/cm³ on April 22 confirmed structure changes of the snow, and was furthermore a useful parameter for the subsequent calculations of SWE during snowmelt periods. The small snow accumulation in the year 2020 was also the result of few heavy precipitation events. Heavy precipitation was in previous years mainly snowfall, which confirms also the

observations of Zhang et al. (2001), who described positive relations of snowfall to heavy precipitation events. These findings implicate, that the moderate precipitation in 2019/2020 was composed of a higher percentage of rain.

Calculations of snow density and SWE using snow depth have been attempted in different locations by many researchers and using various approaches (Durand et al., 1993, Davis et al., 1999, Inoue and Yokoyama, 2003, Narapusetty and Mölders, 2005, Jost et al., 2009, Bormann et al., 2014, Bokhorst et al., 2016, Achleitner and Schöber, 2017). Still, no universal method has been found for modelling snow parameters accurately. The meteorological conditions, relief, vegetation and unique characteristics of every region made it impossible to apply a single method for modelling (Bormann et al., 2014, Notaro et al., 2014). Models for Japan already predicted snow densities of more than 0.5 g/cm³ for the lower meter of deep snowpacks (Saito et al., 2012). However, total SWE for snow covers was often not accurately calculated. YURF has the availability of manual and automatic measurements, which offered the possibility to compare measurements and modelled data in situ. The calculations, described in the chapters 2.7.3.1 and 2.7.3.2, were used because the meteorological conditions, including the high snow cover, offered ideal parameters. Manual measurements from different seminars and manual measurements from the winter 2014/2015 were used to validate the calculations and to evaluate the precision of the model. The accuracy of the model was sufficient to reflect the snow dynamics in YURF. Hence, all graphs in the result section used the modelled snow density and SWE.

4.5.3 Snow accumulation period

Table 4.1: Differences between calculated and measured SWE (accumulation)

Date	Calculated SWE in mm	Actual SWE (±σ) in mm	Difference in mm
Dec. 16, 2014	384	294 (±40)	90
Jan. 8, 2015	702	705 (±32)	-3
Jan. 21, 2015	870	835 (±56)	35
Feb. 16, 2015	1150	1160 (±34)	-10
Feb. 20, 2018	1225	1285 (±85)	-60
Feb. 12, 2019	964	930 (±43)	34
Feb. 21, 2019	1041	973 (±104)	68
Feb. 19, 2020	362	356 (±30)	6

The calculations and modelling for the snow accumulation period were accurate for every year. In some cases the difference between the measured SWE and the calculated SWE was more than 50 mm, but except for December 16, 2014, all modelled values were within the range of the standard deviation of the manual measurements. Further, differences of 60 mm SWE for a snowpack of 1000 mm represent an error of 6%, which was smaller than errors of many other models (Durand et al., 1993, Saito et al., 2012, Kuribayashi et al., 2013, Brod, 2018). The calculations for the SWE were rather simple and used only temperature, precipitation and the DDF, which was calculated for YURF. The model was modified corresponding to the ability of the snowpack to store a certain amount of water from rainfall. The large amount of snow in YURF was probably the reason for the good accuracy of the calculations, because even differences of several millimetres of SWE represented only a small percentage of error for the whole snowpack. Further, snowmelt did not often take place during the snow accumulation period; therefore runoff from the snowpack originated only after rain events.

4.5.4 Snowmelt period

Table 4.2: Differences between calculated and measured SWE (snowmelt)

Date	Calculated SWE in mm	Actual SWE (±σ) in mm	Difference in mm
Mar. 5, 2015	1093	1132 (±86)	-39
Mar. 10, 2015	1045	1115 (±60)	-70
Mar. 15, 2015	1094	1063(±32)	29
Mar. 7, 2018	1395	1385 (±50)	10
Feb. 26, 2019	1004	969 (±96)	35
Feb. 28, 2019	988	987 (±40)	1
Mar. 13, 2019	904	945 (±95)	-41
Mar. 20, 2019	840	819 (±32)	21
Mar. 26, 2019	799	787 (±36)	12
Apr. 2, 2019	790	750 (±41)	40
Apr. 9, 2019	687	685 (±25)	2
Apr. 16, 2019	529	551 (±32)	-22
Apr. 22, 2019	334	345 (±19)	-11
Apr. 28, 2019	145	116 (±4)	29
Feb. 19, 2020	364	356 (±30)	8
Mar. 3, 2020	364	365 (±19)	-1

Similarly to the snow accumulation period, the modelling for the snowmelt period was accurate, except at the beginning and at the end of the snowmelt period. Differences were even smaller than during the snow accumulation period for most days, with usually less than 40 mm difference between calculated and measured SWE (Table 4.2). The differences for the year 2019 were particularly small, because this year was used for the parameterization of the model. The weekly measurements of SWE at the snow profile were ideal for comparisons with the model results in order to adjust the model values and calculation process, achieving greater accuracy in the end. The measuring tower and the manual measurements of different years suggested that the average snow density of the snowpack varied from year to year (Figures 3.51 and 3.53). Hence, it was interesting, that a constant coefficient of density (c_d), which was calculated for the winter 2018/2019 and used for the remaining years, gave accurate model results. The coefficient c_d was $1.4796*10^{-4}$ g/cm^4, which resulted for spring 2019 in an increase in density from 0.454 g/cm³ to 0.491 g/cm³ during the melting season. The snow density at the end of the snowmelt period was low when the initial snow depth was shallow, because the same coefficient was used for every winter. However, different snow densities based on shorter or longer snowmelt periods are realistic and a known process (Colbeck, 1982, Bormann et al., 2014, Bokhorst et al., 2016). Therefore, the small errors of the calculations did not necessitate to calculate a different c_d value for each year; it can be further used as an empirical factor for ongoing modelling in YURF.

The weak point of the model was the connection between the snow accumulation period and the snowmelt period. Since two different methods were used for the two stages of the winter, it was essential to determine the date of the beginning of the snowmelt season of every year. Since the model should work with few input data, namely precipitation and snow depth, an attempt was made to use these two factors to locate the transition between snow accumulation and snowmelt (Vaganov et al., 1999). Decrease in snow depth indicated snowmelt; however it is not a precise indicator, because snow depth started to decrease before SWE decreased. The period between the peak snow depth and peak SWE can be up to two weeks, because less dense snow of the top melts, which decreases snow depth, but does not leave the snowpack (Yamaguchi et al., 2010, BSYSE, 2018). In the winter 2018/2019, the offset between maximum snow depth and maximum SWE was 13 days. These 13 days were regarded as transition between snow accumulation and snowmelt season. Snow depth

offered the possibility to detect the first day of decrease of SWE after these 13 days. After February 25, 2019, snow depth decreased constantly, while it decreased with more variable rates during minor snowmelt events in the months before. Once a linear trend in decrease of snow depth was found for each year, the first day of those time periods was assumed to be the first day of SWE decrease. For the exact determination of the snowmelt season, the data of the measuring tower was used. The date when the maximum SWE was recorded at the tower, was defined as the start of snowmelt. This control method confirmed that the approach of determining a constant decrease of snow depth was suitable to investigate the start of snowmelt.

The two different methods for SWE calculation introduced a second problem, which was related to the SWE value itself. Calculated SWE of the snow accumulation period and for the snowmelt period were different on the day of maximum SWE in the control years 2014/2015 (Feb. 16) and 2018/2019 (Feb. 25). The difference was insignificant, with 10 mm and 45 mm, respectively, but it was with almost 200 mm difference significant in the winter 2017/2018, where only few control measurements were conducted. However, significant differences between measured and modelled SWE were observed only in the early stage of the snowmelt period. For water supply questions, the maximum SWE is of particular importance (Tahir et al., 2011b, Asaoka and Kominami, 2013, Achleitner and Schöber, 2017). It was usually slightly overestimated, but the overestimate was insignificant. Hence, the calculations for YURF were regarded as successfully accurate.

4.5.5 Degree-day factor

The two most important parameters for a DDF calculation are air temperature and SWE. As stated earlier, the SWE values for YURF were artificial and based on the precipitation and the changes in snow depth, because of the malfunction of the weather station. Because of the calculations, smaller changes in SWE and snow density, caused by sudden short-term weather changes, were not perfectly simulated. The SWE decrease and the snow density increase appear more uniform than they would be in reality. Hence, it could be expected that the accumulated snowmelt followed a linear trend for the DDF analysis. However air temperature has not been used for the modelling of SWE. Therefore, it was an independent factor used for the graphical approaches and the calculation of DDFs.

The two approaches (chapter 2.7.4) using the 10-day interval of Martinec (1960) resulted in a higher scattering of DDF values. Especially the original method, adding precipitation to the snowmelt of every day, resulted in higher DDFs, because on rainy days more water discharge was linked to air temperature than in the other three approaches. The difference between approach 3 and the other methods was higher on rainy years, because precipitation was already used to calculate daily SWE. Hence, the modification of the original method was useful and was supported by the small differences between the DDFs of the approaches 4, 1 and 2 (Figure 3.55).

However, the variations of DDFs within one year in the approaches using the 10-day interval were rather high. The method of Martinec (1960) used all intervals, disregarding the amount of days of snowmelt. If only one or two days of snowmelt were within a 10-day period, the resulting DDFs were highly variable. Therefore, significantly high DDFs were calculated especially in the early snowmelt season. Because there were only few days with increasing SWE during the main snowmelt period, the DDF values of the 10-day interval, especially of approach 4, were similar to the DDFs obtained by approaches 1 and 2.

The small differences between the graphical approaches (1 and 2) indicated that the influence of rain on snowmelt was insignificant in YURF. Because snow density was already high at the beginning of the snowmelt season, ROS events were mainly running through the snowpack without influencing the cover itself (Walsh et al., 1985). In particular, wet snow with high densities is characterised by high hydraulic conductivity and fast water flow (Colbeck and Anderson, 1982, Bokhorst et al., 2016). Hence, both approaches, even in rainy spring seasons, could be used simultaneously to calculate DDF values for YURF and for the Asahi Mountains in general. Snow density in other regions increased significantly during the snowmelt season, which explains an increase of the DDF in later stages of the melting period (He at al., 2014, Ismail et al., 2015). But the snow density did not increase significantly in YURF during snowmelt. Therefore, all days of the snowmelt period of every year were plotted together, and all linear regressions had $R^2 > 0.99$. DDFs in YURF ranged between 3 and 5.5 mm/d°C, with smaller DDFs in years where snow depth was less than 3 m. However, for most years the average DDF was around 4.3 mm/d°C, which fits the mean DDF of 4.1 mm/d°C of snow (Zhang et al., 2006) and the average DDF at the Japan Sea coast (Asaoka and Kominami, 2013).

Furthermore, the DDF values between different years did not change much. Many regions around the world have dynamic DDF values, which change during the melting season and from one year to another (Braithwaite, 2008, Butt and Bilal, 2011, Tahir et al., 2011a, Cui et al., 2013, Ismail et al., 2015). Also for Japan DDFs of 3.8 mm/d°C and higher were observed (Asaoka and Kominami, 2013, Nishimura et al., 2019), which means that the DDFs obtained in this study reflect the snowmelt rate of snow in Japan well. The range depended mainly on the amount of snow falling in winter and the air temperature. However, the meteorological conditions in YURF were similar from one year to another. The differences in air temperature among years were less than 5°C in winter (Figure 3.28). Variations in precipitation were higher, but in most years, the total precipitation in winter was around 1500 mm. In every year, ROS and multiple minor snowmelt events increased the snow density of the snowpack during the snow accumulation period. Thus, snow density was similar from year to year at the beginning of the snowmelt season, which was also indicated by the small standard deviation of the monthly average values for March and April (Figure 3.51). Hence, the meteorological conditions in YURF stand for a reproducibility of snowmelt measurements and analysis, as well as for an ideal basis for long term studies and comparisons.

It can be stated, that higher air temperature caused more runoff, because the accumulated snowmelt was constant to air temperature. The linear dependency between air temperature and SWE decrease allows accurate estimations of snowmelt using the DDF (Bagchi, 1983, Brubaker and Rango, 1996). Since the DDF did not change significantly during the snowmelt season, snowmelt could be used on any day during the snowmelt period. However, the calculated DDFs are only applicable in the study site, since snow covers at higher altitudes are known to have different DDFs (Braithwaite, 1995, Cui et al., 2013, Nishimura et al., 2019). Hence, the melting mechanics in higher elevations might be different in YURF and the Asahi mountains in general. The measured peak in stream water level was on April 26, 2019, when the snowmelt was already close to ending. Hence, the peak in water level was caused by snowmelt at higher elevations, further off the measuring point. Since the river water level peak was higher than during the snowmelt in the nearest area, the regions upstream had more snowmelt during the same period and therefore most probably higher SWEs and DDFs (Asaoka and Kominami, 2013, He at al., 2014).

Based on the reliance of stream water discharge on snowmelt from different areas of the watershed, the relation between runoff and stream discharge was not strong (Figure 3.26).

The supply of water from different areas affected the timing of water level and discharge in the stream. Precipitation and snowmelt were found to correlate with river discharge (Shanley and Chalmers, 1999, Masiokas et al., 2006, Dudley et al., 2017). Precipitation and snowmelt, which occurred in the whole YURF area, influenced the stream water level, too. More detailed measurements are needed to quantify the inputs because the correlation was with $R^2 < 0.35$ not significant. Many data points near the y-axis indicate that greater discharge was not necessarily linked to precipitation in YURF. The scattering of data points showed the influence of water discharge of areas upstream. The two different Manning coefficients represent the maximal and the minimal possible discharge, depending on the roughness of the stream bed. Typical values are 0.4 – 0.7 (Akgiray, 2004), therefore these two values were used as boundaries for the real value for the Wasada stream. Figure 3.26 showed that the discharge was generally between 200 and 700 l/s, which are values usual for mountain streams in Japan (Hirayama et al., 2002). However, no accurate identifications and analysis could be performed because the drainage area, which is essential for analysis (Komatsu and Onda, 1996, Hirayama et al., 2002), could not be measured and evaluated completely. It would be necessary to measure the stream discharge at least at the point where the stream entered YURF, in order to calculate the volume of water entering the stream in YURF. With the data obtained in this study, it can be only concluded, that a relation between snowmelt, precipitation and water discharge exists, and that peak river discharge allows the determination of the main snowmelt period.

4.6 HYDRUS 1D

The model results obtained with the parameters measured by the HYPROP system did not reflect the soil moisture data well. The calculated soil moisture increased significantly every month, which was mainly caused by the low value of hydraulic conductivity (Clark et al., 2006). The parameters calculated with the *Neural Network Prediction* showed better agreement with the recorded soil moisture. However, the differences between the three horizons were smaller in the model than in reality. Both input datasets have been modified to find the ideal parameterisation for the model. The parameters that were used differed from the texture data and even more from the HYPROP data. The differences can be explained by measuring discrepancies but also by soil heterogeneity (Sakaki et al., 2008,

Caiqiong and Jun, 2016). Soil texture, physical parameters and the resulting hydrological properties can vary significantly within a few cm (Calamita et al., 2012).

Modelling soil moisture using the HYDRUS 1D model produced overall good results for summer but did have discrepancies, especially in winter. The best results were achieved at *ST*, with usually less than 3 % difference in soil water content. The modelled and measured soil moisture differed only at the beginning and at the end of winter. Differences at *SM* and *SB* were significantly higher, around 2 % in the summer season and up to 10 % in winter (Figure 3.63). The higher difference between the model and the measured soil moisture at the two spots downwards the slope might originate from their position. HYDRUS 1D considers only vertical flow of water, and did not connect the three spots within the model. All models for soil moisture have been calculated separately, and therefore lateral flow within the snowpack, as described earlier, was not regarded. This resulted in a higher volume of water, which was applied to the soil in the model. Hence, soil moisture seemed to increase and did not reflect reality. The effect of ROS events on soil moisture also was not modelled accurately. Instead of just major events with rainfall of more than 10 mm, almost every ROS event produced a soil moisture peak in the model. The model did not seem to be able to use the snow cover as buffering layer. That might originate from the snow density, which was not used for the model (Kojima, 1967), and from the snow structure, which is more complex in YURF than in other regions (Spreitzhofer, 1999, Conner et al., 2016, Kojima et al., 2018).

The HYDRUS model overestimated especially the soil drying process after rainfall. Most peaks were not as sharp in the model as they were in reality. Even model runs with higher values for K_s did not change the decrease rate of soil moisture after the peak event significantly. Furthermore, the model calculated longer and more intensive drying, resulting in significantly lower soil moisture values after peaks (Figure 3.63). The longer drying process could be caused by the parameterisation of the water retention parameters α and n. However, changes affected especially the mean soil water content. Thus, it was not possible to adjust the parameters in a way that achieved a good fit of the modelled soil moisture curve to the measured curve.

Rainfall was reflected directly in the soil moisture in both model and reality. In contrast to the winter months, modelled peak height and timing for most of the rain events was accurate for all three spots and represented the measured data well. It can be concluded

that the parameterisation of the model was suitable to model soil moisture dynamics in YURF at the top of slopes for the whole year, and at all sites in seasons without snow cover. Lateral movement of water and influences of snow cover were not modelled properly, therefore the soil moisture calculations for *SB* and *SM* under snow cover did not represent the measured soil moisture data.

The missing forest cover had an influence on the modelled soil moisture. Plant water uptake was modelled using Feddes parameters of the database of fruit trees. The model lost accuracy in the calculation of root water uptake, because no data for Japanese cedar forest was found. There are other studies which investigated Feddes parameters of evergreen forests (Adane et al., 2018, Rabbel et al., 2018). However, the effect of using different databases for trees was insignificant for the modelling in YURF, because trees never faced drought stress.

The most significant problem of the HYDRUS model was found to be the estimation of snow depth. Since the HYDRUS software was not created for dealing with large amounts of snow, there was no focus on interactions between snow and soil (Šimůnek et al., 2013). The use of a melting factor relating to snow cover decrease (in cm/d) does not represent the reality in YURF well, where snowmelt is stronger related to SWE than to snow depth. Therefore, the model would be improved by using SWE and DDF values for the prediction of snowmelt. However, the model did also underestimate the snow depth in the snow accumulation period. The reason for the small modelled snow depth might be the air temperature. HYDRUS calculated snowmelt for days where the temperature was positive but precipitation fell still as snow. As described in chapter 4.5.4, the transition between rain and snow in YURF is not clear. Since snowfall occurred at positive air temperatures in YURF, snow accumulated, but for the same time rainfall and snowmelt were assumed by the HYDRUS model. The use of different snow models in addition to HYDRUS will improve the accuracy of snow depth calculation (Ismail et al., 2015, Brod, 2018).

However, the modelling of soil moisture was accurate, especially for *SB*, and for all three spots in seasons without snow cover. The model can be improved by using more appropriate values for the plant water uptake calculations (Rabbel et al., 2018), heat transport parameters (Šimůnek et al., 2018) or the soil physical properties (Wessolek et al., 2009, Grinevskiy and Pozdniakov, 2013, Caiqiong and Jun, 2016), e.g. The greatest improvement for the modelling of the slope would occur from using HYDRUS 2D or even HYDRUS 3D to

model the whole watershed and to understand the mechanism in the forest better (Šimůnek et al., 2013, Marthews et al., 2014). As the slope water runoff measurements and soil moisture peak analysis showed, the lateral transport of water was substantial and caused significant differences between the soil moisture curves of *SB* and the other two spots.

4.7 Possible effects on forests

The results revealed that winter precipitation had positive as well as negative impacts on forests in Tōhoku region. On the one hand, water saturated soils due to infiltration of water from ROS or snowmelt events (Hardy et al., 2001) supply plants with sufficient moisture for transpiration in spring (Schwartz and Karl, 1990, Lopez et al., 2015, Osonoi, 2018). Melting processes in spring last longer in forested areas than in clear cut sites, resulting in longer snow cover (Winkler et al., 2005, Jost et al., 2012, Harpold et al., 2015). Unfrozen soil determines the connection between water in the soil surface and the rhizosphere (Edwards et al., 2007, Potopová et al., 2016), as was found in YURF.

On the other hand, drastic decrease in snowfall results in a smaller SWE and shorter melting periods in spring. Water running off in winter was not available for vegetation in spring, which had negative effects on forests due to low precipitation during the initial growing stage (Osonoi, 2018). Forests in mountainous areas might be subject to water shortages in spring, as the snowmelt water supply decreases, and subsurface runoff in mid-winter increases as a result of warmer winters and increase in the number of ROS events (Tague and Peng, 2013, Bokhorst et al., 2016). Thus, it is expected that an increase in the rain/snow ratio will have a strong effect on subsurface water runoff, groundwater levels and stream water discharge in the future, which will probably affect the forest ecosystems (Vaganov et al., 1999, Winkler et al., 2005, Zhang et al., 2005). Since snow stores nutrients like nitrogen, which are distributed to plants during snowmelt, less snow cover does also result in fewer nutrients during the growing season (Clow and Mast, 1995, Kuhn, 2001). Regarding greenhouse gases and climate change, the ability of forest soils to uptake and store methane depends on soil moisture and the duration of snow cover (Borken et al., 2006). Soil drying due to shorter periods of snow cover may lead to smaller uptake of methane as well as less cooling and result hence in increases of air temperature (Cohen and Rind, 1991).

Another factor controlling plant growth is the water isotopic composition (Leonelli et al., 2017). The observed difference in isotope ratio between open sites and forested sites will lead to different isotopic compositions of soil moisture and ground water. The soil moisture isotope ratio will be reflected in the tree xylem water (Zhang et al., 2019) especially in spring, when the trees use the most water (Osonoi, 2018).

4.8 Outlook

In general, the results characterised many hydrological processes in YURF well. However, some datasets were not detailed enough to extrapolate the results of YURF to a larger area. Transferring the methods to other slopes in order to understand the water dynamic of the whole watershed would improve the knowledge about the hydrological cycle significantly. It will be interesting to conduct measurements of bedrock runoff and surface runoff in the future, because the amount of water running off allows quantification of the water use of trees in spring. The water usage pattern of trees and other plants was not taken into consideration in this study, but since other studies are already available, the incorporation of such patterns will be possible without major problems (Osonoi, 2018 Enta et al, 2019, Zhang et al., 2019).

Since this thesis and the measurements focused on snow dynamics and soil moisture, there was less focus on other key aspects of the hydrological cycle. Studying mechanisms like the river discharge or groundwater dynamics will, in combination with the data and experiences of this study, improve the knowledge of the forest water dynamics in YURF. Therefore, continuation of the measurements of soil moisture is planned, and new measurements need to be established to complete and expand the datasets.

Regarding the meteorological conditions in Tōhoku region itself, the next few years will be of high interest. If the winter monsoon and wind streams from Siberia change as a consequence of climate change (Dorman et al., 2004, Shimada and Kawamura, 2004, Asaoka and Kominami, 2013), snowfall might decrease drastically in combination with air temperature increases, which will further increase soil temperatures. Positive air temperatures result then in less precipitation, especially in less snowfall in winter (Takeuchi et al., 2008, Hirabayashi et al., 2010, Luo et al., 2011). As already found in the significantly small amount of snow in the recent winter (2019/2020), the effect of climate change might have a large impact on forest water supply and on agriculture, since the amount of

snowmelt water may decrease significantly over the next years. Combined with changes in the amount of precipitation (Mizuta et al., 2005, Fujita et al., 2014), the meteorological conditions may change more in future (Yamaguchi et al., 2013). Detailed monitoring and analysis in different locations will be needed in order to determine whether the warm and dry winter 2019/2020 was a unique winter or the start of a change in winter climate of Tōhoku and other regions of Japan.

5. Conclusion

The present research at an evergreen forested slope at the Yamagata University Research Forest is a detailed investigation of the hydrological cycle in the region, introducing meteorological parameters and the characteristics of snow and soil interactions.

Soils have been analysed regarding soil type, texture and hydrophysical properties in the main study area, YURF, and in Kaminoyama, where the vineyard classification took place. The water retention curves of most sampling spots represented the soil texture analysis and water repellency data improved the discussion of water movement at the slope in YURF.

Soil moisture measurements revealed different reactions to rainfall in summer and to water infiltration in winter at the three different spots. Surface and bedrock runoff data in relation to soil moisture and precipitation data showed that the water content of the topsoil was one important factor for the distribution of water. In winter, soil moisture reacted to ROS events and snowmelt, when the events produced sufficient amounts of water.

Differences in snow depth, SWE and snow density were found by comparing snow in an evergreen forest and in open sites. Less snow accumulated in the forest, but the snowmelt was slower in forests compared to the open sites.

During winters, several ROS events as well as partial snowmelt due to positive air temperature were observed. Snow density increased during these events, changing the structure and forming icy layers. Events with greater volume of water resulted in peaks in the snow density curve and in soil moisture. Hence, snow density changes were partially irreversible and partially reversible.

SWE was modelled with two different approaches, divided into snow accumulation and snowmelt period. The calculation of SWE for the snowmelt period was more accurate and closer to the results of control measurements than for the snow accumulation period. However, most modelled values showed no significant differences from the control measurements and were therefore regarded as sufficient.

Precipitation and air temperature did not change significantly in most of the years, especially in winter. However, the ratio of rain and snowfall in winter changed to a higher proportion of rain. Snowmelt was similar among years, resulting in small differences in DDFs. Rainfall seemed to have no significant influence on snowmelt in YURF.

Modelled soil moisture reflected the measured values well in summer but had significant discrepancies in winter. Snow cover and precipitation lead to higher modelled soil moisture values under snow cover. Only at ST the difference between modelled and observed soil moisture was minor in winter.

The HYDRUS 1D model already gave good results for the prediction of soil moisture. Using more spots and measurements of soil properties and soil moisture can help to improve the model. Finding a solution for the implementation of snow dynamics would increase the accuracy of the HYDRUS model significantly, especially for the mountainous regions of Japan with heavy snowfall characteristics. For the studied slope and the modelling process, the use of HYDRUS 2D would deliver more data, like surface runoff, e.g., and would improve the calculations of lateral water transport processes.

This study showed the meteorological changes in YURF within the last years and the strong relation between winter precipitation and soil moisture. Climate change affects Tōhoku region and needs to be monitored in detail in the future in order to characterise its impact on the hydrological cycle in Shōnai area.

6. Abbreviations

CN ratio = Carbon Nitrogen ratio

DDF = degree-day factor

ρ_{snow} = snow density

ROS = rain-on-snow

SB = slope bottom

SM = slope middle

ST = slope top

SWE = snow water equivalent

T_{air} = air temperature

T_{soil} = soil temperature

7. Acknowledgements

The three years of my PhD studies did not only required effort of myself to obtain good results and make an effect on the recent science of hydrology and snow dynamics, but included also many supporters and consultants. Therefore, I like to thank in this section all persons who have been part of this work and supported me in many different ways.

At first, I like to thank of course my three supervisors Prof. Hideki Murayama, Prof. Larry Lopez and Prof. Chihiro Kato for their suggestions, help and their great support at any time.

Daisuke Arai and Yoshiaki Iizuka of the Yamagata University Research Forest supported my experiments in the forest and helped preparing the sampling sites, driving me to the research station and equipping me for the measurements. I further like to thank Dr. Felix Seidel for helping me with snow density samples in the winter 2018/2019.

During my internship at Hochschule Koblenz in Germany, Prof. Wolfgang Bogacki and Muhammed Fraz Ismail have been grate hosts, improving research together about snow dynamics and investigating DDFs for YURF. A scientific paper about the DDF results is in work and will hopefully be submitted to a journal, soon.

Thanks for Prof. Jörg Bachmann, Dr. Susanne Woche, Moritz Rahlfs and Martin Volkmann from the soil science institute at the Leibniz University Hannover for their great support and help with the HYPROP system and water repellency measurements. Prof. Bachmann was further a great help in advising experiments, sharing supporting literature and informing me about the usage of HYDRUS software. Dr. Leopold Sauheitl and Anne K. Herwig from the soil science institute at Leibniz University Hannover have been a great help for the CN measurements.

Dr. Jens Groß, Prof. Benjamin Burkhard and Heiko van Wensen from the Institute of Physical Geography at Leibniz University Hannover were supporting my analyses of soil texture.

Ms. Okubo Tsukuba University measured the snow isotopic composition and Ass. Prof. Yoshiko Muto from Iwate University provided her HYPROP measurement system for the water retention measurements at Yamagata University.

During the writing process of the thesis, Professor Friedhelm Schwarz and Dr. Sibylle Weck-Schwarz have been an enormous help in giving advices for the English grammar and proof reading.

Finally, my fiancée Sarah Kentsch and my whole family kept me motivated, helped and supported me in stressful situations and supported my life and study in all possible ways. Especially in the last months, writing my thesis took a lot of time, and the support of Sarah and the rest of my family was an immense help. Sarah also helped a lot proof reading the text and suggesting changes.

All other students of our Laboratory helped me translating texts, filling important documents besides my study and made the student life in Tsuruoka much easier and more interesting. Having that many people involved and having helped with my research I like again to thank everybody again for the way they supported me in the three years.

8. Cited literature

Abdu, H., D. A. Robinson, M. Seyfried, and S. B. Jones. 2008. 'Geophysical Imaging of Watershed Subsurface Patterns and Prediction of Soil Texture and Water Holding Capacity: GEOPHYSICAL IMAGING OF WATERSHED SUBSURFACE'. *Water Resources Research* 44(4).

Abe, Osamu, and Masujiro Shimizu. 2004. 'Equivalent Snow Density to Estimate Snow Load in Extremely Heavy Snow Areas'. 日本雪氷学会誌雲氷 66(1):11–16.

Achleitner, Stefan, and Johannes Schöber. 2017. 'Weiße Wasserspeicher – Analyse und Modellierung der Schneedichte in den österreichischen Alpen und Alpenvorländern'. *Österreichische Wasser- und Abfallwirtschaft* 69(3–4):171–79.

Adane, Zablon A., Paolo Nasta, Vitaly Zlotnik, and David Wedin. 2018. 'Impact of Grassland Conversion to Forest on Groundwater Recharge in the Nebraska Sand Hills'. *Journal of Hydrology: Regional Studies* 15:171–83.

Akgiray, Ömer. 2004. 'Simple Formulae for Velocity, Depth of Flow, and Slope Calculations in Partially Filled Circular Pipes'. *Environmental Engineering Science* 21(3):371–85.

Akitaya, Eizi. 1974. 'Studies on Depth Hoar'. *Contributions from the Institute of Low Temperature Science* A26:1–67.

Alabarse, F. G., J. Haines, O. Cambon, C. Levelut, D. Bourgogne, A. Haidoux, D. Granier, and B. Coasne. 2012. 'Freezing of Water Confined at the Nanoscale'. *Physical Review Letters* 109(3):035701.

Anagnostopoulou, Christina, and Konstantia Tolika. 2012. 'Extreme Precipitation in Europe: Statistical Threshold Selection Based on Climatological Criteria'. *Theoretical and Applied Climatology* 107(3–4):479–89.

Anderson, Eric A. 1973. 'NOAA Technical Memorandum NWS-HYDRO-17'.

Asanuma, Jun, and Hideyuki Kamimera. 2004.'Long-Term Trend of Pan Evaporation Measurements in Japan and Its Relevance to the Variability of the Hydrological Cycle'. Presented at the Symposium on Water Resource and Its Variability in Asia in the 21st Century, Tsukuba.

Asaoka, Yoshihiro, and Yuji Kominami. 2013. 'Incorporation of Satellite-Derived Snow-Cover Area in Spatial Snowmelt Modeling for a Large Area: Determination of a Gridded Degree-Day Factor'. *Annals of Glaciology* 54(62):205–13.

Assouline, S., D. Tessier, and A. Bruand. 1998. 'A Conceptual Model of the Soil Water Retention Curve'. *Water Resources Research* 34(2):223–31.

Avanzi, F., H. Hirashima, S. Yamaguchi, T. Katsushima, and C. De Michele. 2015. 'Laboratory-Based Observations of Capillary Barriers and Preferential Flow in Layered Snow'. *The Cryosphere Discussions* 9(6):6627–59.

Avanzi, Francesco, Tessa P. Maurer, Sami A. Malek, Steven D. Glaser, Roger C. Bales, and Martha H. Conklin. 2018. *Feather River Hydrologic Observatory: Improving Hydrological Snowpack Forecasting for Hydropower Generation Using Intelligent Information Systems*. CNRA-CEC-2018-001. California's Fourth Climate Change Assessment, California Energy Commission.

Bachmann, J., R. Horton, R. R. van der Ploeg, and S. Woche. 2000. 'Modified Sessile Drop Method for Assessing Initial Soil-Water Contact Angle of Sandy Soil'. *Soil Science Society of America Journal* 64(2):564–67.

Bagchi, A. K. 1983. 'A Real Value If Degree-Day Factor'. *Hydrological Sciences* 28(4):499–511.

Baker, Donald G., and David L. Ruschy. 1995. 'Calculated and Measured Air and Soil Freeze-Thaw Frequencies'. *Journal of Applied and Climatology* 34(10):2197–2205.

Bales, Roger C., Jan W. Hopmans, Anthony T. O'Geen, Matthew Meadows, Peter C. Hartsough, Peter Kirchner, Carolyn T. Hunsaker, and Dylan Beaudette. 2011. 'Soil Moisture Response to Snowmelt and Rainfall in a Sierra Nevada Mixed-Conifer Forest'. *Vadose Zone Journal* 10(3):786–99.

Bartsch, Annett, Timo Kumpula, Bruce C. Forbes, and Florian Stammler. 2010. 'Detection of Snow Surface Thawing and Refreezing in the Eurasian Arctic with QuikSCAT: Implications for Reindeer Herding'. *Ecological Applications* 20(8):2346–58.

Beniston, M., F. Keller, and S. Goyette. 2003. 'Snow Pack in the Swiss Alps under Changing Climatic Conditions: An Empirical Approach for Climate Impacts Studies'. *Theoretical and Applied Climatology* 74(1–2):19–31.

Berris, Steven N., and R. Dennis Harr. 1987. 'Comparative Snow Accumulation and Melt during Rainfall in Forested and Clear-Cut Plots in the Western Cascades of Oregon'. *Water Resources Research* 23(1):135–42.

Berset, J. D., M. Ejem, Ruth Holzer, and Peter Lischer. 1999. 'Comparison of Different Drying, Extraction and Detection Techniques for the Determination of Priority Polycyclic Aromatic Hydrocarbons in Background Contaminated Soil Samples'. *Analytica Chimica Acta* 383:263–75.

Bertoldi, Giacomo, Stefano Della Chiesa, Claudia Notarnicola, Luca Pasolli, Georg Niedrist, and Ulrike Tappeiner. 2014. 'Estimation of Soil Moisture Patterns in Mountain Grasslands by Means of SAR RADARSAT2 Images Andhydrological Modeling'. *Journal of Hydrology* 516:245–57.

Besnard, E., C. Chenu, and M. Robert. n.d. 'Influence of Organic Amendments on Copper Distribution among Particle-Size and Density Fractions in Champagne Vineyard Soils'. *Environmental Pollution* 112:329–37.

Betts, Alan K., and John H. Ball. 1997. 'Albedo over the Boreal Forest'. *Journal of Geophysical Research: Atmospheres* 102(D24):28901–9.

Bingham, Marcus A., and Suzanne W. Simard. 2013. 'Seedling Genetics and Life History Outweigh Mycorrhizal Network Potential to Improve Conifer Regeneration under Drought'. *Forest Ecology and Management* 287:132–39.

Blume, Hans-Peter, Gerhard W. Brümmer, Rainer Horn, Ellen Kandeler, Ingrid Kögel-Knabner, Ruben Kretzschmar, Karl Stahr, and Berndt-Michael Wilke. 2010. *Scheffer/Schachtschabel Lehrbuch der Bodenkunde*. 16th ed. Spektrum.

Bokhorst, Stef, Stine Højlund Pedersen, Ludovic Brucker, Oleg Anisimov, Jarle W. Bjerke, Ross D. Brown, Dorothee Ehrich, Richard L. H. Essery, Achim Heilig, Susanne Ingvander, Cecilia Johansson, Margareta Johansson, Ingibjörg Svala Jónsdóttir, Niila Inga, Kari Luojus, Giovanni Macelloni, Heather Mariash, Donald McLennan, Gunhild Ninis Rosqvist, Atsushi Sato, Hannele Savela, Martin Schneebeli, Aleksandr Sokolov, Sergey A. Sokratov, Silvia Terzago, Dagrun Vikhamar-Schuler, Scott Williamson, Yubao Qiu, and Terry V. Callaghan. 2016. 'Changing Arctic Snow Cover: A Review of Recent Developments and Assessment of Future Needs for Observations, Modelling, and Impacts'. *Ambio* 45(5):516–37.

Borken, Werner, Eric A. Davidson, Kathleen Savage, Eric T. Sundquist, and Paul Steudler. 2006. 'Effect of Summer Throughfall Exclusion, Summer Drought, and Winter Snow Cover on Methane Fluxes in a Temperate Forest Soil'. *Soil Biology and Biochemistry* 38(6):1388–95.

Bormann, Kathryn J., Jason P. Evans, and Matthew F. McCabe. 2014. 'Constraining Snowmelt in a Temperature-Index Model Using Simulated Snow Densities'. *Journal of Hydrology* 517:652–67.

Bowen, Gabriel J. 2008. 'Spatial Analysis of the Intra-Annual Variation of Precipitation Isotope Ratios and Its Climatological Corollaries'. *Journal of Geophysical Research: Atmospheres* 113(D5): D05113.

Boyer, Elizabeth W., George M. Homberger, Kenneth E. Bencala, and Diane M. McKnight. 1997. 'Response Characteristics of DOC Flushing in an Alpine Catchment'. *Hydrological Processes* 11:1635–47.

Braithwaite, Roger J. 1995. 'Positive Degree-Day Factors for Ablation on the Greenland Ice Sheet Studied by Energy-Balance Modelling'. *Journal of Glaciology* 41(137):153–60.

Braithwaite, Roger J. 2008. 'Temperature and Precipitation Climate at the Equilibrium-Line Altitude of Glaciers Expressed by the Degree-Day Factor for Melting Snow'. *Journal of Glaciology* 54(186):437–44.

Bramley, R. G. V., J. Ouzman, and P. K. Boss. 2011. 'Variation in Vine Vigour, Grape Yield and Vineyard Soils and Topography as Indicators of Variation in the Chemical Composition of Grapes, Wine and Wine Sensory Attributes: Vineyard Variation in Wines, Grapes and Soils'. *Australian Journal of Grape and Wine Research* 17(2):217–29.

Brod, Fabian. 2018. 'Modeling Snow Distribution in a Forested Area in the Asahi Mountains, Japan'.

Brandt, Alexander C., Qiqin Zhang, Maximo Larry Lopez Caceres, and Hideki Murayama. 2020. 'Soil Temperature and Soil Moisture Dynamics in Winter and Spring under Heavy Snowfall Conditions in North-Eastern Japan'. *Hydrological Processes* hyp.13794.

Brubaker, K. L., and A. Rango. 1996. 'Response of Snowmelt Hydrology to Climate Change'. *Water, Air, and Soil Pollution* 90:335–43.

BSYSE. 2018.'Snowmelt and Frozen Soil (Based on Class Notes by Erin Brooks and the Text by Dingman (2002))'. Presented at the BSYSE 456/556 Lecture 4.

Bulygina, O. N., P. Ya Groisman, V. N. Razuvaev, and N. N. Korshunova. 2011. 'Changes in Snow Cover Characteristics over Northern Eurasia since 1966'. *Environmental Research Letters* 6(4):045204.

Butt, Mohsin Jamil, and Muhammad Bilal. 2011. 'Application of Snowmelt Runoff Model for Water Resource Management'. *Hydrological Processes* 25(24):3735–47.

Caiqiong, Yi, and Fan Jun. 2016. 'Application of HYDRUS-1D Model to Provide Antecedent Soil Water Contents for Analysis of Runoff and Soil Erosion from a Slope on the Loess Plateau'. *CATENA* 139:1–8.

Calamita, G., L. Brocca, A. Perrone, S. Piscitelli, V. Lapenna, F. Melone, and T. Moramarco. 2012. 'Electrical Resistivity and TDR Methods for Soil Moisture Estimation in Central Italy Test-Sites'. *Journal of Hydrology* 454–455:101–12.

Callaghan, Terry V., Margareta Johansson, Ross D. Brown, Pavel Ya. Groisman, Niklas Labba, Vladimir Radionov, Roger G. Barry, Olga N. Bulygina, Richard L. H. Essery, D. M. Frolov, Vladimir N. Golubev, Thomas C. Grenfell, Marina N. Petrushina, Vyacheslav N. Razuvaev, David A. Robinson, Peter Romanov, Drew Shindell, Andrey B. Shmakin, Sergey A. Sokratov, Stephen Warren, and Daquing Yang. 2011. 'The Changing Face of Arctic Snow Cover: A Synthesis of Observed and Projected Changes'. *AMBIO* 40(S1):17–31.

Cayan, Daniel R. 1996. 'Interannual Climate Variability and Snowpack in the Western United States'. *Journal of Climate* 9:928–48.

Clark, Martyn P., Andrew G. Slater, Andrew P. Barrett, Lauren E. Hay, Gregory J. McCabe, Balaji Rajagopalan, and George H. Leavesley. 2006. 'Assimilation of Snow Covered Area Information into Hydrologic and Land-Surface Models'. *Advances in Water Resources* 29(8):1209–21.

Cline, Donald W. 1997. 'Snow Surface Energy Exchanges and Snowmelt at a Continental, Midlatitude Alpine Site'. *Water Resources Research* 33(4):689–701.

Clow, David W., and Alisa Mast. 1995. 'Composition of Precipitation, Bulk Deposition, and Runoff at a Granitic Bedrock Catchment in the Loch Vale Watershed, Colorado, USA'. *AHS Publications-Series of Proceedings and Reports-Intern Assoc Hydrological Sciences* 228:235–42.

Colbeck, S. C. 1982. 'An Overview of Seasonal Snow Metamorphism'. *Reviews of Geophysics* 20(1):45.

Colbeck, S. C., and Eric S. Anderson. 1982. 'The Permeability of a Melting Snow Cover'. *Water Resources Research* 18(4):904–8.

Coléou, Cécile, and Bernard Lesaffre. 1998. 'Irreducible Water Saturation in Snow: Experimental Results in a Cold Laboratory'. *Annals of Glaciology* 26:64–68.

Conner, Lafe G., Richard A. Gill, and Jayne Belnap. 2016. 'Soil Moisture Response to Experimentally Altered Snowmelt Timing Is Mediated by Soil, Vegetation, and Regional Climate Patterns'. *Ecohydrology* 9(6):1006–16.

Coulson, S. J., I. D. Hodkinson, A. T. Strathdee, W. Block, N. R. Webb, J. S. Bale, and M. R. Worland. 1995. 'Thermal Environments of Arctic Soil Organisms during Winter'. *Arctic, Antarctic and Alpine Research* 27(4):364–70.

Cristiano, Giuseppe, Salvatore Camposeo, Mariano Fracchiolla, Gaetano Vivaldi, Barbara De Lucia, and Eugenio Cazzato. 2016. 'Salinity Differentially Affects Growth and Ecophysiology of Two Mastic Tree (Pistacia Lentiscus L.) Accessions'. *Forests* 7(12):156.

Cui, Yuhuan, Baisheng Ye, Jie Wang, and Youcun Liu. 2013. 'Influence of Degree-Day Factor Variation on the Mass Balance of Glacier No. 1 at the Headwaters of Ürümqi River, China'. *Journal of Earth Science* 24(6):1008–22.

Davis, Robert E., Michael B. Lowit, Paul C. Knappenberger, and David R. Legates. 1999. 'A Climatology of Snowfall-Temperature Relationships in Canada'. *Journal of Geophysical Research: Atmospheres* 104(D10):11985–94.

De la Hera, M. L., P. Romero, E. Gómez-Plaza, and A. Martinez. 2007. 'Is Partial Root-Zone Drying an Effective Irrigation Technique to Improve Water Use Efficiency and Fruit Quality in Field-Grown Wine Grapes under Semiarid Conditions?' *Agricultural Water Management* 87(3):261–74.

de Quervain, M. R. 1973. 'Snow Structure, Heat, and Mass Flux through Snow'. *The Role of Snow and Ice in Hydrology* 105(14):203–26.

Detert, Martin, and Gary Parker. 2010. 'Estimation of the Washout Depth of Fine Sediments from a Granular Bed'. *Journal of Hydraulic Engineering* 136(10):790–93.

Di Ferrante, N., R. D. Leachman, P. Angelini, P. V. Donnelly, G. Francis, A. Almazan, G. Segni, C. Franzblau, and R. E. Jordan. 1975. 'Ehlers-Danlos Type V (X-Linked Form): A Lysyl Oxidase Deficiency'. *Birth Defects Original Article Series* 11(6):31–37.

Dorman, C. E., R. C. Beardsley, N. A. Dashko, C. A. Friehe, D. Kheilf, K. Cho, R. Limeburner, and S. M. Varlamov. 2004. 'Winter Marine Atmospheric Conditions over the Japan Sea'. *Journal of Geophysical Research* 109(C12):C12011.

Dörner Fernández, José Miguel. 2005. 'Anisotropie von Bodenstrukturen und Porenfunktionen in Böden und deren Auswirkungen auf Transportprozesse im gesättigten und ungesättigten Zustand'.

Dudley, R. W., G. A. Hodgkins, M. R. McHale, M. J. Kolian, and B. Renard. 2017. 'Trends in Snowmelt-Related Streamflow Timing in the Conterminous United States'. *Journal of Hydrology* 547:208–21.

Durand, Y., E. Brun, L. Merindol, G. Guyomarc'h, B. Lesaffre, and E. Martin. 1993. 'A Meteorological Estimation of Relevant Parameters for Snow Models'. *Annals of Glaciology* 18:65–71.

Durner, Wolfgang. 1994. 'Hydraulic Conductivity Estimation for Soils with Heterogeneous Pore Structure'. *Water Resources Research* 30(2):211–23.

Dusek, Jaromir, Tomas Vogel, Michal Dohnal, Johannes A. C. Barth, Martin Sanda, Anne Marx, and Jakub Jankovec. 2017. 'Dynamics of Dissolved Organic Carbon in Hillslope Discharge: Modeling and Challenges'. *Journal of Hydrology* 546:309–25.

Ebuchi, Naoto, Hiroshi Kawamura, and Yoshiaki Toba. 1992. 'Growth of Wind Waves with Fetch Observed by the Geosat Altimeter in the Japan Sea under Winter Monsoon'. *Journal of Geophysical Research* 97(C1):809.

Edwards, Anthony C., Riccardo Scalenghe, and Michele Freppaz. 2007. 'Changes in the Seasonal Snow Cover of Alpine Regions and Its Effect on Soil Processes: A Review'. *Quaternary International* 162–163:172–81.

Eickelmann, Wolf, H. Sponagel, W. Grottenthaler, K. J. Hartmann, R. Hartwich, P. Janetzko, H. Joisten, D. Kühn, K. J. Sabel, and R. Traidl. 2005. *Bodenkundliche Kartieranleitung. KA5*. 5th ed. Hannover: Bundesanstalt für Geowissenschaften und Rohstoffe in Zusammenarbeit mit den Staatlichen Geologischen Diensten.

Enta, Ayako, Mika Hayashi, Maximo Larry Lopez Caceres, Lei Fujiyoshi, Toshiro Yamanaka, Akira Oikawa, and Felix Seidel. 2019. 'Nitrogen Resorption and Fractionation during Leaf Senescence in Typical Tree Species in Japan'. *Journal of Forestry Research*.

Essery, R., E. Martin, H. Douville, A. Fernandez, and E. Brun. 1999. 'A Comparison of Four Snow Models Using Observations from an Alpine Site'. *Climate Dynamics* 15:583–89.

Feddes, R. A., H. Zaradny, and P. Kowalik. 1977. 'Simulation of Evapotranspiration with Different Root Water-Uptake Functions'. *American Geophysical Union* 58:900.

Fernández-González, S., F. Valero, J. L. Sánchez, E. Gascón, L. López, E. García-Ortega, and A. Merino. 2015. 'Numerical Simulations of Snowfall Events: Sensitivity Analysis of Physical Parameterizations'. *Journal of Geophysical Research: Atmospheres* 120(19).

Floyd, William, and Markus Weiler. 2008. 'Measuring Snow Accumulation and Ablation Dynamics during Rain-on-Snow Events: Innovative Measurement Techniques'. *Hydrological Processes* 22(24):4805–12.

Forbes, Bruce C., and Florian Stammler. 2009. 'Arctic Climate Change Discourse: The Contrasting Politics of Research Agendas in the West and Russia'. *Polar Research* 28(1):28–42.

Franchitto, Nicolas, Peggy Gandia-Mailly, Bernard Georges, Anne Galinier, Norbert Telmon, Jean Louis Ducassé, and Daniel Rougé. 2008. 'Acute Copper Sulphate Poisoning: A Case Report and Literature Review'. *Resuscitation* 78(1):92–96.

Fu, Qiang, Renjie Hou, Tianxiao Li, Ruiqi Jiang, Peiru Yan, Ziao Ma, and Zhaoqiang Zhou. 2018. 'Effects of Soil Water and Heat Relationship under Various Snow Cover during Freezing-Thawing Periods in Songnen Plain, China'. *Scientific Reports* 8(1):1325.

Fujihara, Yoichi, Keiji Takase, Shunsuke Chono, Eiji Ichion, Akira Ogura, and Kenji Tanaka. 2017. 'Influence of Topography and Forest Characteristics on Snow Distributions in a Forested Catchment'. *Journal of Hydrology* 546:289–98.

Fujita, Mikiko, Hiroshi G. Takahashi, Noriko N. Ishizaki, and Fujio Kimura. 2014. 'Long-Term Variation of Winter Precipitation Linked to Sea-Surface Heat Fluxes around the Japan/East Sea'. *Atmospheric Science Letters* 15:275–81.

Gerke, Kirill M., Roy C. Sidle, and Dirk Mallants. 2015. 'Preferential Flow Mechanisms Identified from Staining Experiments in Forested Hillslopes: Preferential Flow Mechanisms Identified from Staining Experiments'. *Hydrological Processes* 29(21):4562–78.

Giddings, J. C., and E. LaChapelle. 1962. 'The Formation Rate of Depth Hoar'. *Journal of Geophysical Research* 67(6):2377–83.

Godsey, Sarah E., Danny Marks, Patrick R. Kormos, Mark S. Seyfried, Clarissa L. Enslin, Adam H. Winstral, James P. McNamara, and Timothy E. Link. 2018. 'Eleven Years of Mountain Weather, Snow, Soil Moisture and Streamflow Data from the Rain–Snow Transition Zone – the Johnston Draw Catchment, Reynolds Creek Experimental Watershed and Critical Zone Observatory, USA'. *Earth System Science Data* 10(3):1207–16.

Goebel, Marc-O., Jörg Bachmann, Markus Reichstein, Ivan A. Janssens, and Georg Guggenberger. 2011. 'Soil Water Repellency and Its Implications for Organic Matter Decomposition - Is There a Link to Extreme Climatic Events?: EXTREME EVENTS AND SOIL WATER REPELLENCY'. *Global Change Biology* 17(8):2640–56.

Gottfried, Gerald J., Daniel G. Neary, Peter F. Ffolliott, and Donald G. Decker. 2006. 'Impacts of a High-Intensity Summer Rainstorm on Two Small Oak Savanna Watersheds in the Southwestern Borderlands'. *Hydrology and Water Resources in Arizona and the Southwest* 36:67–73.

Grayson, Rodger B., Andrew W. Western, Francis H. S. Chiew, and Günter Blöschl. 1997. 'Preferred States in Spatial Soil Moisture Patterns: Local and Nonlocal Controls'. *Water Resources Research* 33(12):2897–2908.

Greilinger, Marion, Wolfgang Schöner, Wilfried Winiwarter, and Anne Kasper-Giebl. 2016. 'Temporal Changes of Inorganic Ion Deposition in the Seasonal Snow Cover for the Austrian Alps (1983–2014)'. *Atmospheric Environment* 132:141–52.

Grinevskiy, Sergey O., and Sergey P. Pozdniakov. n.d. 'The Use of HYDRUS-1D for Groundwater Recharge Estimation in Boreal Environments'. in Vol. Proceedings of the 4th International Conference "HYDRUS Software Applications to Subsurface Flow and Contaminant Transport Problems". Dept. of Soil Science and Geology, Czech University of Life Sciences Prague, Czech Republic.

Hardy, Janet P., Peter M. Groffman, Ross D. Fitzhugh, Karen S. Henry, Adam T. Welman, Jason D. Demers, Timothy J. Fahey, Charles T. Driscoll, Geraldine L. Tierney, and Scott Nolan. 2001. 'Snow Depth Manipulation and Its Influence on Soil Frost and Water Dynamics in a Northern Hardwood Forest'. *Biogeochemistry* 56(2):151–74.

Harpold, Adrian A., Noah P. Molotch, Keith N. Musselman, Roger C. Bales, Peter B. Kirchner, Marcy Litvak, and Paul D. Brooks. 2015. 'Soil Moisture Response to Snowmelt Timing in Mixed-Conifer Subalpine Forests'. *Hydrological Processes* 29(12):2782–98.

Hart, George, and Howard W. Lull. 1963. *SOME RELATIONSHIPS AMONG AIR, SNOW, AND SOIL TEMPERATURES AND SOIL FROST*. U.S. FOREST SERVICE RESEARCH NOTE NE-3. Northeastern Forest Experiment Station.

Hayashi, Masaki, Tomoyoshi Hirota, Yukiyoshi Iwata, and Izuru Takayabu. 2005. 'Snowmelt Energy Balance and Its Relation to Foehn Events in Tokachi, Japan'. *Journal of the Meteorological Society of Japan* 83(5):783–98.

He, Z. H., J. Parajka, F. Q. Tian, and G. Blöschl. 2014. 'Estimating Degree-Day Factors from MODIS for Snowmelt Runoff Modeling'. *Hydrology and Earth System Sciences* 18(12):4773–89.

Helling, Charles S., G. Chesters, and R. B. Corey. 1964. 'Contribution of Organic Matter and Clay to Soil Cation-Exchange Capacity as Affected by the PH of the Saturating Solution'. *Soil Science Society of America Journal* 28(4):517–20.

Hepper, E. N., D. E. Buschiazzo, G. G. Hevia, A. Urioste, and L. Antón. 2006. 'Clay Mineralogy, Cation Exchange Capacity and Specific Surface Area of Loess Soils with Different Volcanic Ash Contents'. *Geoderma* 135:216–23.

Hestnes, Erik. 1985. 'A Contribution to the Prediction of Slush Avalanches'. *Annals of Glaciology* 6:1–4.

Hillel, Daniel. 1998. *Environmental Soil Physics*. San Diego, California: Academic Press.

Hirabayashi, Yukiko, Petra Döll, and Shinjiro Kanae. 2010. 'Global-Scale Modeling of Glacier Mass Balances for Water Resources Assessments: Glacier Mass Changes between 1948 and 2006'. *Journal of Hydrology* 390(3–4):245–56.

Hirashima, Hiroyuki, Francesco Avanzi, and Satoru Yamaguchi. 2016. 'A Multi-Dimensional Model of Water Transport into Layered Snowpack: A Validation by Comparison with Laboratory Experiments'. Breckenridge, Colorado.

Hirashima, Hiroyuki, Nander Wever, Francesco Avanzi, Satoru Yamaguchi, and Yoshiyuki Ishii. 2018. 'SIMULATING LIQUID WATER INFILTRATION - COMPARISON BETWEEN A THREE-DIMENSIONAL WATER TRANSPORT MODEL AND A DUAL-DOMAIN APPROACH USING SNOWPACK'. Innsbruck, Austria.

Hirayama, Kenichi, Makoto Yamazaki, and Hung Tao Shen. 2002. 'Aspects of River Ice Hydrology in Japan'. *Hydrological Processes* 16(4):891–904.

Iijima, Yoshihiro, Tetsu Nakamura, Hotaek Park, Yoshihiro Tachibana, and Alexander N. Fedorov. 2016. 'Enhancement of Arctic Storm Activity in Relation to Permafrost Degradation in Eastern Siberia: ARCTIC STORM ACTIVITY IN RELATION TO PERMAFROST DEGRADATION'. *International Journal of Climatology* 36(13):4265–75.

Inoue, Satoshi, and Kotaro Yokoyama. 2003. 'Estimates of Snowfall Depth, Maximum Snow Depth, and Snow Pack Environments under Global Warming in Japan from Five Sets of Predicted Data'. *Journal of Agricultural Meteorology* 59(3):227–36.

Isard, Scott A., and Randall J. Schaetzl. 1998. 'EFFECTS OF WINTER WEATHER CONDITIONS ON SOIL FREEZING IN SOUTHERN MICHIGAN'. *Physical Geography* 19(1):71–94.

Ishizaka, Masaaki. 2004. 'Climatic Response of Snow Depth to Recent Warmer Winter Seasons in Heavy-Snowfall Areas in Japan'. *Annals of Glaciology* 38:299–304.

Ismail, Muhammad Fraz, Habib-ur Rehman, Wolfgang Bogacki, and Noor Muhammad. 2015. 'Degree Day Factor Models for Forecasting the Snowmelt Runoff for Naran Watershed'. *Science International (Lahore)* 27(3):1961–69.

Japan Meteorological Agency: https://www.jma.go.jp/jma/menu/menureport.html

Jennings, Keith S., Taylor S. Winchell, Ben Livneh, and Noah P. Molotch. 2018. 'Spatial Variation of the Rain–Snow Temperature Threshold across the Northern Hemisphere'. *Nature Communications* 9(1):1148.

Jin, G., Y. Shimizu, S. Onodera, M. Saito, and K. Matsumori. 2015. 'Evaluation of Drought Impact on Groundwater Recharge Rate Using SWAT and Hydrus Models on an Agricultural Island in Western Japan'. *Proceedings of the International Association of Hydrological Sciences* 371:143–48.

Jost, Georg, R. Dan Moore, Markus Weiler, David R. Gluns, and Younes Alila. 2009. 'Use of Distributed Snow Measurements to Test and Improve a Snowmelt Model for Predicting the Effect of Forest Clear-Cutting'. *Journal of Hydrology* 376(1–2):94–106.

Jost, Georg, R. Dan Moore, Russell Smith, and David R. Gluns. 2012. 'Distributed Temperature-Index Snowmelt Modelling for Forested Catchments'. *Journal of Hydrology* 420–421:87–101.

Kachanoski, R. G., R. P. Voroney, and E. G. Gregorich. 1988. 'ULTRASONIC DISPERSION OF AGGREGATES: DISTRIBUTION OF ORGANIC MATTER IN SIZE FRACTIONS'. *Canadian Journal of Soil Science* 68(2):395–403.

Kanno, Hiromitsu. 1997. 'Classification of the Yamase (Cold Northeasterly Wind around Northeastern Japan) Based upon Its Air-Mass Vertical Structures'. *Journal of the Meteorological Society of Japan* 75(6):1053–71.

Kato, Chihiro, Taku Nishimura, Hiromi Imoto, and Tsuyoshi Miyazaki. 2011. 'Predicting Soil Moisture and Temperature of Andisols under a Monsoon Climate in Japan'. *Vadose Zone Journal* 10(2):541–51.

Kato, Chihiro, and Taku Nishimura. 2017. 'Predicting Soil Moisture Condition in Arbitrary Agricultural Lands Using the Digital Soil Map and Soil Physical Properties Database'. *Paddy and Water Environment* 15(1):159–69.

Kattelmann, Richard. 1987. 'Some Measurements of Water Movement and Storage in Snow'. *International Association of Hydrological Sciences Publication* 162:245–54.

Kawahigashi, Masayuki, Klaus Kaiser, Karsten Kalbitz, Andrej Rodionov, and Georg Guggenberger. 2004. 'Dissolved Organic Matter in Small Streams along a Gradient from Discontinuous to Continuous Permafrost'. *Global Change Biology* 10(9):1576–86.

Kawase, Hiroaki, Akira Yamazaki, Hajime Iida, Kazuma Aoki, Wataru Shimada, Hidetaka Sasaki, Akihiko Murata, and Masaya Nosaka. 2018. 'Simulation of Extremely Small Amounts of Snow Observed at High Elevations over the Japanese Northern Alps in the 2015/16 Winter'. *SOLA* 14(0):39–45.

Kazama, So, Hirokazu Izumi, Priyantha Ranjan Sarukkalige, Takayuki Nasu, and Masaki Sawamoto. 2008. 'Estimating Snow Distribution over a Large Area and Its Application for Water Resources'. *Hydrological Processes* 22(13):2315–24.

Kellomäki, Seppo, Matti Maajärvi, Harri Strandman, Antti Kilpeläinen, and Heli Peltola. 2010. 'Model Computations on the Climate Change Effects on Snow Cover, Soil Moisture and Soil Frost in the Boreal Conditions over Finland'. *Silva Fennica* 44(2):213–33.

Kirdyanov, Alexander, Malcolm Hughes, Eugene Vaganov, Fritz Schweingruber, and Pavel Silkin. 2003. 'The Importance of Early Summer Temperature and Date of Snow Melt for Tree Growth in the Siberian Subarctic'. *Trees* 17(1):61–69.

Klein Tank, A. M. G., and G. P. Können. 2003. 'Trends in Indices of Daily Temperature and Precipitation Extremes in Europe,1946–99'. *Journal of Climate* 16(22):3665–80.

Kohl, B., M. Fuchs, G. Markart, and G. Patzelt. 2001. 'Heavy Rain on Snow Cover'. *Annals of Glaciology* 32:33–38.

Kojima, Kenji. 1967. 'Densification of Seasonal Snow Cover'. *Physics of Snow and Ice: Proceedings* 1(2):929–52.

Kojima, Yuki, Joshua L. Heitman, Masaru Sakai, Chihiro Kato, and Robert Horton. 2018. 'Bulk Density Effects on Soil Hydrologic and Thermal Characteristics: A Numerical Investigation'. *Hydrological Processes* 32(14):2203–16.

Kokkonen, Teemu, Harri Koivusalo, Tony Jakeman, and J. P. Norton. 2006. 'Construction of a Degree-Day Snow Model in the Light of the Ten Iterative Steps in Model Development'. Burlington, Vermont, USA.

Komatsu, Yosuke, and Yuichi Onda. 1996. 'Spatial Variation in Specific Discharge of Base Flow in a Small Catchments, Oe-Yama Region, Western Japan'. *Journal of Japan Society of Hydrology and Water Resources* 9(6):489–97.

Kominami, Yuji, Nobuyuki Tanaka, Yasoichi Endo, and Shoji Niwano. 2005. 'Estimation of Snow Distribution under Global Warming Using Data from Remote Weather Stations (AMeDAS)'. *Journal of Agricultural Meteorology* 60(5):445–50.

Kondo, Junsei, and Takeshi Yamazaki. 1990. 'A Prediction Model for Snowmelt, Snow Surface Temperature and Freezing Depth Using a Heat Balance Method'. *Journal of Applied Meteorology* 29(5):375–84.

Krasting, John P., Anthony J. Broccoli, Keith W. Dixon, and John R. Lanzante. 2013. 'Future Changes in Northern Hemisphere Snowfall'. *Journal of Climate* 26(20):7813–28.

Kudo, Ryoji, Takeo Yoshida, and Takao Masumoto. 2017. 'Uncertainty Analysis of Impacts of Climate Change on Snow Processes: Case Study of Interactions of GCM Uncertainty and an Impact Model'. *Journal of Hydrology* 548:196–207.

Kuhn, Michael. 2001. 'The Nutrient Cycle through Snow and Ice, a Review': *Aquatic Sciences* 63(2):150–67.

Kumagai, Tomo'omi, Makiko Tateishi, Takanori Shimizu, and Kyoichi Otsuki. 2008. 'Transpiration and Canopy Conductance at Two Slope Positions in a Japanese Cedar Forest Watershed'. *Agricultural and Forest Meteorology* 148(10):1444–55.

Kuribayashi, Masatoshi, Nam Jin Noh, Taku M. Saitoh, Ichiro Tamagawa, Yasutaka Wakazuki, and Hiroyuki Muraoka. 2013. 'Comparison of Snow Water Equivalent Estimated in Central Japan by High-Resolution Simulations Using Different Land-Surface Models'. *SOLA* 9(0):148–52.

Kuusinen, Nea, Pasi Kolari, Janne Levula, Albert Porcar-Castell, Pauline Stenberg, and Frank Berninger. 2012. 'Seasonal Variation in Boreal Pine Forest Albedo and Effects of Canopy Snow on Forest Reflectance'. *Agricultural and Forest Meteorology* 164:53–60.

Lakshmi, Venkat. 2013. 'Remote Sensing of Soil Moisture'. *ISRN Soil Science* 2013:1–33.

Lamparter, A., J. Bachmann, M. O. Goebel, and S. K. Woche. 2009. 'Carbon Mineralization in Soil: Impact of Wetting–Drying, Aggregation and Water Repellency'. *Geoderma* 150(3–4):324–33.

Laryea, K. B., P. Pathak, J. C. Katyal, International Crops Research Institute for the Semi-Arid Tropics, and Central Research Institute for Dryland Agriculture (India). 1997. *Measuring Soil Processes in Agricultural Research*. Patancheru, Andrah Pradesh, India: ICRISAT : CRIDA.

Le Bissonnais, Y., D. Blavet, G. De Noni, J. Y. Laurent, J. Asseline, and C. Chenu. 2007. 'Erodibility of Mediterranean Vineyard Soils: Relevant Aggregate Stability Methods and Significant Soil Variables'. *European Journal of Soil Science* 58(1):188–95.

Le, Phuong Dong, Michael Leonard, and Seth Westra. 2018. 'Modeling Spatial Dependence of Rainfall Extremes Across Multiple Durations'. *Water Resources Research* 54(3):2233–48.

Lehning, Michael, Ingo Völksch, David Gustafsson, Tuan Anh Nguyen, Manfred Stähli, and Massimiliano Zappa. 2006. 'ALPINE3D: A Detailed Model of Mountain Surface Processes and Its Application to Snow Hydrology'. *Hydrological Processes* 20(10):2111–28.

Leonelli, Giovanni, Giovanna Battipaglia, Paolo Cherubini, Matthias Saurer, Rolf T. W. Siegwolf, Maurizio Maugeri, Barbara Stenni, Stella Fusco, Valter Maggi, and Manuela Pelfini. 2017. 'Larix Decidua Δ18O Tree-Ring Cellulose Mainly Reflects the Isotopic Signature of Winter Snow in a High-Altitude Glacial Valley of the European Alps'. *Science of The Total Environment* 579:230–37.

Liao, Kaihua, Zhiwen Zhou, Xiaoming Lai, Qing Zhu, and Huihui Feng. 2017. 'Evaluation of Different Approaches for Identifying Optimal Sites to Predict Mean Hillslope Soil Moisture Content'. *Journal of Hydrology* 547:10–20.

Lindström, Göran, Kevin Bishop, and Mikaell Ottosson Löfvenius. 2002. 'Soil Frost and Runoff at Svartberget, Northern Sweden-Measurements and Model Analysis. *Hydrological Processes* 16(17):3379–92.

Lopez C., M. Larry, A. Brouchkov, H. Nakayama, F. Takakai, A. N. Fedorov, and M. Fukuda. 2007. 'Epigenetic Salt Accumulation and Water Movement in the Active Layer of Central Yakutia in Eastern Siberia'. *Hydrological Processes* 21(1):103–9.

Lopez C., M. Larry, Chitoshi Mizota, Toshiro Yamanaka, and Yoshihiro Nobori. 2010. 'Temporal Changes in Tree-Ring Nitrogen of Pinus Thunbergii Trees Exposed to Black-Tailed Gull (Larus Crassirostris) Breeding Colonies'. *Applied Geochemistry* 25(11):1699–1702.

Lopez C., M. Larry, Hayashida, S. Mori, Ashitani, and Yoshihiro Nobori. 2014 a. *Field Science Center University Forest: Watershed Preservation Division: 8th Forest Plan*. Tsuruoka, Yamagata, Japan: Yamagata University, Faculty of Agriculture.

Lopez C., M. Larry, C. Mizota, Y. Nobori, T. Sasaki, and T. Yamanaka. 2014 b. 'Temporal Changes in Nitrogen Acquisition of Japanese Black Pine (Pinus Thunbergii) Associated with Black Locust (Robinia Pseudoacacia)'. *Journal of Forestry Research* 25(3):585–89.

Lopez C., M. Larry, F. Takakai, G. Iwahana, A. N. Fedorov, Y. Iijima, R. Hatano, and M. Fukuda. 2015. 'Snowmelt and the Hydrological Interaction of Forest-Grassland Ecosystems in Central Yakutia, Eastern Siberia. *Hydrological Processes* 29(14):3074–83.

Lundmark, Annika, and Per-Erik Jansson. 2008. 'Estimating the Fate of De-Icing Salt in a Roadside Environment by Combining Modelling and Field Observations'. *Water, Air, and Soil Pollution* 195(1–4):215–32.

Luo, Jing-Jia, Swadhin K. Behera, Yukio Masumoto, and Toshio Yamagata. 2011. 'Impact of Global Ocean Surface Warming on Seasonal-to-Interannual Climate Prediction'. *Journal of Climate* 24(6):1626–46.

Madi, Raneem, Gerrit Huibert de Rooij, Henrike Mielenz, and Juliane Mai. 2018. 'Parametric Soil Water Retention Models: A Critical Evaluation of Expressions for the Full Moisture Range'. *Hydrology and Earth System Sciences* 22(2):1193–1219.

Magono, Choji, and Katsuhiro Kikuchi. 1980. 'Some Observations of Snowfall and Meteorological Conditions in Arctic Canada'. *Monthly Weather Review* 108(10):1656–64.

Marthews, T. R., C. A. Quesada, D. R. Galbraith, Y. Malhi, C. E. Mullins, M. G. Hodnett, and I. Dharssi. 2014. 'High-Resolution Hydraulic Parameter Maps for Surface Soils in Tropical South America'. *Geoscientific Model Development* 7(3):711–23.

Martinec, Jaroslav. 1960. 'The Degree-Day Factor for Snowmelt Runoff Forecasting'. *IUGG General Assembly of Helsinki, IAHS Commission of Surface Waters* 51:468–77.

Masiokas, M.H., Villalba, R., Luckman, B.H., Le Quesne, C., Aravena, J.C., 2006. Snowpack Variations in the Central Andes of Argentina and Chile, 1951–2005: Large-Scale Atmospheric Influences and Implications for Water Resources in the Region. *Journal of Climate* 19:6334–6352

Matsubaya, Osamu, and Hiroshi Kawaraya. 2014. 'Hydrogen and Oxygen Isotopic Characteristics of Precipitation in Coastal Areas of Japan Determined by Observations for 23 Years at Akita and for 1-2 Years at Other Several Localities'. *GEOCHEMICAL JOURNAL* 48(4):397–408.

Matsumoto, Masakazu, Shinji Saito, and Iwao Ohmine. 2002. 'Molecular Dynamics Simulation of the Ice Nucleation and Growth Process Leading to Water Freezing'. *Nature* 416(6879):409–13.

Matsuoka, Norikazu. 1996. 'Soil Moisture Variability in Relation to Diurnal Frost Heaving on Japanese High Mountain Slopes'. *Permafrost and Periglacial Processes* 7:139–51.

McNamara, James P., David Chandler, Mark Seyfried, and Shiva Achet. 2005. 'Soil Moisture States, Lateral Flow, and Streamflow Generation in a Semi-Arid, Snowmelt-Driven Catchment'. *Hydrological Processes* 19(20):4023–38.

Mesic, Milan, Marta Birkas, Zeljka Zgorelec, Ivica Kisic, Aleksandra Jurisic, and Ivana Sestak. 2012. 'Carbon Content and C/N Ratio in Pannonian and Mediterranean Soils'. in *Impact of tillage and fertilization on probable climate threats in Hungary and Croatia, soil vulnerability and protection*. Szent Istvan University Press.

Meyer, Hanno, Alexander Dereviagin, Christine Siegert, Lutz Schirrmeister, and Hans-W. Hubberten. 2002. 'Palaeoclimate Reconstruction on Big Lyakhovsky Island, North Siberia?Hydrogen and Oxygen Isotopes in Ice Wedges'. *Permafrost and Periglacial Processes* 13(2):91–105.

Mizuta, Ryo, Takao Uchiyama, Kenji Kamiguchi, Akio Kitoh, and Akira Noda. 2005. 'Changes in Extremes Indices over Japan Due to Global Warming Projected by a Global 20-Km-Mesh Atmospheric Model'. *SOLA* 1:153–56.

Monteith, J. L. 2007. 'Evaporation and Surface Temperature'. *Quarterly Journal of the Royal Meteorological Society* 107(451):1–27.

Motoya, Ken, and Junsei Kondo. 1999. 'Estimating the Seasonal Variations of Snow Water Equivalent, Runoff and Water Temperature of a Stream in a Basin Using the New Bucket Model.' *Journal of Japan Society of Hydrology and Water Resources* 12(5):391–407.

Motoya, Ken, Takeshi Yamazaki, and Nobuhisa Yasuda. 2001. 'Evaluating the Spatial and Temporal Distribution of Snow Accumulation, Snowmelts and Discharge in a Multi Basin Scale: An Application to the Tohoku Region, Japan'. *Hydrological Processes* 15(11):2101–29.

Musselman, Keith N., Noah P. Molotch, Steven A. Margulis, Peter B. Kirchner, and Roger C. Bales. 2012. 'Influence of Canopy Structure and Direct Beam Solar Irradiance on Snowmelt Rates in a Mixed Conifer Forest'. *Agricultural and Forest Meteorology* 161:46–56.

Nagata, Masashi. 1987. 'On the Structure of a Convergent Cloud Band over the Japan Sea in Winter; a Prediction Experiment'. *Journal of the Meteorological Society of Japan. Ser. II* 65(6):871–83.

Nakai, Sento, Koyuru Iwanami, Ryohei Misumi, Sang-Goon Park, and Toshiichi Kobayashi. 2005. 'A Classification of Snow Clouds by Doppler Radar Observations at Nagaoka, Japan'. *SOLA* 1:161–64.

Nakamura, Tsutomu, and Osamu Abe. 1993. 'Estimated Seasonal Snow Cover and Snowfall in Japan'. *Annals of Glaciology* 18:179–84.

Nakatsuka, Takeshi, Keiko Ohnishi, Toshihiko Hara, Akihiro Sumida, Daisuke Mitsuishi, Naoyuki Kurita, and Shigeru Uemura. 2004. 'Oxygen and Carbon Isotopic Ratios of Tree-Ring Cellulose in a Conifer-Hardwood Mixed Forest in Northern Japan'. *GEOCHEMICAL JOURNAL* 38(1):77–88.

Narapusetty, Balachandrudu, and Nicole Mölders. 2005. 'Evaluation of Snow Depth and Soil Temperatures Predicted by the Hydro–Thermodynamic Soil–Vegetation Scheme Coupled with the Fifth-Generation Pennsylvania State University–NCAR Mesoscale Model'. *Journal of Applied Meteorology* 44(12):1827–43.

Nawrot, Adam P., Krzysztof Migała, Bartłomiej Luks, Paulina Pakszys, and Piotr Głowacki. 2016. 'Chemistry of Snow Cover and Acidic Snowfall during a Season with a High Level of Air Pollution on the Hans Glacier, Spitsbergen'. *Polar Science* 10(3):249–61.

Neumann, T. A., M. R. Albert, R. Lomonaco, C. Engel, Z. Courville, and F. Perron. 2008. 'Experimental Determination of Snow Sublimation Rate and Stable-Isotopic Exchange'. *Annals of Glaciology* 49:1–6.

Ninomiya, K. 1964. 'Water-Substance Budget over the Japan Sea and the Japan Islands during the Period of Heavy Snow Storm'. *Journal of the Meteorological Society of Japan. Ser. II* 42(5):317–29.

Nishimura, Motoshi, Akihiko Sasaki, and Keisuke Suzuki. 2019. 'Long-Term Fluctuations, Modelling and Predictions of the Snow Accumulation and Ablation Process in Norikura Highland: Study Using an Energy Balance Analysis and Ablation Models'. *Journal of Geography (Chigaku Zasshi)* 128(1):61–75.

Niu, Guo-Yue, and Zong-Liang Yang. 2006. 'Effects of Frozen Soil on Snowmelt Runoff and Soil Water Storage at a Continental Scale'. *Journal of Hydrometeorology* 7(5):937–52.

Notaro, Michael, David Lorenz, Christopher Hoving, and Michael Schummer. 2014. 'Twenty-First-Century Projections of Snowfall and Winter Severity across Central-Eastern North America'. *Journal of Climate* 27(17):6526–50.

Ogawa, Mayumi, and Michio Nogami. 1994. 'Precipitation Amount Separated by Precipitation Type Using Discriminating Temperature During Winter Season'. *Journal of Japan Society of Hydrology and Water Resources* 7(1):421–27.

Ohta, Takeshi, Tetsuya Hiyama, Hiroki Tanaka, Takashi Kuwada, Trofim C. Maximov, Tetsuo Ohata, and Yoshihiro Fukushima. 2001. 'Seasonal Variation in the Energy and Water Exchanges above and below a Larch Forest in Eastern Siberia'. *Hydrological Processes* 15(8):1459–76.

Osonoi, Takahiro. 2018. 'Evaluation of Snowmelt Water Used by Japanese Cedar at the Start of the Growing Season in Shonai Region'.

Osumi, Katsuhiro, Shigeto Ikeda, and Toru Okamoto. 2003. 'Vegetation Patterns and Their Dependency on Site Conditions in the Pre-Industrial Landscape of North-Eastern Japan'. *Ecological Research* 18(6):753–65.

Parfitt, R. L., D. J. Giltrap, and J. S. Whitton. 1995. 'Contribution of Organic Matter and Clay Minerals to the Cation Exchange Capacity of Soils'. *Communications in Soil Science and Plant Analysis* 26(9–10):1343–55.

Perry, Katharine B. 1998. 'Basics of Frost and Freeze Protection for Horticultural Crops'. *HortTechnology* 8(1):10–15.

Peters, A., and W. Durner. 2006. 'Improved Estimation of Soil Water Retention Characteristics from Hydrostatic Column Experiments: ESTIMATION OF WATER RETENTION CHARACTERISTICS'. *Water Resources Research* 42(11).

Potopová, Vera, Constanţa Boroneanţ, Martin Možný, and Josef Soukup. 2016. 'Driving Role of Snow Cover on Soil Moisture and Drought Development during the Growing Season in the Czech Republic'. *International Journal of Climatology* 36(11):3741–58.

Rabbel, Inken, Heye Bogena, Burkhard Neuwirth, and Bernd Diekkrüger. 2018. 'Using Sap Flow Data to Parameterize the Feddes Water Stress Model for Norway Spruce'. *Water* 10(3):279.

Reba, Michele L., John Pomeroy, Danny Marks, and Timothy E. Link. 2012. 'Estimating Surface Sublimation Losses from Snowpacks in a Mountain Catchment Using Eddy Covariance and Turbulent Transfer Calculations: SUBLIMATION LOSSES FROM SNOWPACKS'. *Hydrological Processes* 26(24):3699–3711.

Reiweger, I., and J. Schweizer. 2013. 'Weak Layer Fracture: Facets and Depth Hoar'. *The Cryosphere* 7(5):1447–53.

Richard, C., and D. J. Gratton. 2001. 'The Importance of the Air Temperature Variable for the Snowmelt Runoff Modelling Using the SRM'. *Hydrological Processes* 15(18):3357–70.

Romano, N., P. Nasta, G. Severino, and J. W. Hopmans. 2011. 'Using Bimodal Lognormal Functions to Describe Soil Hydraulic Properties'. *Soil Science Society of America Journal* 75(2):468–80.

Røyne, Anja, Bjørn Jamtveit, Joachim Mathiesen, and Anders Malthe-Sørenssen. 2008. 'Controls on Rock Weathering Rates by Reaction-Induced Hierarchical Fracturing'. *Earth and Planetary Science Letters* 275(3–4):364–69.

Saito, Kazuyuki, Satoru Yamaguchi, Hiroki Iwata, Yoshinobu Harazono, Kenji Kosugi, Michael Lehning, and Martha Shulski. 2012. 'Climatic Physical Snowpack Properties for Large-Scale Modeling Examined by Observations and a Physical Model'. *Polar Science* 6(1):79–95.

Sakaki, Toshihiro, Anuchit Limsuwat, Kathleen M. Smits, and Tissa H. Illangasekare. 2008. 'Empirical Two-Point α-Mixing Model for Calibrating the ECH_2O EC-5 Soil Moisture Sensor in Sands'. *Water Resources Research* 44(4).

Salve, Rohit, Teamrat A. Ghezzehei, and Robert Jones. 2008. 'Infiltration into Fractured Bedrock'. *Water Resources Research* 44(1).

Sándor, Renáta, and Nándor Fodor. 2012. 'Simulation of Soil Temperature Dynamics with Models Using Different Concepts'. *The Scientific World Journal* 2012:1–8.

Sasaki, Takehiro, Masatoshi Katabuchi, Chiho Kamiyama, Masaya Shimazaki, Tohru Nakashizuka, and Kouki Hikosaka. 2014. 'Vulnerability of Moorland Plant Communities to Environmental Change: Consequences of Realistic Species Loss on Functional Diversity' edited by V. Devictor. *Journal of Applied Ecology* 51(2):299–308.

Schelker, J., L. Kuglerová, K. Eklöf, K. Bishop, and H. Laudon. 2013. 'Hydrological Effects of Clear-Cutting in a Boreal Forest – Snowpack Dynamics, Snowmelt and Streamflow Responses'. *Journal of Hydrology* 484:105–14.

Schwartz, Mark D., and Thomas R. Karl. 1990. 'Spring Phenology: Nature's Experiment to Detect the Effect of "Green-Up" on Surface Maximum Temperatures'. *Monthly Weather Review* 118:883–90.

Seidel, Felix, M. Larry Lopez C, Georg Guggenberger, and Yoshihiro Nobori. 2017. 'Impact of a Low Severity Fire on Soil Organic Carbon and Nitrogen Characteristics in Japanese Cedar Soil, Yamagata Prefecture, Japan'. *Open Journal of Forestry* 07(02):270–84.

Seidel, Felix, M. Larry Lopez C., Luisella Celi, Eleonora Bonifacio, Akira Oikawa, and Toshiro Yamanaka. 2019. 'N Isotope Fractionation in Tree Tissues During N Reabsorption and Remobilization in Fagus Crenata Blume'. *Forests* 10(4):330.

Shanley, James B., and Ann Chalmers. 1999. 'The Effect of Frozen Soil on Snowmelt Runoff at Sleepers River, Vermont'. *Hydrological Processes* 13:1843–57.

Shimada, Teruhisa, and Hiroshi Kawamura. 2004. 'Wind Jets and Wind Waves off the Pacific Coast of Northern Japan under Winter Monsoon Captured by Combined Use of Scatterometer, Synthetic Aperture Radar, and Altimeter'. *Journal of Geophysical Research* 109(C12):C12027.

Sicart, Jean Emmanuel, Richard L. H. Essery, John W. Pomeroy, Janet P. Hardy, Timothy E. Link, and Danny Marks. 2004. 'A Sensitivity Study of Daytime Net Radiation during Snowmelt to Forest Canopy and Atmospheric Conditions'. *Journal of Hydrometeorology* 5(5):774–84.

Sidle, Roy C., Tomonori Hirano, Takashi Gomi, and Tomomi Terajima. 2007. 'Hortonian Overland Flow from Japanese Forest Plantations—an Aberration, the Real Thing, or Something in Between?' *Hydrological Processes* 21(23):3237–47.

Simard, Suzanne W., David A. Perry, Melanie D. Jones, David D. Myrold, Daniel M. Durall, and Randy Molina. 1997. 'Net Transfer of Carbon between Ectomycorrhizal Tree Species in the Field'. *Nature* 388(6642):579–82.

Šimůnek, Jirka, Martinus Th. van Genuchten, and Miroslav Šejna. 2008. 'Development and Applications of the HYDRUS and STANMOD Software Packages and Related Codes'. *Vadose Zone Journal* 7(2):587.

Šimůnek, Jirka, Miroslav Šejna, M. Saito, M. Sakai, and Martinus Th. van Genuchten. 2013 a. *The HYDRUS-1D Software Package for Simulating the One-Dimensional Movement of Water, Heat, and Multiple Solutes in Variably-Saturated Media; Version4.17*. Riverside, California: DEPARTMENT OF ENVIRONMENTAL SCIENCES UNIVERSITY OF CALIFORNIA RIVERSIDE.

Šimůnek, Jirka, Diederik Jacques, Günter Langergrber, Scott A. Bradford, Miroslav Šejna, and Martinus Th. van Genuchten. 2013 b. 'Numerical Modeling of Contaminant Transport Using HYDRUS and Its Specialized Modules'. *Journal of the Indian Institute of Science* 93(2):265–84.

Šimůnek, Jirka, Martinus Th. van Genuchten, and Miroslav Šejna. 2016. 'Recent Developments and Applications of the HYDRUS Computer Software Packages'. *Vadose Zone Journal* 15(7):0.

Sinha, Tushar, and Keith A. Cherkauer. 2010. 'Impacts of Future Climate Change on Soil Frost in the Midwestern United States'. *Journal of Geophysical Research* 115(D8):D08105.

Skogland, Terje. 1978. 'Characteristics of the Snow Cover and Its Relationship to Wild Mountain Reindeer (Rangifer Tarandus Tarandus L.) Feeding Strategies'. *Arctic and Alpine Research* 10(3):569–79.

Soylu, Mehmet Evren, Christopher J. Kucharik, and Steven P. Loheide. 2014. 'Influence of Groundwater on Plant Water Use and Productivity: Development of an Integrated Ecosystem – Variably Saturated Soil Water Flow Model'. *Agricultural and Forest Meteorology* 189–190:198–210.

Spreitzhofer, G. 1999. 'Spatial, Temporal and Intensity Characteristics of Heavy Snowfall Events over Austria'. *Theoretical and Applied Climatology* 62(3–4):209–19.

Stadler, Daniel, Hans Wunderli, Adrian Auckenthaler, Hannes Flühler, and Michael Bründl. 1996. 'Measurement of Frost-induced Snowmelt Runoff in a Forest Soil'. *Hydrological Processes* 10:1293–1304.

Tague, Christina, and Hui Peng. 2013. 'The Sensitivity of Forest Water Use to the Timing of Precipitation and Snowmelt Recharge in the California Sierra: Implications for a Warming Climate'. *Journal of Geophysical Research: Biogeosciences* 118(2):875–87.

Tahir, A. A., P. Chevallier, Y. Arnaud, and B. Ahmad. 2011 a. 'Snow Cover Dynamics and Hydrological Regime of the Hunza River Basin, Karakoram Range, Northern Pakistan'. *Hydrology and Earth System Sciences* 15(7):2275–90.

Tahir, Adnan Ahmad, Pierre Chevallier, Yves Arnaud, Luc Neppel, and Bashir Ahmad. 2011 b. 'Modeling Snowmelt-Runoff under Climate Scenarios in the Hunza River Basin, Karakoram Range, Northern Pakistan'. *Journal of Hydrology* 409(1–2):104–17.

Takeuchi, Yukari, Yasoichi Endo, and Shigeki Murakami. 2008. 'High Correlation between Winter Precipitation and Air Temperature in Heavy-Snowfall Areas in Japan'. *Annals of Glaciology* 49:7–14.

Tanabe, Satoru. 2020. 'Assessing the Impact of Climate Change on Larch and Cedar Forests Using Stable Isotope Analysis'.

Tanaka, Yukio, and Yohei Sato. 2005. 'Farmers Managed Irrigation Districts in Japan: Assessing How Fairness May Contribute to Sustainability'. *Agricultural Water Management* 77(1–3):196–209.

Tischler, M., M. Garcia, C. Peterslidard, M. Moran, S. Miller, D. Thoma, S. Kumar, and J. Geiger. 2007. 'A GIS Framework for Surface-Layer Soil Moisture Estimation Combining Satellite Radar

Measurements and Land Surface Modeling with Soil Physical Property Estimation'. *Environmental Modelling & Software* 22(6):891–98.

Uchida, Masaki, Wenhong Mo, Takayuki Nakatsubo, Yuki Tsuchiya, Takao Horikoshi, and Hiroshi Koizumi. 2005. 'Microbial Activity and Litter Decomposition under Snow Cover in a Cool-Temperate Broad-Leaved Deciduous Forest'. *Agricultural and Forest Meteorology* 134(1–4):102–9.

UMS GmbH. 2015. 'Operation Manual HYPROP'.

Vaganov, E. A., M. K. Hughes, A. V. Kirdyanov, F. H. Schweingruber, and P. P. Silkin. 1999. 'Influence of Snowfall and Melt Timing on Tree Growth in Subarctic Eurasia'. *Nature* 400(6740):149–51.

van Genuchten, M. Th. 1980. 'A Closed-Form Equation for Predicting the Hydraulic Conductivity of Unsaturated Soils'. *Soil Science Society of America Journal* 44(5):892–98.

van Leeuwen, Boudewijn. 2015. 'GIS Workflow for Continuous Soil Moisture Estimation Based on Medium Resolution Satellite Data'. Lisbon, Portugal.

Venäläinen, A., H. Tuomenvirta, M. Heikinheimo, S. Kellomäki, H. Peltola, H. Strandman, and H. Väisänen. 2001. 'Impact of Climate Change on Soil Frost under Snow Cover in a Forested Landscape'. *Climate Research* 17:63–72.

Wagner, Annette. 2009. *Literature Study on the Correction of Precipitation Measurements*. FutMon C1-Met-29(BY). Freising, Germany: Bayerische Landesanstalt für Wald und Forstwirtschaft.

Wakahama, Gorou. 1968. 'Permeation of Melt Water into Snow Cover'. *Journal of the Japanese Society of Snow and Ice* 30(6):175–88.

Waldner, Peter A., Martin Schneebeli, Ute Schultze-Zimmermann, and Hannes Flühler. 2004. 'Effect of Snow Structure on Water Flow and Solute Transport'. *Hydrological Processes* 18(7):1271–90.

Walker, Jeffrey P., and Paul R. Houser. 2004. 'Requirements of a Global Near-Surface Soil Moisture Satellite Mission: Accuracy, Repeat Time, and Spatial Resolution'. *Advances in Water Resources* 27(8):785–801.

Walsh, John E. 1985. 'Influences of Snow Cover and Soil Moisture on Monthly Air Temperature'. Monthly Weather Reviewer(113):756–68.

Wang, Genxu, Yuanshou Li, Hongchang Hu, and Yibo Wang. 2008. 'Synergistic Effect of Vegetation and Air Temperature Changes on Soil Water Content in Alpine Frost Meadow Soil in the Permafrost Region of Qinghai-Tibet'. *Hydrological Processes* 22(17):3310–20.

Wang, Yin Quan, and Frank Schuchardt. 2010. 'Effect of C/N Ratio on the Composting of Vineyard Pruning Residues'. *Landbauforschung - VTI Agriculture and Forestry Researc* 3(60):131–38.

Wessolek, Gerd, Martin Kaupenjohann, Manfried Renger, and Michael Facklam. 2009. *Bodenphysikalische Kennwerte und Berechnungsverfahren für die Praxis*. Vol. 40. Berlin: Technische Universität Berlin.

Whisenant, Steve. 2005. 'First Steps in Erosion Control'. Pp. 350–56 in *Forest Restoration in Landscapes*. New York: Springer.

Winkler, R. D., D. L. Spittlehouse, and D. L. Golding. 2005. 'Measured Differences in Snow Accumulation and Melt among Clearcut, Juvenile, and Mature Forests in Southern British Columbia'. *Hydrological Processes* 19(1):51–62.

Yamaguchi, Satoru, Takafumi Katsushima, Atsushi Sato, and Toshiro Kumakura. 2010. 'Water Retention Curve of Snow with Different Grain Sizes'. *Cold Regions Science and Technology* 64(2):87–93.

Yamaguchi, Satoru, Osamu Abe, Sento Nakai, and Atsushi Sato. 2011. 'Recent Fluctuations of Meteorological and Snow Conditions in Japanese Mountains'. *Annals of Glaciology* 52(58):209–15.

Yamaguchi, Satoru, Kunio Watanabe, Takafumi Katsushima, Atsushi Sato, and Toshiro Kumakura. 2012. 'Dependence of the Water Retention Curve of Snow on Snow Characteristics'. *Annals of Glaciology* 53(61):6–12.

Yamaguchi, Satoru, Katsushi Iwamoto, and Sento Nakai. 2013. 'Interannual Fluctuations of the Relationship between Winter Precipitation and Air Temperature in the Heavy-Snowfall Zone of Japan'. *Annals of Glaciology* 54(62):183–88.

Yamazaki, Takeshi, and Junsei Kondo. 1992. 'The Snowmelt and Heat Balance in Snow-Covered Forested Areas'. *Journal of Applied Meteorology* 31:1322–27.

Yan, Hongxiang, and Hamid Moradkhani. 2016. 'Combined Assimilation of Streamflow and Satellite Soil Moisture with the Particle Filter and Geostatistical Modeling'. *Advances in Water Resources* 94:364–78.

Yasunaga, Kazuaki, and Masashi Tomochika. 2017. 'An Increasing Trend in the Early Winter Precipitation during Recent Decades along the Coastal Areas of the Sea of Japan'. *Journal of Hydrometeorology* 18(11):2893–2906.

Zhai, Lu, Jiang Jiang, Donald DeAngelis, and Leonel da Silveira Lobo Sternberg. 2016. 'Prediction of Plant Vulnerability to Salinity Increase in a Coastal Ecosystem by Stable Isotope Composition (Δ18O) of Plant Stem Water: A Model Study'. *Ecosystems* 19(1):32–49.

Zhan, ZhiMing, QiMing Qin, Abduwasit Ghulan, and DongDong Wang. 2007. 'NIR-Red Spectral Space Based New Method for Soil Moisture Monitoring'. *Science in China Series D: Earth Sciences* 50(2):283–89.

Zhang, Xuebin, W. D. Hogg, and Éva Mekis. 2001. 'Spatial and Temporal Characteristics of Heavy Precipitation Events over Canada'. *Journal of Climate* 14:1923–36.

Zhang, Tingjun. 2005. 'Influence of the Seasonal Snow Cover on the Ground Thermal Regime: An Overview'. *Reviews of Geophysics* 43(4):RG4002.

Zhang, Yu, Wenjun Chen, Sharon L. Smith, Daniel W. Riseborough, and Josef Cihlar. 2005. 'Soil Temperature in Canada during the Twentieth Century: Complex Responses to Atmospheric Climate Change'. *Journal of Geophysical Research* 110(D3):D03112.

Zhang, Yong, Shiyin Liu, and Yongjian Ding. 2006. 'Observed Degree-Day Factors and Their Spatial Variation on Glaciers in Western China'. *Annals of Glaciology* 43:301–6.

Zhang, Qiqin, M. Larry Lopez C., Alexander C. Brandt, Jordi Voltas, Takeshi Nakatsuka, and Mónica Aguilera. 2019. 'Using Water Stable Isotopes to Trace Water Sources of Three Typical Japanese Tree Species under Heavy Rainfall Conditions'. *Open Journal of Forestry* 10(01):7–21.

Zhou, P., O. Luukkanen, T. Tokola, and J. Nieminen. 2008. 'Effect of Vegetation Cover on Soil Erosion in a Mountainous Watershed'. *CATENA* 75(3):319–25.

9. Supplementary Materials

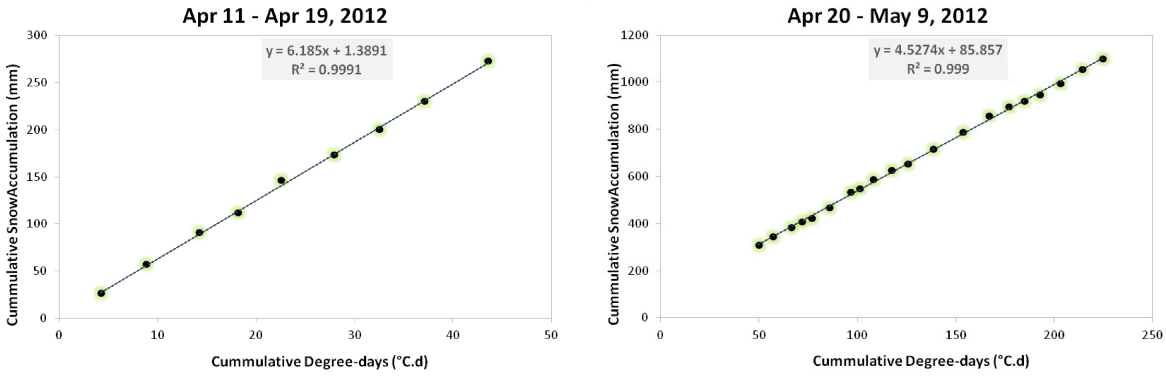

Figure 8.1 a-b: DDF graphs for the snowmelt season 2012

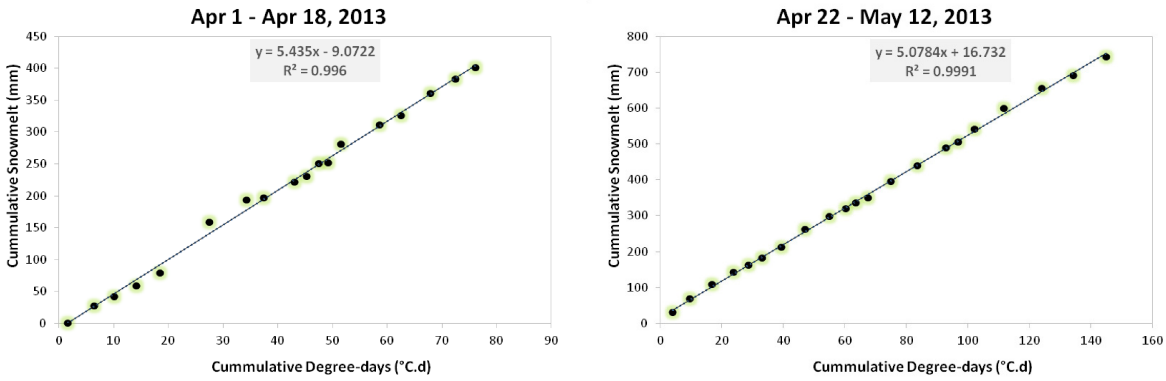

Figure 8.2 a-b: DDF graphs for the snowmelt season 2013

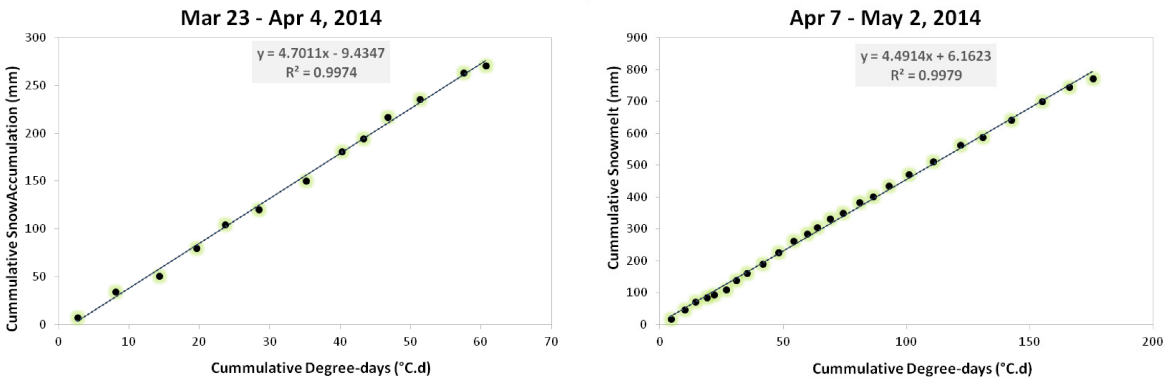

Figure 8.3 a-b: DDF graphs for the snowmelt season 2014

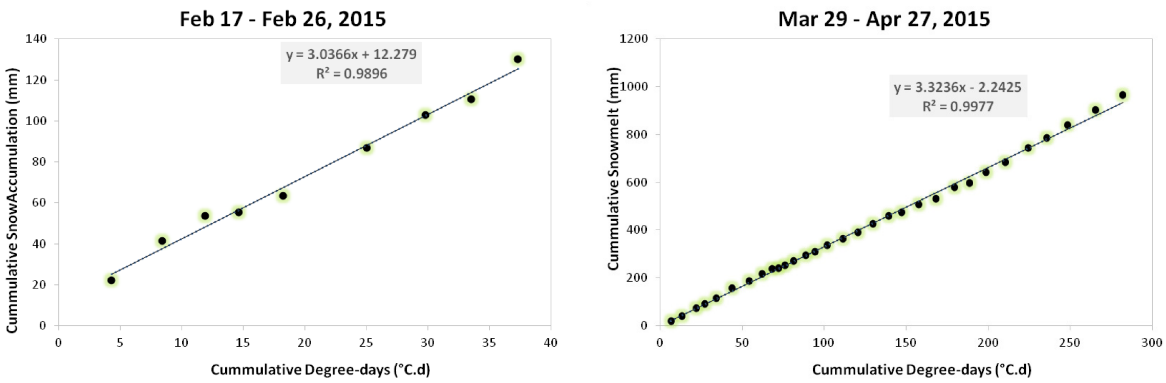

Figure 8.4 a-b: DDF graphs for the snowmelt season 2015

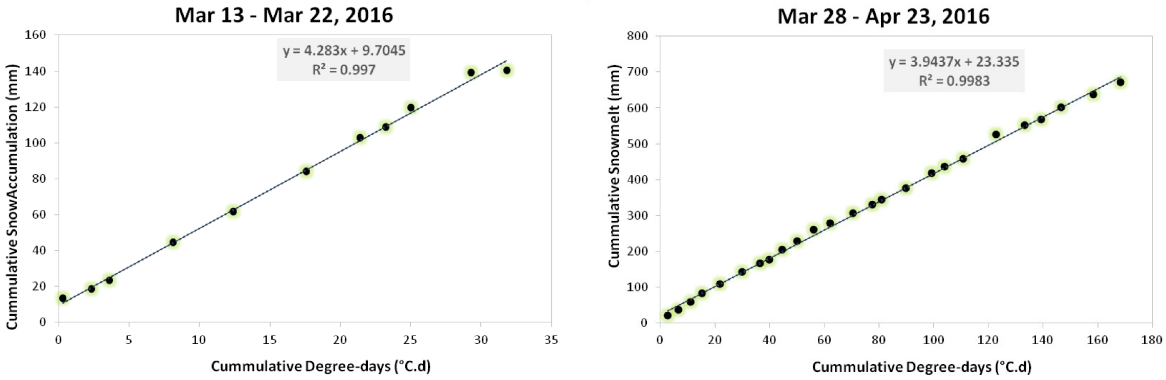

Figure 8.5 a-b: DDF graphs for the snowmelt season 2016

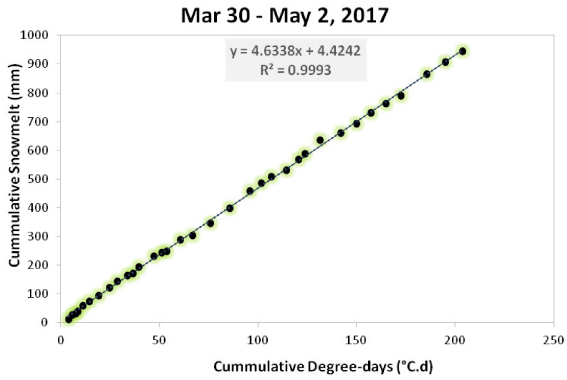

Figure 8.6: DDF graph for the snowmelt season 2017

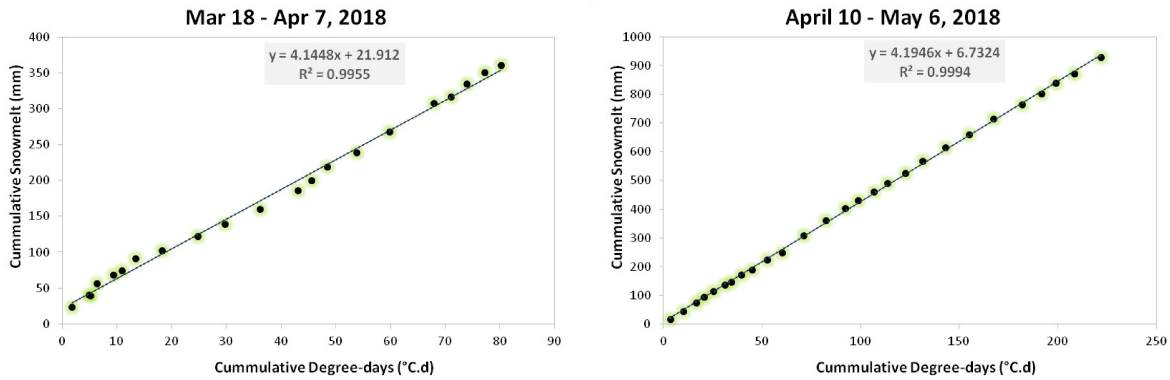

Figure 8.7 a-b: DDF graphs for the snowmelt season 2018

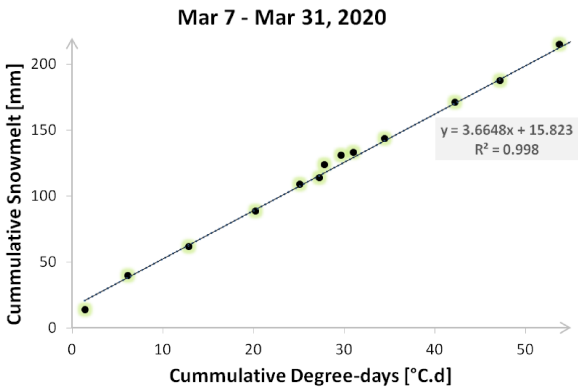

Figure 8.8: DDF graph for the snowmelt season 2020

Table 8.1: Soil moisture peak analysis of rain and snowmelt events (2020)

date of peak	SM increase in vol.%	$\Delta t_{increase}$ in h	increase rate in vol.%/h	Precipitation (rain) in mm	SWE change in mm	causing event
29.12.2019	2.05**	4	0.5125	2.5 (0.5)	-1	both
03.01.2020	1.52**	4	0.3800	4.5 (1)	11	rain
08.01.2020	2.05**	10	0.2050	6.5 (6.5)	4	both
14.01.2020	1.59**	4	0.3975	6 (1.5)	-2	both
20.01.2020	1.59**	4	0.3975	5.5 (5.5)	8	rain
22.01.2020	1.37**	4	0.3425	0 (0)	-1	melt
28.01.2020	1.56**	14	0.1114	0.5 (0.5)	-16	melt
01.02.2020	2.35**	4	0.5875	13.5 (2)	22	rain
03.02.2020	1.75**	4	0.4375	5.5 (5.5)	14	rain
05.02.2020	2.51**	6	0.4183	15.5 (7.5)	20	rain
13.02.2020	2.05**	12	0.1708	5 (5)	-2	both
17.02.2020	1.67**	10	0.1670	13 (13)	6	both
19.02.2020	1.22**	4	0.3050	5 (1)	9	both
24.02.2020	1.75**	4	0.4375	6 (5.5)	10	rain
29.02.2020	1.82**	6	0.3033	0.5 (0.5)	-6	melt

†: The peak was too close to a previous event, only one day (‡: two days) before the event was/were regarded
**: significance level $p < 0.01$

Table 8.2: DDFs (in mm/d°C) calculated with approach 3

Period	2012	2013	2014	2015	2016	2017	2018	2019	2020
11.2. - 20.2.				4.21					
21.2.-29.2.				3.75					
1.3. - 10.3.		7.77		3.59	7.37			4.17	7.39
11.3. - 20.3.	14.33	12.18	11.63	3.97	5.47	8.43	5.59	6.75	5.97
21.3. - 31.3.	15.12	8.66	5.74	2.93	6.04	5.99	4.59	6.01	5.64
1.4. - 10.4.	12.48	6.88	5.34	4.34	4.85	5.49	6.37	5.64	
11.4. - 20.4.	6.26	7.64	5.06	3.62	4.51	6.1	5.09	6.34	
21.4. - 30.4.	4.88	6.13	4.3	3.87	3.44	5.02	4.7	5.21	
1.5. - 10.5.	5.09	6.63	4.91			4.31	4.46		
11.5. - 20.5.	3.99	4.95							

Table 8.3: DDFs (in mm/d°C) calculated with approach 4

Period	2012	2013	2014	2015	2016	2017	2018	2019	2020
11.2. - 20.2.				3.79					
21.2.-29.2.				2.90	36.28			21.95	
1.3. - 10.3.		6.16		2.76	5.78		6.78	3.96	4.89
11.3. - 20.3.	9.12	8.26	7.10	3.28	4.69	6.46	5.28	4.79	3.23
21.3. - 31.3.	10	8.04	4.49	2.65	4.82	4.01	4.06	4.34	3.69
1.4. - 10.4.	7.09	5.1	4.39	3.35	3.97	4.93	4.39	4.37	
11.4. - 20.4.	6.15	5.61	4.95	3.12	3.92	4.71	4.08	5.46	
21.4. - 30.4.	4.55	5.41	4.28	3.76	3.21	4.52	4.35	4.51	
1.5. - 10.5.	4.38	5.18	3.47			4.31	3.99		
11.5. - 20.5.	3.41	4.17							

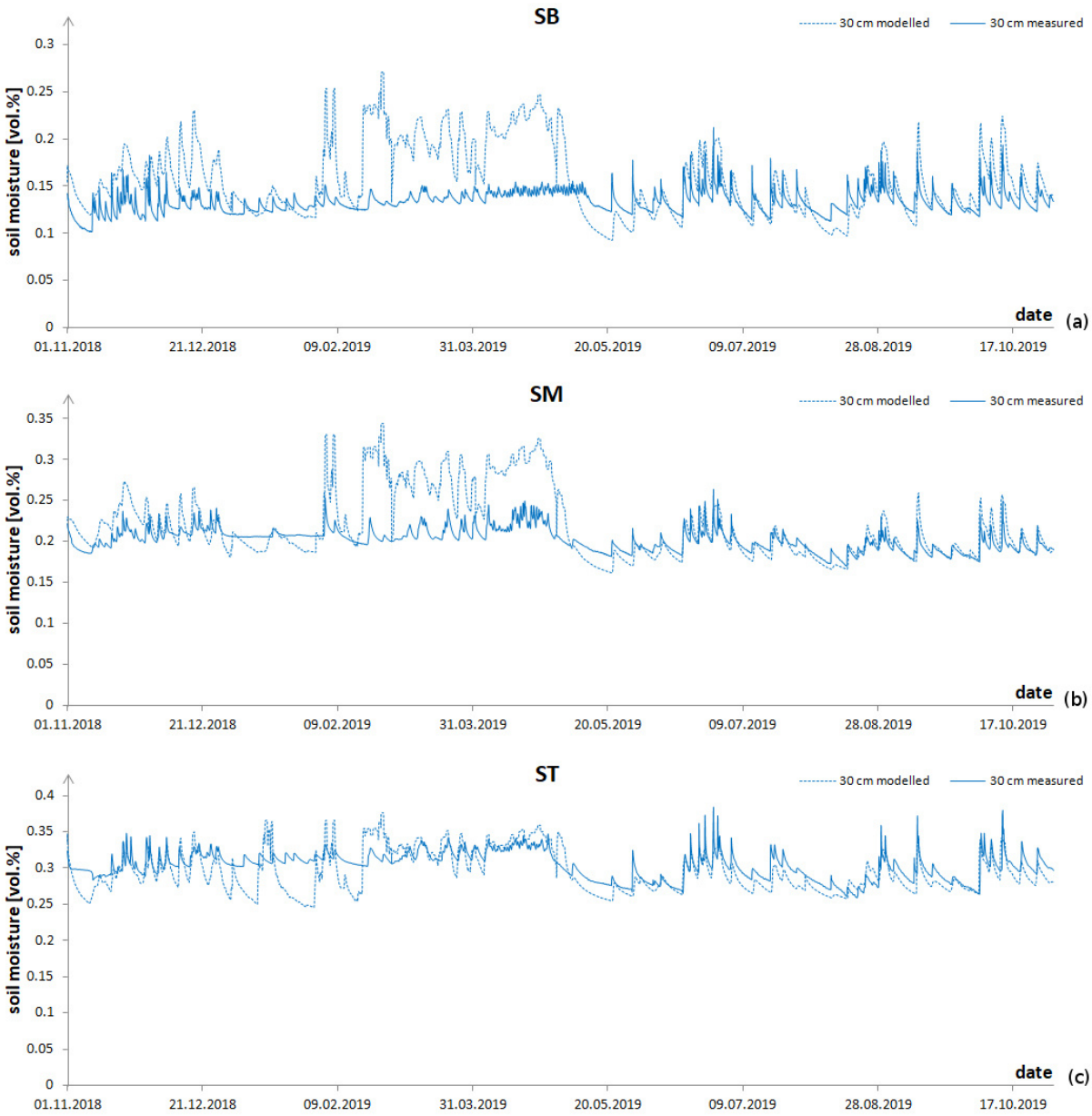

Figure 8.9 a-c: HYDRUS 1D modelled soil moisture for *SB*, *SM* and *ST* (30 cm)

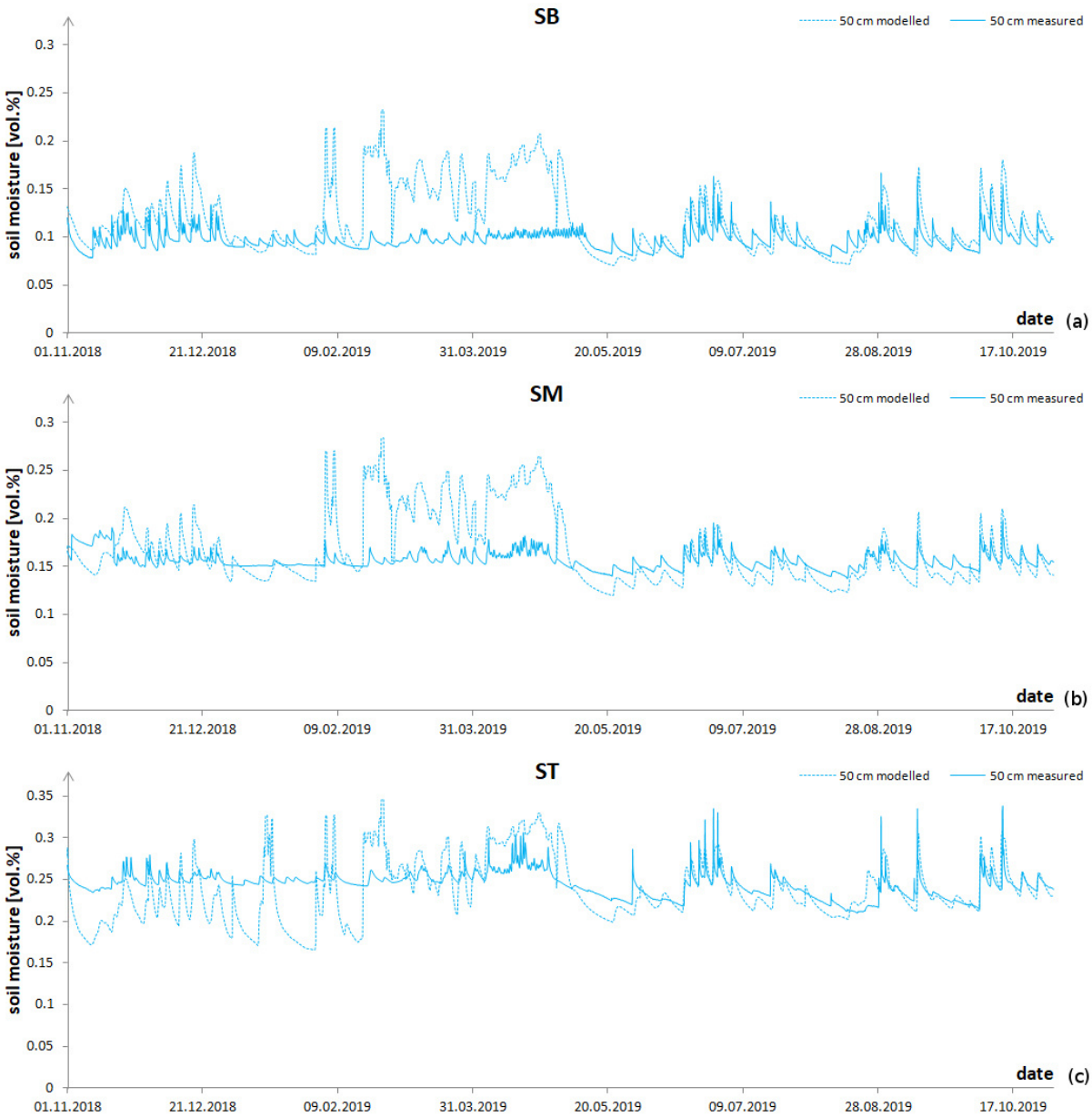

Figure 8.10 a-c: HYDRUS 1D modelled soil moisture for *SB*, *SM* and *ST* (50 cm)